OGO-E SPACE VEHICLE RESPONSE TO TRANSIENT LOADING AT ATLAS BOOSTER ENGINE CUTOFF

900-128 April 1968

Approved by:

M. E. Alper, Manager
Applied Mechanics Section

W. H. Gayman, Ass't. Manager
Applied Mechanics Section
Co-Author

M. R. Trubert
Member of Technical Staff
Applied Mechanics Section
Co-Author

J. A. Garba, Senior Engineer
Applied Mechanics Section
Co-Author

JET PROPULSION LABORATORY
CALIFORNIA INSTITUTE OF TECHNOLOGY
PASADENA, CALIFORNIA

PRECEDING PAGE BLANK NOT FILMED.

CONTENTS

I. Introduction 1

II. Normal Mode Analysis 1

A. Input Data 1

1. The OGO-E spacecraft 1
2. The Atlas/Agena launch vehicle 2

B. Data Processing 2

1. The OGO-E spacecraft 2
2. The Atlas/Agena launch vehicle 5
3. The composite vehicle 5

C. Free-Free Torsional Modes 5

III. Response Analyses 7

A. Method 7

B. Input Data 9

C. Normal Modes 10

D. Damping 10

E. Responses 10

References 13

Appendix A. Conversion From Normal-Mode Coordinates of a Cantilever Structure to an Equivalent Lumped-Parameter System A-1

Appendix B. The OGO-E Generalized Mass Matrix B-1

Appendix C. Numerical Values for the Atlas/Agena/OGO-E Mathematical Model C-1

Appendix D. Free-Free Torsional Modes for the OGO-E Space Vehicle D-1

Appendix E. Response Plots E-1

CONTENTS (contd)

TABLES

1. Acceleration responses for 3% modal damping (RA-6, 7, 8, 9 data input) 11

2. Torque 12

3. Effect of modal damping of Atlas/Agena/OGO space vehicle, pulse 3 excitation 12

D-1. Pertinent modal information D-23

FIGURES

1. Mathematical model of the Atlas/Agena interface 3

2. Ideal representation of structure for spacecraft base torque determination 8

A-1. Oscillator A-2

A-2. Mathematical model of the OGO-E spacecraft A-5

C-1. Mathematical model of the Atlas/Agena OGO-E space vehicle C-6

D-1. Atlas/Agena/OGO torsion mode shape (mode 1) F = 4.93 Hz D-1

D-2. Atlas/Agena/OGO torsion mode shape (mode 2) F = 9.30 Hz D-2

D-3. Atlas/Agena/OGO torsion mode shape (mode 3) F = 11.74 Hz D-3

D-4. Atlas/Agena/OGO torsion mode shape (mode 4) F = 13.09 Hz D-4

D-5. Atlas/Agena/OGO torsion mode shape (mode 5) F = 15.64 Hz D-5

D-6. Atlas/Agena/OGO torsion mode shape (mode 6) F = 19.13 Hz D-6

D-7. Atlas/Agena/OGO torsion mode shape (mode 7) F = 21.80 Hz D-7

CONTENTS (contd)

FIGURES (contd)

D-8. Atlas/Agena/OGO torsion mode shape (mode 8) F = 24.68 Hz D-8

D-9. Atlas/Agena/OGO torsion mode shape (mode 9) F = 28.24 Hz D-9

D-10. Atlas/Agena/OGO torsion mode shape (mode 10) F = 34.63 Hz D-10

D-11. Atlas/Agena/OGO torsion mode shape (mode 11) F = 39.87 Hz D-11

D-12. Atlas/Agena/OGO torsion mode shape (mode 12) F = 42.58 Hz D-12

D-13. Atlas/Agena/OGO torsion mode shape (mode 13) F = 45.83 Hz D-13

D-14. Atlas/Agena/OGO torsion mode shape (mode 14) F = 48.27 Hz D-14

D-15. Atlas/Agena/OGO torsion mode shape (mode 15) F = 58.83 Hz D-15

D-16. Atlas/Agena/OGO torsion mode shape (mode 16) F = 59.02 Hz D-16

D-17. Atlas/Agena/OGO torsion mode shape (mode 17) F = 67.50 Hz D-17

D-18. Atlas/Agena/OGO torsion mode shape (mode 18) F = 79.66 Hz D-18

D-19. Atlas/Agena/OGO torsion mode shape (mode 19) F = 82.99 Hz D-19

D-20. Atlas/Agena/OGO torsion mode shape (mode 20) F = 92.20 Hz D-20

D-21. Atlas/Agena/OGO torsion mode shape (mode 21) F = 97.26 Hz D-21

D-22. Atlas/Agena/OGO torsion mode shape (mode 22) F = 98.04 Hz D-22

E-1. RA-6 torsional flight acceleration, time history (pulse 1) . . E-1

CONTENTS (contd)

FIGURES (contd)

E-2. RA-6 torsional flight acceleration, Fourier transform, modulus (pulse 1) E-2

E-3. RA-6 torsional flight acceleration, Fourier transform, phase angle (pulse 1) E-3

E-4. RA-7 torsional flight acceleration, time history (pulse 2) E-4

E-5. RA-7 torsional flight acceleration, Fourier transform, modulus (pulse 2) E-5

E-6. RA-7 torsional flight acceleration, Fourier transform, phase angle (pulse 2) E-6

E-7. RA-8 torsional flight acceleration, time history (pulse 3) . . . E-7

E-8. RA-8 torsional flight acceleration, Fourier transform, modulus (pulse 3) E-8

E-9. RA-8 torsional flight acceleration, Fourier transform, phase angle (pulse 3) E-9

E-10. RA-9 torsional flight acceleration, time history (pulse 4) . . . E-10

E-11. RA-9 torsional flight acceleration, Fourier transform, modulus (pulse 4) E-11

E-12. RA-9 torsional flight acceleration, Fourier transform, phase angle (pulse 4) E-12

E-13. Spacecraft base acceleration, Joint 7, time history (pulse 1) E-13

E-14. Spacecraft base acceleration, Joint 7, Fourier transform, modulus (pulse 1) E-14

E-15. Spacecraft base acceleration, Joint 7, Fourier transform, phase angle (pulse 1) E-15

E-16. Spacecraft base acceleration, Joint 7, time history (pulse 2) E-16

E-17. Spacecraft base acceleration, Joint 7, Fourier transform, modulus (pulse 2) E-17

E-18. Spacecraft base acceleration, Joint 7, Fourier transform, phase angle (pulse 2) E-18

CONTENTS (contd)

FIGURES (contd)

E-19. Spacecraft base acceleration, Joint 7, time history (pulse 3) E-19

E-20. Spacecraft base acceleration, Joint 7, Fourier transform, modulus (pulse 3) E-20

E-21. Spacecraft base acceleration, Joint 7, Fourier transform, phase angle (pulse 3) E-21

E-22. Spacecraft base acceleration, Joint 7, time history (pulse 4) E-22

E-23. Spacecraft base acceleration, Joint 7, Fourier transform, modulus (pulse 4) E-23

E-24. Spacecraft base acceleration, Joint 7, Fourier transform, phase angle (pulse 4) E-24

E-25. Joint 1, x_1 time history (pulse 1). E-25

E-26. Joint 1, x_1 Fourier transform, modulus (pulse 1) E-26

E-27. Joint 1, x_1 Fourier transform, phase angle (pulse 1) E-27

E-28. Joint 1, x_1 time history (pulse 2). E-28

E-29. Joint 1, x_1 Fourier transform, modulus (pulse 2) E-29

E-30. Joint 1, x_1 Fourier transform, phase angle (pulse 2) E-30

E-31. Joint 1, x_1 time history (pulse 3) E-31

E-32. Joint 1, x_1 Fourier transform, modulus (pulse 3) E-32

E-33. Joint 1, x_1 Fourier transform, phase angle (pulse 3) E-33

E-34. Joint 1, x_1 time history (pulse 4). E-34

E-35. Joint 1, x_1 Fourier transform, modulus (pulse 4) E-35

E-36. Joint 1, x_1 Fourier transform, phase angle (pulse 4) E-36

E-37. Joint 1, x_5 time history (pulse 1) E-37

E-38. Joint 1, x_5 Fourier transform, modulus (pulse 1) E-38

E-39. Joint 1, x_5 Fourier transform, phase angle (pulse 1) E-39

CONTENTS (contd)

FIGURES (contd)

E-40. Joint 1, x_5 time history (pulse 2) E-40
E-41. Joint 1, x_5 Fourier transform, modulus (pulse 2) E-41
E-42. Joint 1, x_5 Fourier transform, phase angle (pulse 2) E-42
E-43. Joint 1, x_5 time history (pulse 3) E-43
E-44. Joint 1, x_5 Fourier transform, modulus (pulse 3) E-44
E-45. Joint 1, x_5 Fourier transform, phase angle (pulse 3) E-45
E-46. Joint 1, x_5 time history (pulse 4) E-46
E-47. Joint 1, x_5 Fourier transform, modulus (pulse 4) E-47
E-48. Joint 1, x_5 Fourier transform, phase angle (pulse 4) E-48
E-49. Joint 5, x_5 time history (pulse 1) E-49
E-50. Joint 5, x_5 Fourier transform, modulus (pulse 1) E-50
E-51. Joint 5, x_5 Fourier transform, phase angle (pulse 1) E-51
E-52. Joint 5, x_5 time history (pulse 2) E-52
E-53. Joint 5, x_5 Fourier transform, modulus (pulse 2) E-53
E-54. Joint 5, x_5 Fourier transform, phase angle (pulse 2) E-54
E-55. Joint 5, x_5 time history (pulse 3) E-55
E-56. Joint 5, x_5 Fourier transform, modulus (pulse 3) E-56
E-57. Joint 5, x_5 Fourier transform, phase angle (pulse 3) E-57
E-58. Joint 5, x_5 time history (pulse 4) E-58
E-59. Joint 5, x_5 Fourier transform, modulus (pulse 4) E-59
E-60. Joint 5, x_5 Fourier transform, phase angle (pulse 4) E-60
E-61. Joint 23, x_1 time history (pulse 1) E-61
E-62. Joint 23, x_1 Fourier transform, modulus (pulse 1) E-62
E-63. Joint 23, x_1 Fourier transform, phase angle (pulse 1). . . . E-63

CONTENTS (contd)

FIGURES (contd)

E-64. Joint 23, x_1 time history (pulse 2) E-64

E-65. Joint 23, x_1 Fourier transform, modulus (pulse 2) E-65

E-66. Joint 23, x_1 Fourier transform, phase angle (pulse 2) E-66

E-67. Joint 23, x_1 time history (pulse 3) E-67

E-68. Joint 23, x_1 Fourier transform, modulus (pulse 3) E-68

E-69. Joint 23, x_1 Fourier transform, phase angle (pulse 3) E-69

E-70. Joint 23, x_1 time history (pulse 4) E-70

E-71. Joint 23, x_1 Fourier transform, modulus (pulse 4) E-71

E-72. Joint 23, x_1 Fourier transform, phase angle (pulse 4) E-72

E-73. Joint 23, x_3 time history (pulse 1) E-73

E-74. Joint 23, x_3 Fourier transform, modulus (pulse 1) E-74

E-75. Joint 23, x_3 Fourier transform, phase angle (pulse 1) E-75

E-76. Joint 23, x_3 time history (pulse 2) E-76

E-77. Joint 23, x_3 Fourier transform, modulus (pulse 2) E-77

E-78. Joint 23, x_3 Fourier transform, phase angle (pulse 2) E-78

E-79. Joint 23, x_3 time history (pulse 3) E-79

E-80. Joint 23, x_3 Fourier transform, modulus (pulse 3) E-80

E-81. Joint 23, x_3 Fourier transform, phase angle (pulse 3) E-81

E-82. Joint 23, x_3 time history (pulse 4) E-82

E-83. Joint 23, x_3 Fourier transform, modulus (pulse 4) E-83

E-84. Joint 23, x_3 Fourier transform, phase angle (pulse 4) E-84

E-85. Base of spacecraft torque, Joint 7, time history (pulse 1) E-85

E-86. Base of spacecraft torque, Fourier transform, modulus (pulse 1) E-86

CONTENTS (contd)

FIGURES (contd)

E-87. Base of spacecraft torque, Joint 7, Fourier transform, phase angle (pulse 1) E-87

E-88. Base of spacecraft torque, Joint 7, time history (pulse 2) . . E-88

E-89. Base of spacecraft torque, Fourier transform, modulus (pulse 2) E-89

E-90. Base of spacecraft torque, Joint 7, Fourier transform, phase angle (pulse 2) E-90

E-91. Base of spacecraft torque, Joint 7, time history (pulse 3) E-91

E-92. Base of spacecraft torque, Fourier transform, modulus (pulse 3) E-92

E-93. Base of spacecraft torque, Joint 7, Fourier transform, phase angle (pulse 3) E-93

E-94. Base of spacecraft torque, Joint 7, time history (pulse 4) E-94

E-95. Base of spacecraft torque, Joint 7, Fourier transform, modulus (pulse 4) E-95

E-96. Base of spacecraft torque, Joint 7, Fourier transform, phase angle (pulse 4) E-96

E-97. Joint 1, x_1 time history (pulse 3) 1% damping E-97

E-98. Joint 1, x_1 Fourier transform, modulus (pulse 3) 1% damping E-98

E-99. Joint 1, x_1 Fourier transform, phase angle (pulse 3) 1% damping E-99

E-100. Joint 1, x_1 time history (pulse 3) 2% damping E-100

E-101. Joint 1, x_1 Fourier transform, modulus (pulse 3) 2% damping E-101

E-102. Joint 1, x_1 Fourier transform, phase angle (pulse 3) 2% damping E-102

E-103. Joint 1, x_1 time history (pulse 3) 4% damping E-103

CONTENTS (contd)

FIGURES (contd)

E-104. Joint 1, x_1 Fourier transform, modulus (pulse 3) 4% damping E-104

E-105. Joint 1, x_1 Fourier transform, phase angle (pulse 3) 4% damping E-105

E-106. Joint 23, x_1 time history (pulse 3) 0.1% damping E-106

E-107. Joint 23, x_1 Fourier transform, modulus (pulse 3) 0.1% damping E-107

E-108. Joint 23, x_1 Fourier transform, phase angle (pulse 3) 0.1% damping E-108

E-109. Joint 23, x_1 time history (pulse 3) 0.5% damping E-109

E-110. Joint 23, x_1 Fourier transform, modulus (pulse 3) 0.5% damping E-110

E-111. Joint 23, x_1 Fourier transform, phase angle (pulse 3) 0.5% damping E-111

E-112. Joint 23, x_1 time history (pulse 3) 1% damping E-112

E-113. Joint 23, x_1 Fourier transform, modulus (pulse 3) 1% damping E-113

E-114. Joint 23, x_1 Fourier transform, phase angle (pulse 3) 1% damping E-114

E-115. Joint 23, x_1 time history (pulse 3) 2% damping E-115

E-116. Joint 23, x_1 Fourier transform, modulus (pulse 3) 2% damping E-116

E-117. Joint 23, x_1 Fourier transform, phase angle (pulse 3) 2% damping E-117

E-118. Joint 23, x_1 time history (pulse 3) 4% damping E-118

E-119. Joint 23, x_1 Fourier transform, modulus (pulse 3) 4% damping E-119

E-120. Joint 23, x_1 Fourier transform, phase angle (pulse 3) 4% damping E-120

E-121. Joint 23, x_1 time history (pulse 3) 10% damping E-121

CONTENTS (contd)

FIGURES (contd)

E-122. Joint 23, x_1 Fourier transform, modulus (pulse 3) 10% damping E-122

E-123. Joint 23, x_1 Fourier transform, phase angle (pulse 3) 10% damping E-123

E-124. Joint 23, x_1 time history (pulse 3) 50% damping E-124

E-125. Joint 23, x_1 Fourier transform, modulus (pulse 3) 50% damping E-125

E-126. Joint 23, x_1 Fourier transform, phase angle (pulse 3) 50% damping E-126

E-127. Variations of peak acceleration with Atlas/Agena/OGO modal damping E-127

OGO-E SPACE VEHICLE RESPONSE TO TRANSIENT LOADING AT ATLAS BOOSTER ENGINE CUTOFF

I. INTRODUCTION

The analyses described herein were undertaken in response to a request[1] made by the NASA Goddard Space Flight Center (GSFC). They have utilized analysis concepts and computer programs developed by the Applied Mechanics Section of JPL for treating various classes of problems in the field of structural dynamics. The specific problem dealt with in this document is the prediction of the Orbiting Geophysical Observatory (OGO-E) spacecraft structural response to be expected during Atlas booster engine cut-off (BECO).

II. NORMAL MODE ANALYSIS

A. Input Data

Input data for the normal mode analysis were obtained from two sources: 1) the OGO-E spacecraft model was supplied to JPL by the TRW Systems Group, Redondo Beach, California, as authorized by GSFC; 2) the model for the launch vehicle system, consisting of GD/C SLV-3A Atlas data and LMSC Agena data, including the nose fairing, was supplied by NASA Lewis Research Center (LeRC), Cleveland, Ohio.

1. The OGO-E spacecraft. The OGO-E spacecraft structural model as used in this analysis is described in Refs. 1 and 2. Frequencies and modal deflections for one quadrant of the OGO-E spacecraft, including the interstage adapter structure, were obtained by TRW Systems using the Stiffness Matrix Structural Analysis Program described in Ref. 3.

[1] GSFC letter, File No. 16113, dated Feb. 6, 1968 to Dr. W.H. Pickering, Director, JPL from John F. Clark, Director, GSFC; Subj: Torsional Mode Analysis of the OGO-E Combined Launch Vehicle.

The TRW Systems model assumes the OGO-E spacecraft structure to have symmetry about two orthogonal planes intersecting at the longitudinal axis of the launch vehicle system.

The data obtained by JPL from TRW was in the following form: 1) input data cards for the computer program, Ref. 3, defining the mass properties for each joint of the lumped mass model, the joint coordinates, member properties and stiffness matrix elements, 2) output cards defining the modal deflections for the first 18 elastic modes of the structure cantilevered at the bottom of the interstage adapter structure, and 3) computer printout containing the 18 frequencies corresponding to the 18 normal modes of 2) above.

2. The Atlas/Agena launch vehicle. The data describing the Atlas/Agena launch vehicle, including the nose fairing, were transmitted to JPL via Ref. 4. Two enclosures were contained in Ref. 4: the GD/C Atlas SLV-3A model description, Ref. 5, and the Agena and nose fairing description, Refs. 6 and 7.

The launch vehicle model description consists of a lumped parameter representation of the Atlas/Agena vehicle including the nose fairing. As requested by the Lewis Research Center (LeRC) in Ref. 4, the Agena model described by GD/C in Ref. 5 was updated using LMSC data of Ref. 6. The magnesium door data was used in the Agena model.

Clarification of the Atlas/Agena interface area was provided by LeRC verbally. The model is defined in Fig. 1.

In addition, LeRC informed JPL that the model, as described in Ref. 4, accounts for an OGO-E spacecraft inertia of 91 slug-ft^2 at Joint 7.

B. Data Processing

1. The OGO-E spacecraft. The cantilever normal modes of the OGO-E spacecraft obtained from TRW Systems were converted to equivalent single-degree-of-freedom systems by the same technique used for the Ranger and Surveyor spacecrafts, Ref. 8. The general method used is described in Appendix A and Ref. 9.

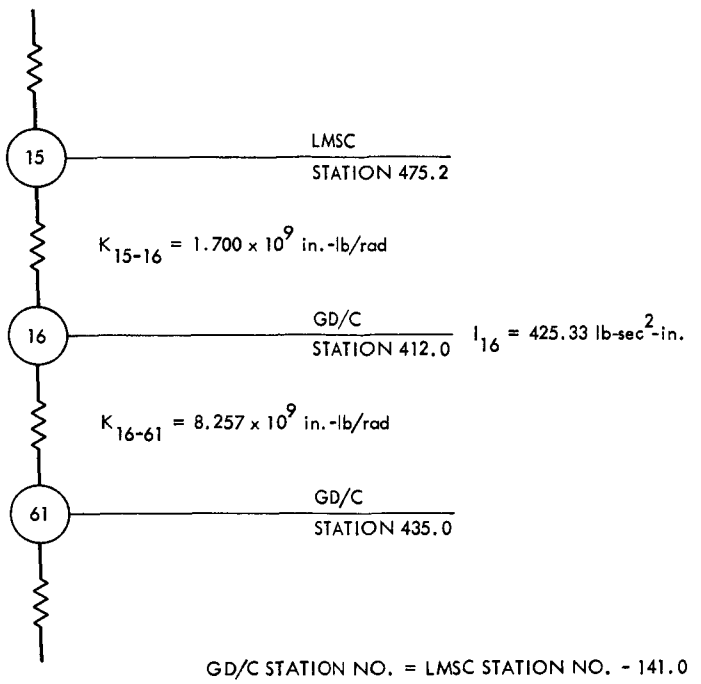

Fig. 1. Mathematical model of the Atlas/Agena interface

The conversion from cantilever normal modes to single-degree-of-freedom systems requires the calculation of the rigid-elastic coupling terms for the cantilever structure. This was accomplished by dividing the OGO-E spacecraft structure into two parts, shifting the origin of the coordinate axes, and then calculating the rigid-elastic coupling terms for each of these parts within the Modal Combination Program, Ref. 10.

The elastic-elastic and rigid-elastic description of the whole OGO-E spacecraft structure was obtained by first adding the respective terms of the two subsystems and then multiplying the result by four. The multiplication by four converts the spacecraft model for one quadrant to the complete spacecraft.

The generalized mass matrix for the OGO-E spacecraft is of the following form:

$$\left[M \right] = \begin{bmatrix} M_{RR} & M_{RE} \\ M_{ER} & M_{EE} \end{bmatrix} \tag{1}$$

Since the rigid-elastic coupling terms have been computed only for a rotation about the vehicle longitudinal axis, the M_{RE} matrix is a row matrix having 18 columns representing the 18 normal modes. The elements of the M_{RE} and M_{EE} matrices are given in Appendix A.

The normal modes are renormalized such that

$$(m^*_{re})_j = (m^*_{ee})_j \tag{2}$$

for the jth normal mode.

Using renormalization factors

$$\mu_j = \left(\frac{m_{re}}{m_{ee}}\right)_j \tag{3}$$

results in a new mass matrix for the spacecraft

$$\left[M^*\right] = \begin{bmatrix} M_{RR} & M^*_{RE} \\ M^*_{ER} & M^*_{EE} \end{bmatrix} \tag{4}$$

Using the above matrix, 18 single-degree-of-freedom systems have been obtained. Thus, the spacecraft is described by Joints 26 through 43 and the associated spring constants connecting each of these joints to Joint 7 on the main vehicle, as shown in Appendix B.

In the discussion to follow the jth inertia term, I_j, represents the effective mass of the jth cantilever normal mode. Hence, for the spacecraft model the subscript j is common to mass point and normal mode. The method of conversion from normal modes to equivalent lumped parameters is described in Appendix A.

In deriving the connecting spring constants the analytically obtained modal frequencies were adjusted by a factor of 0.915 as justified in Ref. 2. While Ref. 2 applies this factor only to the dominant torsion mode, TRW Systems instructed JPL verbally to use this factor on all the normal modes considered.

2. The Atlas/Agena launch vehicle. The Atlas/Agena launch vehicle used in this analysis was described in 2. of Section II. The inertia at Joint 7 had to be modified to be compatible with the treatment of the spacecraft model.

First, the spacecraft inertia, as used by LMSC, 91 slug-ft^2, was removed from Joint 7. Then, the additional inertia of 3.4 slug-ft^2 was added to the inertia at Joint 7 in order to preserve the proper rigid-body representation consistent with the 18 normal modes used. (Ref. Eq. A-13, Appendix A.)

3. The composite vehicle. All pertinent data of the composite vehicle are given in Appendix C. In the processing of the composite vehicle data to obtain normal modes, the vehicle was first divided into two parts at GD/C Station 577.195. The cantilevered normal modes of each part of the vehicle were obtained using the Stiffness Matrix Structural Analysis Program, Ref. 3.

The two parts of the composite vehicle were then combined to obtain the overall vehicle normal modes using the Modal Combination Program, Ref. 10.

C. Free-Free Torsional Modes

Appendix D contains plots of the first 22 free-free normal modes of the composite vehicle as well as other pertinent modal data in tabular form. Spacecraft deflections shown at GD/C Station 95.0 are actually the participation factors of the spacecraft centilever modes as finally normalized.

Modal deflections for joints within the OGO-E spacecraft were obtained as required for the response analysis requested by TRW Systems in Ref. 11.

In obtaining the modal deflections for joints within the OGO-E spacecraft, the original TRW modal data had to be renormalized by the factor $-\mu_j$. The negative sign is required to make the TRW analysis coordinate axes convention compatible with the JPL composite vehicle analysis axes.

Thus,

$$\Phi_{1n}^{k} = -\sum_{j=1}^{18} \mu_j \, \Phi_{oj}^{k} \, U_{jn} \tag{5}$$

where

Φ_{1n}^{k} = modal deflection of kth point in the OGO-E spacecraft in the nth overall launch vehicle free-free mode.

μ_j = renormalization factor for the jth mode, from Eq. (3).

Φ_{oj}^{k} = modal deflection of the kth point in the OGO-E spacecraft in the jth cantilever mode in original TRW coordinate axes.

U_{jn} = the nth mode shape at point j in the overall launch vehicle free-free mode.

Values of Φ_{in}^{k} are listed in Appendix D for the five points for which response time histories have been requested by TRW Systems.

Rotational acceleration and torque at OGO Station 400 were requested by TRW Systems in Ref. 11. Since no spacecraft mass point was provided at that station, it was verbally agreed with TRW Systems to supply the acceleration and torque at Joint 7, GD/C Station 106.1.

The computation of the torque at Joint 7, as described in Section III, requires the evaluation of the following quantity:

$$I_n^* = \sum_{j=1}^{18} (m_{re}^*)_j \, U_{jn} = \sum_{j=1}^{18} I_j \, U_{jn} \tag{6}$$

where

I_n^* = modal quantity used to compute torque response

$(m_{re}^*)_j$ = the mass, in this case inertia, representing the jth OGO cantilever mode from Eqs. (3) and (4)

I_j = same as $(m_{re}^*)_j$

U_{jn} = the nth mode shape at point j in the overall launch vehicle free-free mode.

Values of I_n^* are listed in Appendix D.

III. RESPONSE ANALYSES

A. Method

The method used to compute the response of the spacecraft at booster engine cut-off (BECO) is indicated in the JPL Technical Memorandum 33-350 (Ref. 12) modified to accommodate certain types of responses.

Three types of responses were required:

1) Angular acceleration of the spacecraft base (Station 106.1) and at two points of the spacecraft (Joint 1, x_5 and Joint 5, x_5).
2) Linear acceleration at 3 points of the spacecraft (Joint 1, x_1, Joint 23, x_1, and Joint 23, x_3).
3) Torque at the spacecraft base (Station 106.1).

Item 1 is readily computed by the digital program of Ref. 12, for which Φ_{1n} is identical to Φ_{1n}^k of Eq (5).

Item 2 can also be computed by the same program if one notes that the mode shapes Φ_{1n} (n = 0, 1, 2, ... N) of Ref. 12 corresponding to the points on the spacecraft must be linear mode shapes rather than angular mode shapes. Particularly, it must be noted that the rigid body linear mode shape Φ_{10} is no longer unity if the gimbal block angular rigid body mode shape Φ_{20} is normalized to unity. Finally, the response $u_2(t)$ (Eq. 18 of Ref. 12) is a linear acceleration (in./sec^2) instead of an angular acceleration (rad/sec^2), again Φ_{1n} is identical to Φ_{1n}^k.

Item 3 requires a slight modification in the interpretation of Eq. 8 of Ref. 12 in order to use the same program as indicated below.

Torque computation. The torque $T_B = T_B(t)$ at the spacecraft base is the sum of the inertia torques due to the elements of inertia I_j (j = 1, 2, ... M), of each mass point j of the spacecraft model (cantilever normal mode of spacecraft) about the longitudinal axis above the spacecraft base (Fig. 2).

The inertia torque due to each inertia I_j is:

$$T_j = I_j \ddot{\theta}_j = I_j \sum_{n=o}^{N} U_{jn} \ddot{q}_n \tag{7}$$

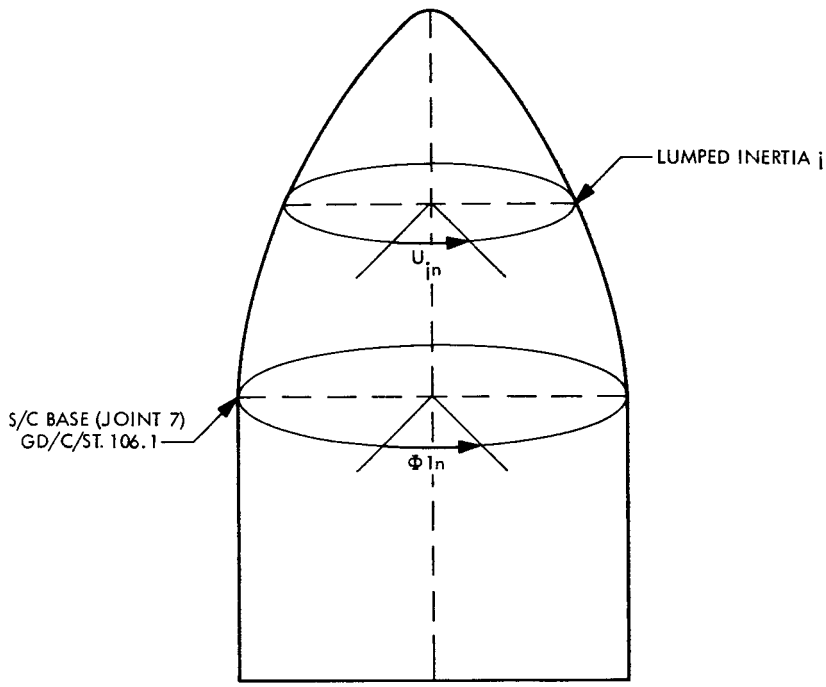

Fig. 2. Ideal representation of structure for spacecraft base torque determination

where

$\ddot{\theta}_j$ = the angular rotation at mass point j

U_{jn} = the nth mode shape at mass point j in the overall vehicle free-free modes

$\ddot{q}_n$ = the nth generalized coordinate

The total torque at the spacecraft base is the summation of T_j on all mass points j of the spacecraft.

$$T_B = \sum_{j=1}^{M} I_j \sum_{n=o}^{N} U_{jn} \ddot{q}_n \tag{8}$$

$$T_B = \sum_{n=0}^{N} \left(\sum_{j=1}^{M} I_j \; U_{jn} \right) \ddot{q}_n \tag{9}$$

Let

$$\sum_{j=1}^{M} I_j \, U_{jn} = I_n^* \qquad (M=18) \tag{10}$$

then the torque at the spacecraft base is

$$T_B = \sum_{n=o}^{N} \ddot{q}_n \, I_n^* \tag{11}$$

Taking the Fourier transform of T_B and using Eq. (5) of Ref. 12 we finally obtain:

$$F_B(\omega) = F(\omega) \sum_{n=o}^{N} \frac{\Phi_{2n} \, I^*}{m_n} \cdot \frac{1}{1 - \left(\frac{\omega_n}{\omega}\right)^2 - 2i \, \xi_n \frac{\omega_n}{\omega}} \tag{12}$$

This is the same as Eq. (8) of Ref. 12 if we replace

$$\Phi_{1n} \quad \text{by} \quad I_n^*$$

$$V_1(\omega) \text{ by } F_B(\omega)$$

The column of I_n^* used in the computation of the torque is indicated in Appendix D.

B. Input Data

The input data were the flight data obtained during the Ranger flight, Ranger VI through IX, at booster engine cut-off (BECO), as determined in Ref. 13. In Appendix E, Figs. E-1 through E-12 show the time histories of the four transients and their Fourier transforms.

C. Normal Modes

In addition to the rigid-body mode, the first 19 elastic free-free normal modes covering a frequency range from 4.93 to 82.99 cps were retained to represent the Atlas/Agena/OGO vehicle. (See Appendix D.)

As previously done, 9 modes were retained for the Atlas/Agena/Ranger vehicle as shown in Table B-1 of Ref. 13.

D. Damping

A modal damping of 3% critical $\left(\xi = \frac{C}{C_c}\right)$ was used for all modes of the Atlas/Agena/Ranger vehicle in accordance with previous calculations (Refs. 12 and 13). A modal damping of 3% was also used for most of the calculations pertaining to the Atlas/Agena/OGO vehicle. However, modal dampings ranging from 0.1% to 50% were also used for joint 23, X_1 responses to show the influence of the damping. (See Table 3.) Modal dampings of 1, 2, 3, and 4% were also used for joint 1, x_1.

E. Responses

The time histories of the responses were computed together with their Fourier transforms. Peak responses were noted and are indicated in Tables 1 through 3. Time histories and Fourier transforms are shown in Appendix E, Figs. E-13 through E-126.

Finally, it must be noted that since the amount of energy contained in each pulse is limited, the peak response tends to level out for small damping ξ as shown in Fig. E-127 in Appendix E.

Table 1. Acceleration responses for 3% modal damping (RA-6, 7, 8, 9 data input)

Location	Excitation	Peak acceleration	
Base of S/C Accel. (Joint 7)	Pulse 1	20.4 rad/sec^2	
	Pulse 2	21.2 rad/sec^2	
	Pulse 3	24.2 rad/sec^2	
	Pulse 4	21.3 rad/sec^2	
Joint 1, x_1	Pulse 1	151.6 in./sec^2	0.393g
	Pulse 2	192.3 in./sec^2	0.498g
	Pulse 3	192.9 in./sec^2	0.500g
	Pulse 4	187.8 in./sec^2	0.486g
Joint 1, x_5	Pulse 1	70.8 rad/sec^2	
	Pulse 2	75.6 rad/sec^2	
	Pulse 3	121.4 rad/sec^2	
	Pulse 4	75.3 rad/sec^2	
Joint 5, x_5	Pulse 1	30.7 rad/sec^2	
	Pulse 2	52.4 rad/sec^2	
	Pulse 3	76.0 rad/sec^2	
	Pulse 4	41.2 rad/sec^2	
Joint 23, x_1	Pulse 1	759.0 in./sec^2	1.97g
	Pulse 2	1158.0 in./sec^2	3.0g
	Pulse 3	1520.0 in./sec^2	3.94g
	Pulse 4	1106.0 in./sec^2	2.86g
Joint 23, x_3	Pulse 1	592.0 in./sec^2	1.53g
	Pulse 2	1000.0 in./sec^2	2.59g
	Pulse 3	1446.0 in./sec^2	3.74g
	Pulse 4	890.0 in./sec^2	2.30g

Table 2. Torque

Location	Excitation	Peak torque
Base of S/C torque	Pulse 1	22690 lb-in.
	Pulse 2	37989 lb-in.
	Pulse 3	50018 lb-in.
(Joint 7)	Pulse 4	29574 lb-in.

Table 3. Effect of modal damping of Atlas/Agena/OGO space vehicle - pulse 3 excitation

Location	Modal damping	Peak acceleration	
Joint 1, x_1	1%	281.3 in./sec^2	0.728g
	2%	215.3 in./sec^2	0.558g
	3%	192.9 in./sec^2	0.500g
	4%	171.4 in./sec^2	0.444g
Joint 23, x_1	0.1%	2638.0 in./sec^2	6.83g
	0.5%	2415.0 in./sec^2	6.25g
	1%	2215.0 in./sec^2	5.74g
	2%	1830.0 in./sec^2	4.74g
	3%	1520.0 in./sec^2	3.94g
	4%	1307.0 in./sec^2	3.34g
	10%	721.0 in./sec^2	1.87g
	50%	45.0 in./sec^2	0.11g

REFERENCES

1. TRW Systems Interoffice Correspondence No. 67-3343.2-119 to John Kugler from A. R. Von Waldburg and T. K. Hasselman, "OGO Modal Computations," dated 7/31/67.

2. TRW Systems Interoffice Correspondence No. 67-3343.2-129 to John Kugler from T. K. Hasselman, "Preliminary OGO Modal Computations, Torsional Modes," dated 8/29/67.

3. Wada, B. K.; "Stiffness Matrix Structural Analysis." JPL Technical Report 32-774, dated 31 October 1965.

4. Correspondence to W. E. Scull, NASA-GSFC from H. W. Plohr, NASA-LeRC, "SLV-3A Torsional Model and Vibration Analysis," Reference 9440:JCG, dated 1/9/68.

5. GD/C Interoffice Correspondence No. SD-67-087-LVP to L. F. Buss from J. G. Greene, "SLV-3A Torsional Modes," dated 5/9/67.

6. LMSC Report SS/1167/5522, LMSC/A839166, "Torsional Dynamic Model ATS-B/SS-01B," dated 4 November 1966, page 9, Figure 1.

7. LMSC Report SS/1202/5522, LMSC/A876600, dated 3 May 1967, pages 36 and 37, Figs. 1a and 1b.

8. Garba, J. A.; Gayman, W. H.; and Wada, B. K.; "Computation of Torsional Vibration Modes of Ranger and Surveyor Space Vehicles." JPL Technical Memorandum 33-277, 1 April 1968.

9. Bamford, R. M.; and Wada, B. K.; "Equivalent Spring-Mass System for Normal Modes." JPL Technical Memorandum 33-380 (to be published).

10. Bamford, R. M.; "A Modal Combination Program for Dynamic Analysis of Structures." JPL Technical Memorandum 33-290, 15 August 1966.

11. TRW Systems Interoffice Correspondence No. 67-3343.2-212 to J. Kugler from T. K. Hasselman, "OGO Torsional Vibration," dated 12/29/67.

12. Trubert, M. R.; "A Fourier Transform Technique for the Prediction of Torsional Transients for a Spacecraft from Flight Data of Another Spacecraft Using the Same Booster." JPL Technical Memorandum 33-350, 15 October 1967.

13. Trubert M. R.; "Use of Ranger Flight Data in the Synthesis of a Torsional Acceleration Transient for Surveyor Vibration Qualification Testing." JPL Technical Memorandum 33-237, 19 April 1966.

14. Timoshenko, S.; Vibration Problems in Engineering; D. Van Nostrand Co., Inc.; New York, New York; 1955; pp 297-300.

APPENDIX A

CONVERSION FROM NORMAL-MODE COORDINATES OF A CANTILEVER STRUCTURE TO AN EQUIVALENT LUMPED-PARAMETER SYSTEM

APPENDIX A

CONVERSION FROM NORMAL-MODE COORDINATES OF A CANTILEVER STRUCTURE TO AN EQUIVALENT LUMPED-PARAMETER SYSTEM

In the absence of the availability of Ref. 9, it is intended that this appendix convey the physical and mathematical concepts of converting the cantilever normal-mode data computed for the OGO-E spacecraft into an equivalent lumped-parameter system compatible with the launch vehicle representation.

The concepts are most easily introduced by first considering the axial cantilever modes of a uniform bar of length, ℓ, and mass-per-unit length, μ. From Ref. 14 it can be shown, using Timoshenko's notation, that the circular frequency of the ith mode is given by

$$p_i = \frac{\pi}{2}\left(\frac{a}{\ell}\right)i \qquad i = 1, 3, 5 \ldots \tag{A-1}$$

where

$$a = \left(\frac{E}{\mu}\right)^{1/2}$$

and the modal amplitude a distance, x, from the root is

$$X_i = D_i \sin\left(\frac{i\pi x}{2\ell}\right) \qquad i = 1, 3, 5 \ldots \tag{A-2}$$

where D_i is, in general, an arbitrary normalization factor. However, here it will be shown that, for each mode, a relationship can be established for D_i giving an equivalence between the continuous system and a simple oscillator.

The generalized mass of the ith mode is

$$M_{ii} = \int_0^{\ell} X_i^2 \mu \, dx$$

$$= \frac{\mu\ell}{2} D_i^2 \tag{A-3}$$

The axial load at the root of the bar is

$$P_i = p_i^2 M_{ri}$$

where M_{ri} is the inertial coupling between the ith cantilever mode and a rigid-body axial translation, $X_r = 1$, i.e.,

$$M_{ri} = \int_0^{\ell} X_r X_i \, \mu \, dx$$

$$= \frac{2\mu\ell}{i\pi} D_i \qquad i = 1, 3, 5, \ldots \tag{A-4}$$

With a simple oscillator (Fig. A-1), the generalized mass is m, and the inertia force, $-m\ddot{x}$, is the axial force applied at the base.

The continuous system may be converted to an equivalent simple oscillator by modal renormalizations that equate M_{ii} and M_{ri} for all applicable values of i. Thus, from Eqs. (A-3) and (A-4),

$$D_i = \frac{4}{i\pi} \tag{A-5}$$

Substituting this expression in Eq. (A-2), and performing the integrations indicated in Eqs. (A-3) and (A-4) gives

$$M_{ii} = M_{ri} = \frac{8\mu\ell}{i^2\pi^2} \tag{A-6}$$

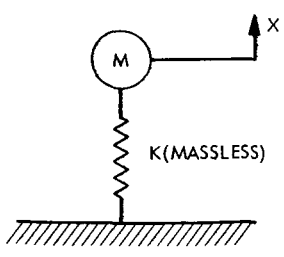

Figure A-1. Oscillator

The continuous system has an infinite number of modes, each of which may be represented by a simple oscillator with a point mass defined by Eq. (A-6). It is pertinent to note that

$$\sum_{i=1}^{\infty} M_{ii} = \frac{8\mu\ell}{\pi 2} \sum_{i=1}^{\infty} \frac{1}{(2i-1)^2} \qquad i = 1, 2, 3, \ldots$$

$$= \mu\ell$$

$$= M_{rr}$$

the "rigid-rigid" term in the generalized mass matrix, i.e.,

$$\int_0^{\ell} X_r^2 \mu dx$$

$$[M] = \begin{bmatrix} M_{rr} & M_{re} \\ M_{er} & M_{ee} \end{bmatrix} \tag{A-7}$$

wherein M_{ee} is the diagonal matrix of which M_{ii} is an element.

With respect to the OGO-E spacecraft, the initial mass matrix, $\overline{M}_{ee}$, is the diagonal matrix applying to modal normalizations giving unit displacement at the point of maximum amplitude in each mode. The ith element of this matrix is of the form

$$\overline{M}_{ii} = \sum_{k=1}^{k=n} \vec{\phi}_{ik} \cdot \vec{\phi}_{ik}\, m_k \tag{A-8}$$

wherein the dot product is meant to signify that all six components of motion (i.e., three translations and three rotations) are appropriately treated with the applicable m_k to account, in effect, for all of the kinetic energy in the mode.

The inertial coupling between the ith elastic mode and a rigid-body rotation of 1 rad. about the roll axis is of the form

$$\overline{M}_{ri} = \sum_{k=1}^{k=n} \phi_{ik} m_k \tag{A-9}$$

wherein ϕ_{ik} is meant as only that component of the total motion of m_k that has the sense of torsion.

If, now, the ith elastic mode is to be renormalized by a factor, D_i, the new mass matrix elements are

$$M_{ii} = D_i^2 \overline{M}_{ii} \tag{A-10}$$

$$M_{ri} = D_i \overline{M}_{ri} \tag{A-11}$$

Equating M_{ii} and M_{ri} gives

$$D_i = \frac{\overline{M}_{ri}}{\overline{M}_{ii}} \tag{A-12}$$

Since only a certain number, N, of cantilever modes need be used in an engineering analysis, an incremental rigid mass,

$$\Delta M_{rr} = M_{rr} - \sum_{i=1}^{i=N} M_{ii} \tag{A-13}$$

must be added at the "ground plane" of the system of n independent simple oscillators as shown in Fig. A-2.

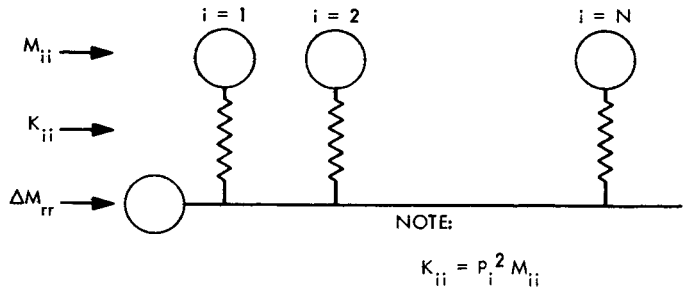

Fig. A-2. Mathematical model of the OGO-E spacecraft

APPENDIX B

THE OGO-E GENERALIZED MASS MATRIX

FOLDOUT FRAME

FOLDOUT FRAME

APPENDIX B

THE OGO-E GENERALIZED MASS MATRIX

The elements of the OGO-E spacecraft mass matrix are as follows:

j	1	2	3	4	5	6	7	8	9	10	11	12	13	14	15	16	17	18
$(m_{re})_j$	0.9411	1.1177	-1.2044	-0.0411	-1.7212	1.0042	-2.1900	-1.4431	3.1042	10.5132	-0.1216	-0.4456	-0.3315	-0.0293	0.0996	-0.0548	0.0232	0.0084
$(m_{ee})_j$	0.0472	0.0436	0.2018	0.0152	0.0587	0.0545	0.0688	0.0454	0.0593	0.2360	0.0104	0.0753	0.0881	0.0487	0.0471	0.1089	0.0165	0.0286
μ_j	19.93	25.63	-5.97	-2.70	-29.30	18.43	-31.83	-31.77	52.36	44.55	-11.71	-5.92	-3.76	-0.60	2.11	-0.50	1.40	0.29
$(m^*_{re})_j$	18.756	28.647	7.190	0.111	50.431	18.507	69.708	45.847	162.536	468.360	1.424	2.638	1.246	0.017	0.210	0.027	0.032	0.002

NOTE

$m_{rr} = 916.8$

The units of m_{rr}, m_{ee}, and m_{re} are lb-in.-sec^2

$(m^*_{re})_j = (m^*_{ee})_j = \mu_j (m_{re})_j$

APPENDIX C

NUMERICAL VALUES FOR THE ATLAS/AGENA/OGO-E MATHEMATICAL MODEL

ATLAS/AGENA/OGO TORSION MODEL INPUT DATA

JOINT COORDINATES

JOINT	GD/C STATION, INCHES
1	-99.9
2	-59.9
3	-22.1
4	19.3
5	59.3
6	95.6
7	106.1
8	118.9
9	137.1
10	163.7
11	194.0
12	225.1
13	263.8
14	304.9
15	334.2
16	412.0
17	301.0
61	435.0
62	455.0
63	475.0
64	495.0
65	515.1
66	528.65
67	547.13
68	577.195
69	607.265
70	636.855
71	665.965
72	695.075
73	724.185
74	753.295
75	782.405
76	811.515
77	840.625
78	869.73
79	899.84
80	927.67
81	951.34
82	977.57
83	1008.75
84	1041.25
85	1073.75
86	1106.25
87	1127.75
45	1133.0
46	1160.0
47	1176.0
48	1198.0
49	1210.0
50	1212.0
51	1158.0
52	1182.0
53	1212.0
54	1235.0
55	1212.0
56	1242.0

SPACECRAFT REPRESENTATION

26	95.0
27	95.0
28	95.0
29	95.0
30	95.0
31	95.0
32	95.0
33	95.0
34	95.0
35	95.0
36	95.0
37	95.0
38	95.0
39	95.0
40	95.0
41	95.0
42	95.0
43	95.0

JOINT INERTIAS

JOINT	INERTIA,POUND INCHES SQUARED
1	.56824 E5
2	.81167 E5
3	.81631 E5
4	.90626 E5
5	.90966 E5
6	.14131 E6
7	.91291 E5
8	.22128 E6
9	.10289 E6
10	.81642 E5
11	.58400 E5
12	.62987 E5
13	.19669 E6
14	.84336 E5
15	.10275 E6
16	.16435 E6
17	.22029 E5
61	.88810 E5
62	.81619 E5
63	.10526 E6
64	.13364 E6
65	.16751 E6
66	.11554 E6
67	.19852 E6
68	.19859 E6
69	.19859 E6
70	.19225 E6
71	.19225 E6
72	.19225 E6
73	.28925 E6
74	.36954 E6
75	.21486 E6
76	.23748 E6
77	.33434 E6
78	.43350 E6

79	.77792	E6
80	.84974	E6
81	.76633	E6
82	.13688	E7
83	.16217	E7
84	.15170	E7
85	.12906	E7
86	.86234	E6
87	.12835	E7
45	.40652	E6
46	.52767	E6
47	.47759	E6
48	.30278	E6
49	.23555	E6
50	.51422	E6
51	.15093	E7
52	.42825	E7
53	.63826	E7
54	.57388	E7
55	.10000	E2
56	.66051	E7

SPACECRAFT REPRESENTATION

26	.72489	E4
27	.11068	E5
28	.23537	E4
29	.42846	E2
30	.19484	E5
31	.71523	E4
32	.26935	E5
33	.17715	E5
34	.62807	E5
35	.18100	E6
36	.55052	E3
37	.10192	E4
38	.48200	E3
39	.67983	E1
40	.81376	E2
41	.10652	E2
42	.12562	E2
43	.96256	E0

SPRING CONSTANTS

JOINT A	JOINT B	K, IN-LB/RADIAN	
1	2	.21500	E09
2	3	.94400	E09
3	4	.81000	E09
4	5	.96500	E09
5	6	.13360	E10
6	7	.53300	E10
7	8	.43700	E10
8	9	.38000	E10
9	10	.28830	E10
10	11	.13240	E10
11	12	.14930	E10
12	13	.15450	E10
13	14	.14000	E10
13	17	.20000	E09
14	15	.19590	E10
15	16	.17000	E10
16	61	.82570	E10
61	62	.82190	E10
62	63	.75660	E10
63	64	.97940	E10
64	65	.12480	E11
65	66	.15360	E11
66	67	.68460	E11
67	68	.79200	E10
68	69	.79200	E10
69	70	.79200	E10
70	71	.81800	E10
71	72	.81800	E10
72	73	.81800	E10
73	74	.81800	E10
74	75	.81800	E10
75	76	.92400	E10
76	77	.10200	E11
77	78	.11140	E11
78	79	.11770	E11
79	80	.10690	E11
80	81	.17080	E11
81	82	.18690	E11
82	83	.14150	E11
83	84	.13000	E11
84	85	.13470	E11
85	86	.13830	E11
86	87	.14300	E11
87	45	.97060	E11
45	46	.11100	E11
46	47	.13116	E11
47	48	.12720	E10
48	49	.20880	E09
49	50	.20880	E09
45	51	.34320	E11
51	52	.36600	E11
52	53	.29940	E11
53	54	.39180	E11
53	55	.10440	E09
55	56	.10000	E12

SPACECRAFT REPRESENTATION

7	26	.17990	E05
7	27	.97930	E05
7	28	.33070	E05
7	29	.10710	E04
7	30	.73290	E06
7	31	.34870	E06
7	32	.17430	E07
7	33	.21340	E07
7	34	.11280	E08
7	35	.34950	E08
7	36	.13090	E06
7	37	.36010	E06
7	38	.22410	E06
7	39	.47790	E04
7	40	.78570	E05
7	41	.10450	E05
7	42	.14830	E05
7	43	.13280	E04

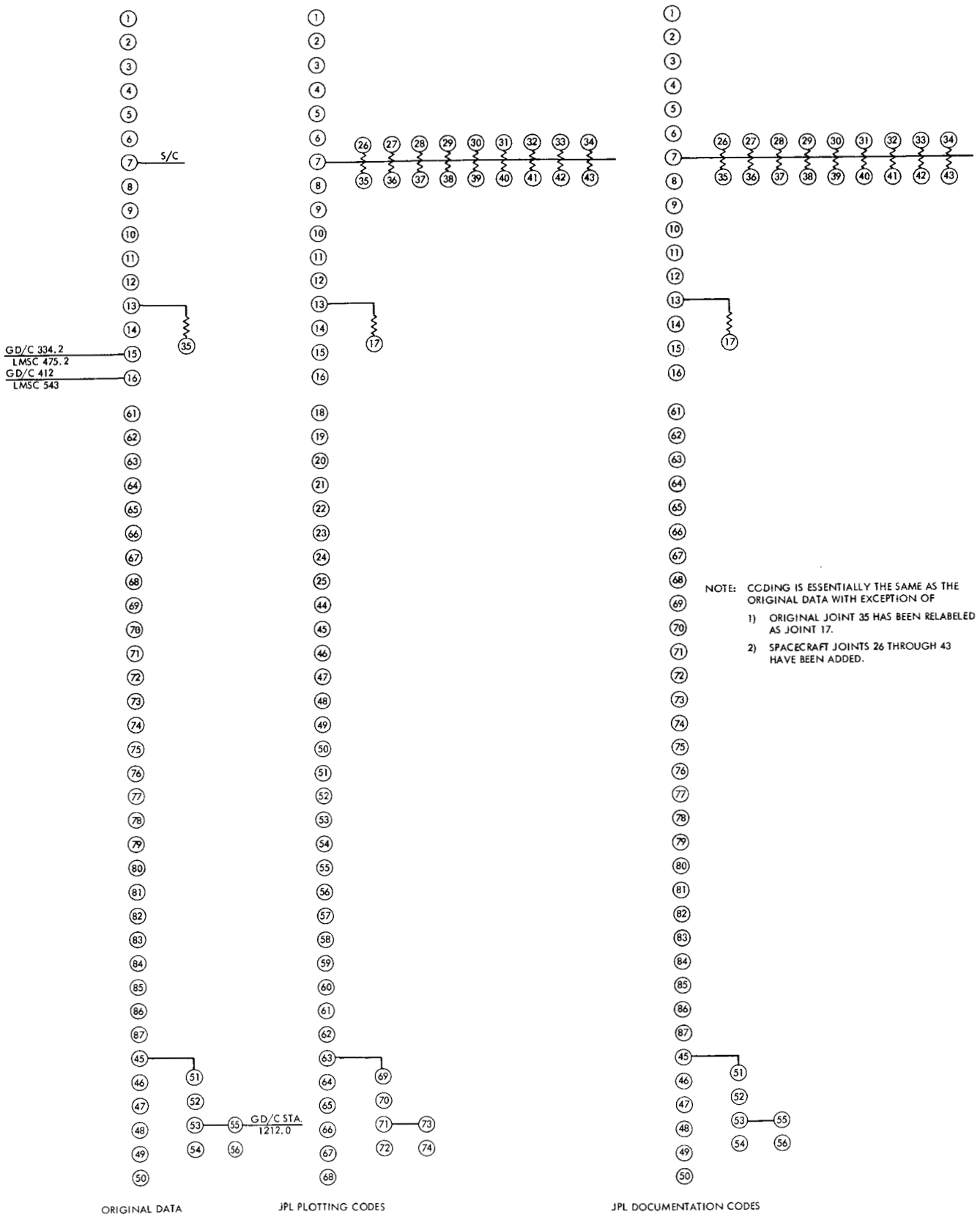

Fig. C-1. Mathematical model of the Atlas/Agena OGO-E space vehicle

APPENDIX D

FREE-FREE TORSIONAL MODES FOR THE OGO-E SPACE VEHICLE

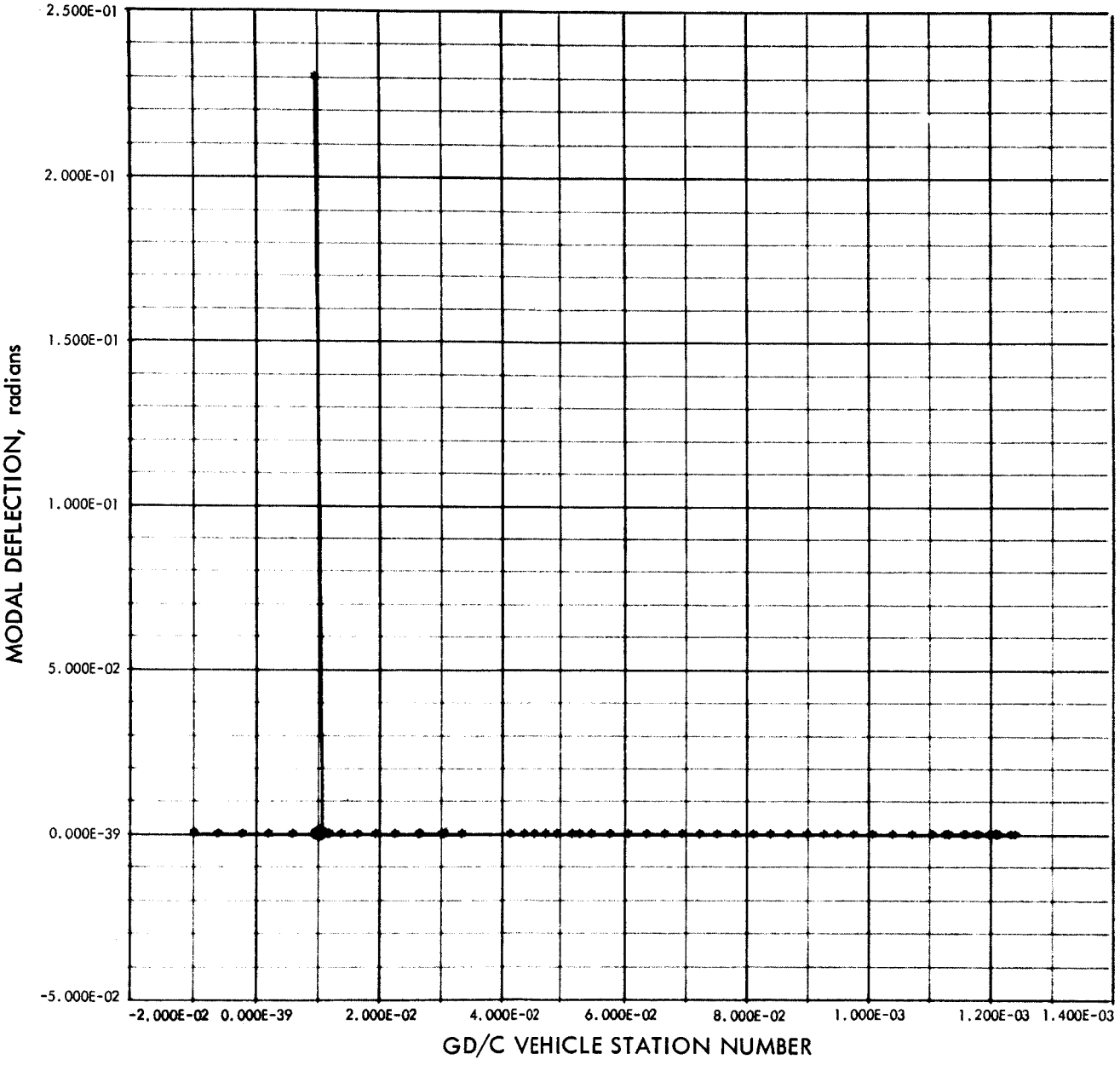

Fig. D-1. Atlas/Agena/OGO torsion mode shape (mode 1) F = 4.93 Hz

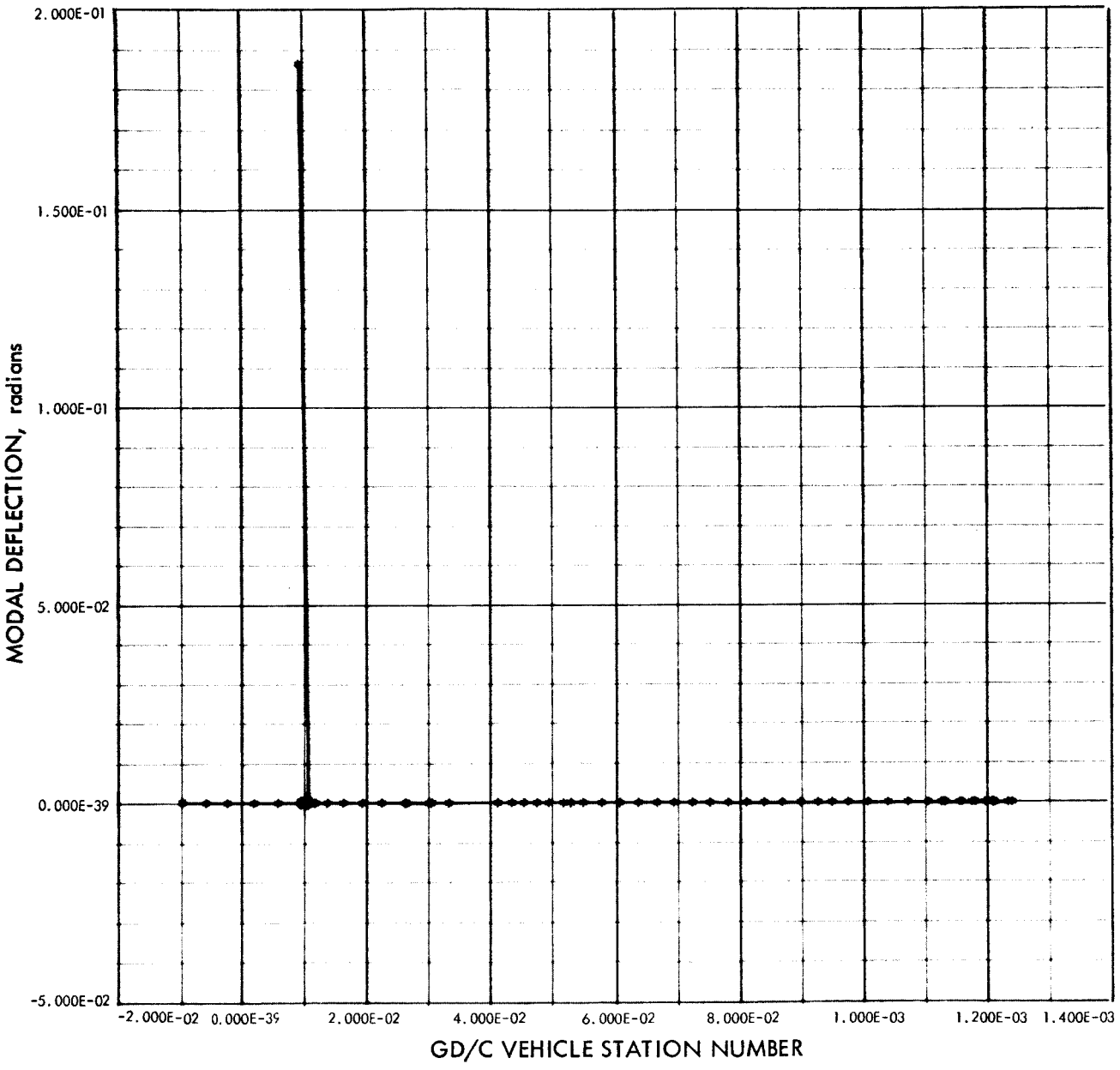

Fig. D-2. Atlas/Agena/OGO torsion mode shape (mode 2) F = 9.30 Hz

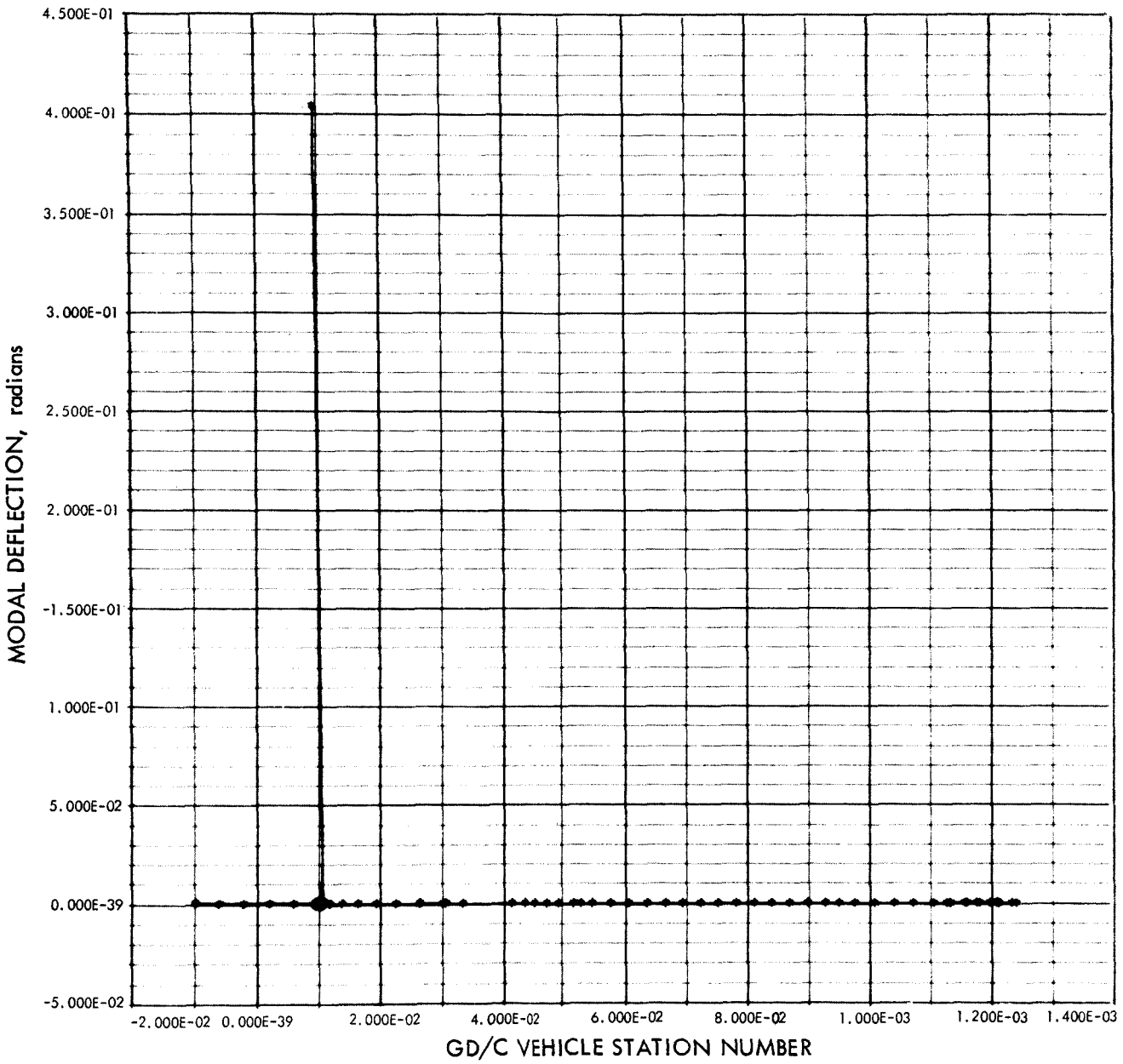

Fig. D-3. Atlas/Agena/OGO torsion mode shape (mode 3) F = 11.74 Hz

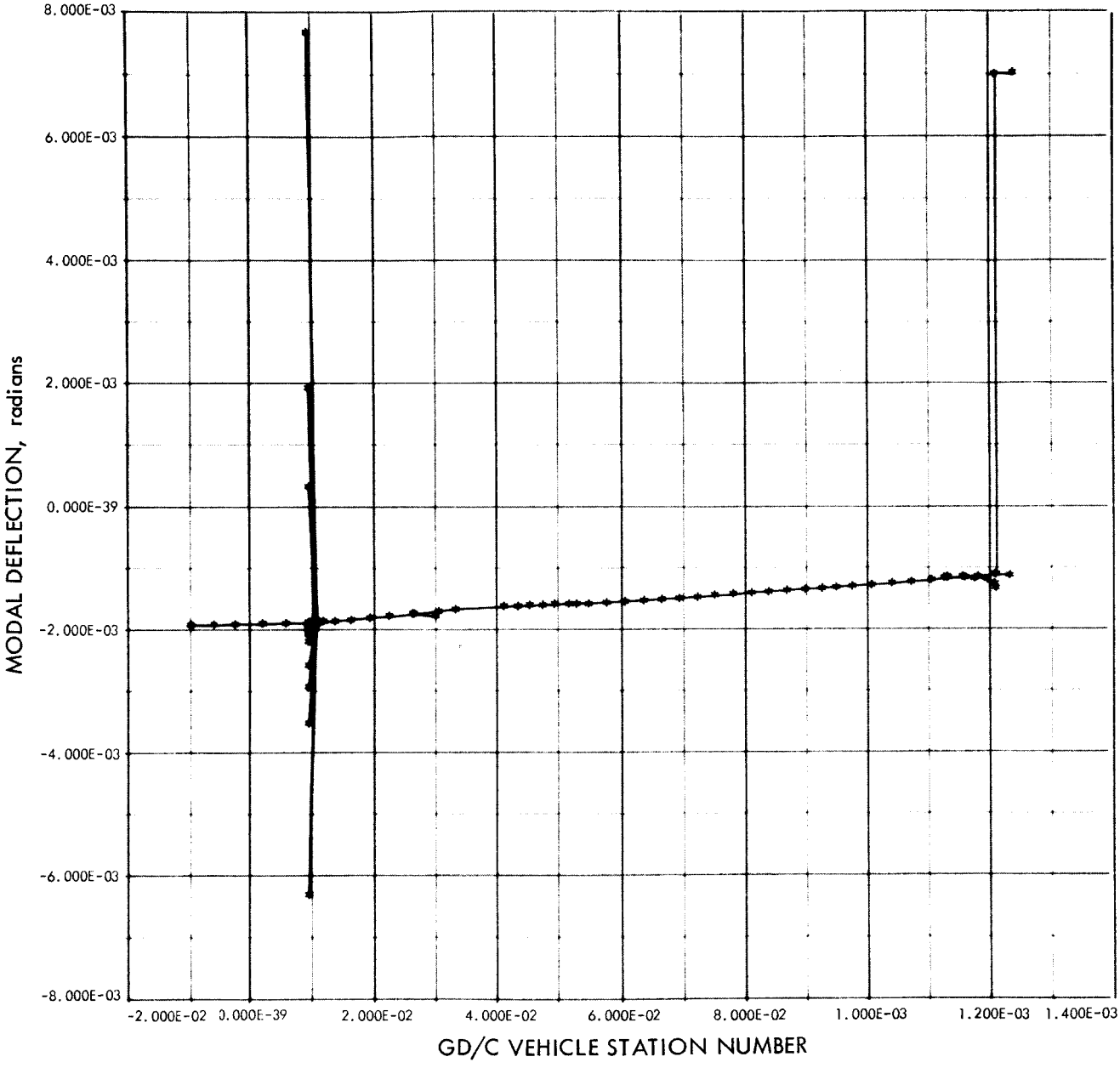

Fig. D-4. Atlas/Agena/OGO torsion mode shape (mode 4) F = 13.09 Hz

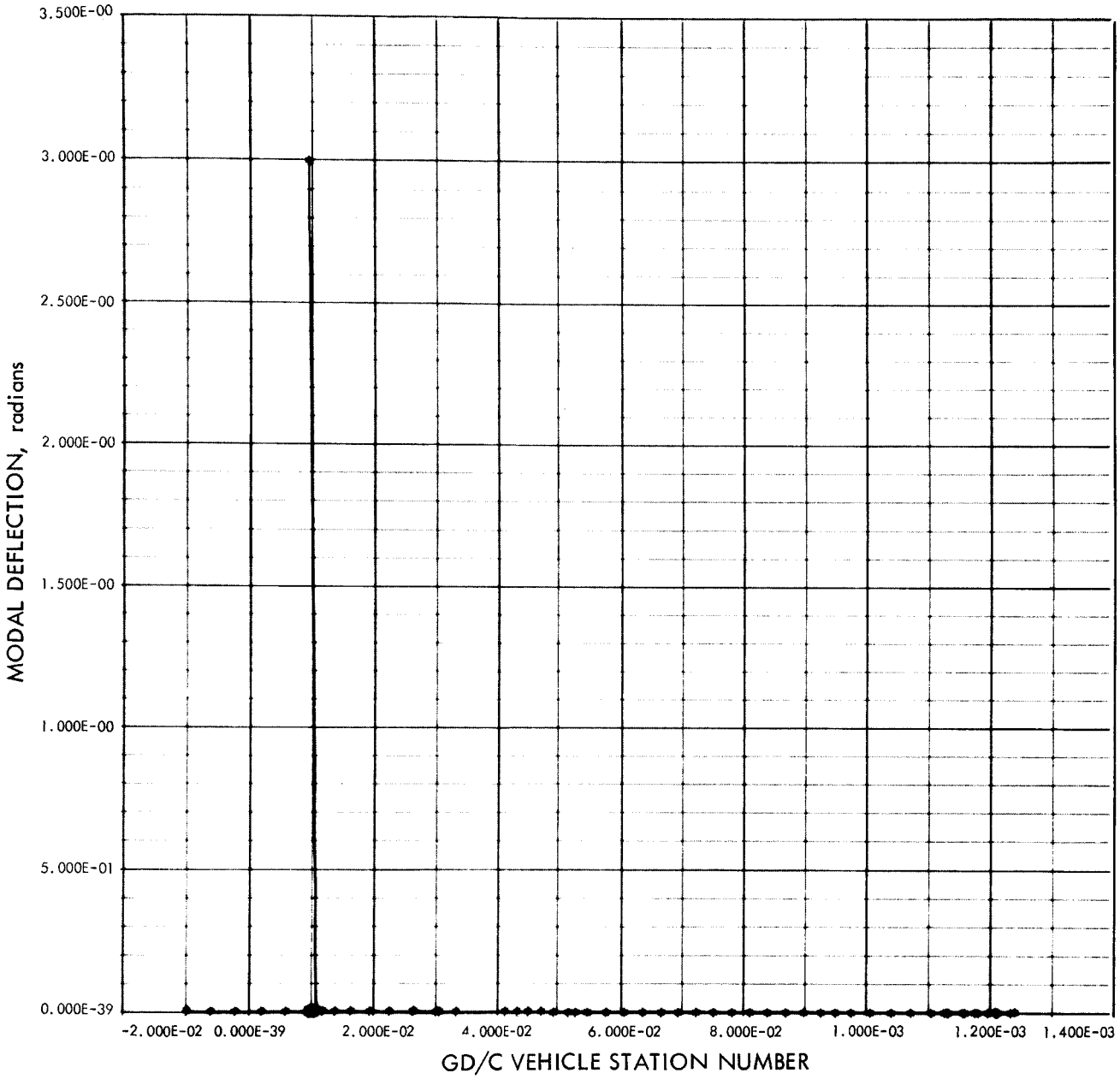

Fig. D-5. Atlas/Agena/OGO torsion mode shape (mode 5) F = 15.64 Hz

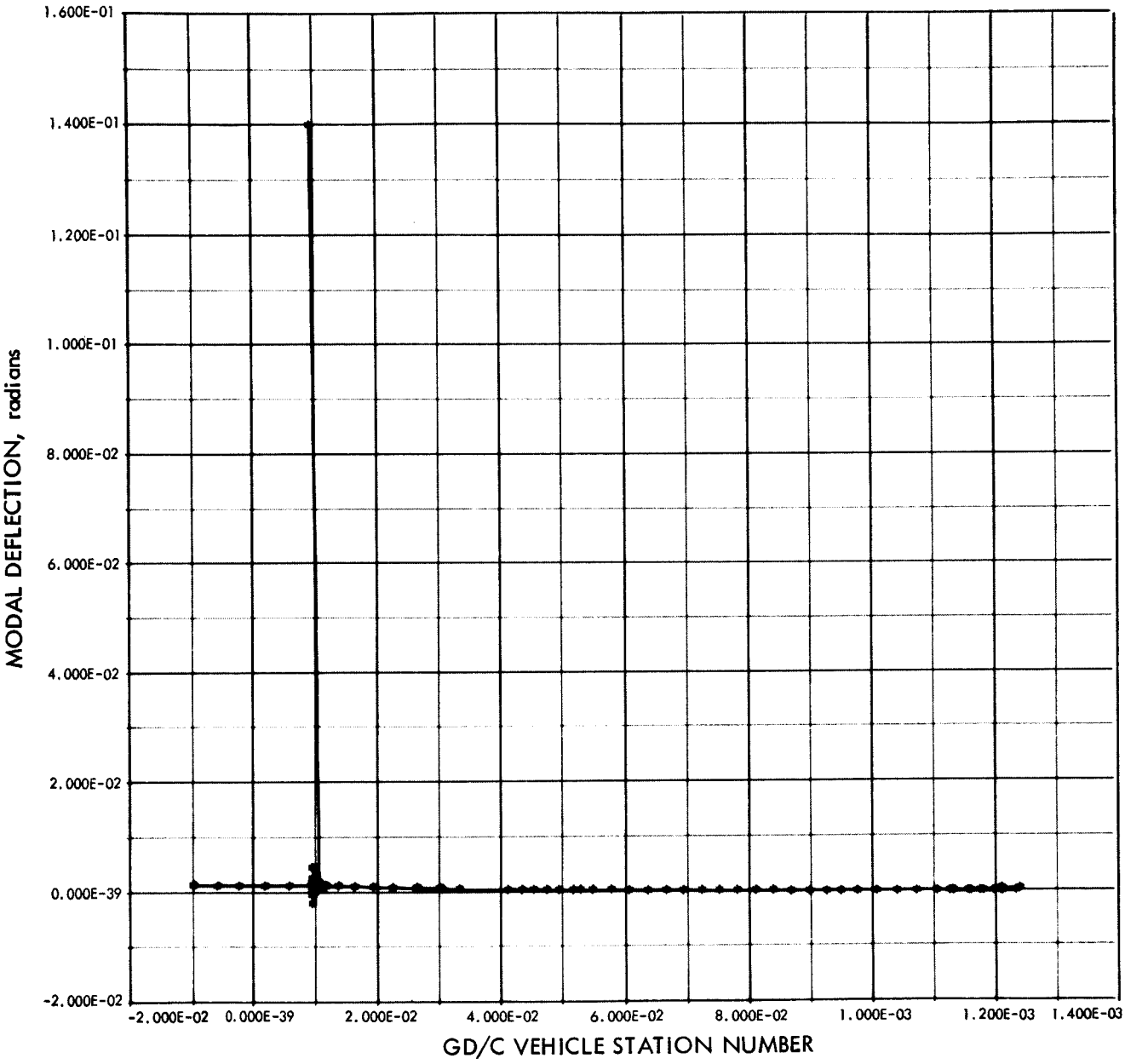

Fig. D-6. Atlas/Agena/OGO torsion mode shape (mode 6) F = 19.13 Hz

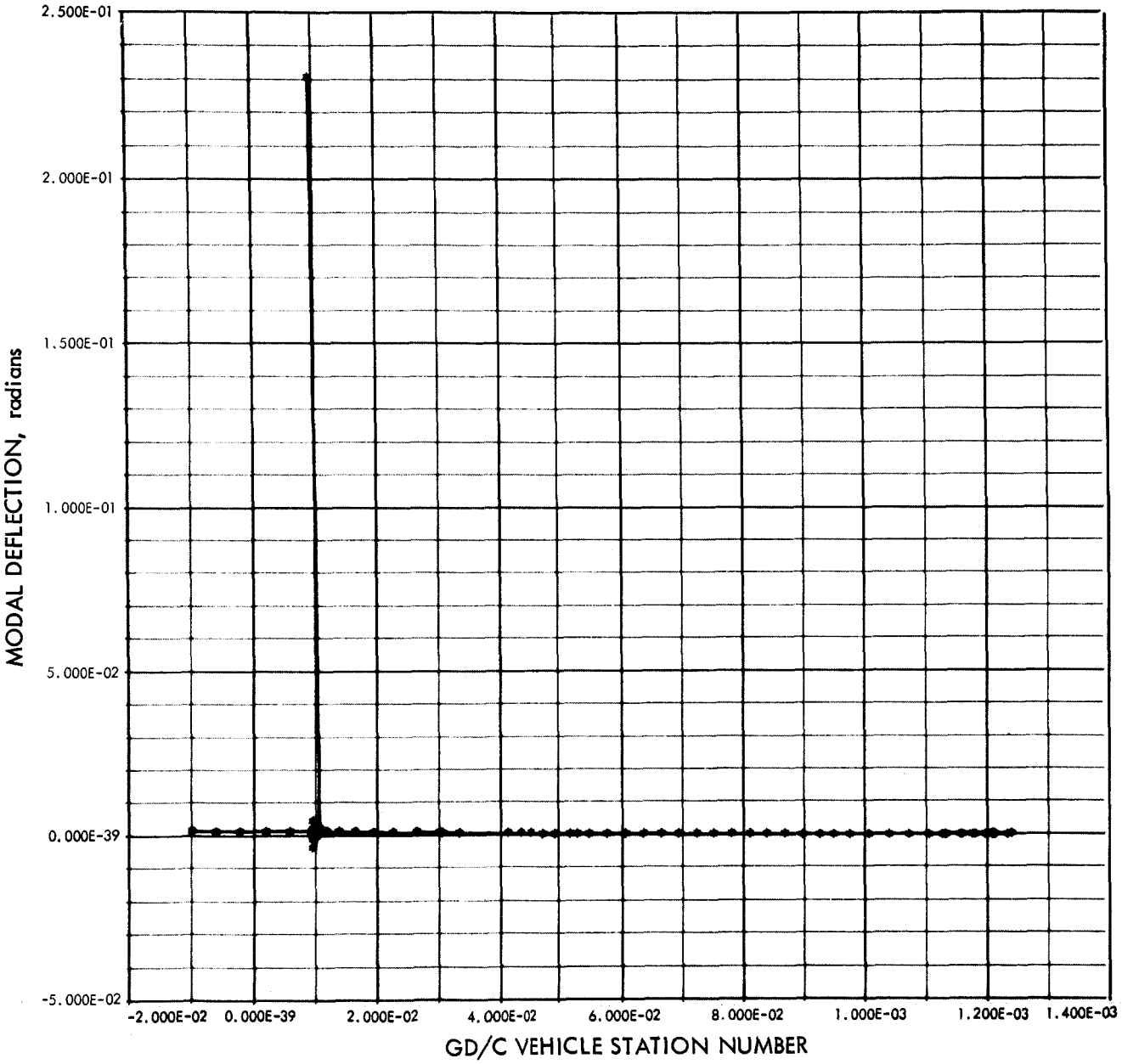

Fig. D-7. Atlas/Agena/OGO torsion mode shape (mode 7) F = 21.80 Hz

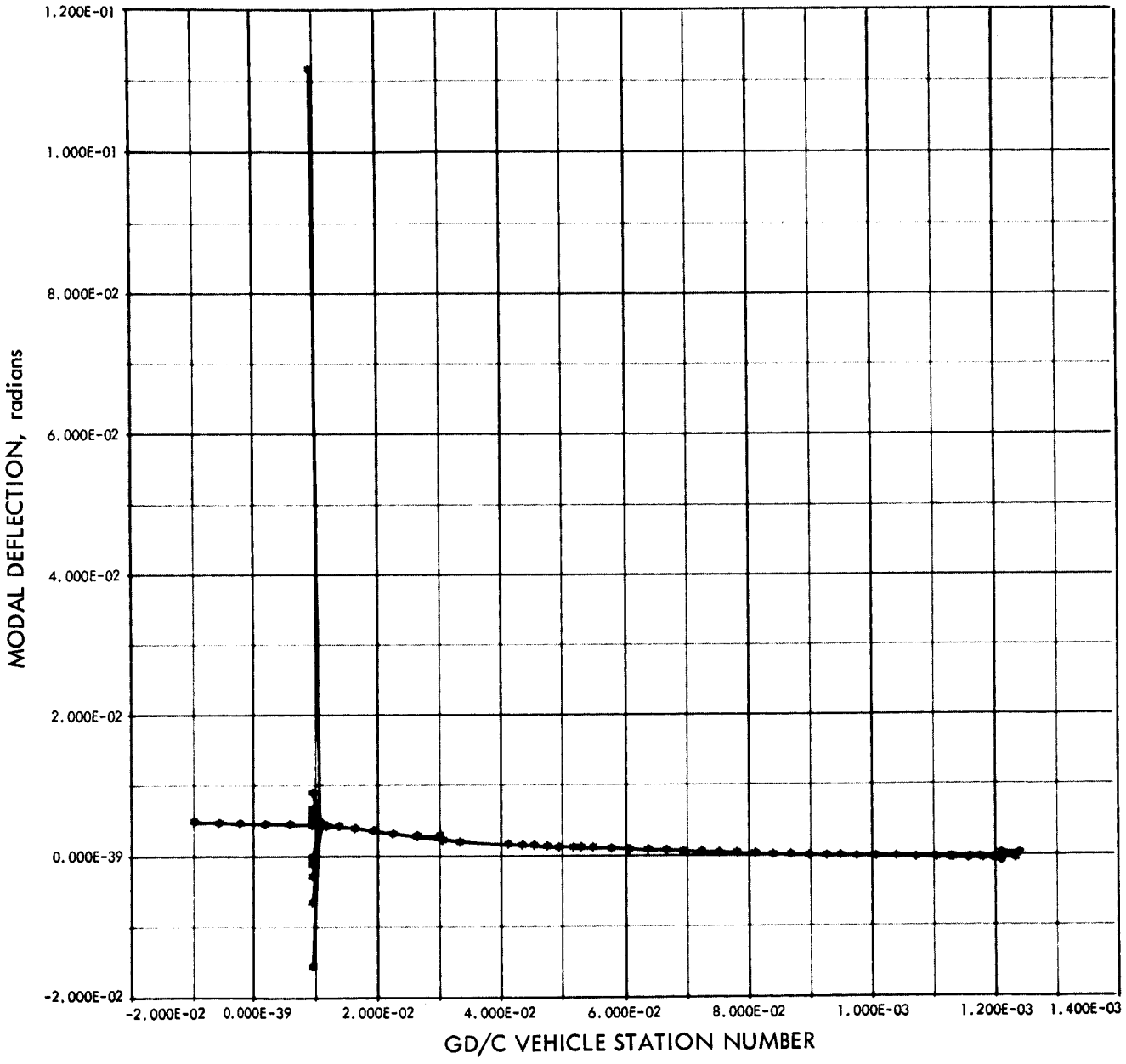

Fig. D-8. Atlas/Agena/OGO torsion mode shape (mode 8) F = 24.68 Hz

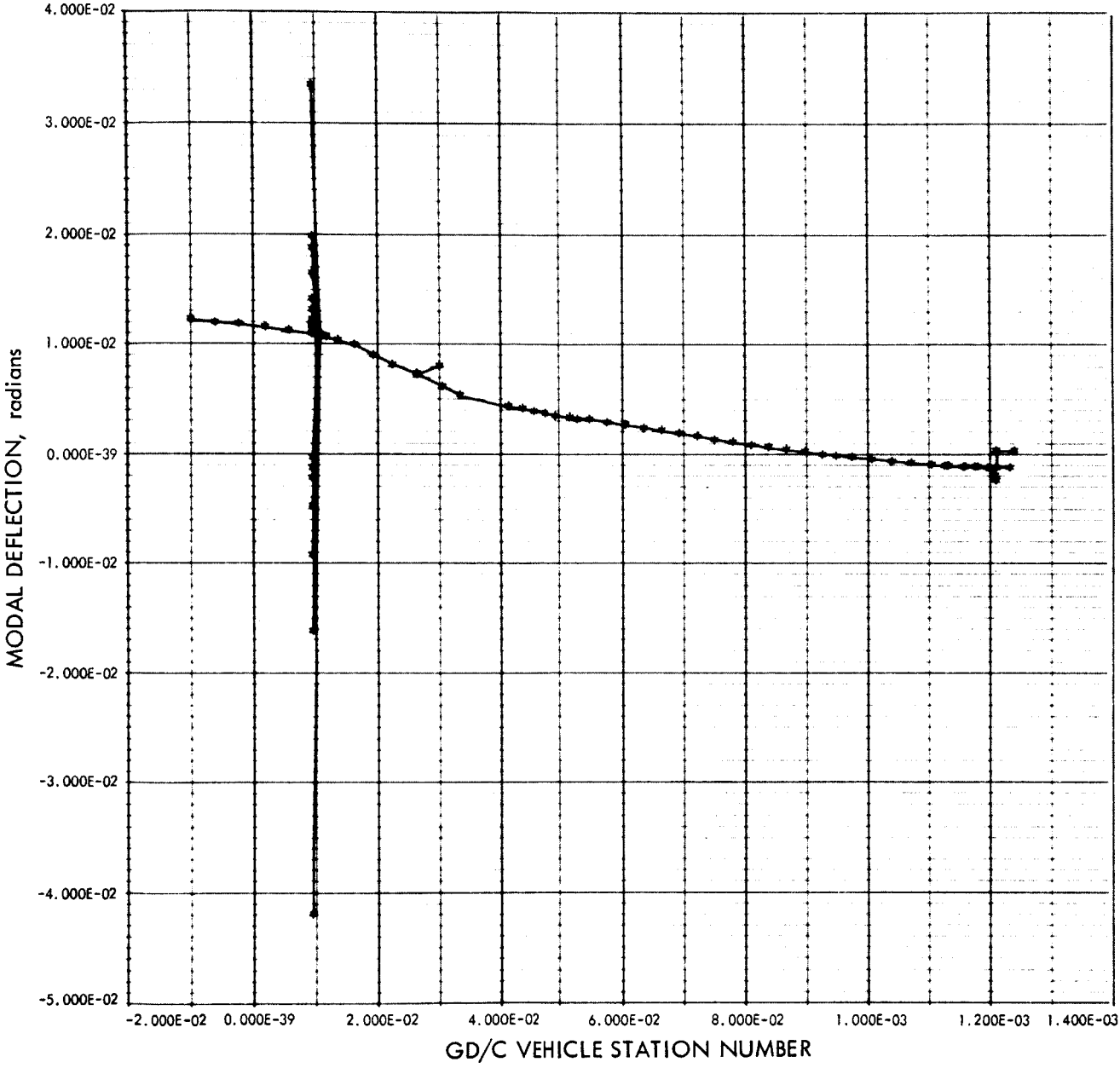

Fig. D-9. Atlas/Agena/OGO torsion mode shape (mode 9) F = 28.24 Hz

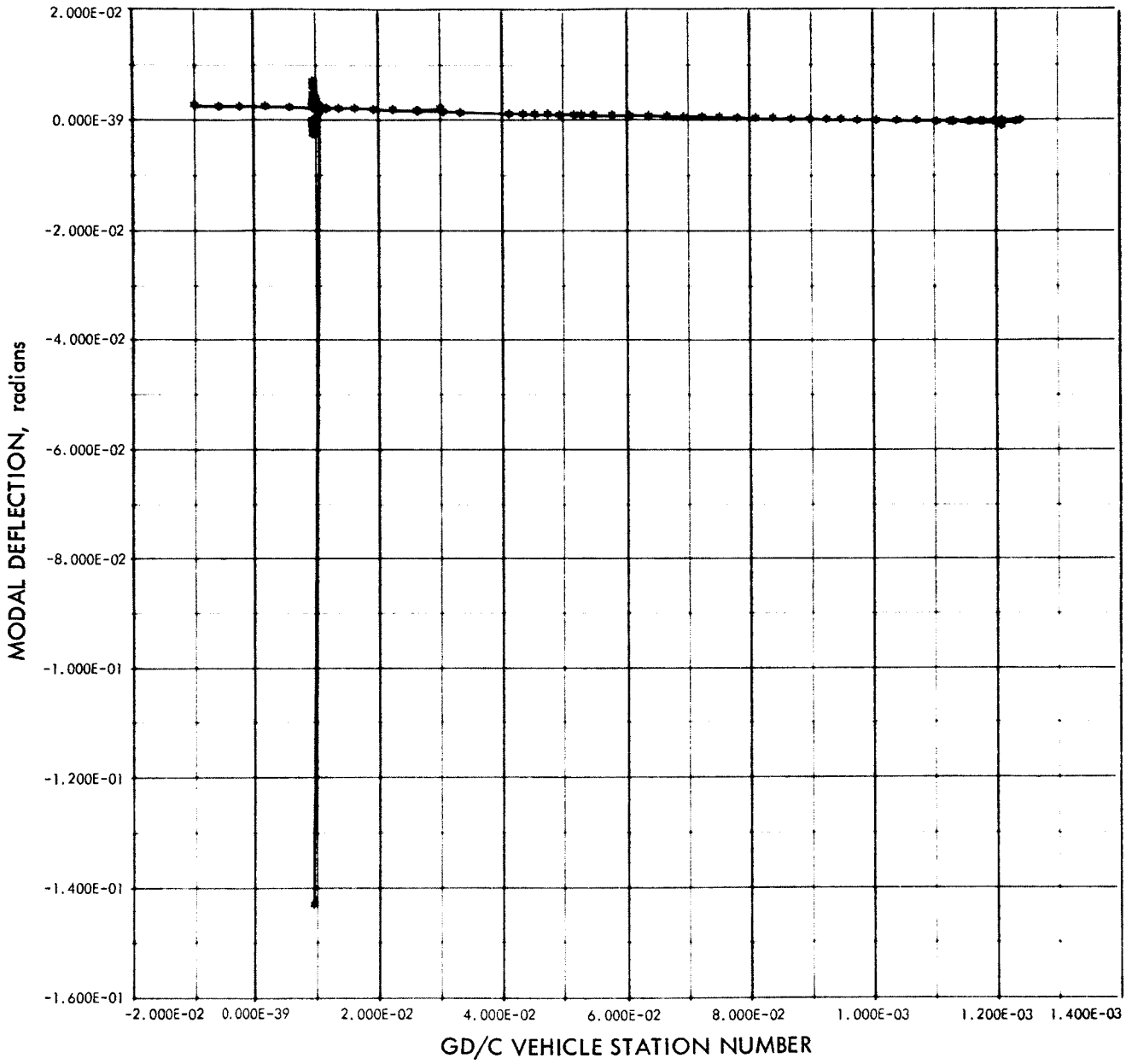

Fig. D-10. Atlas/Agena/OGO torsion mode shape (mode 10) F = 34.63 Hz

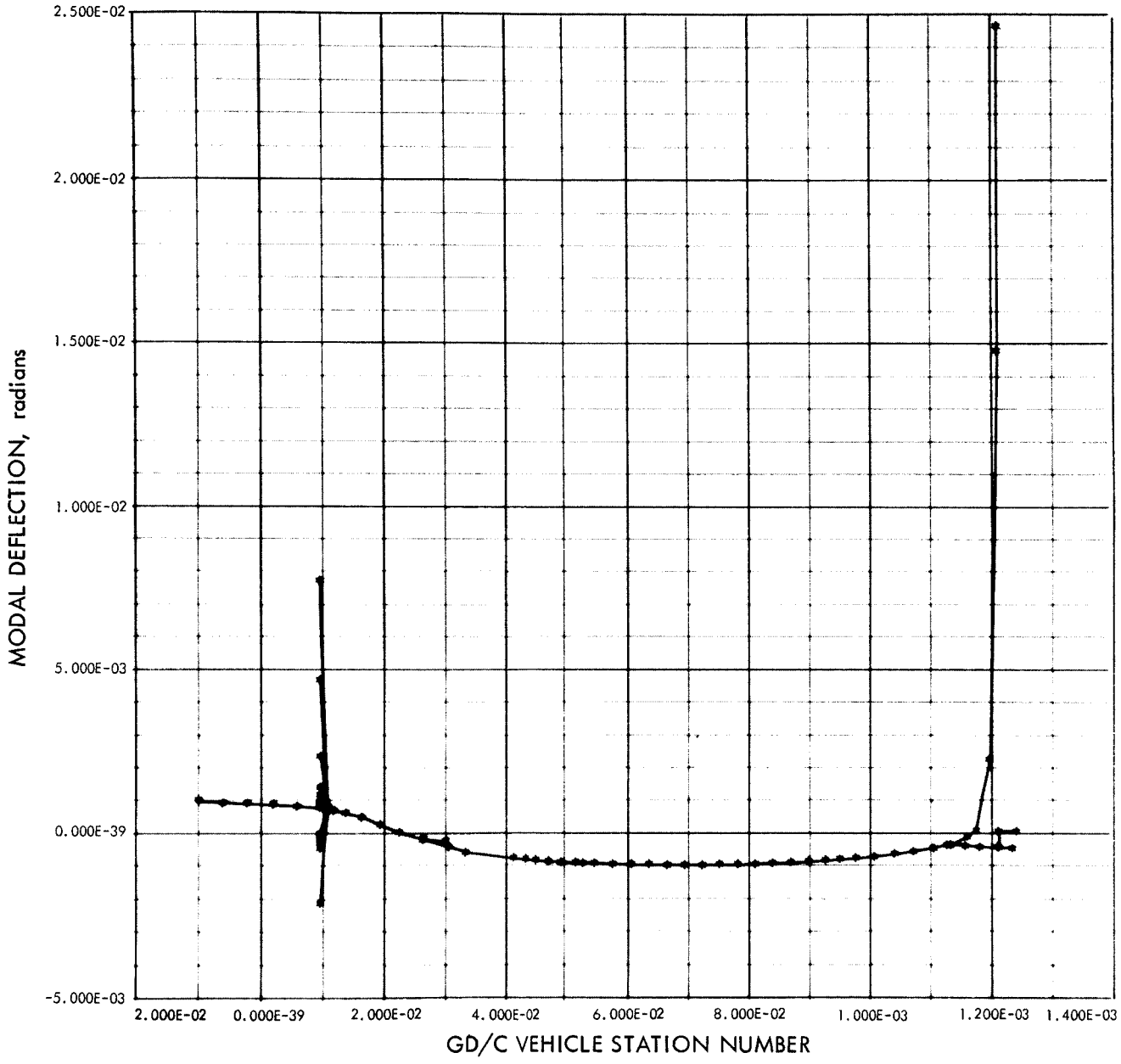

Fig. D-11. Atlas/Agena/OGO torsion mode shape (mode 11) F = 39.87 Hz

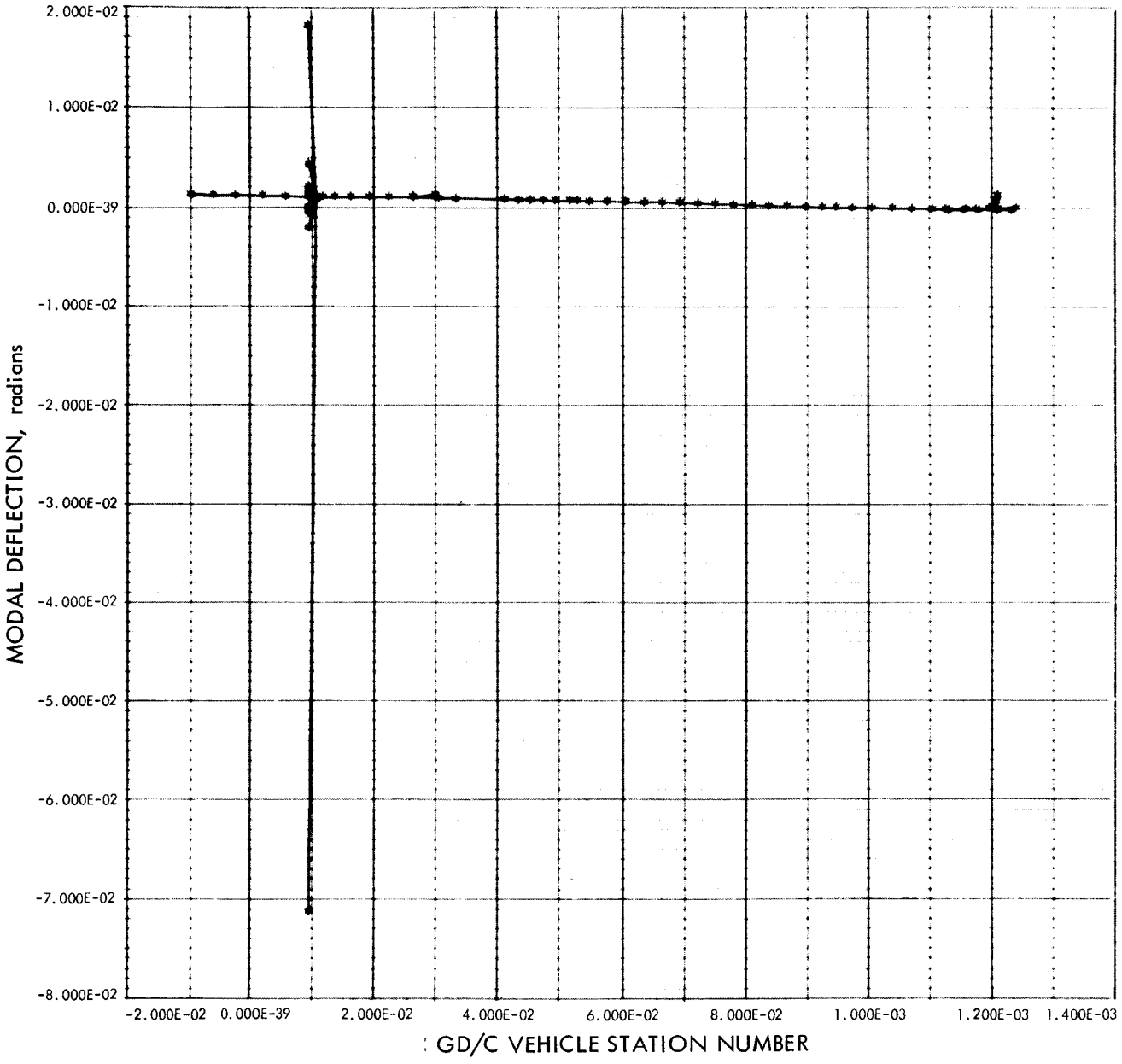

Fig. D-12. Atlas/Agena/OGO torsion mode shape (mode 12) F = 42.58 Hz

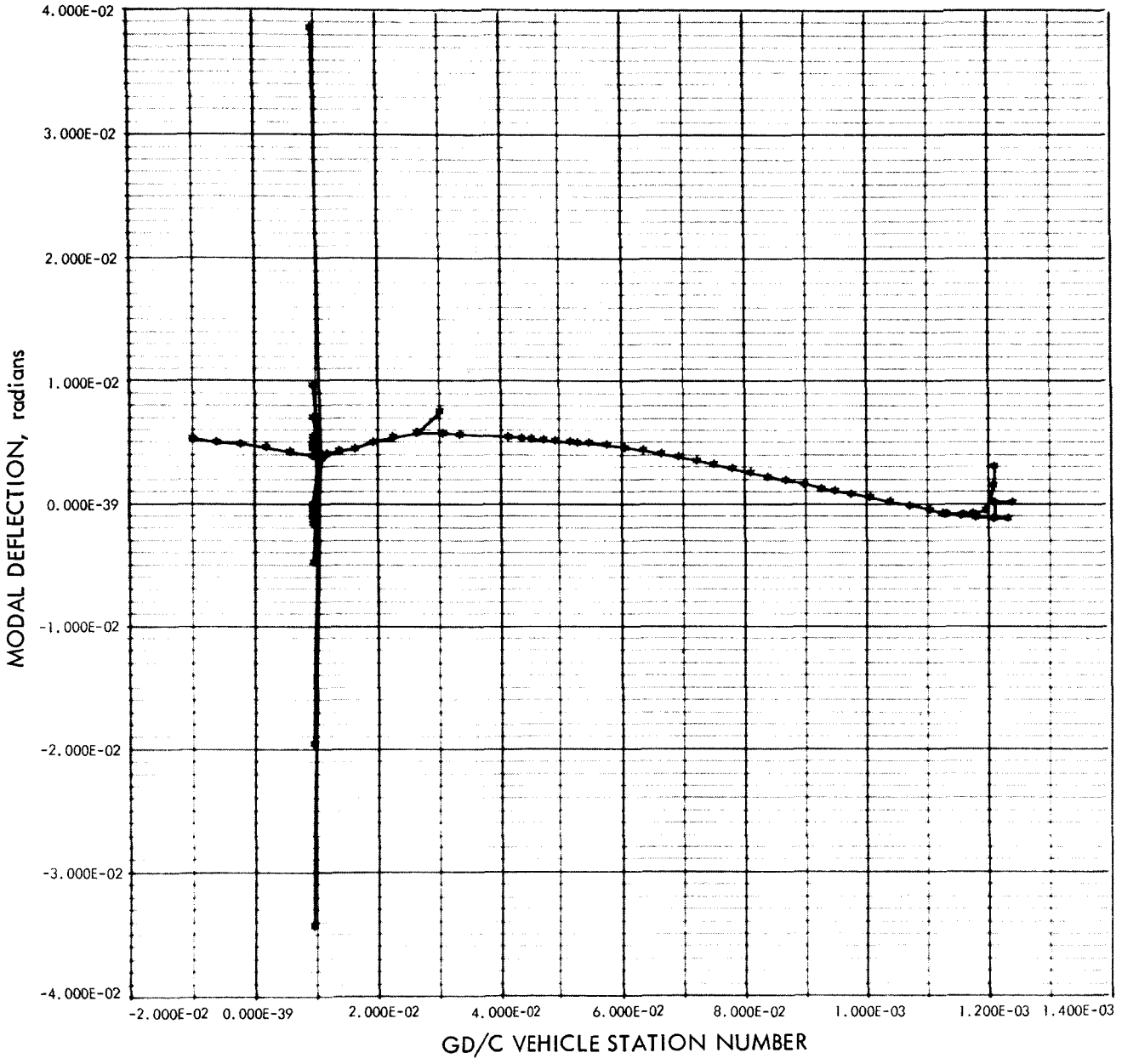

Fig. D-13. Atlas/Agena/OGO torsion mode shape (mode 13) F = 45.83 Hz

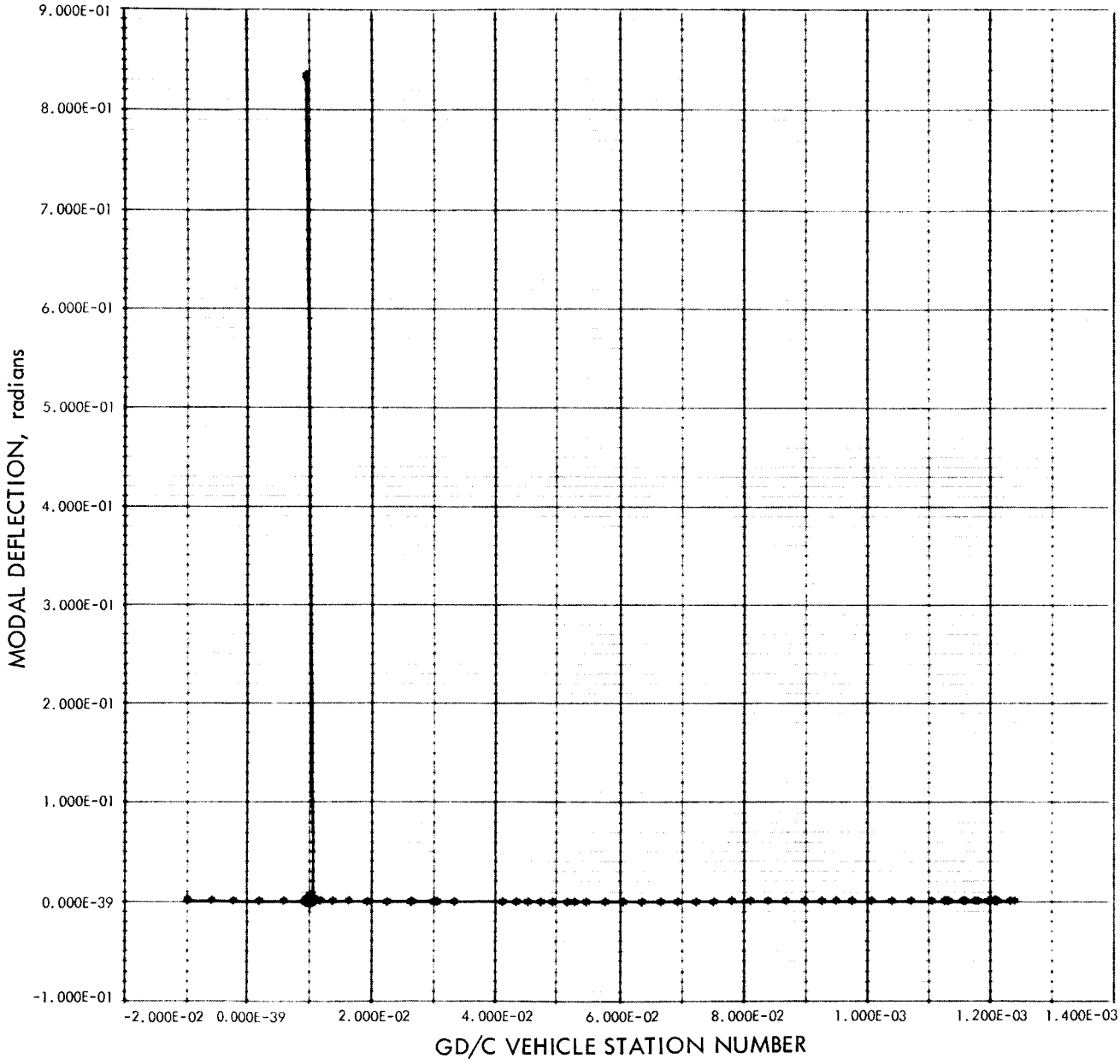

Fig. D-14. Atlas/Agena/OGO torsion mode shape (mode 14) F = 48.27 Hz

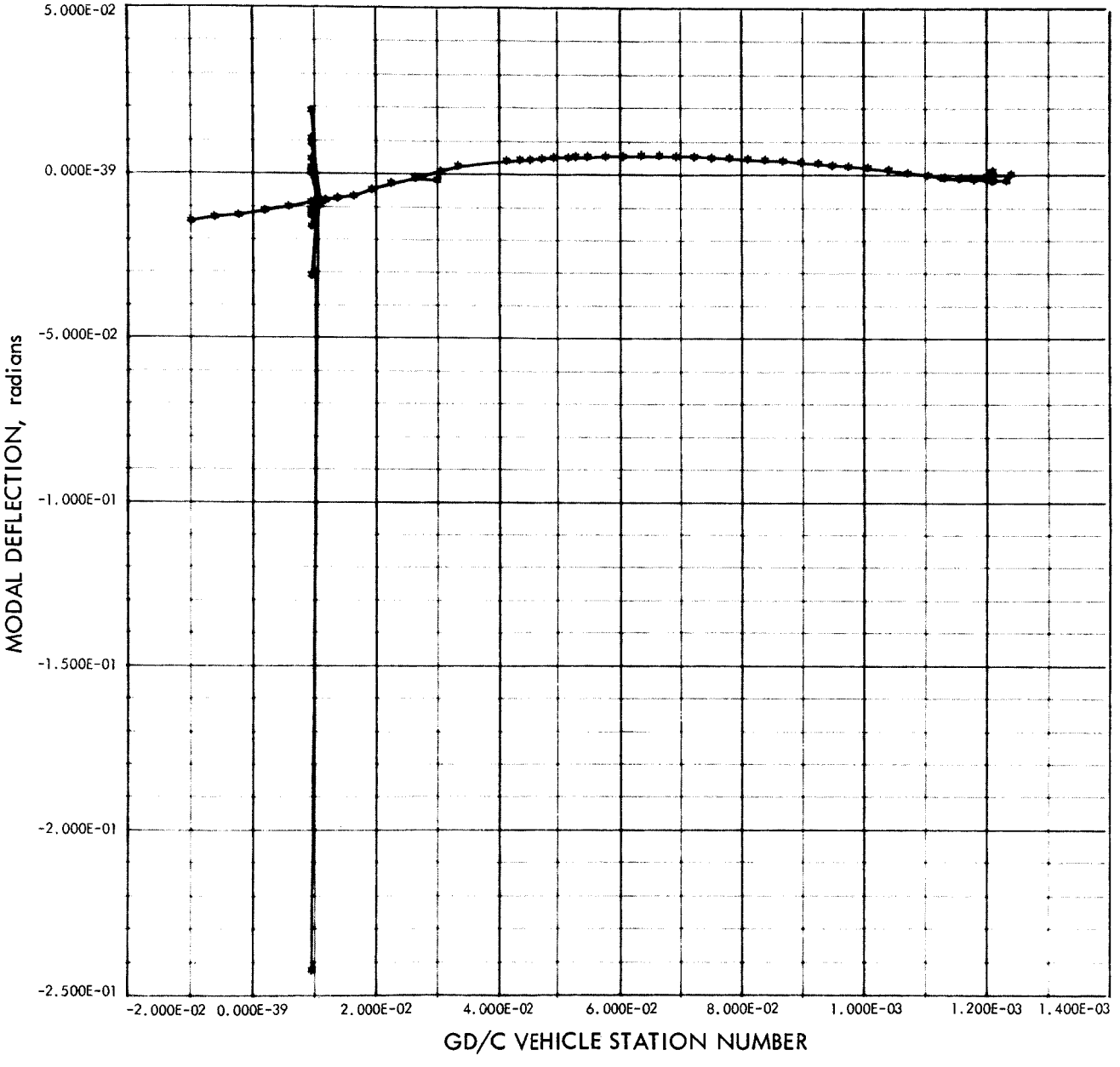

Fig. D-15. Atlas/Agena/OGO torsion mode shape (mode 15) F = 58.83 Hz

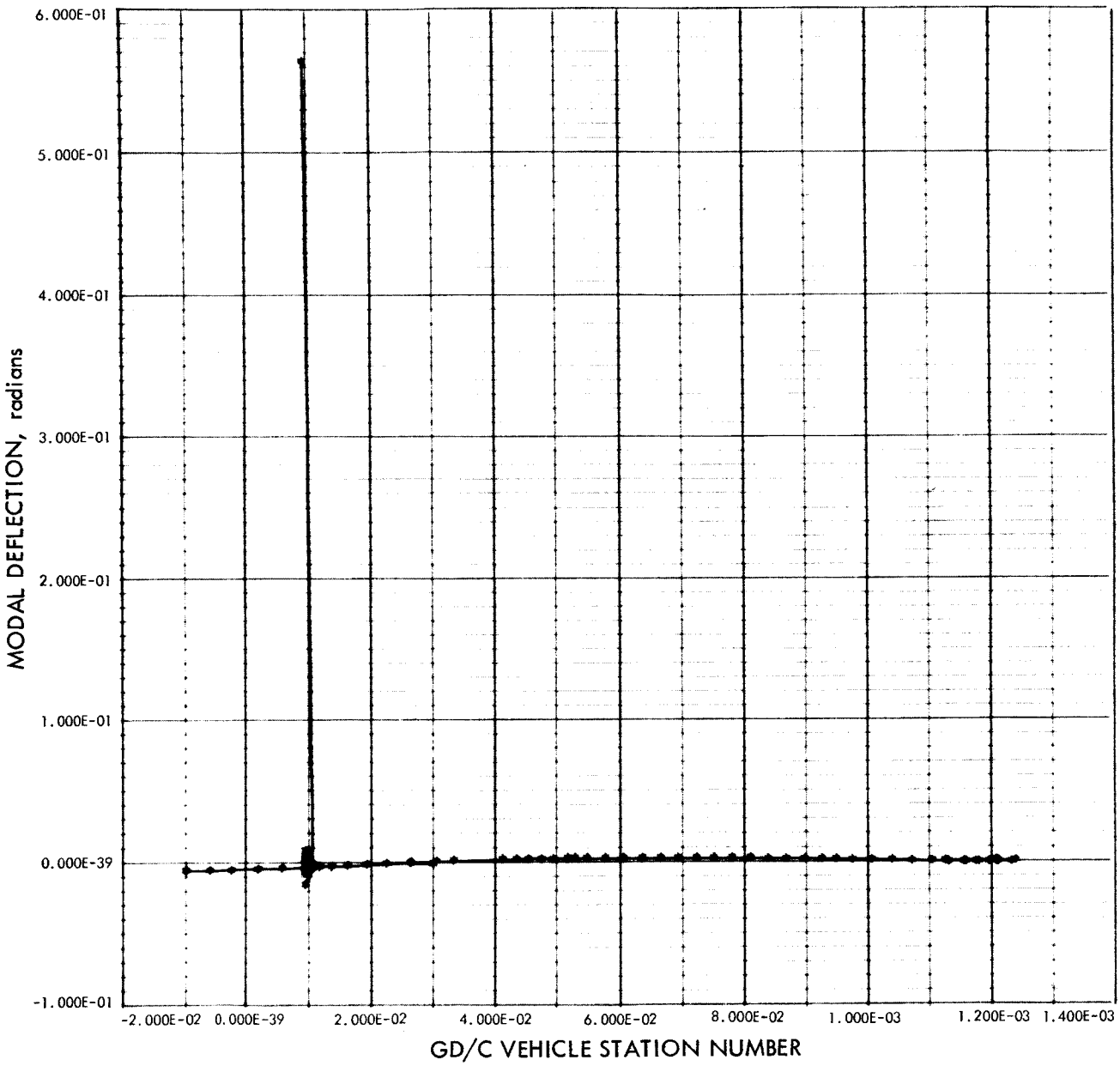

Fig. D-16. Atlas/Agena/OGO torsion mode shape (mode 16) F = 59.02 Hz

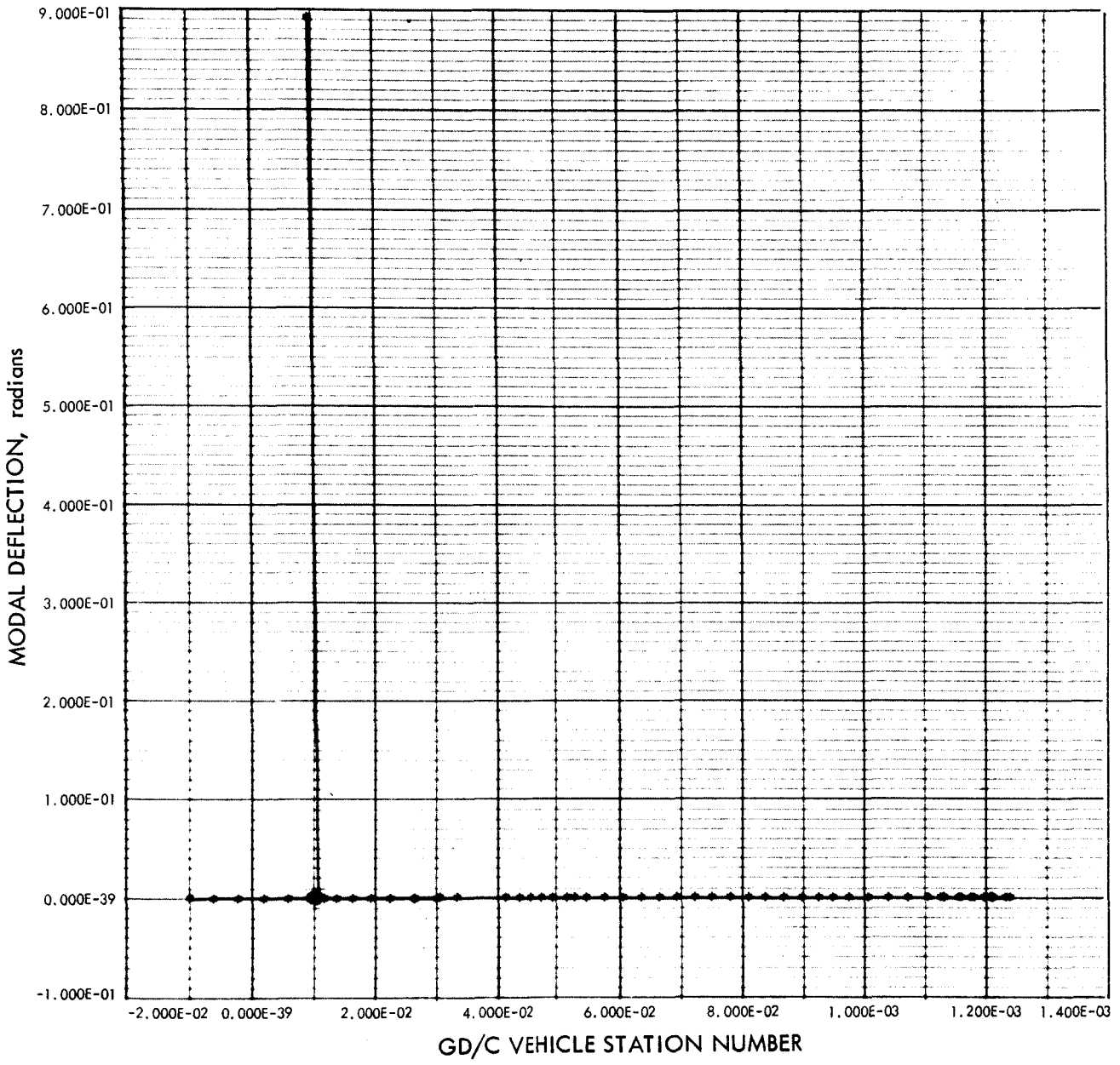

Fig. D-17. Atlas/Agena/OGO torsion mode shape (mode 17) F = 67.50 Hz

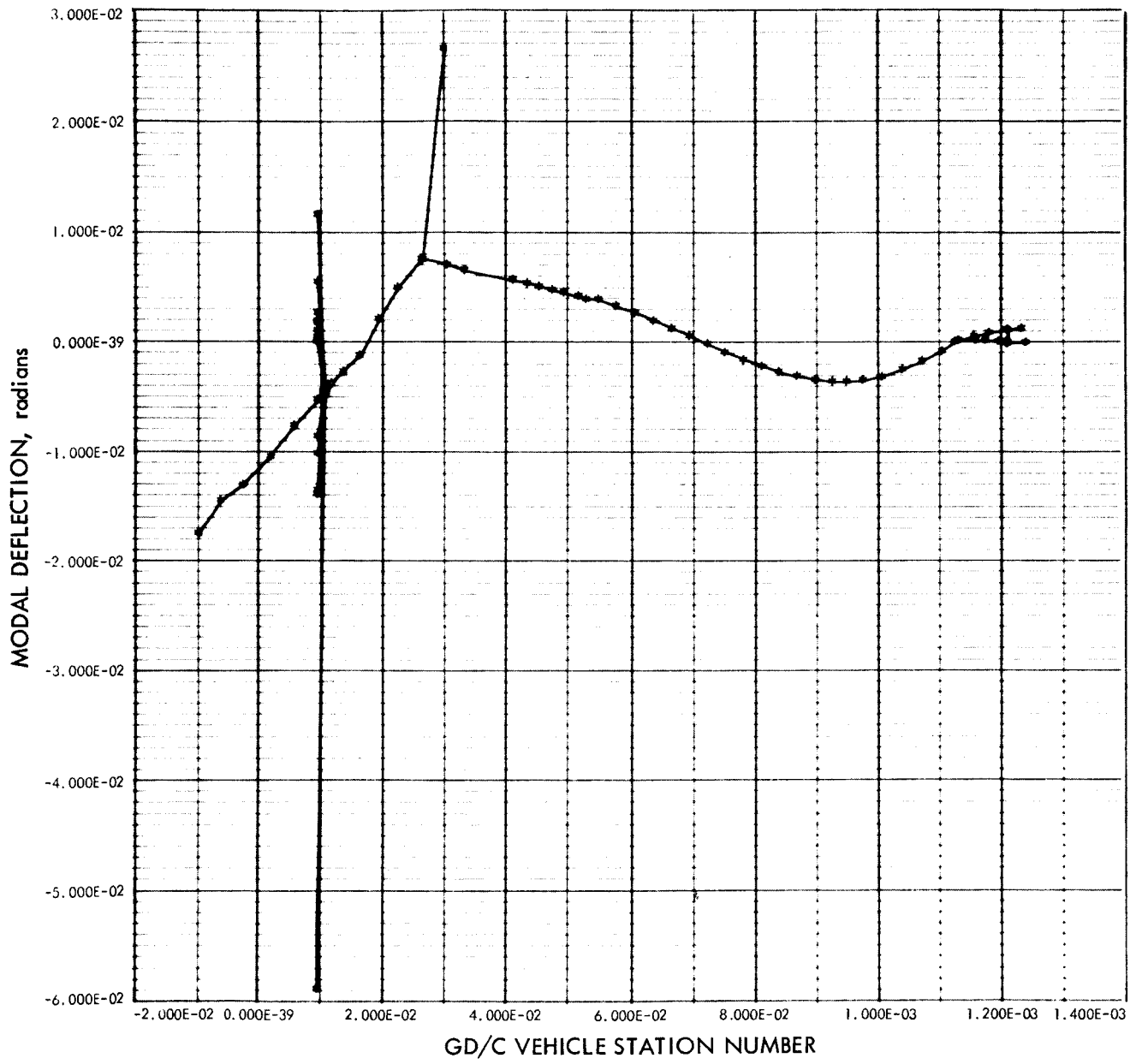

Fig. D-18. Atlas/Agena/OGO torsion mode shape (mode 18) F = 79.66 Hz

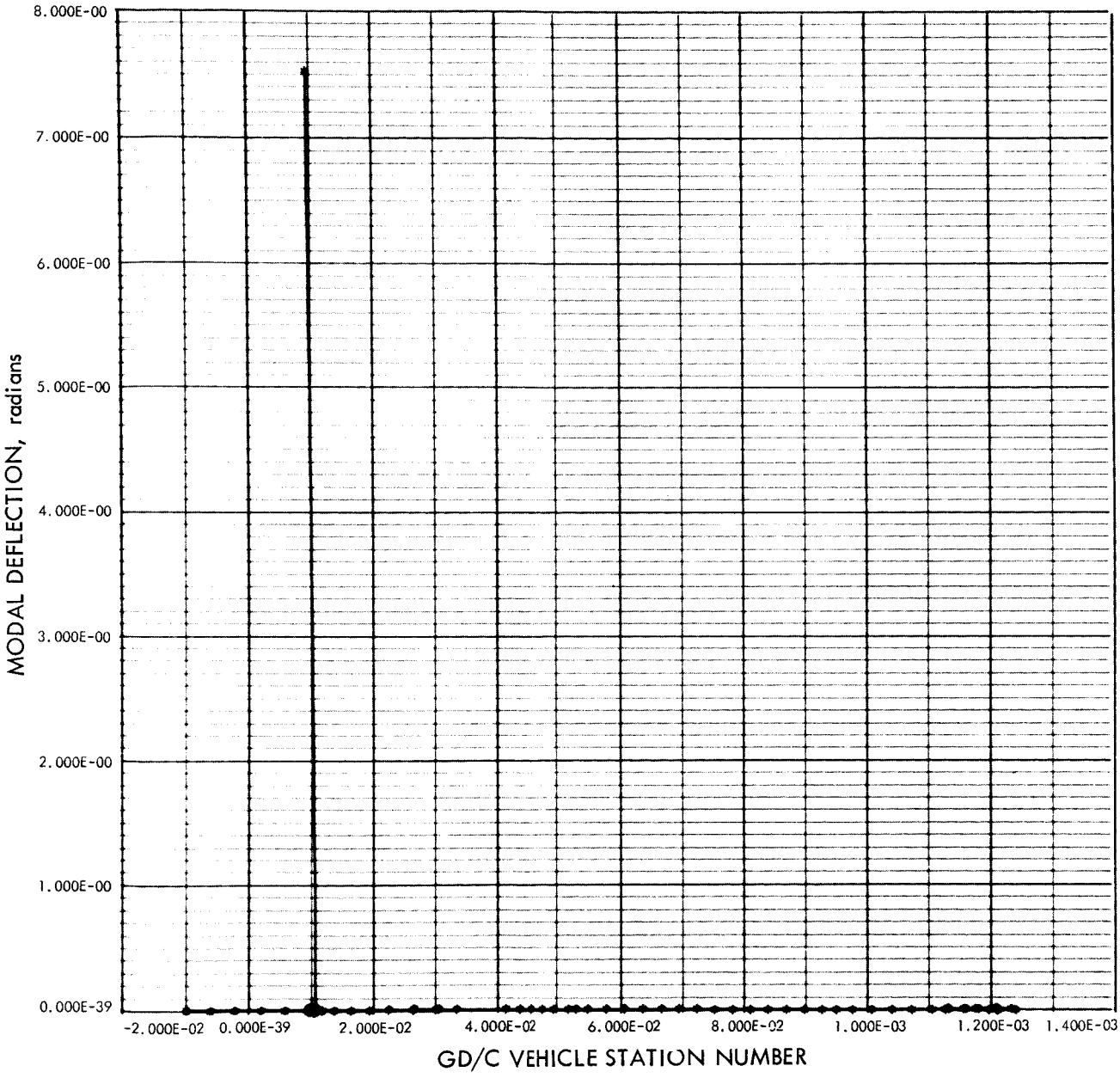

Fig. D-19. Atlas/Agena/OGO torsion mode shape (mode 19) F = 82.99 Hz

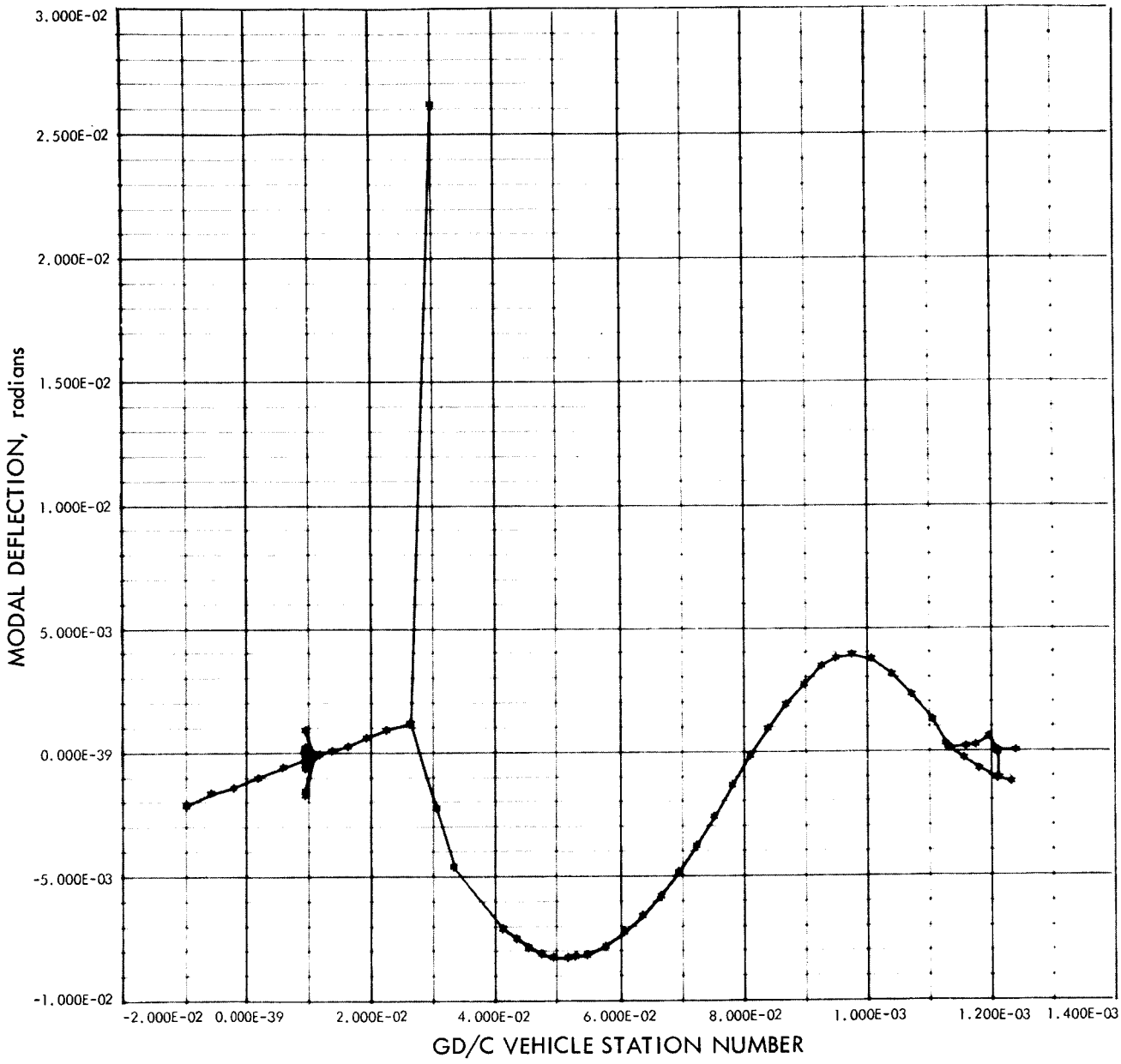

Fig. D-20. Atlas/Agena/OGO torsion mode shape (mode 20) F = 92.20 Hz

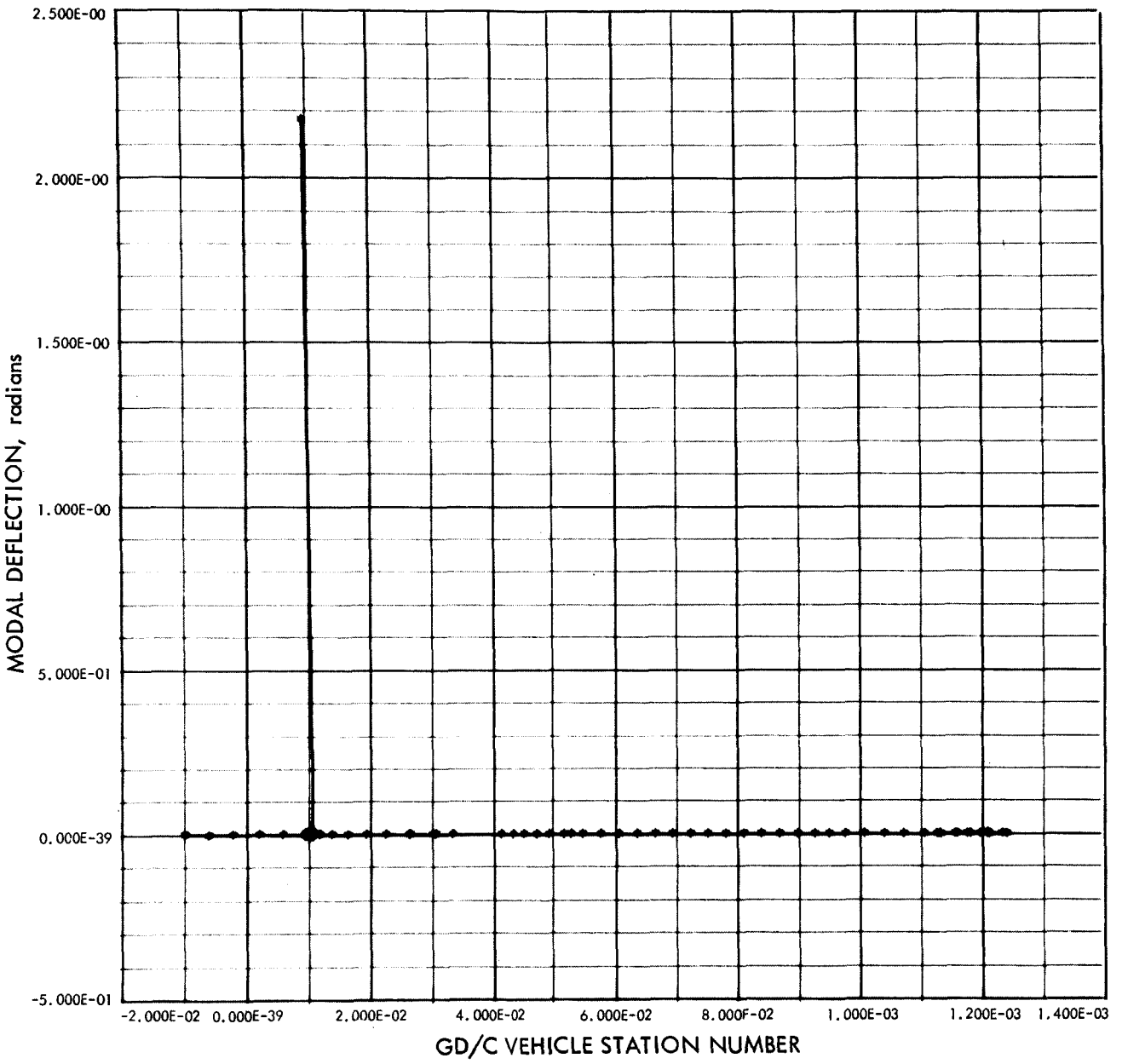

Fig. D-21. Atlas/Agena/OGO torsion mode shape (mode 21) F = 97.26 Hz

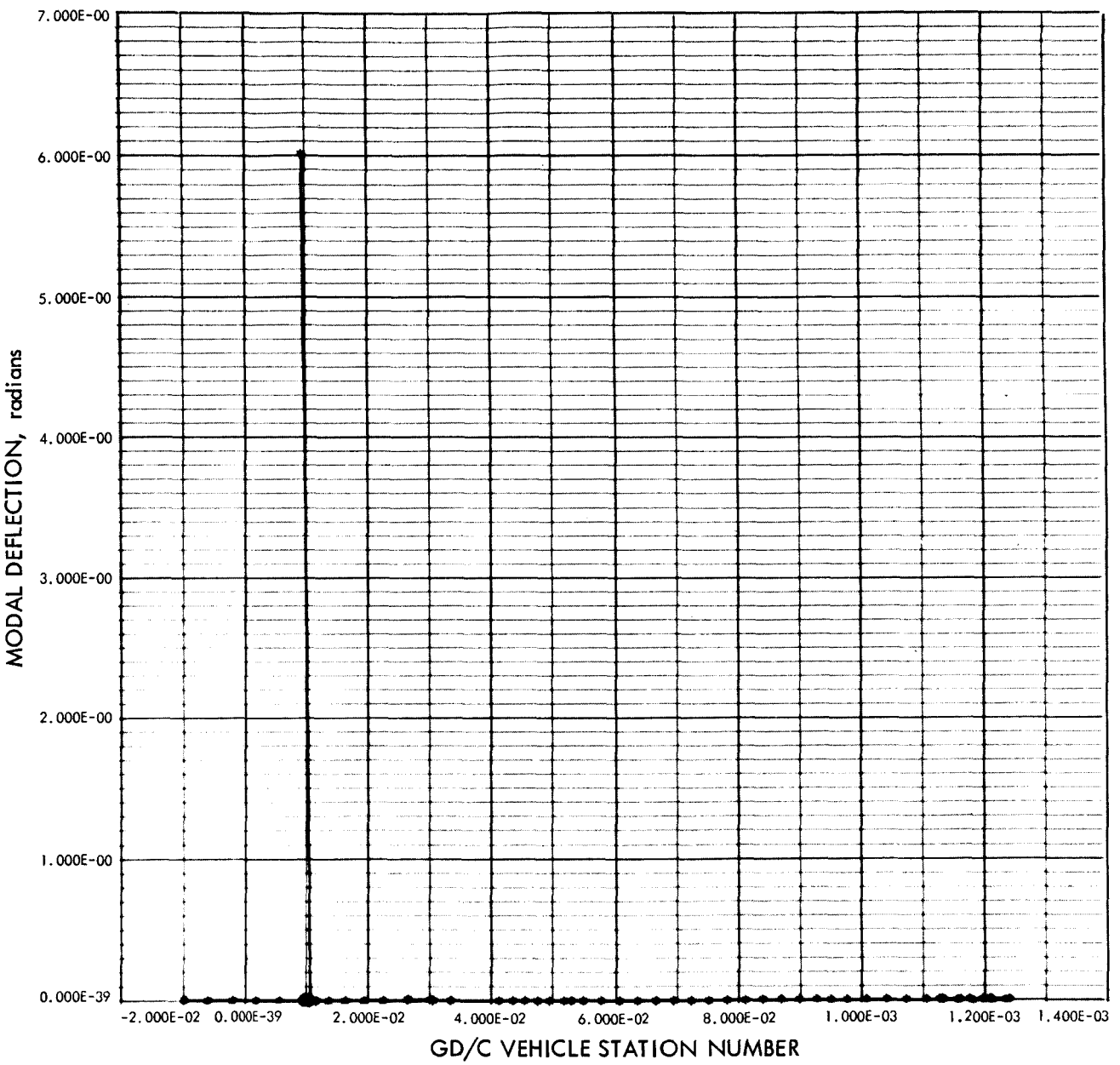

Fig. D-22. Atlas/Agena/OGO torsion mode shape (mode 22) F = 98.04 Hz

Table D-1. Pertinent modal information

Mode No. n	Generalized mass (inertia) m_n lb-in.-sec^2	Freq. Hz	Gimbal block deflection JT. 53 rad (ϕ_{2n})	S/C attachment point deflection JT. 7 rad (ϕ_{1n})	I_n^* lb-in.-sec^2	JT. 1 x_1 in. (ϕ_{1n})	JT. 1 x_5 rad (ϕ_{1n})	JT. 5 x_5 rad (ϕ_{1n})	JT. 23 x_1 in. (ϕ_{1n})	JT. 23 x_3 in. (ϕ_{1n})
0	112,200	0	1	1	0.91680×10^{3}	0.13080×10^{2}	1	1	0.17810×10^{2}	0.18700×10^{2}
1	1	4.93	-0.39344×10^{-4}	-0.97712×10^{-5}	0.43221×10^{1}	0.36078×10^{0}	-0.10088×10^{0}	-0.68965×10^{-4}	-0.12383×10^{0}	0.40279×10^{1}
2	1	9.30	-0.47015×10^{-4}	0.96596×10^{-4}	0.57223×10^{1}	-0.60301×10^{0}	-0.11102×10^{0}	-0.45138×10^{-3}	0.11089×10^{0}	0.20276×10^{1}
3	1	11.74	-0.92961×10^{-5}	0.11162×10^{-3}	0.30107×10^{1}	0.24202×10^{1}	0.93608×10^{-1}	-0.43514×10^{-3}	-0.15691×10^{0}	0.18576×10^{1}
4	1	13.09	-0.11284×10^{-2}	-0.18899×10^{-2}	-0.17213×10^{1}	0.10091×10^{-1}	-0.33550×10^{-3}	0.21046×10^{-2}	-0.56628×10^{-1}	0.11165×10^{0}
5	1	15.64	-0.79790×10^{-5}	0.20924×10^{-4}	0.35579×10^{0}	-0.30572×10^{0}	-0.35083×10^{-1}	-0.71982×10^{-4}	-0.34752×10^{0}	0.51943×10^{0}
6	1	19.13	-0.20208×10^{-3}	0.10186×10^{-2}	0.81779×10^{1}	0.94652×10^{0}	0.71441×10^{-1}	-0.32691×10^{-2}	0.14634×10^{0}	-0.13134×10^{1}
7	1	21.80	-0.17099×10^{-3}	0.11145×10^{-2}	0.54235×10^{1}	0.51751×10^{0}	0.44364×10^{-1}	-0.30495×10^{-2}	0.13412×10^{1}	-0.11332×10^{1}
8	1	24.68	-0.55251×10^{-3}	0.43171×10^{-2}	0.11638×10^{2}	0.15858×10^{0}	0.43836×10^{-2}	-0.96658×10^{-2}	0.21922×10^{1}	-0.10893×10^{1}
9	1	28.24	-0.12207×10^{-2}	0.10868×10^{-1}	0.98768×10^{1}	-0.28722×10^{0}	-0.46590×10^{-1}	-0.16772×10^{-1}	-0.97823×10^{0}	0.10291×10^{1}
10	1	34.63	-0.24596×10^{-3}	0.22651×10^{-2}	-0.27607×10^{1}	0.26455×10^{0}	0.38579×10^{-1}	0.27676×10^{-3}	-0.16740×10^{1}	-0.14112×10^{1}
11	1	39.87	-0.46547×10^{-3}	0.74762×10^{-3}	0.33086×10^{1}	-0.56577×10^{-2}	-0.10859×10^{-1}	-0.47243×10^{-2}	-0.13197×10^{0}	0.86207×10^{-1}
12	1	42.25	-0.20223×10^{-3}	0.10341×10^{-2}	-0.31517×10^{1}	0.19141×10^{0}	0.23376×10^{0}	0.32254×10^{-2}	-0.29464×10^{0}	-0.29161×10^{1}
13	1	45.83	-0.12038×10^{-2}	0.37928×10^{-2}	-0.19622×10^{2}	-0.54311×10^{-1}	0.46301×10^{-2}	0.27483×10^{-1}	0.60619×10^{0}	0.45262×10^{0}
14	1	48.27	0.11416×10^{-3}	-0.16547×10^{-3}	0.16223×10^{1}	-0.33427×10^{-1}	0.10210×10^{0}	-0.27025×10^{-2}	0.10861×10^{0}	-0.74356×10^{0}
15	1	57.83	-0.16480×10^{-2}	-0.82257×10^{-2}	0.62753×10^{1}	0.96730×10^{-1}	-0.76770×10^{-1}	-0.92156×10^{-2}	-0.16513×10^{0}	-0.45767×10^{0}
16	1	59.02	-0.67915×10^{-3}	-0.37755×10^{-2}	0.43929×10^{1}	-0.13482×10^{0}	0.12658×10^{0}	-0.41777×10^{-2}	-0.23835×10^{-1}	0.68468×10^{0}
17	1	67.50	-0.64118×10^{-4}	-0.41132×10^{-3}	0.13126×10^{1}	-0.45108×10^{0}	0.37914×10^{0}	-0.41083×10^{-2}	0.58557×10^{0}	0.33689×10^{1}
18	1	79.66	0.11656×10^{-2}	-0.45823×10^{-2}	0.13314×10^{1}	0.12034×10^{-3}	0.49851×10^{-2}	-0.17792×10^{-2}	-0.17328×10^{-1}	0.99605×10^{-1}
19	1	82.99	0.68973×10^{-5}	-0.57035×10^{-4}	0.14742×10^{0}	-0.10789×10^{0}	0.11904×10^{-1}	-0.70776×10^{-3}	0.15543×10^{0}	-0.26273×10^{1}
20	1	92.20	0.44178×10^{-3}	-0.17325×10^{-3}	0.33741×10^{-1}	0.31892×10^{-3}	0.10262×10^{-3}	-0.42960×10^{-4}	-0.12513×10^{-2}	0.48258×10^{-2}
21	1	97.26	0.12512×10^{-6}	-0.84885×10^{-5}	0.46019×10^{0}	-0.49159×10^{0}	0.42220×10^{-1}	-0.32791×10^{-2}	0.12858×10^{1}	-0.45934×10^{1}
22	1	98.04	-0.17227×10^{-8}	-0.17916×10^{-6}	0.16607×10^{0}	0.30539×10^{0}	-0.23938×10^{0}	-0.11916×10^{-2}	-0.25085×10^{0}	-0.30298×10^{1}

Note: The modal quantities are normalized such as to give a unit generalized mass for the composite launch vehicle in all elastic modes, n>0.

APPENDIX E

RESPONSE PLOTS

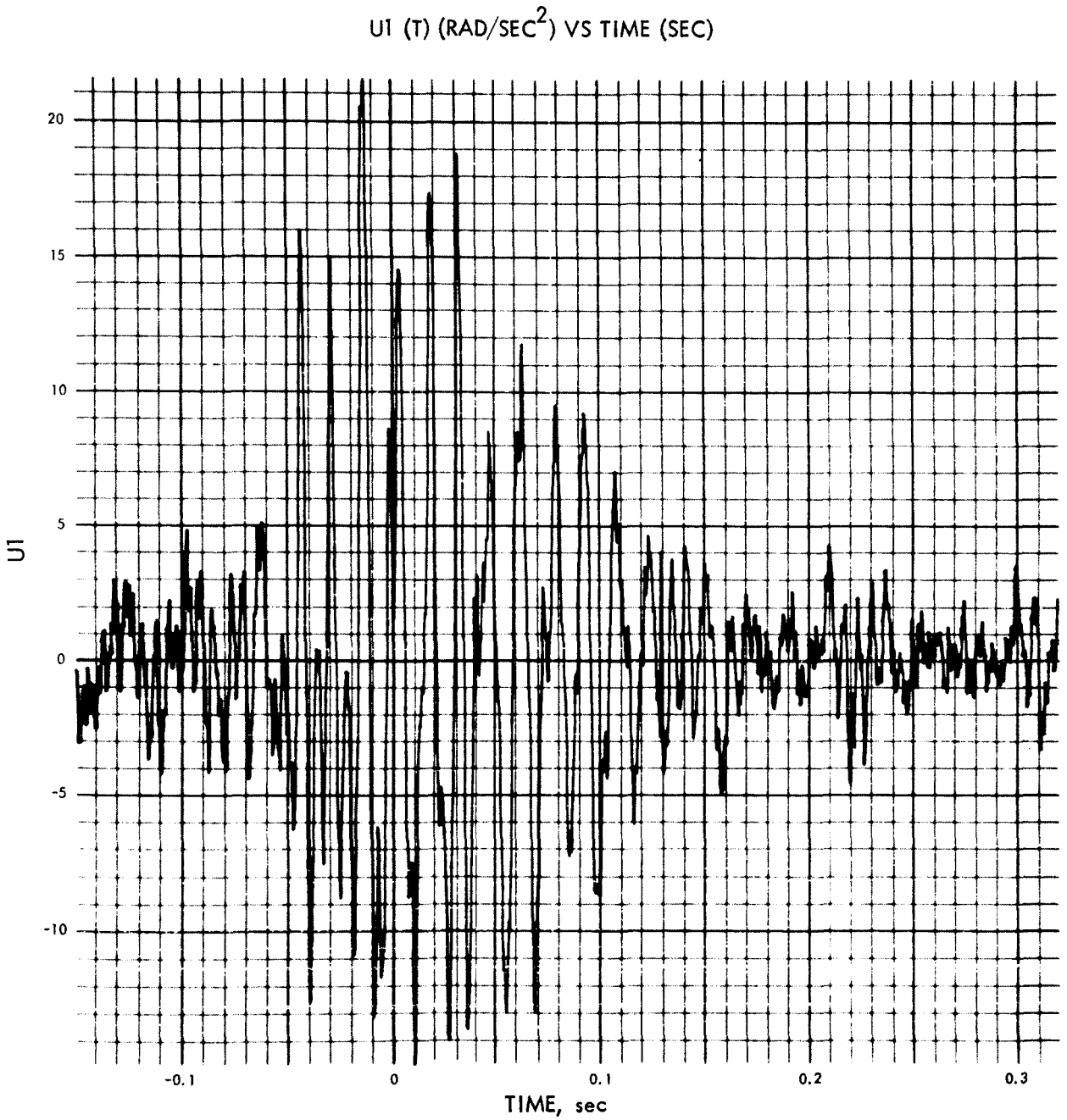

Fig. E-1. RA-6 torsional flight acceleration, time history (pulse 1)

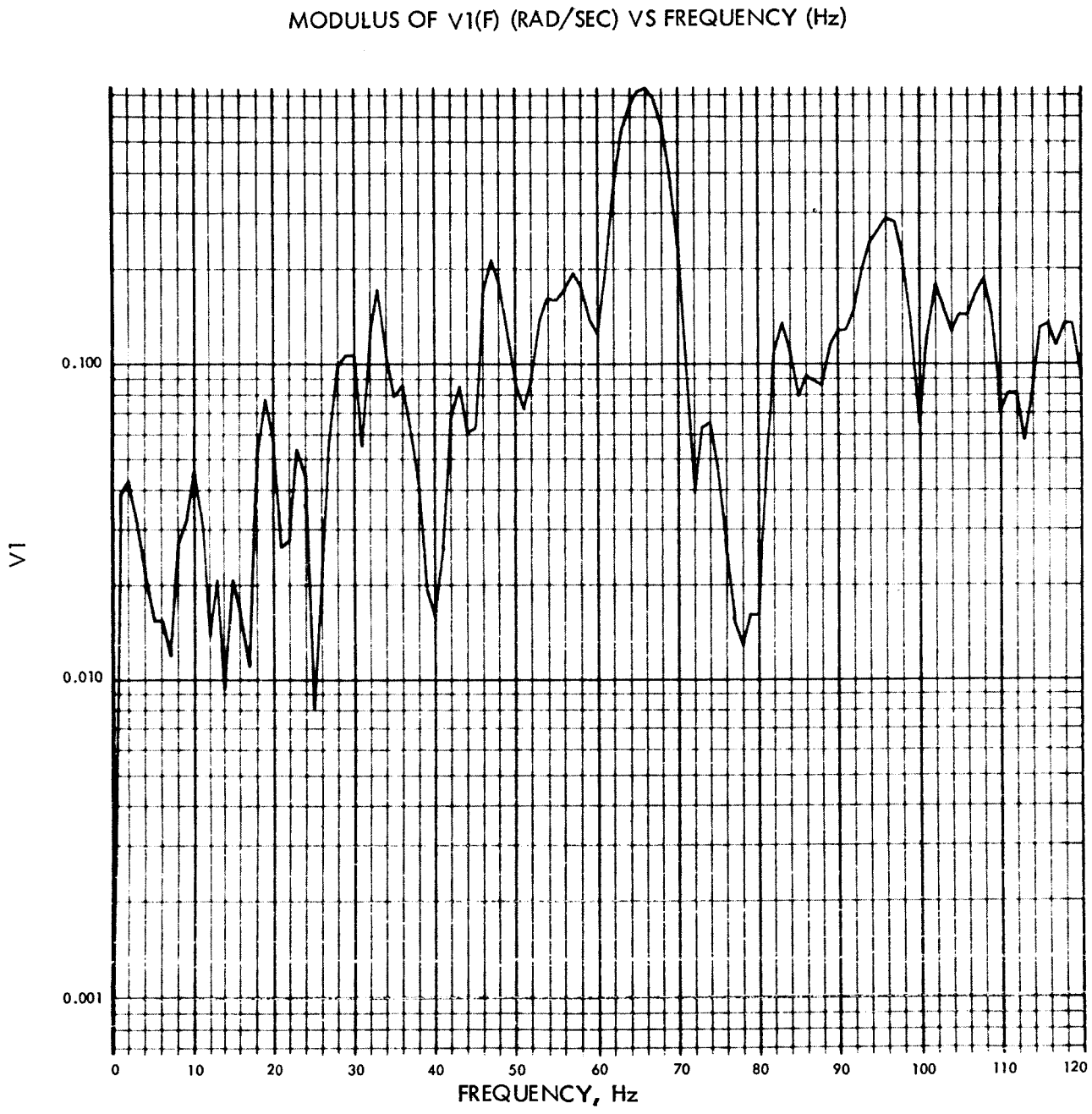

Fig. E-2. RA-6 torsional flight acceleration, Fourier transform, modulus (pulse 1)

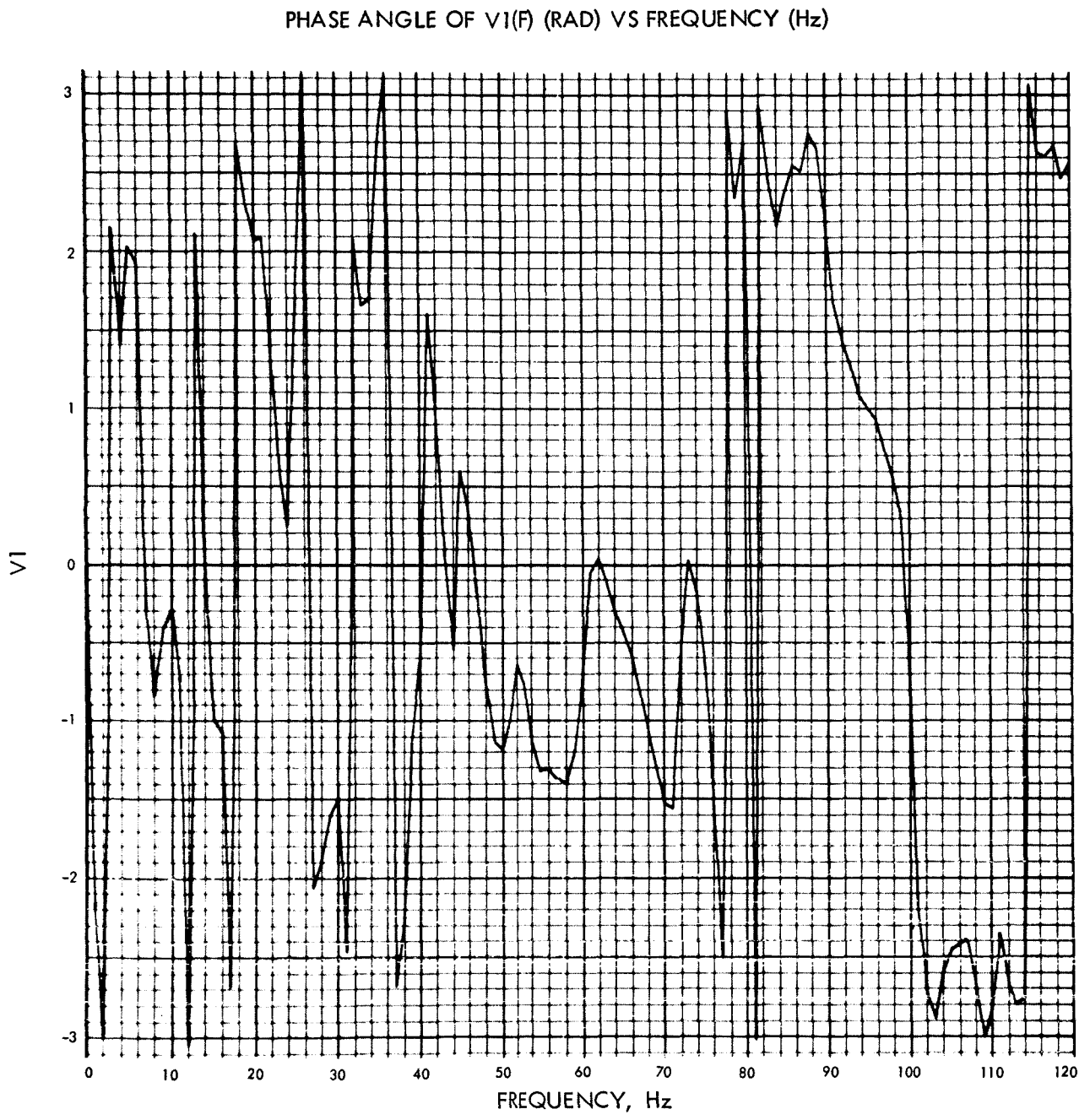

Fig. E-3. RA-6 torsional flight acceleration, Fourier transform, phase angle (pulse 1)

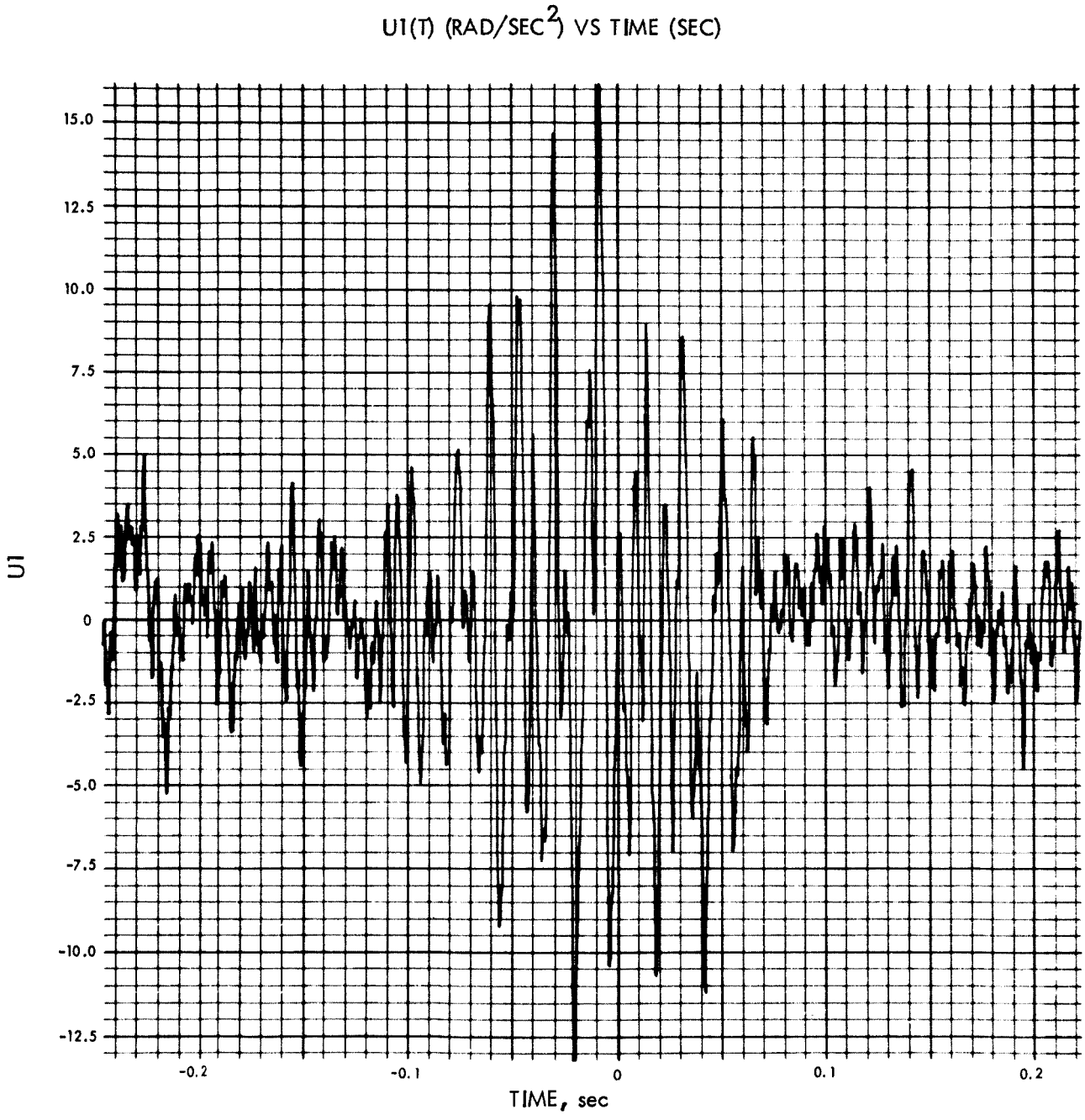

Fig. E-4. RA-7 torsional flight acceleration, time history (pulse 2)

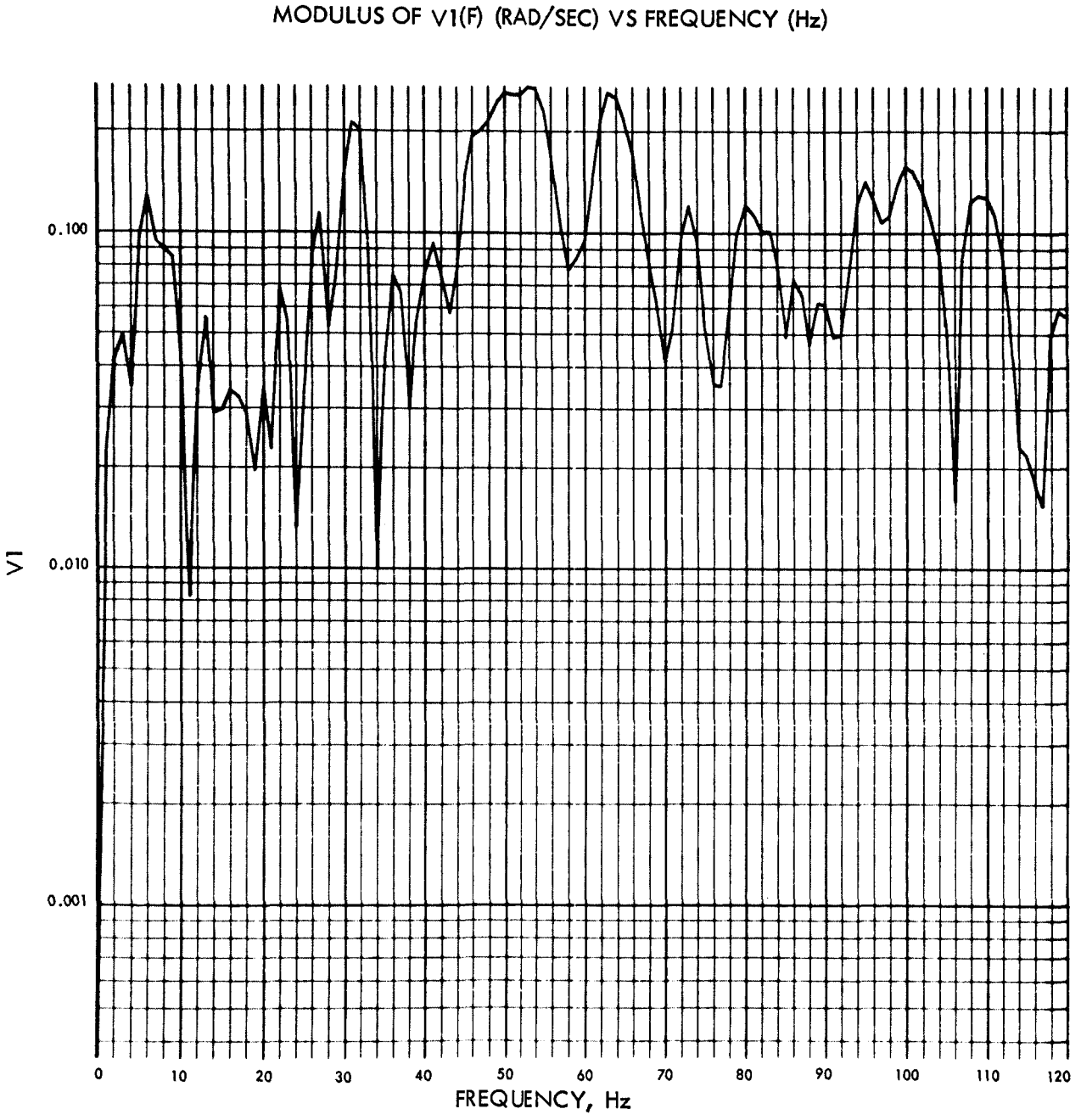

Fig. E-5. RA-7 torsional flight acceleration, Fourier transform, modulus (pulse 2)

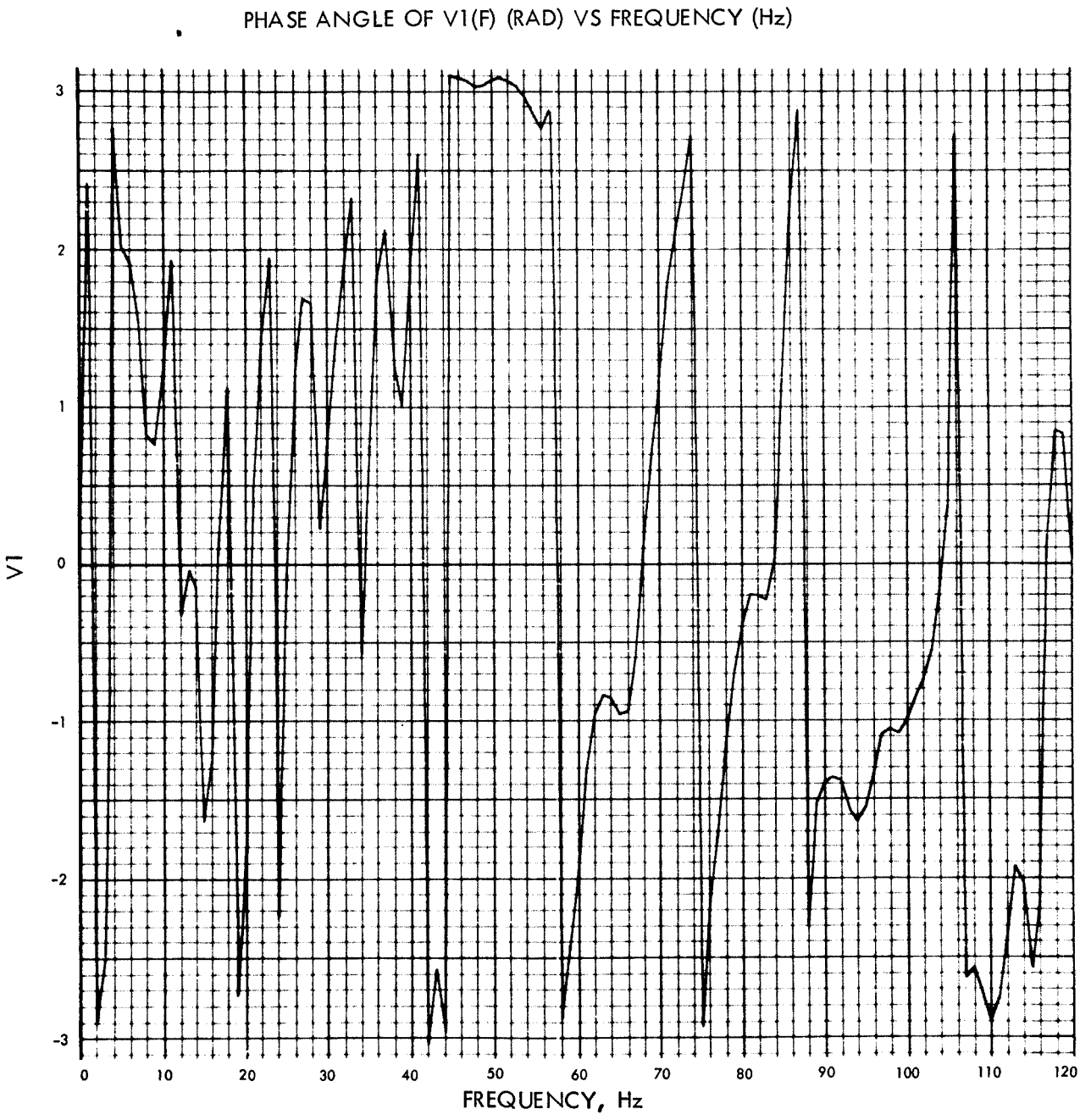

Fig. E-6. RA-7 torsional flight acceleration, Fourier transform, phase angle (pulse 2)

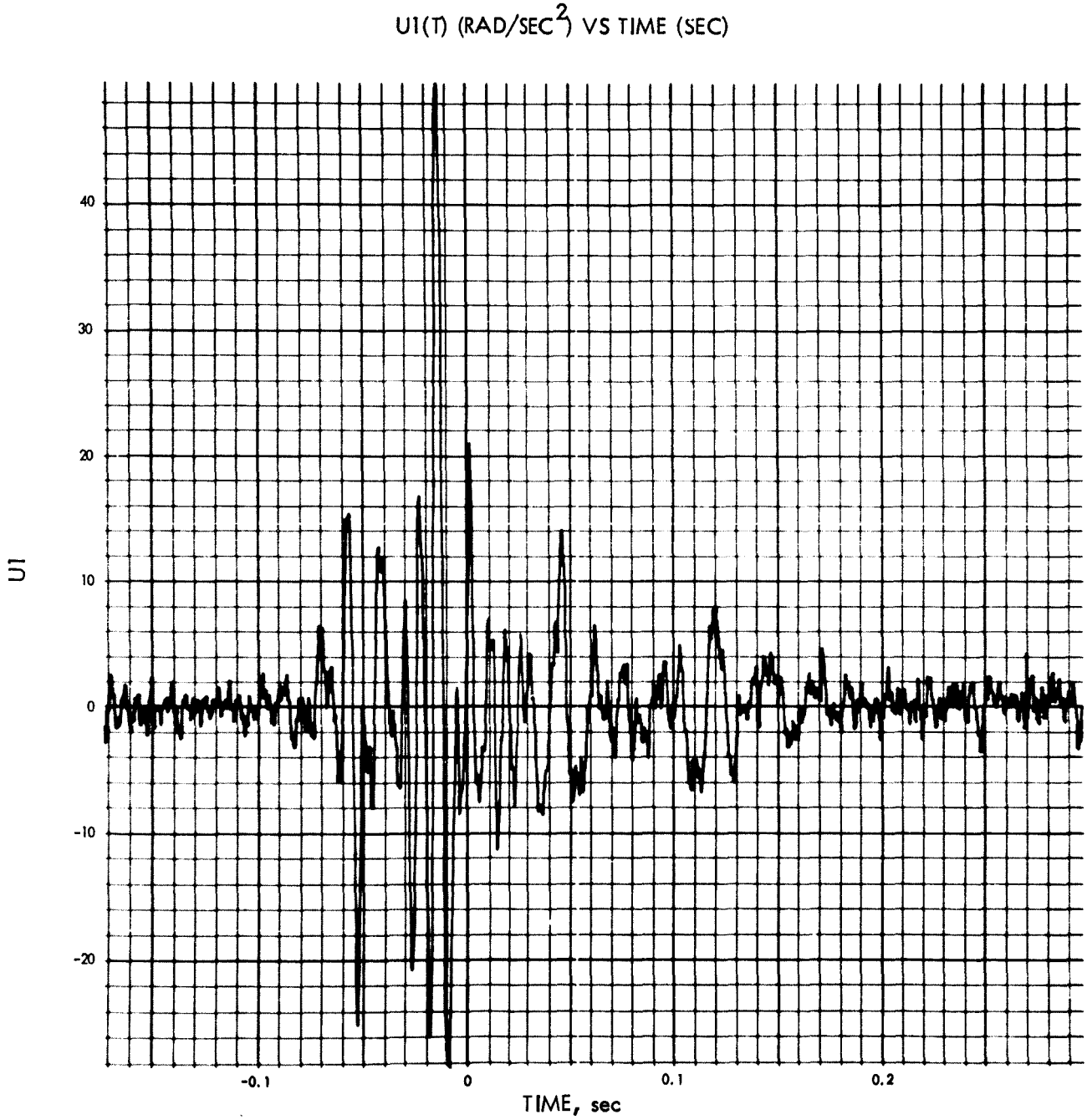

Fig. E-7. RA-8 torsional flight acceleration, time history (pulse 3)

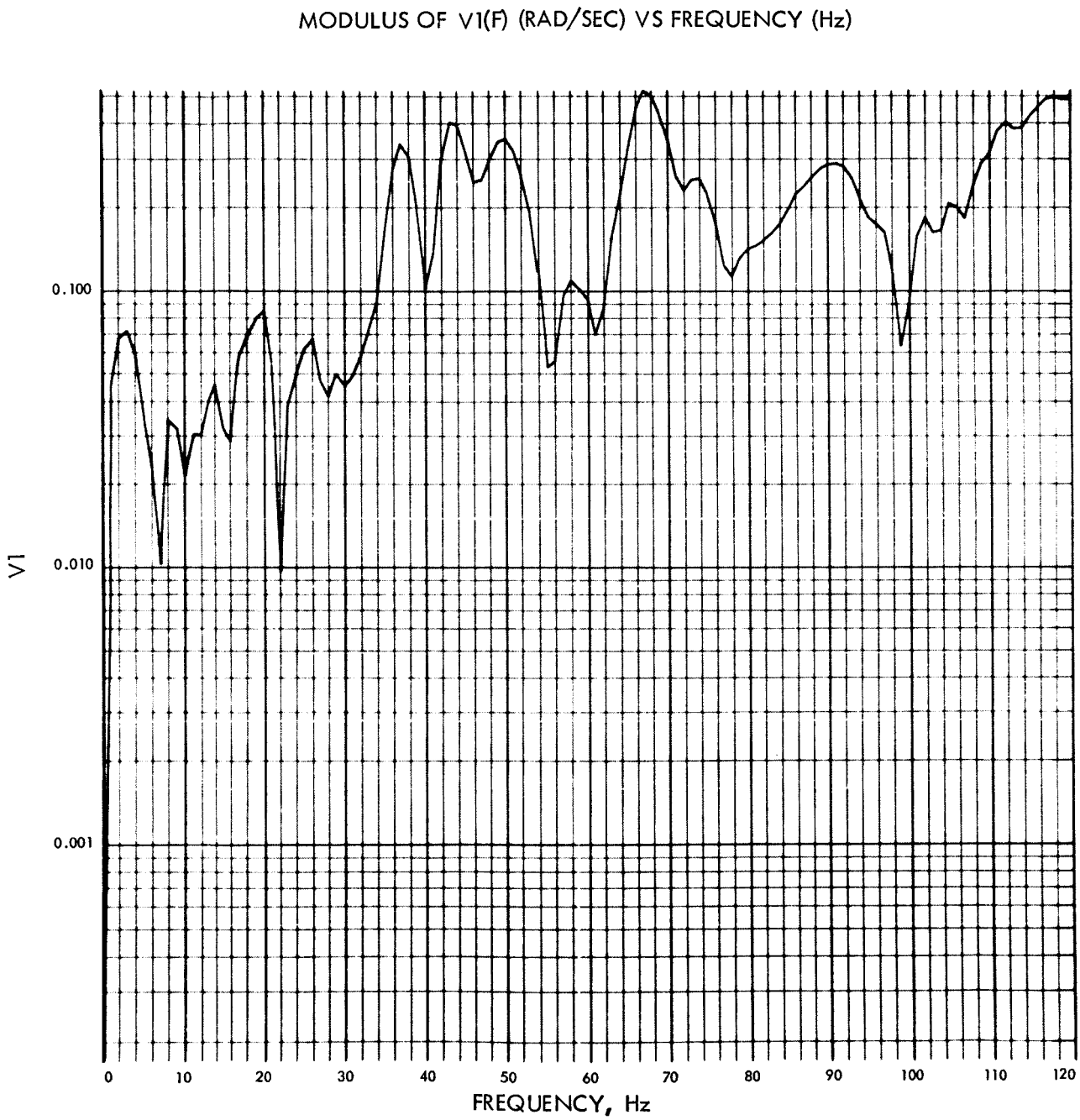

Fig. E-8. RA-8 torsional flight acceleration, Fourier transform, modulus (pulse 3)

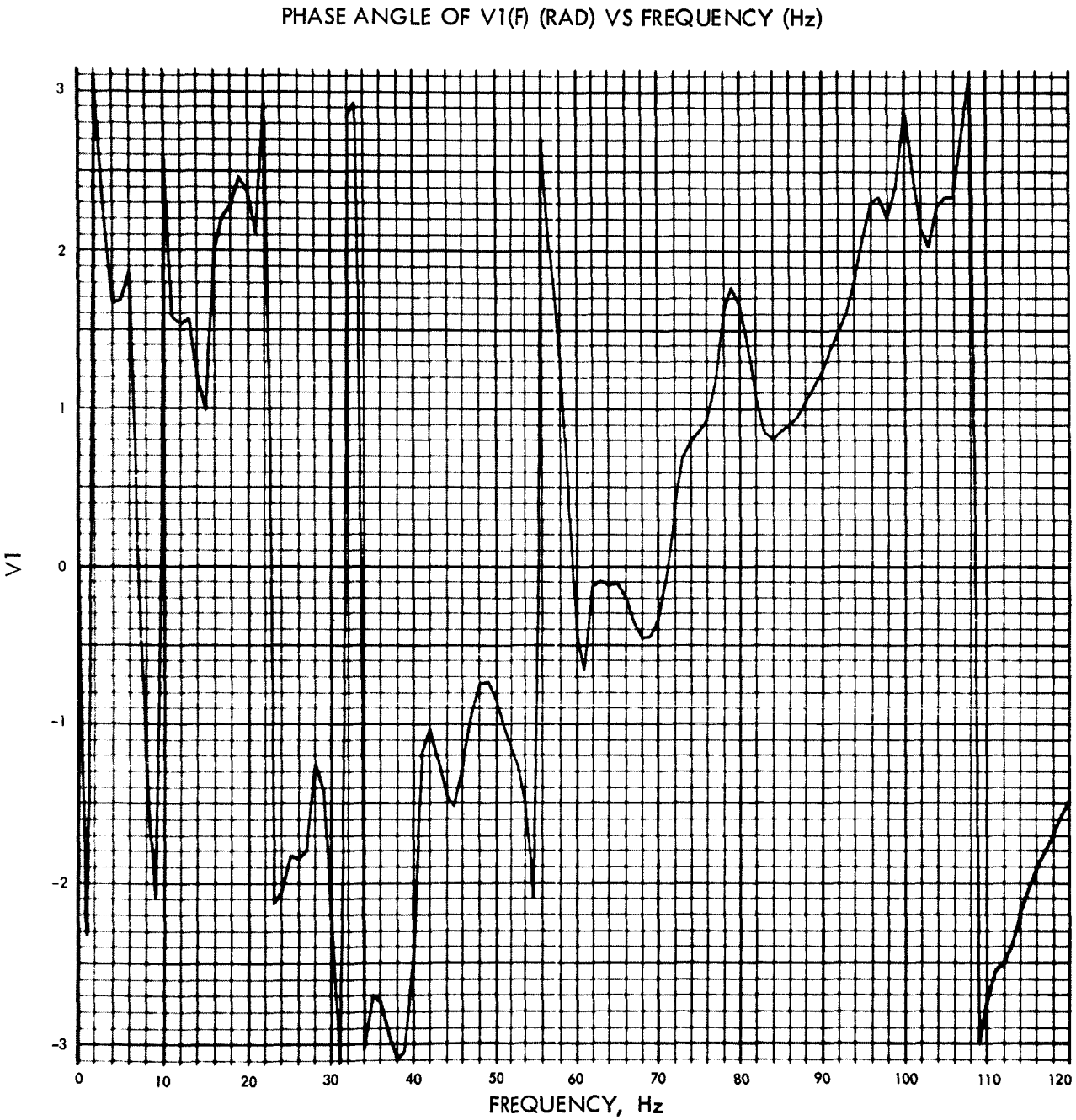

Fig. E-9. RA-8 torsional flight acceleration, Fourier transform, phase angle (pulse 3)

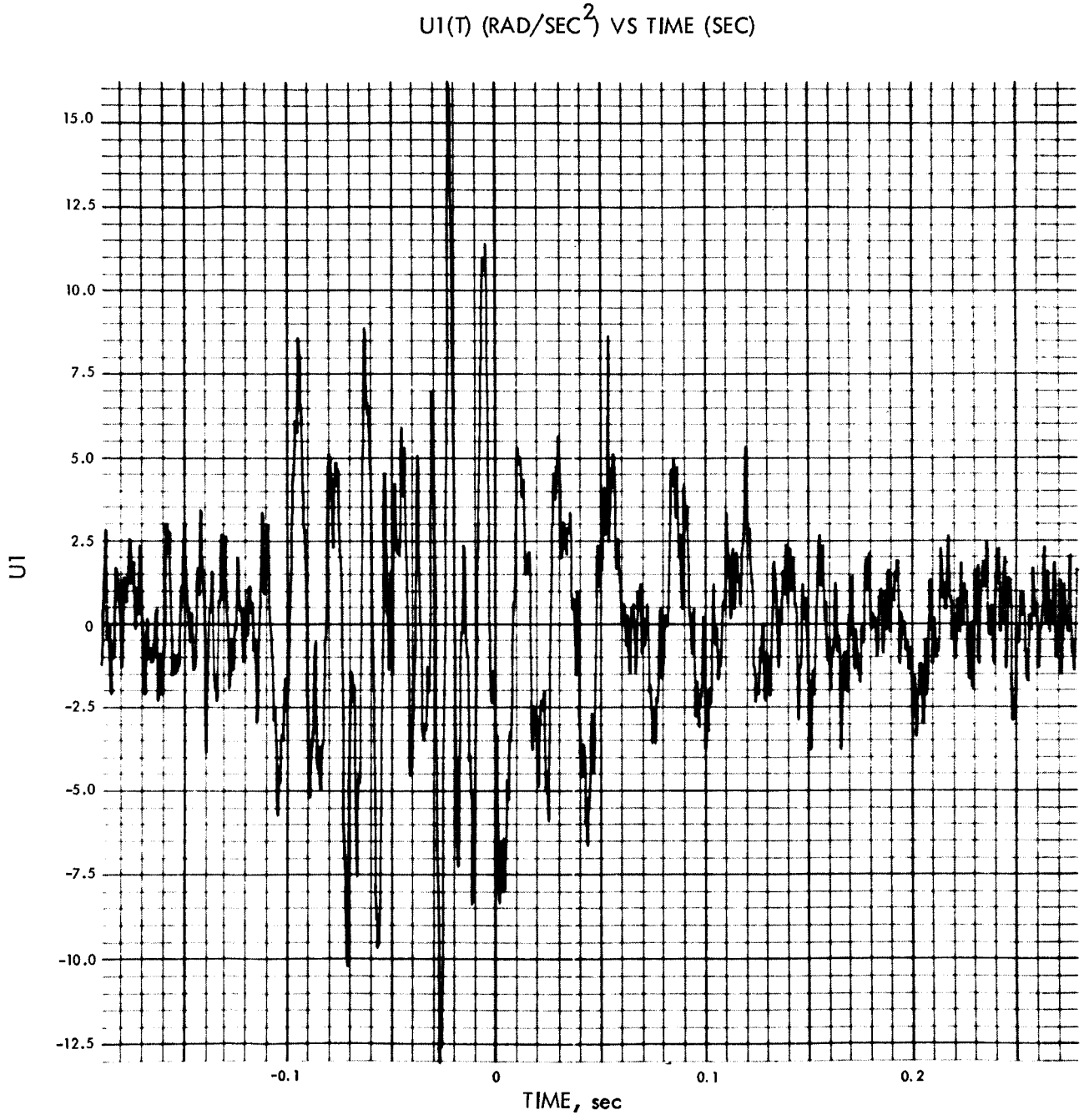

Fig. E-10. RA-9 torsional flight acceleration, time history (pulse 4)

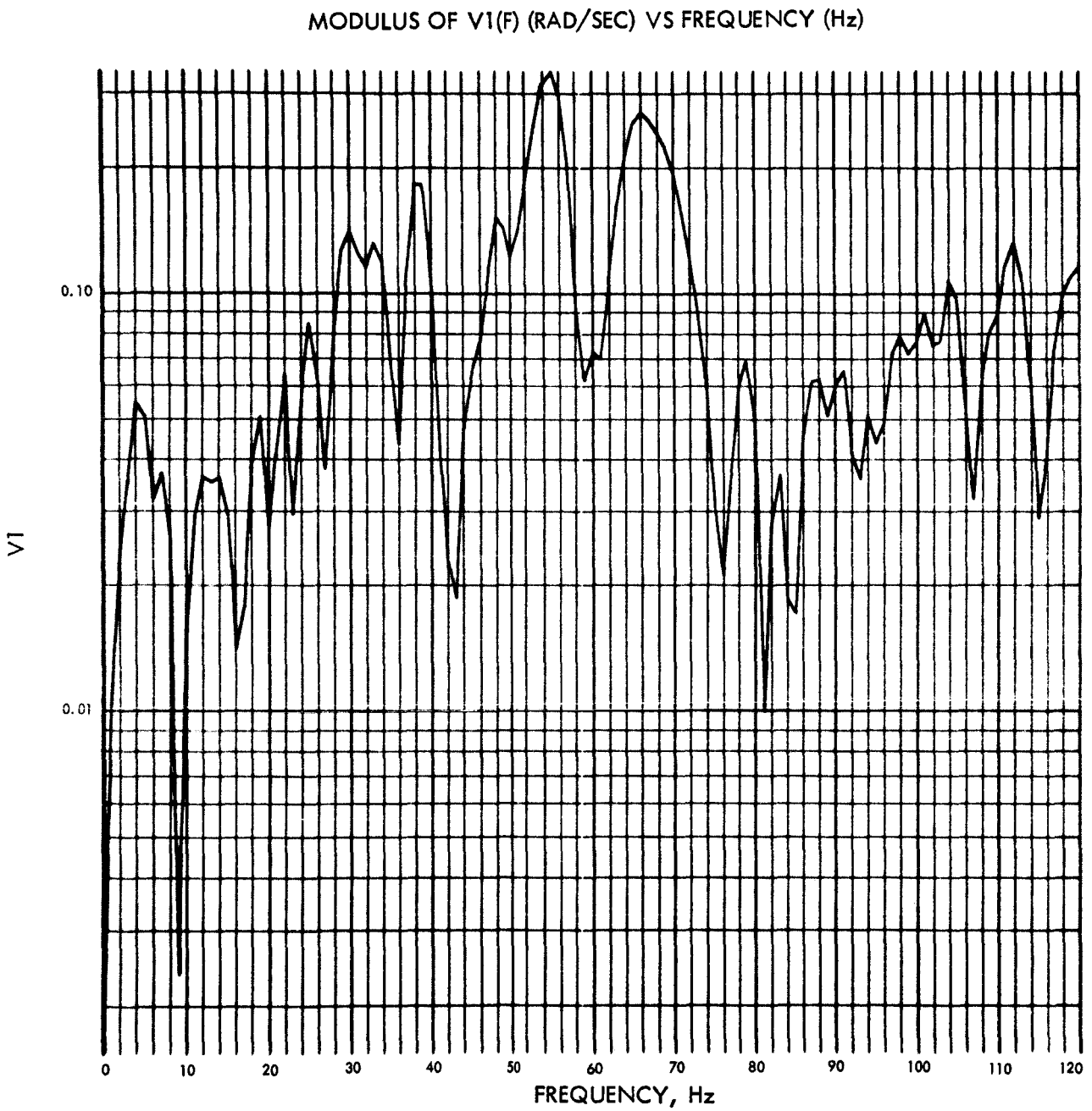

Fig. E-11. RA-9 torsional flight acceleration, Fourier transform, modulus (pulse 4)

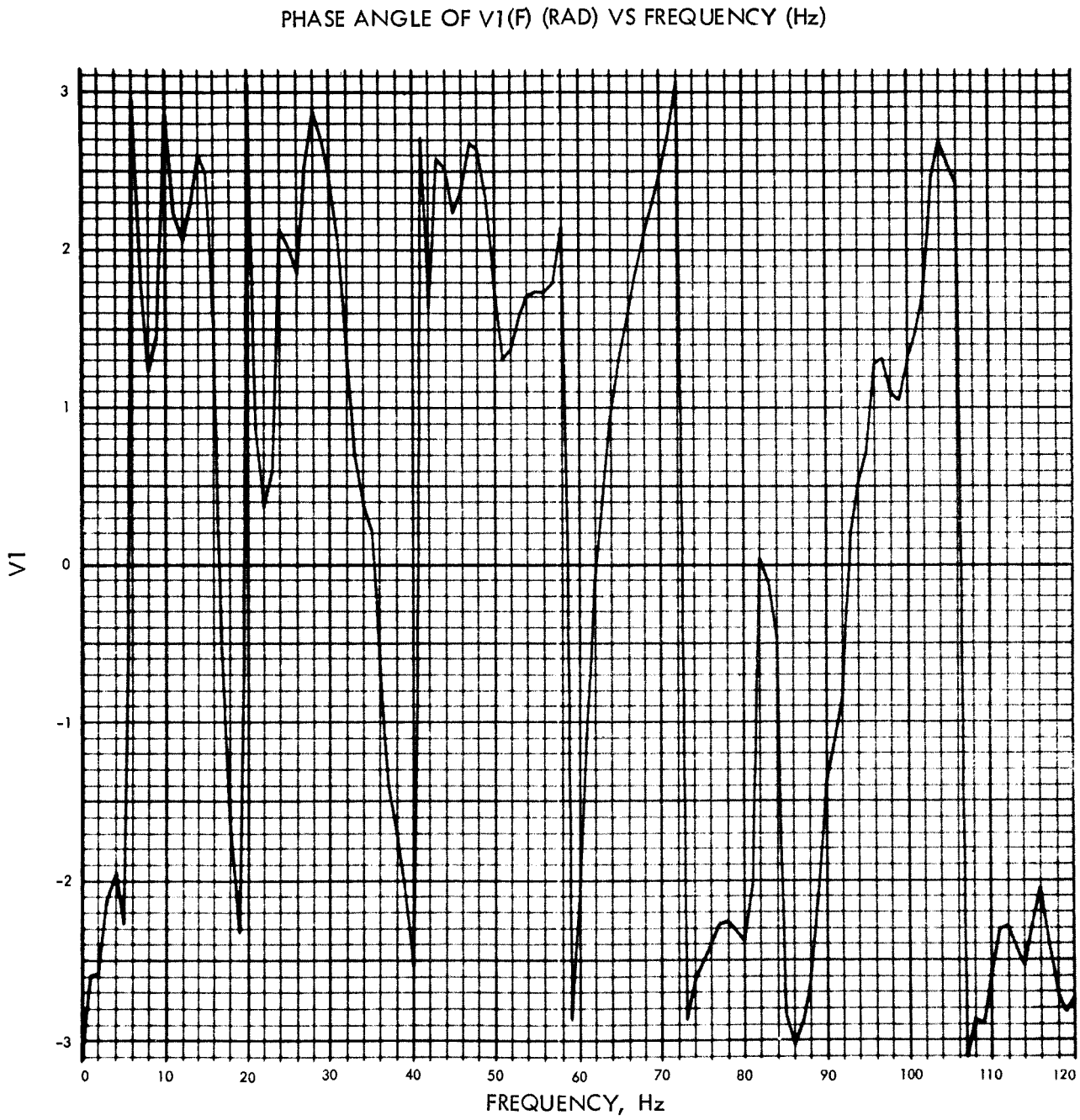

Fig. E-12. RA-9 torsional flight acceleration, Fourier transform, phase angle (pulse 4)

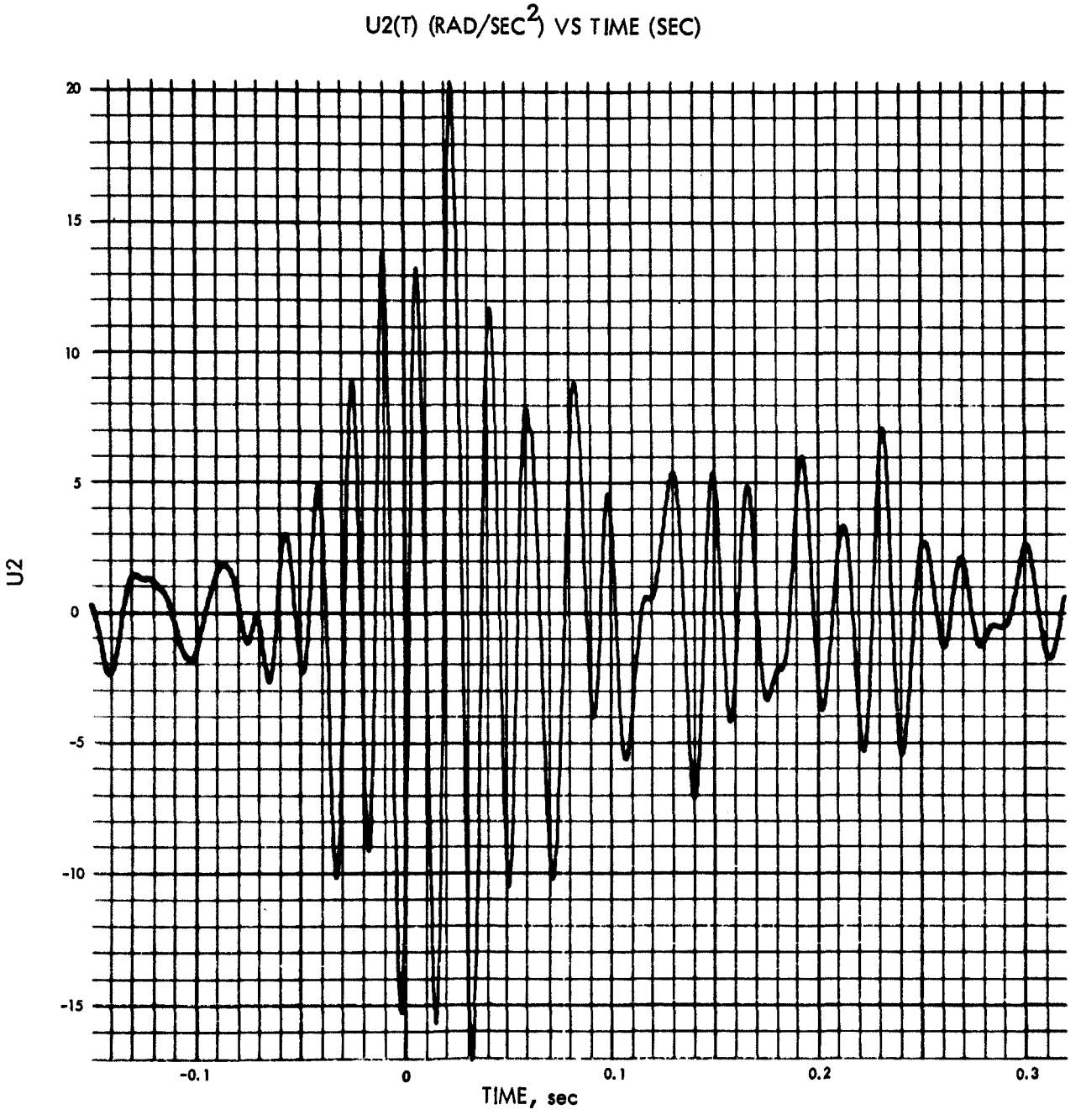

Fig. E-13. Spacecraft base acceleration, Joint 7, time history (pulse 1)

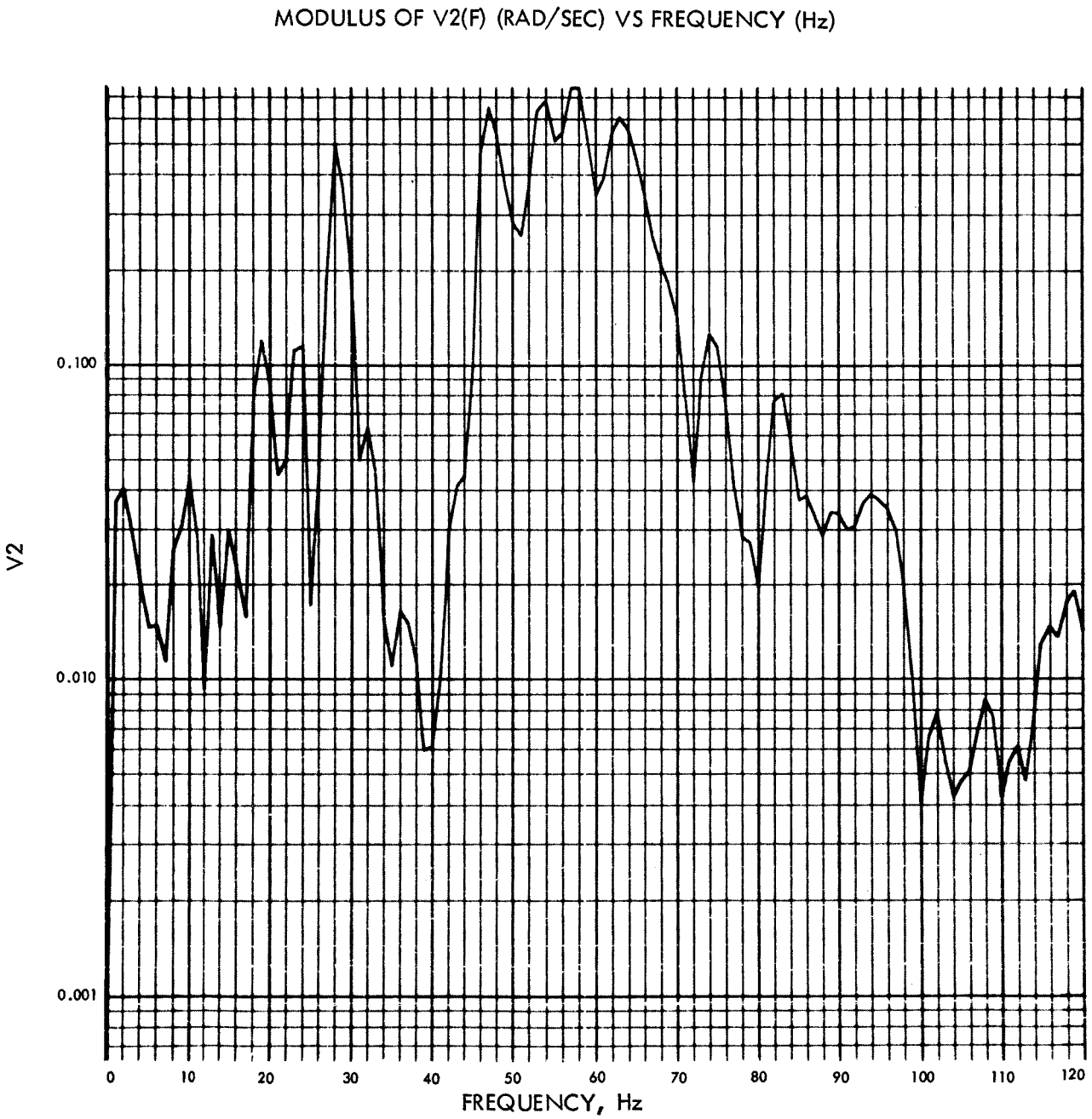

Fig. E-14. Spacecraft base acceleration, Joint 7, Fourier transform, modulus (pulse 1)

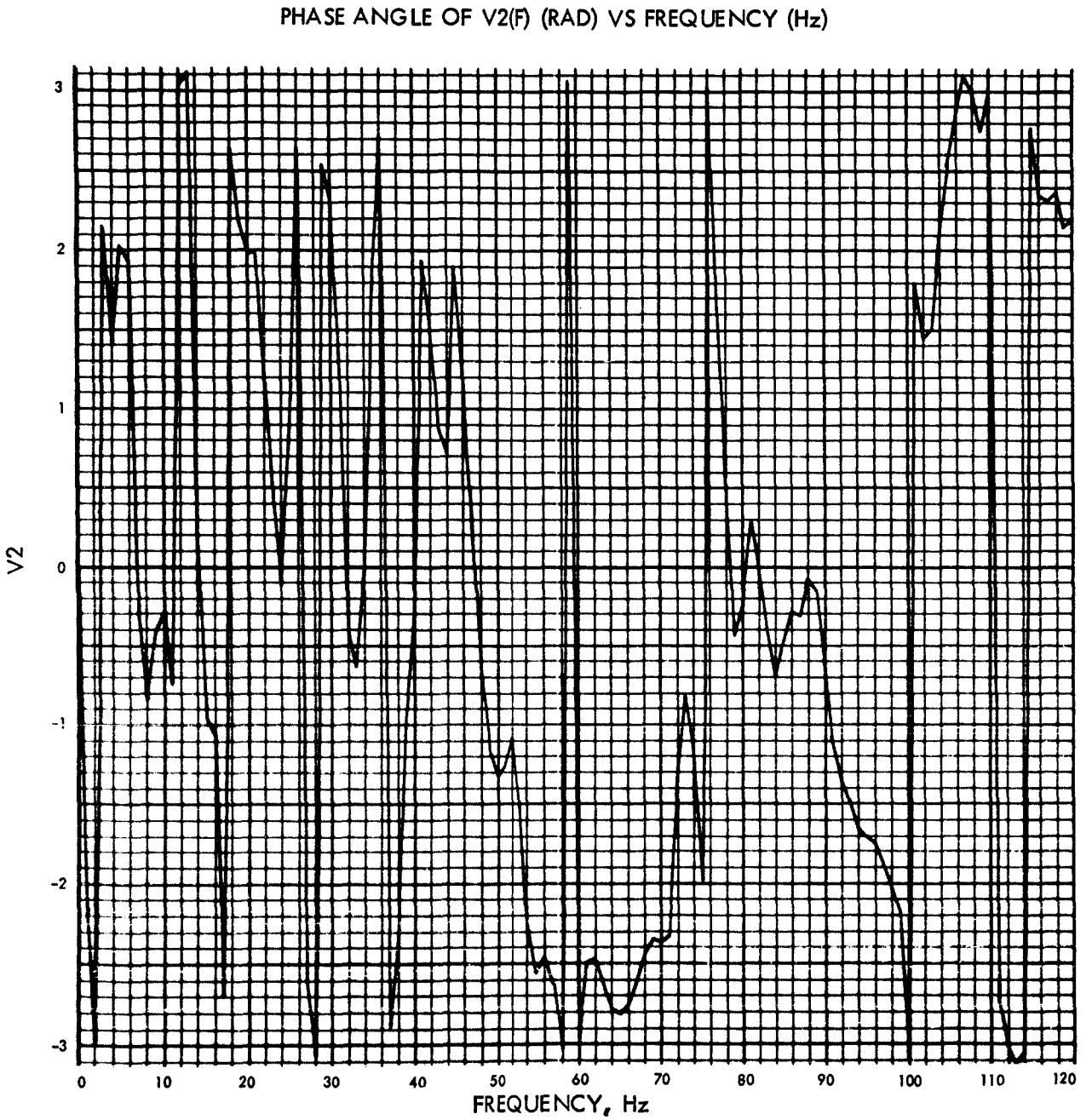

Fig. E-15. Spacecraft base acceleration, Joint 7, Fourier transform, phase angle (pulse 1)

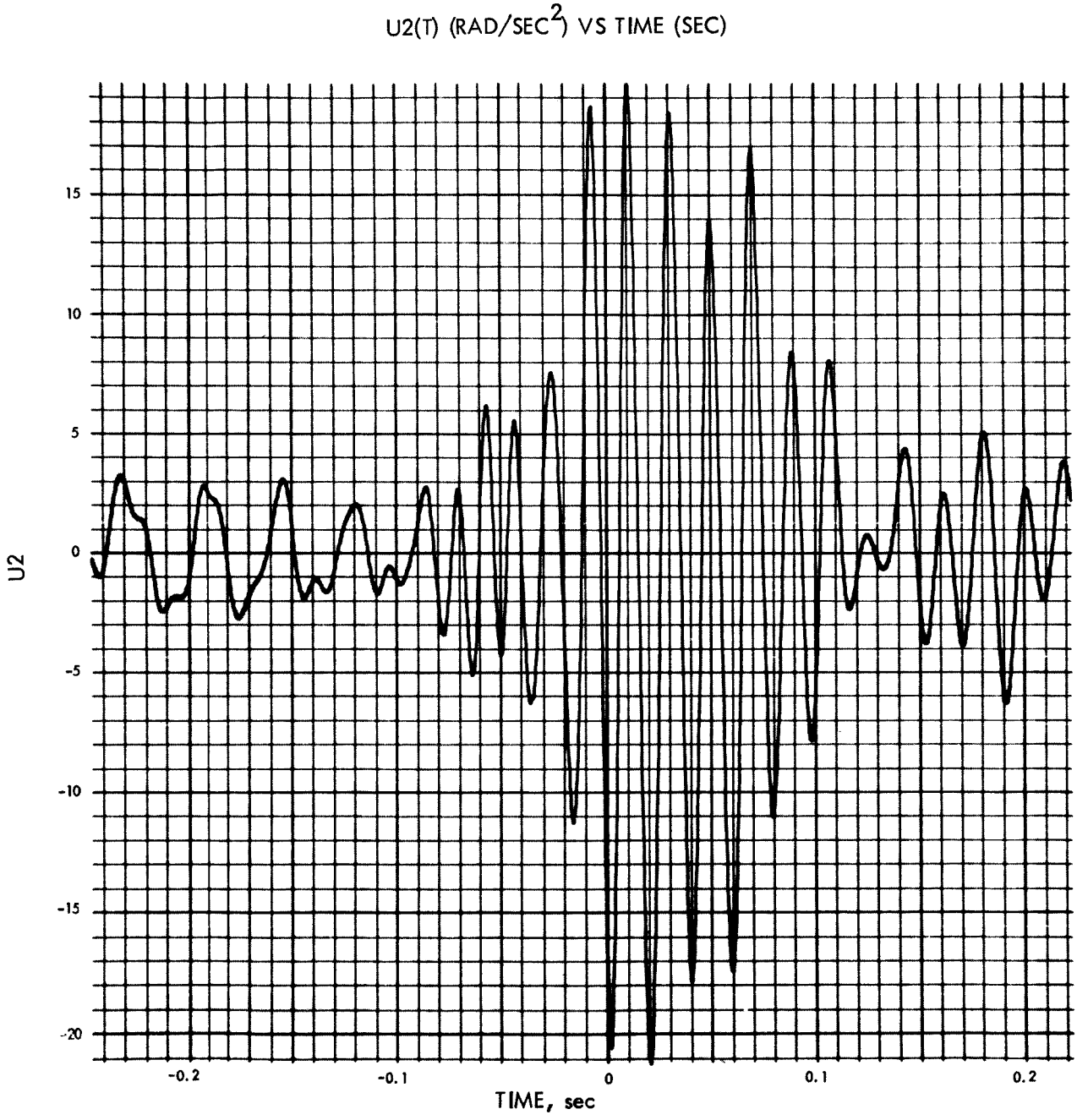

Fig. E-16. Spacecraft base acceleration, Joint 7, time history (pulse 2)

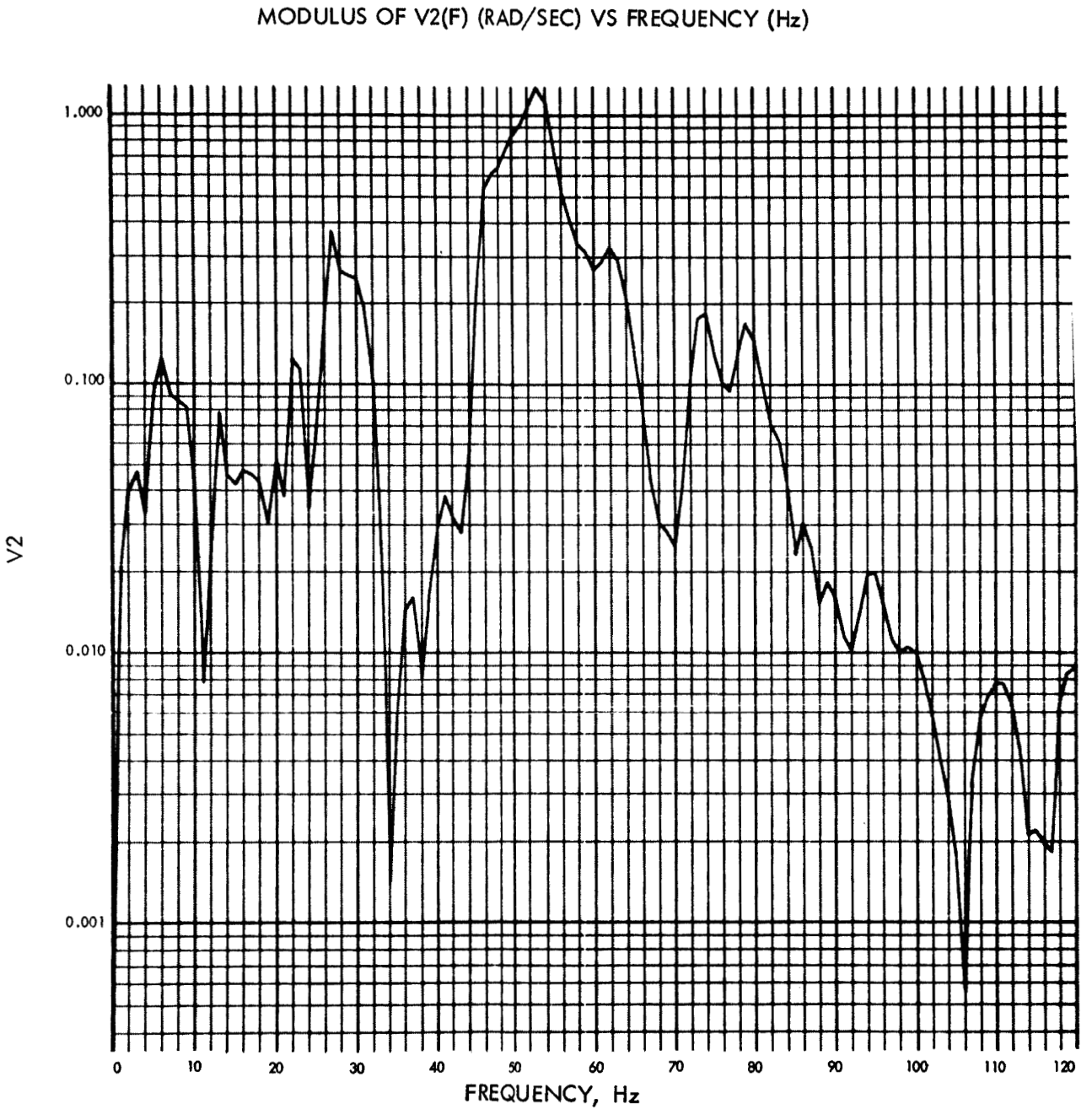

Fig. E-17. Spacecraft base acceleration, Joint 7, Fourier transform, modulus (pulse 2)

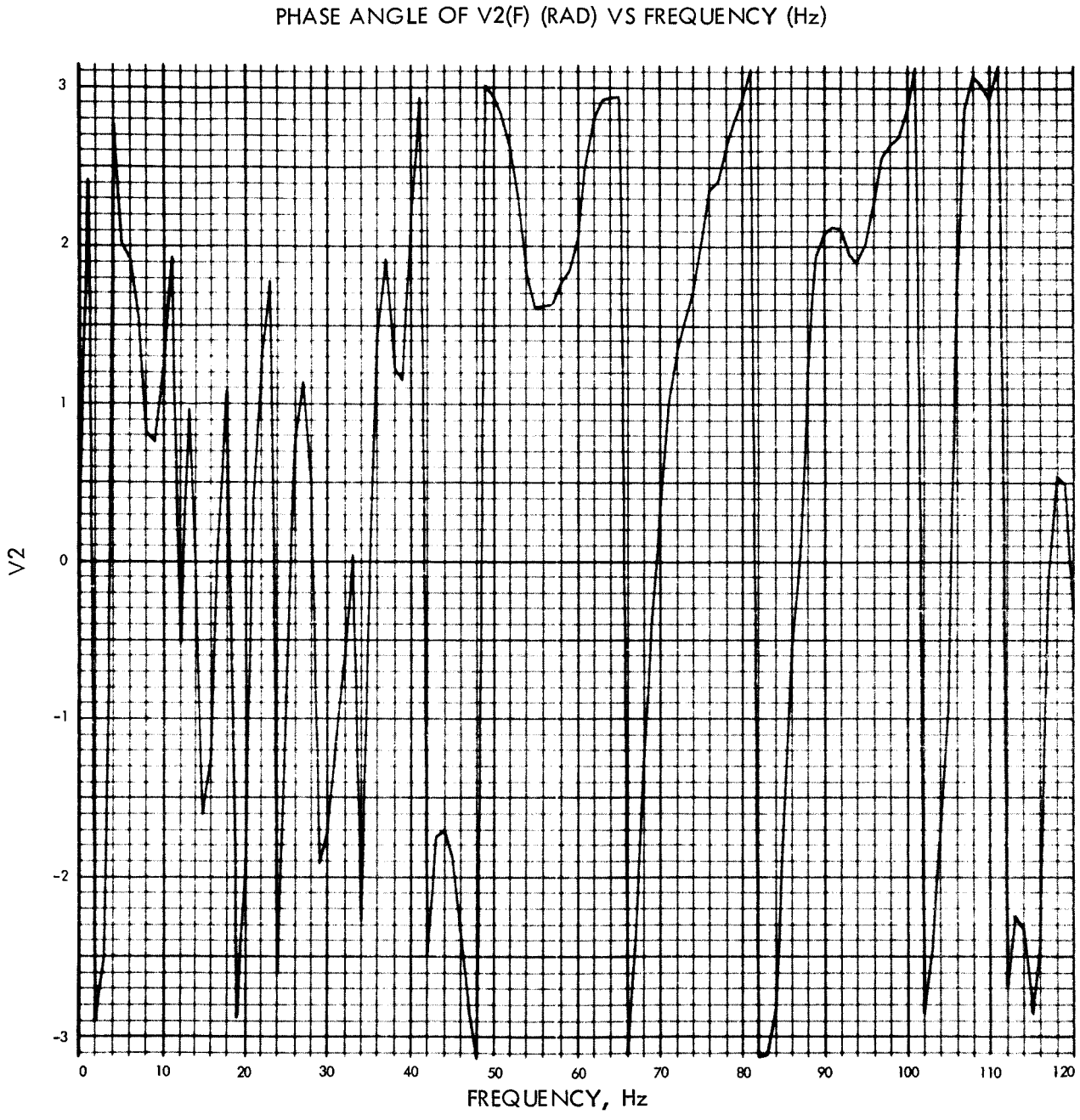

Fig. E-18. Spacecraft base acceleration, Joint 7, Fourier transform, phase angle (pulse 2)

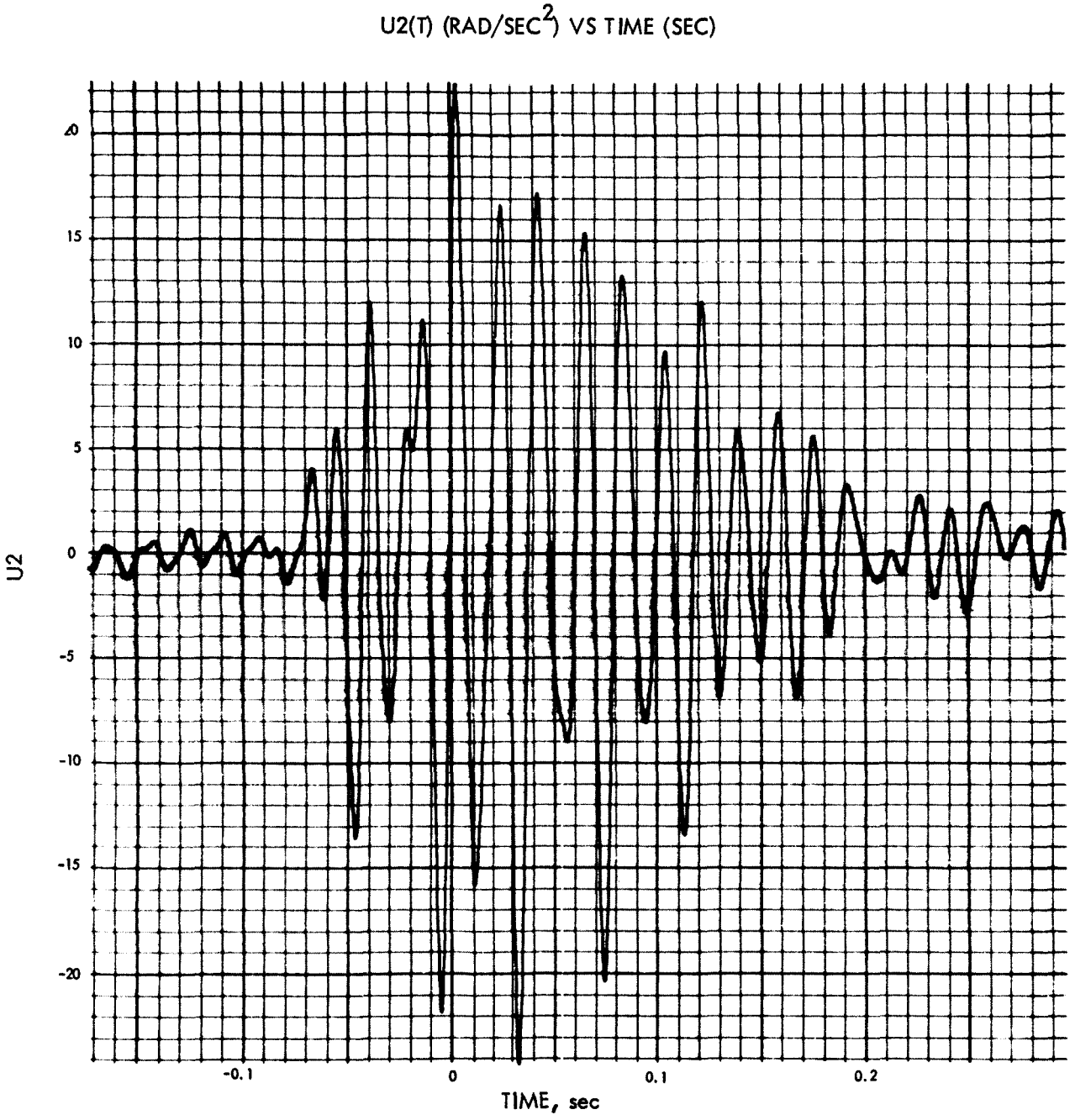

Fig. E-19. Spacecraft base acceleration, Joint 7, time history (pulse 3)

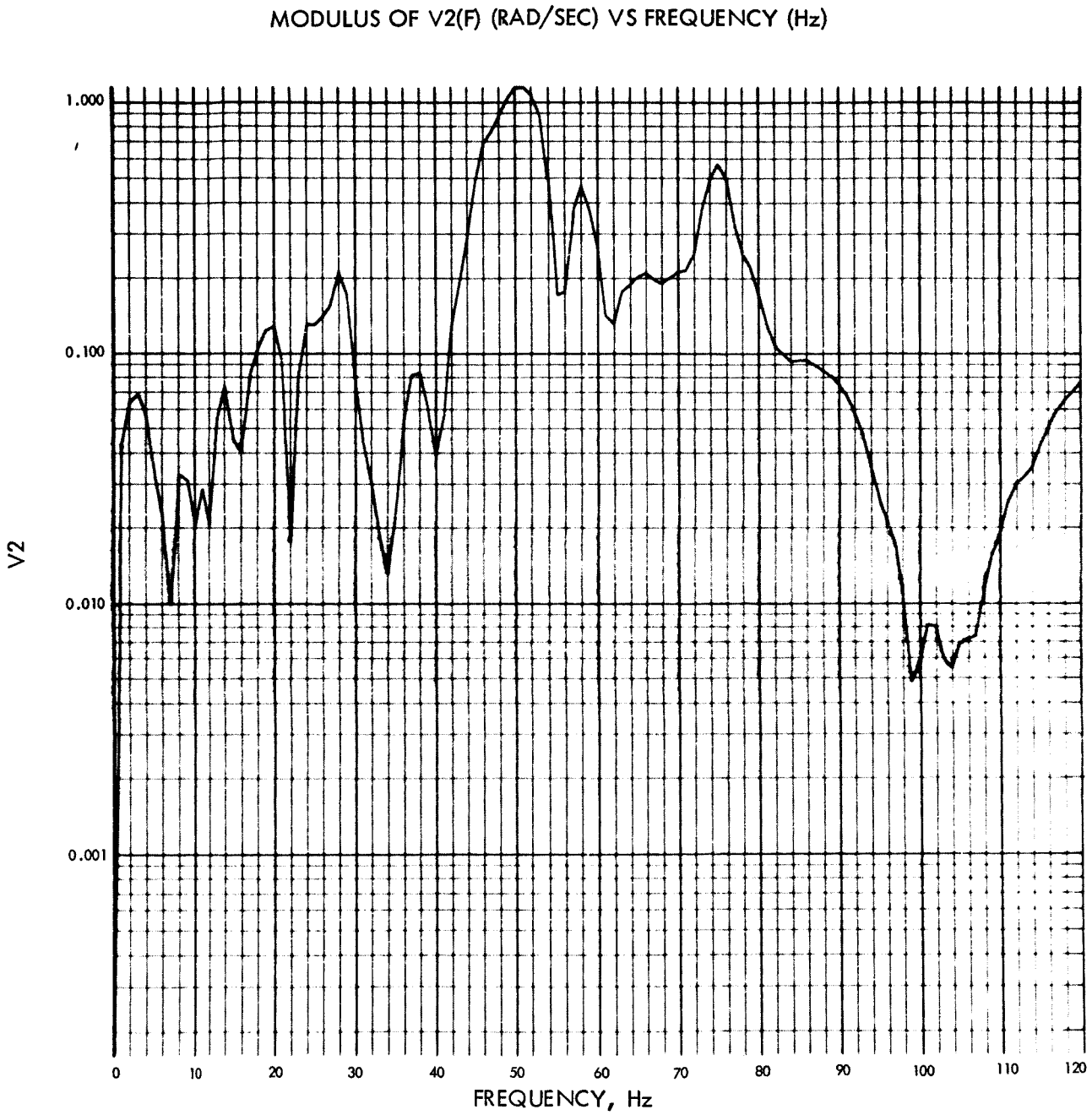

Fig. E-20. Spacecraft base acceleration, Joint 7, Fourier transform, modulus (pulse 3)

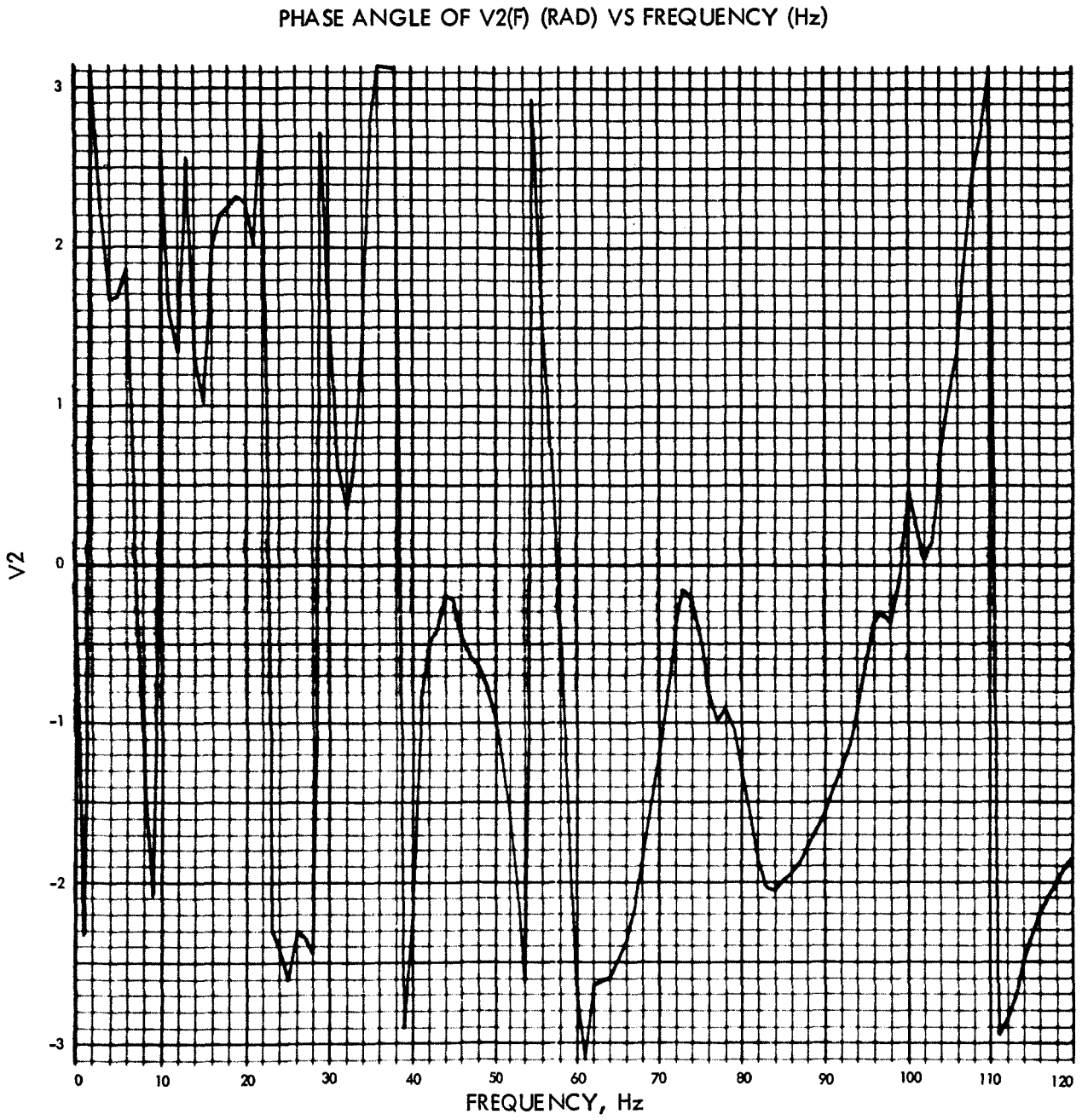

Fig. E-21. Spacecraft base acceleration, Joint 7, Fourier transform, phase angle (pulse 3)

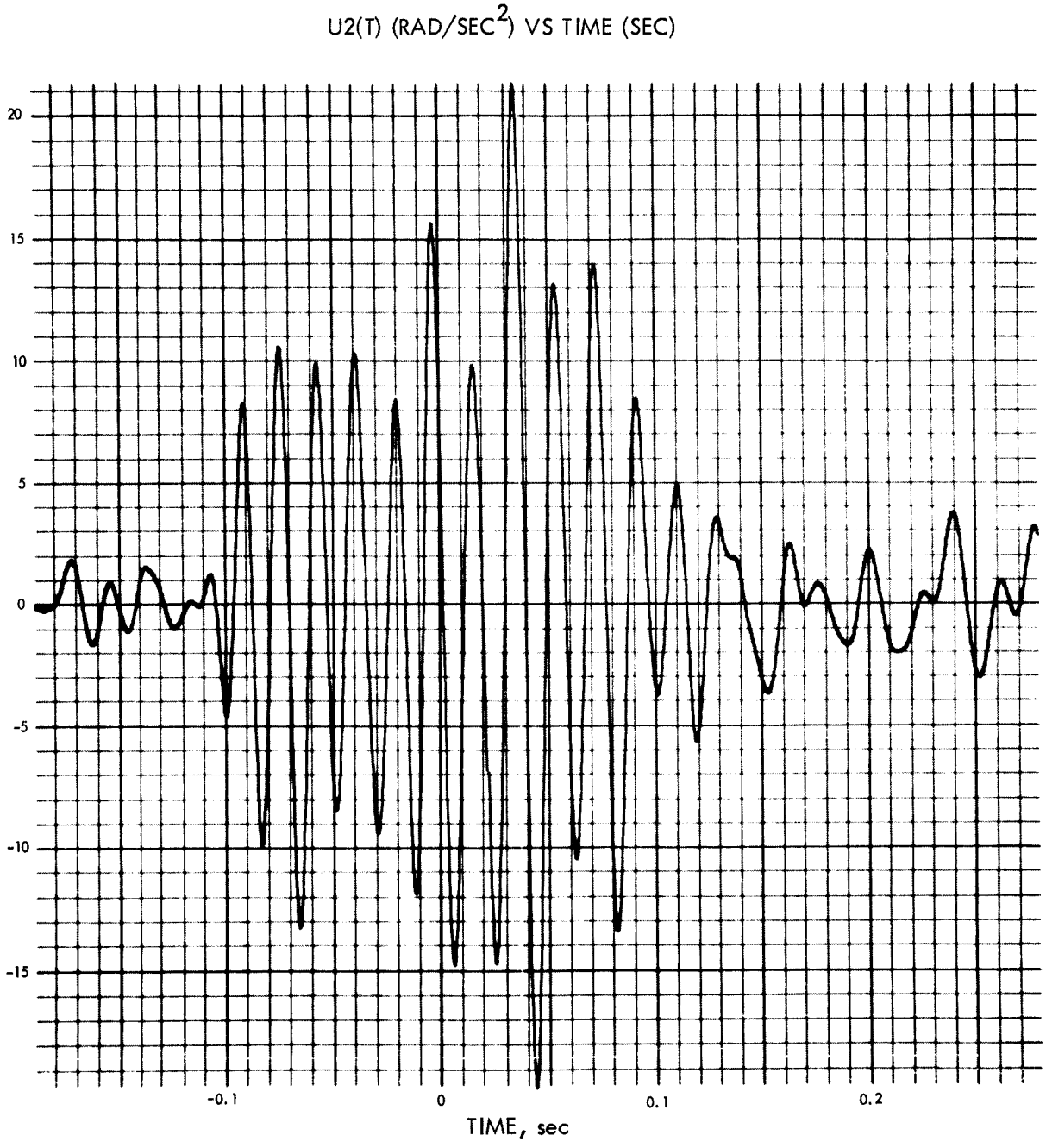

Fig. E-22. Spacecraft base acceleration, Joint 7, time history (pulse 4)

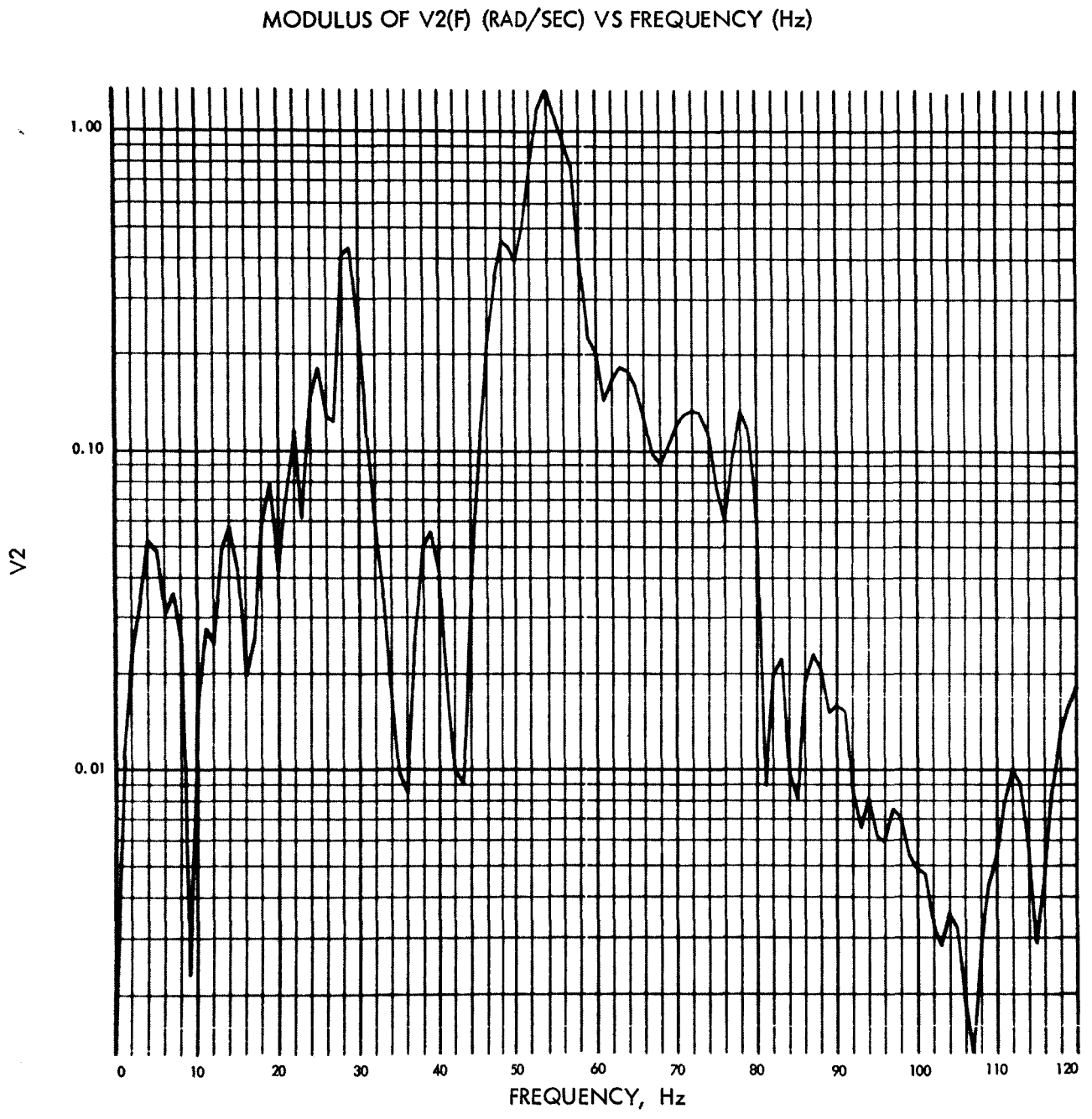

Fig. E-23. Spacecraft base acceleration, Joint 7, Fourier transform, modulus, (pulse 4)

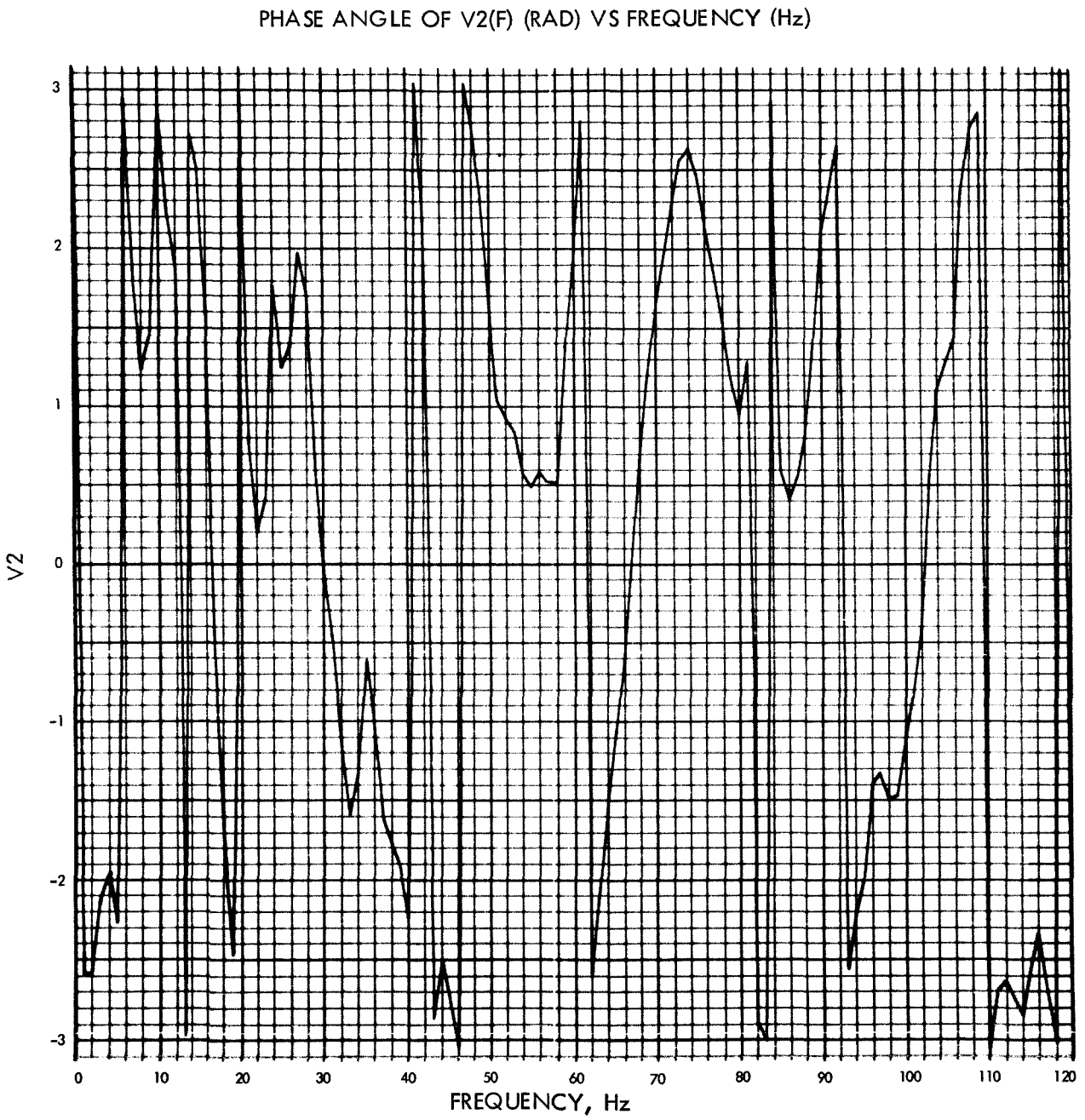

Fig. E-24. Spacecraft base acceleration, Joint 7, Fourier transform, phase angle (pulse 4)

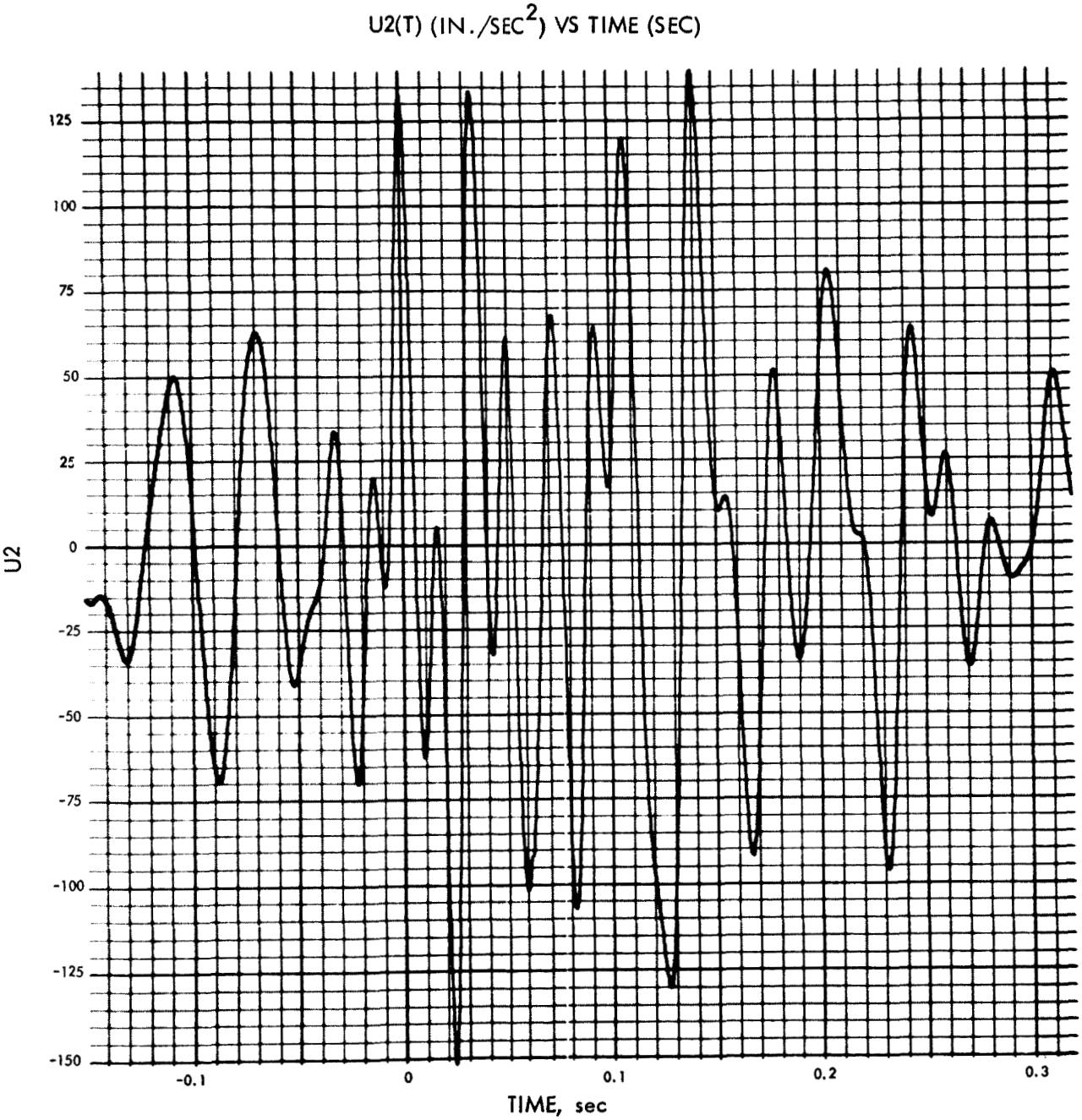

Fig. E-25. Joint 1, x_1 time history (pulse 1)

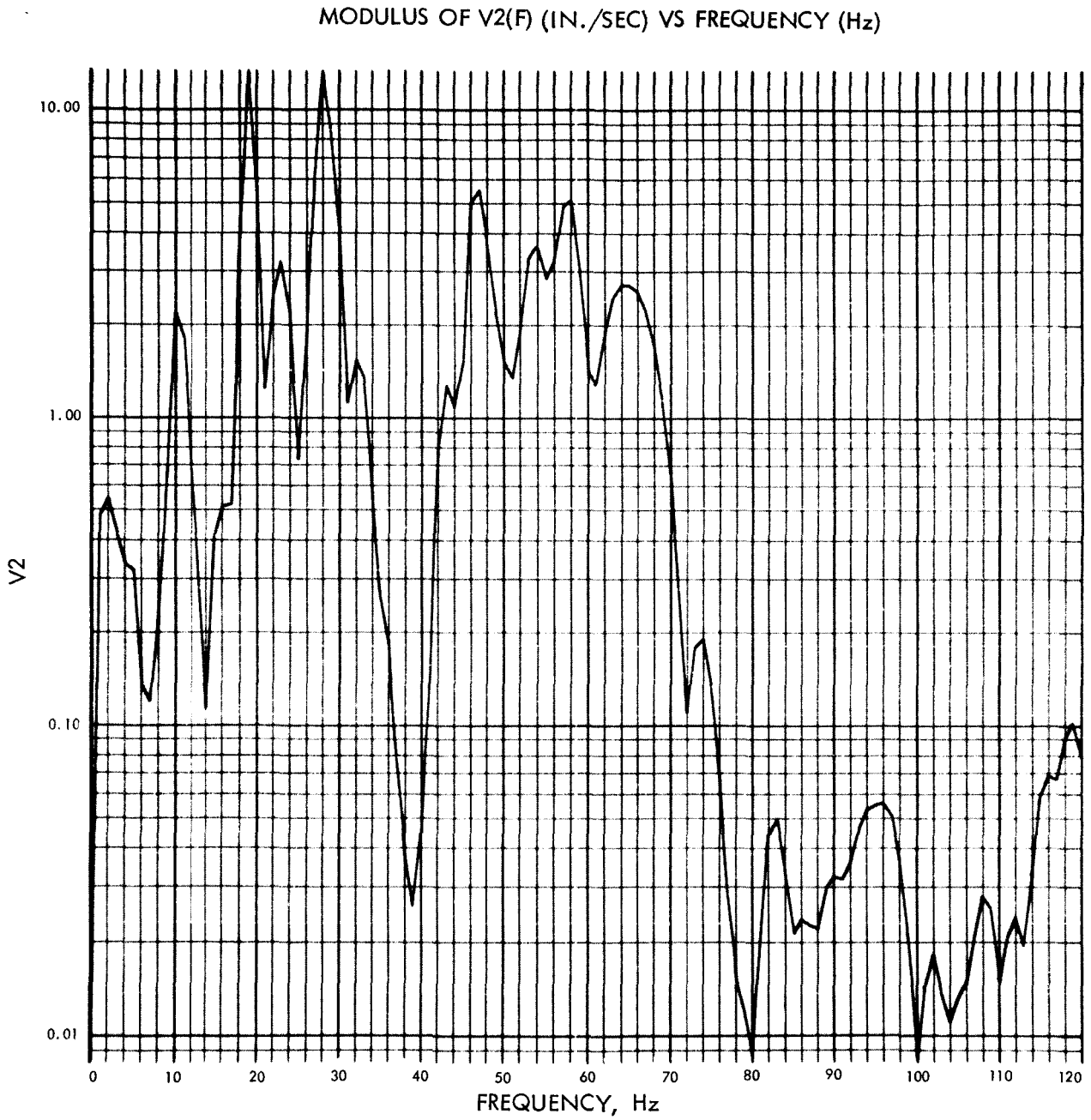

Fig. E-26. Joint 1, x_1 Fourier transform, modulus (pulse 1)

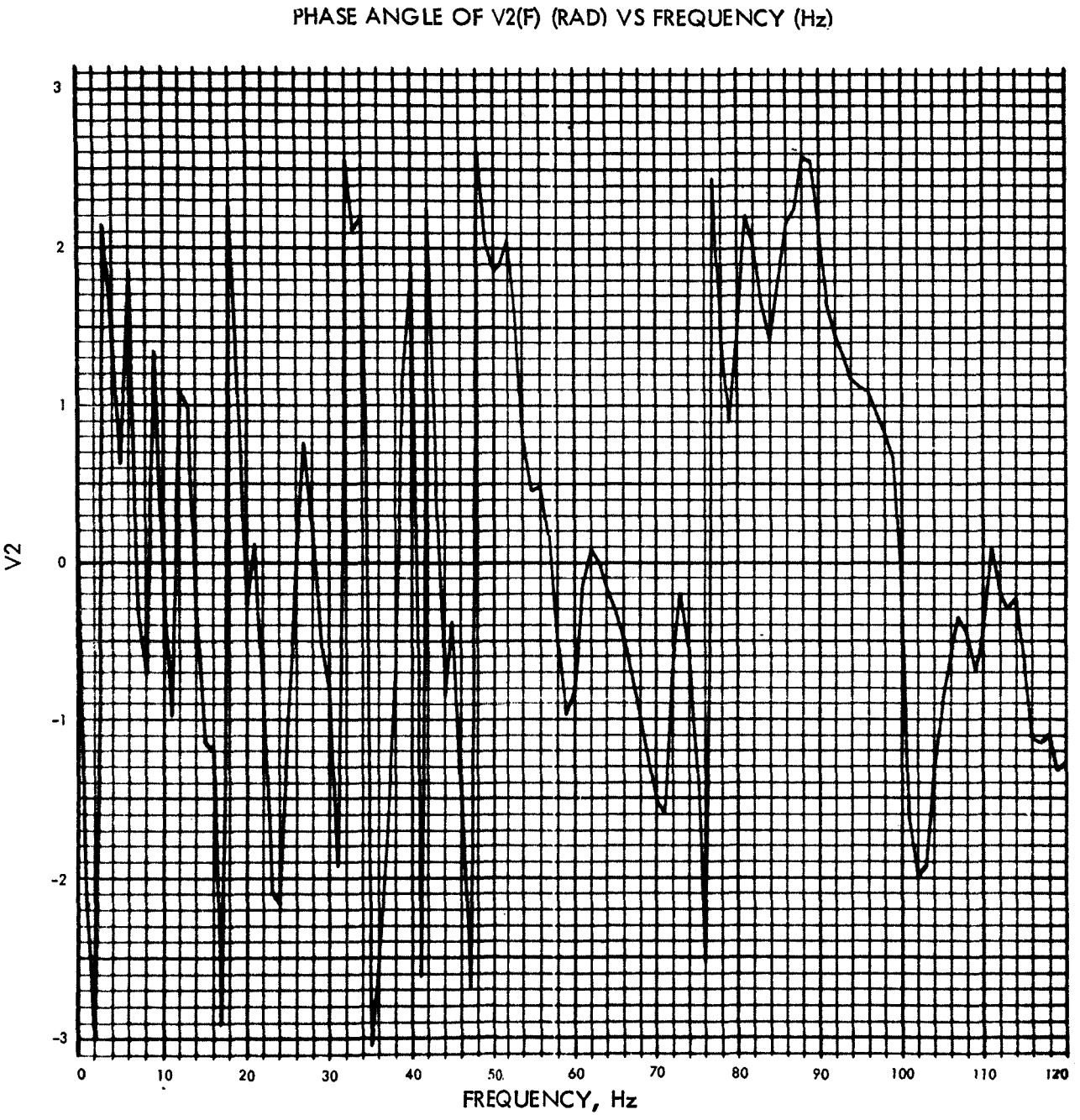

Fig. E-27. Joint 1, x_1 Fourier transform, phase angle (pulse 1)

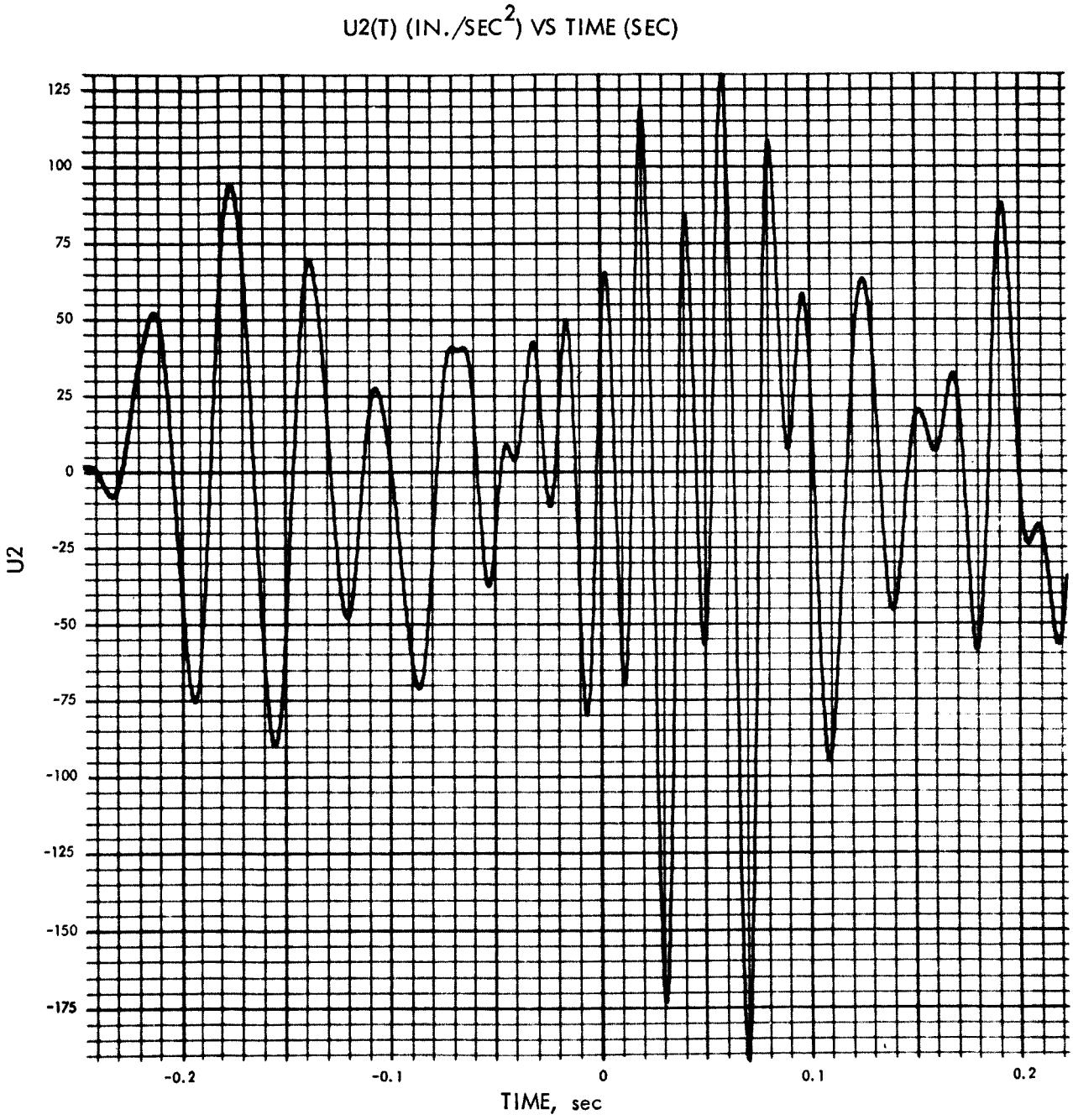

Fig. E-28. Joint 1, x_1 time history (pulse 2)

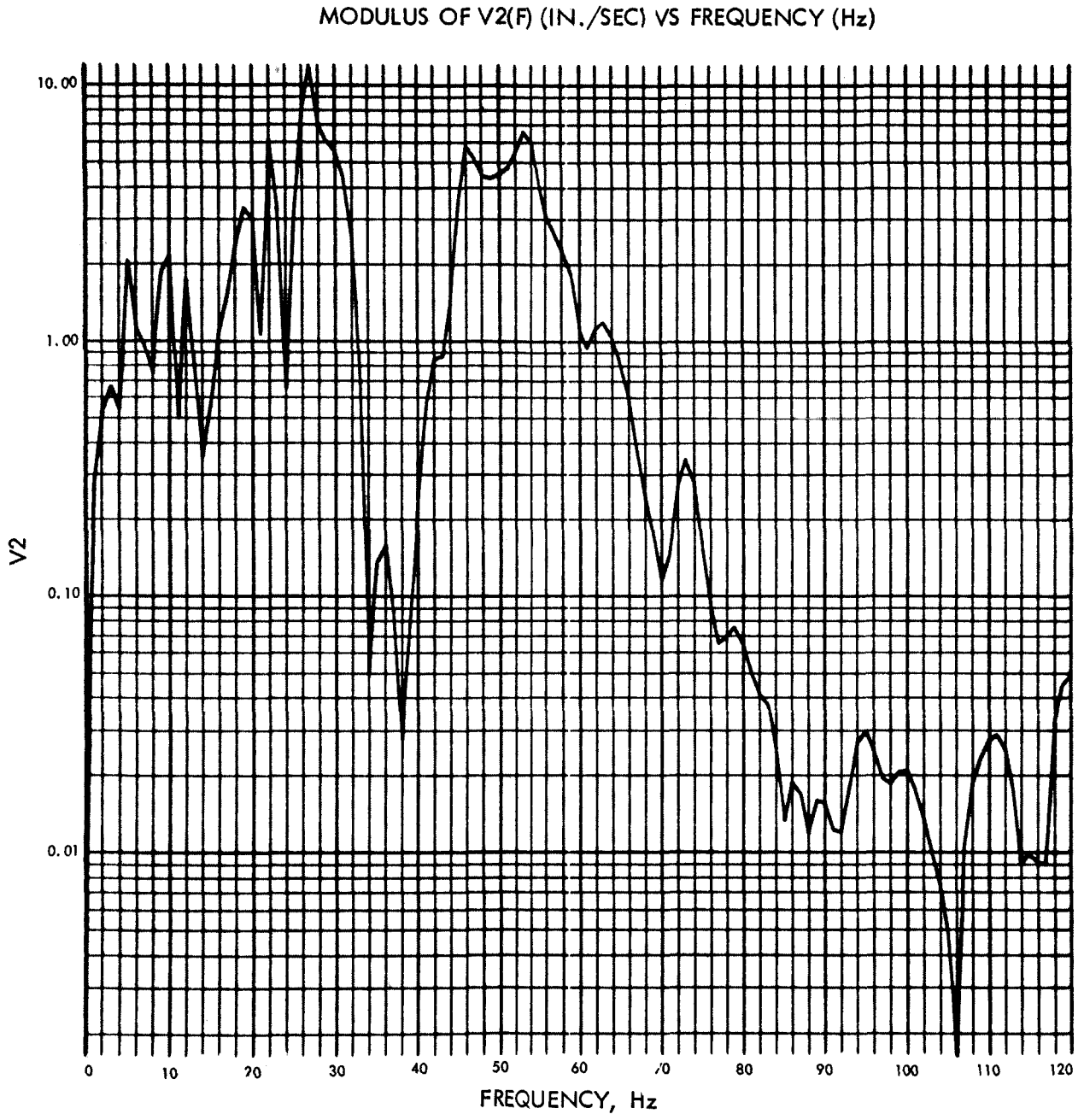

Fig. E-29. Joint 1, x_1 Fourier transform, modulus (pulse 2)

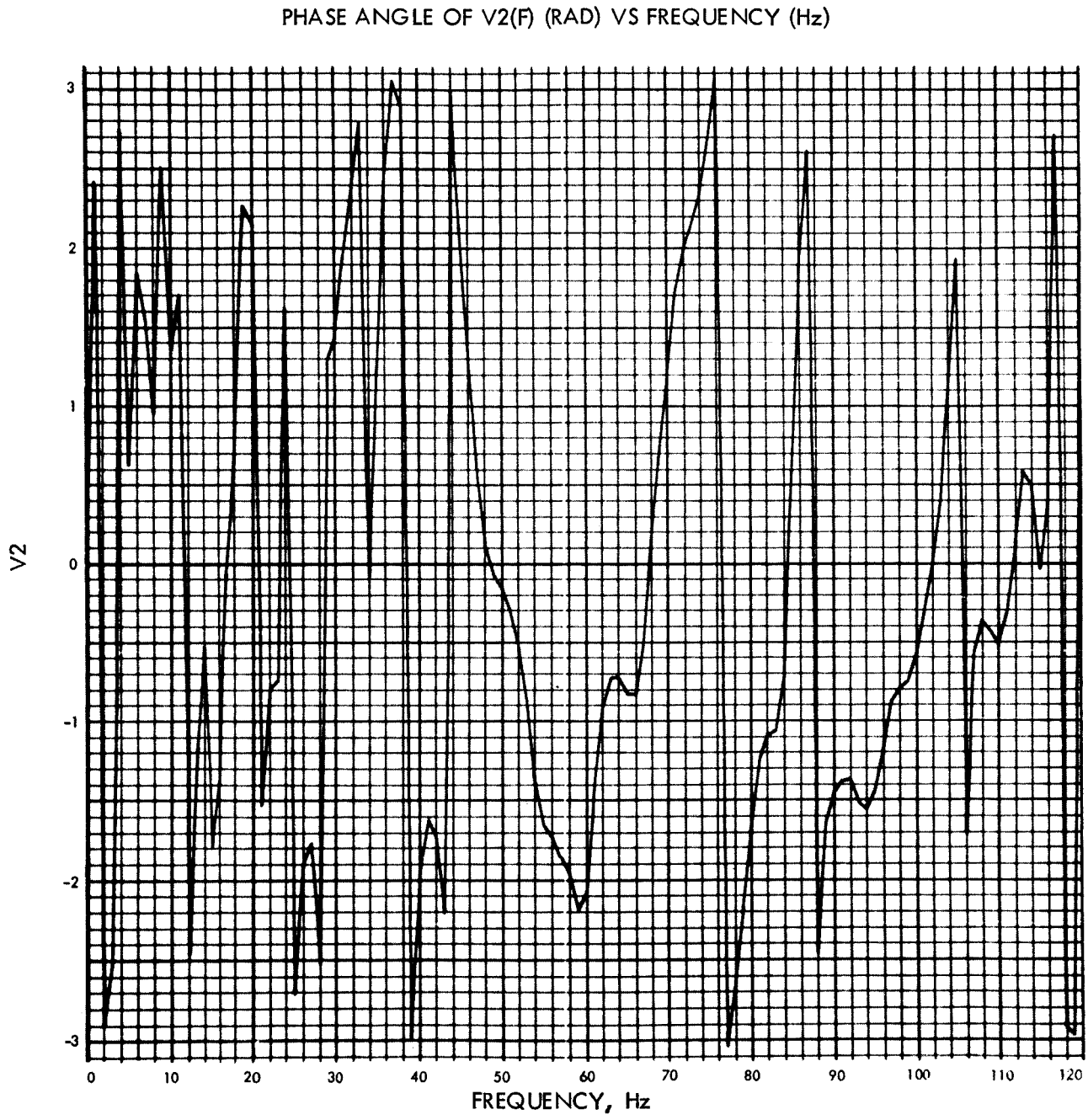

Fig. E-30. Joint 1, x_1 Fourier transform, phase angle (pulse 2)

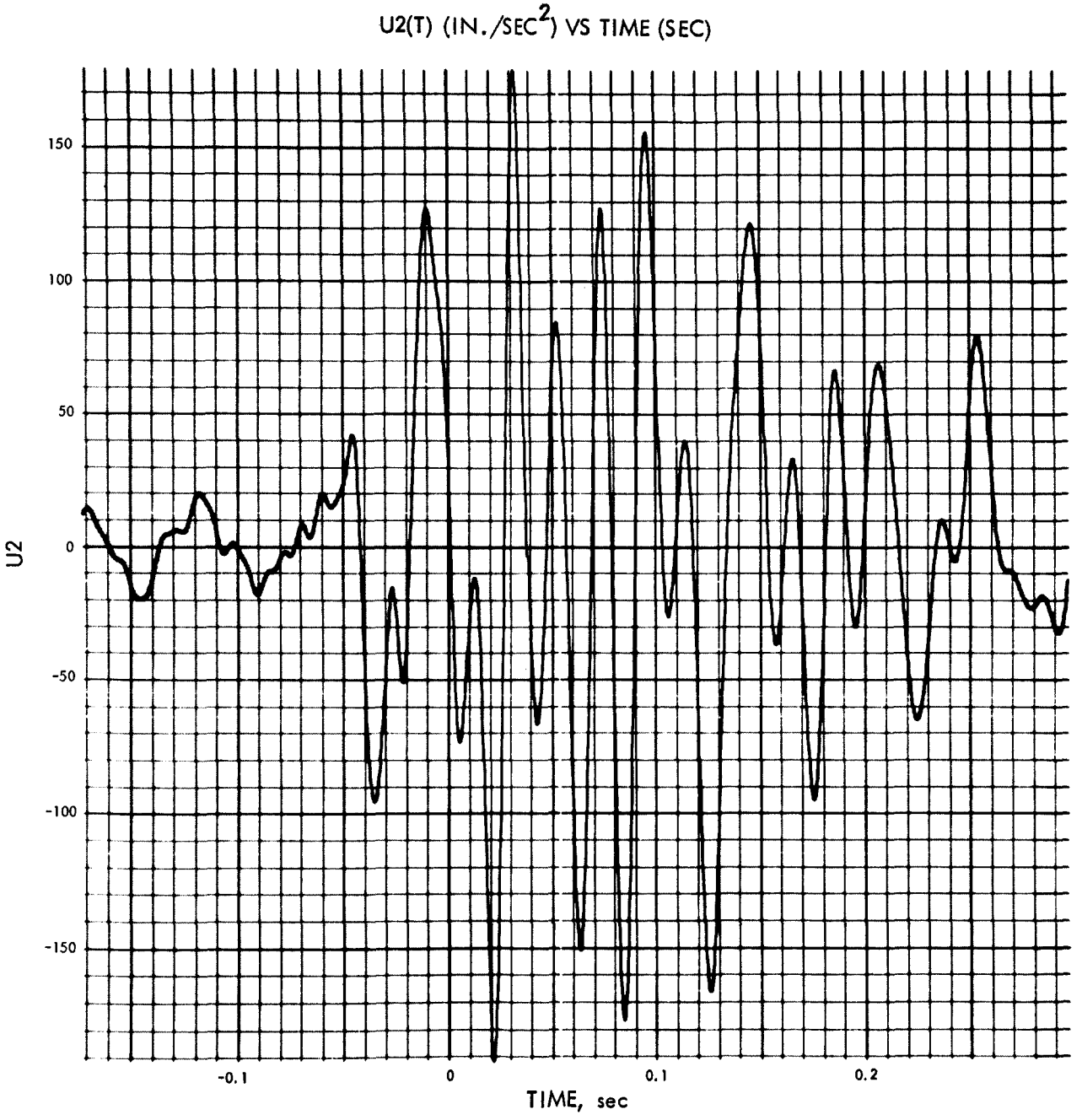

Fig. E-31. Joint 1, x_1 time history (pulse 3)

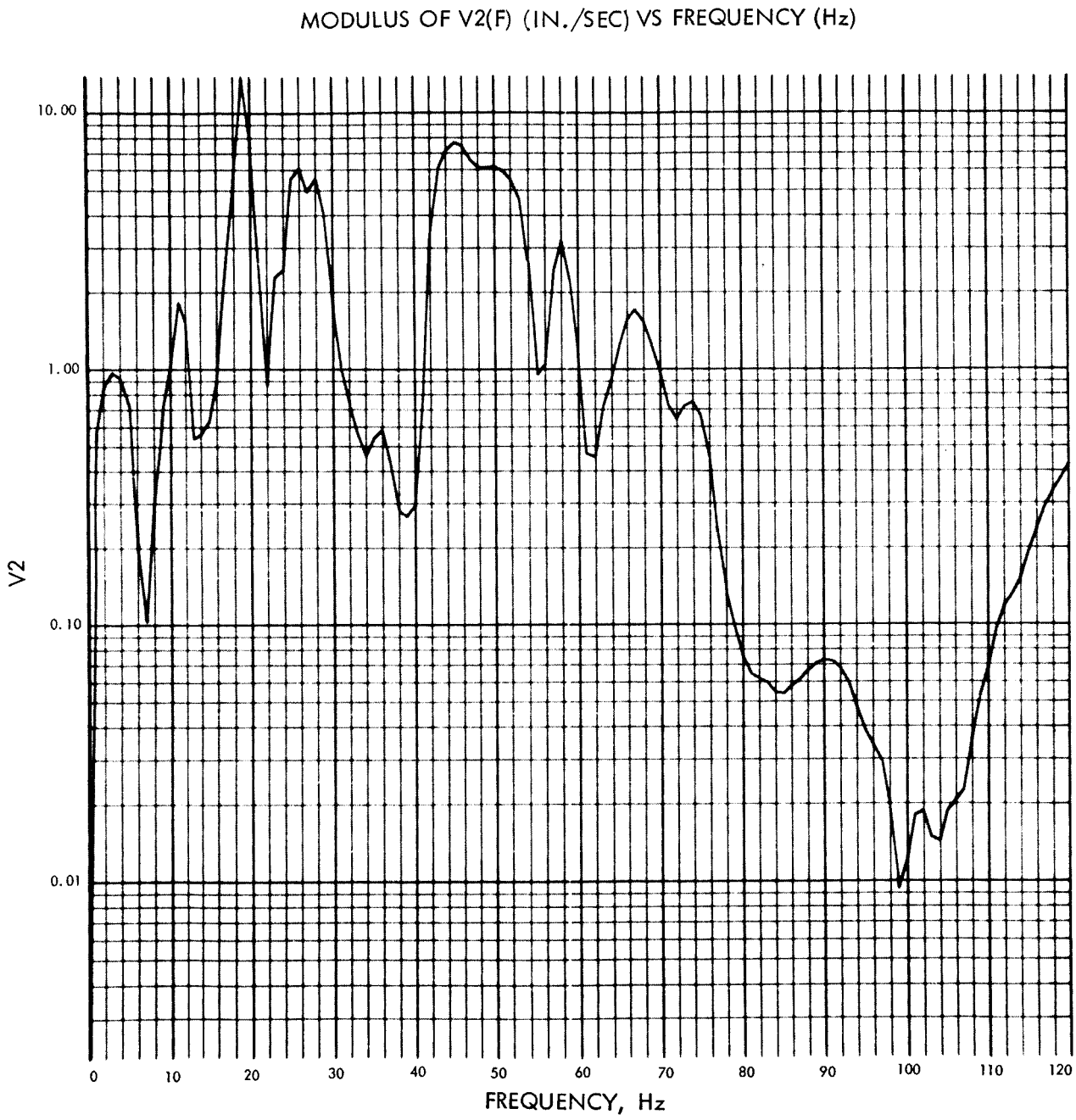

Fig. E-32. Joint 1, x_1 Fourier transform, modulus (pulse 3)

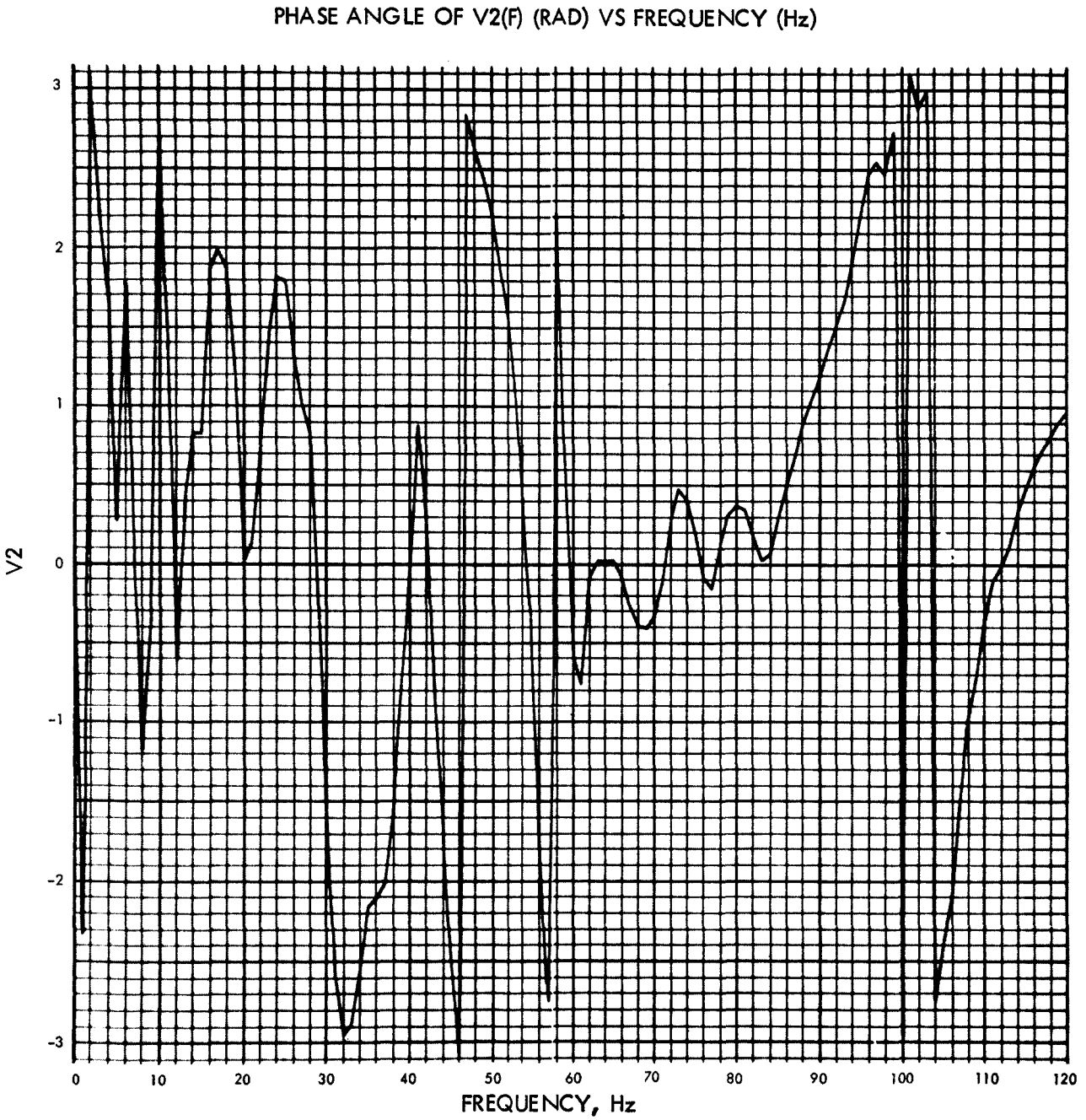

Fig. E-33. Joint 1, x_1 Fourier transform, phase angle (pulse 3)

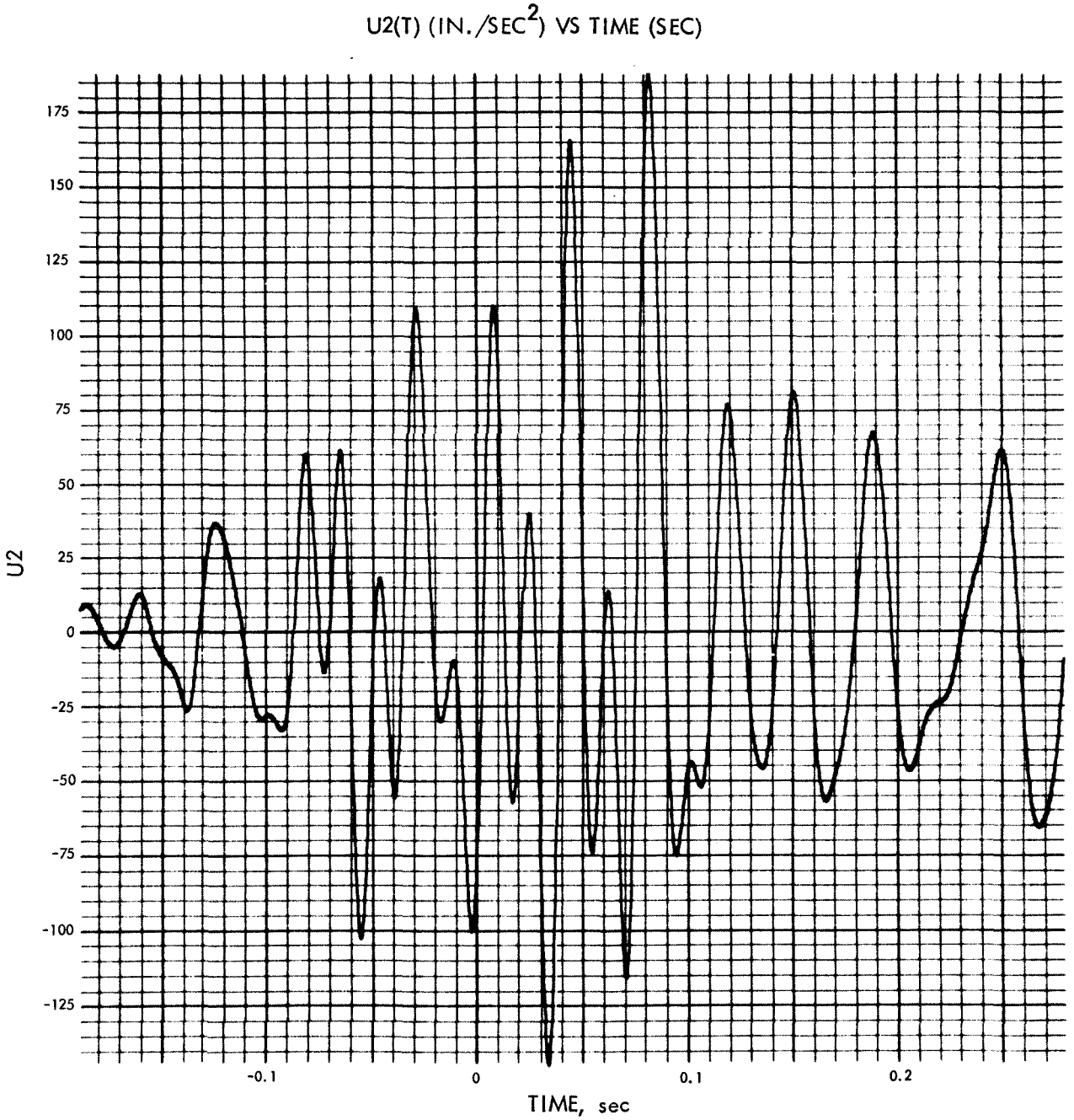

Fig. E-34. Joint 1, x_1 time history (pulse 4)

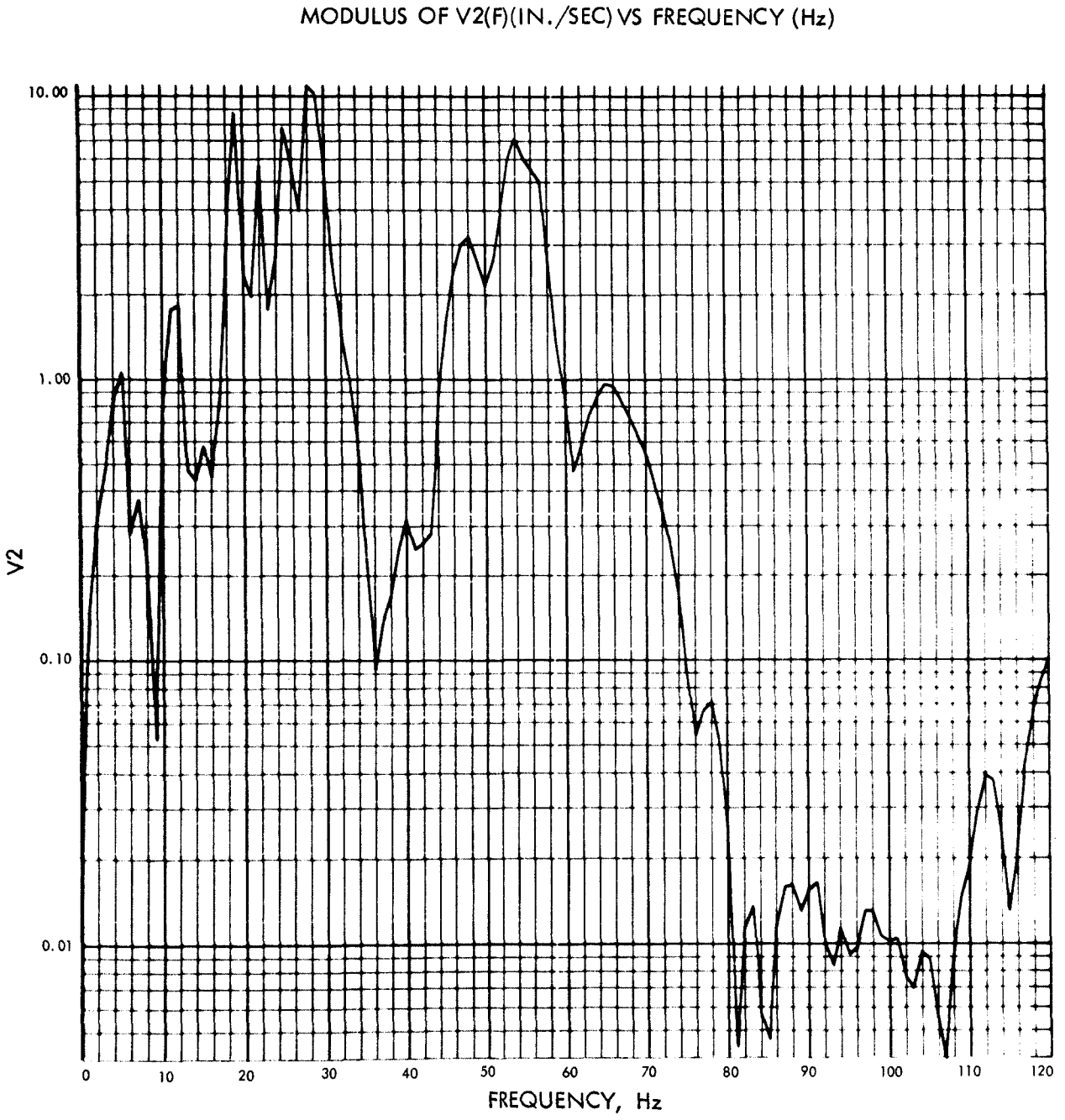

Fig. E-35. Joint 1, x_1 Fourier transform, modulus (pulse 4)

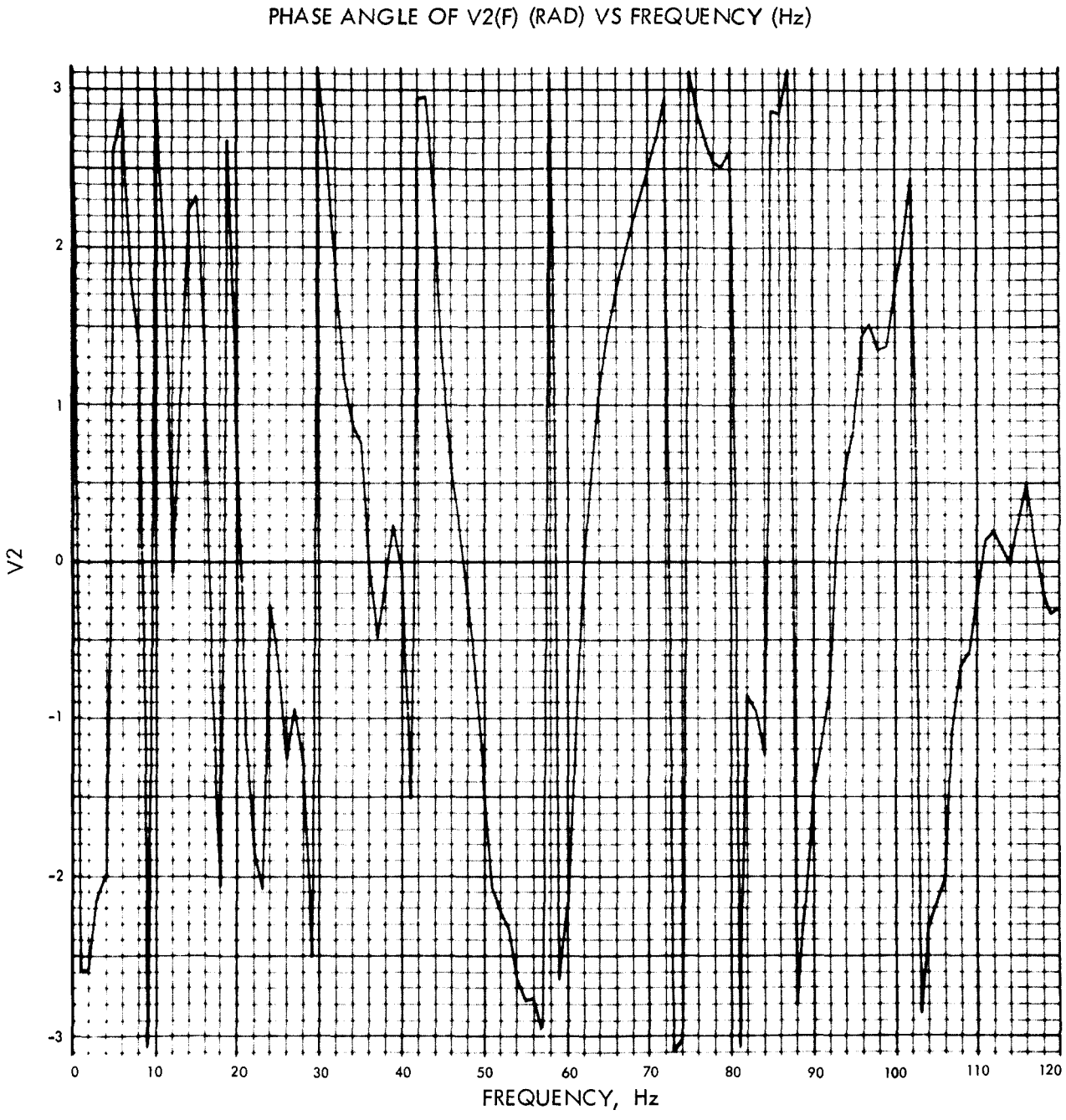

Fig. E-36. Joint 1, x_1 Fourier transform, phase angle (pulse 4)

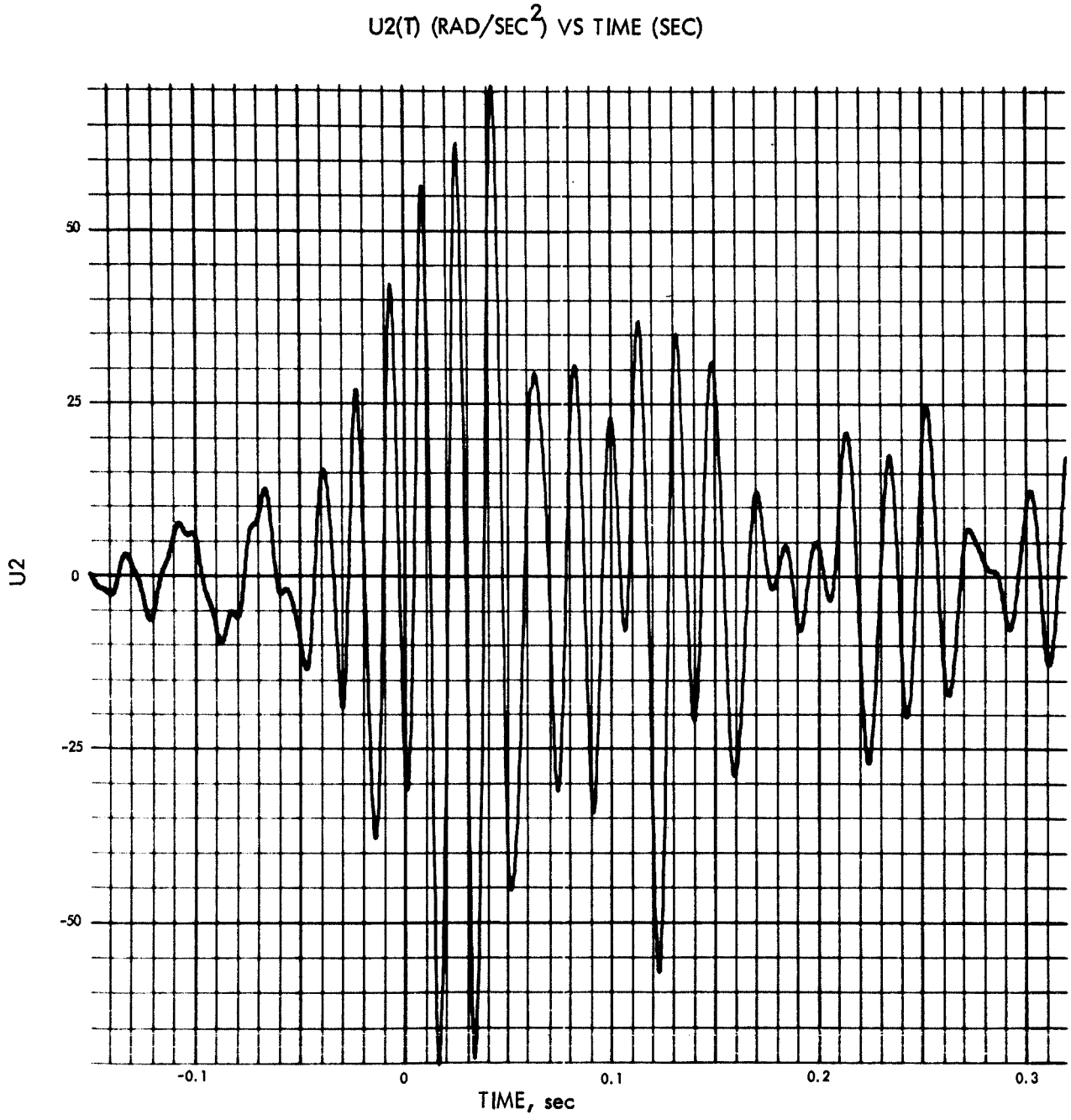

Fig. E-37. Joint 1, x_5 time history (pulse 1)

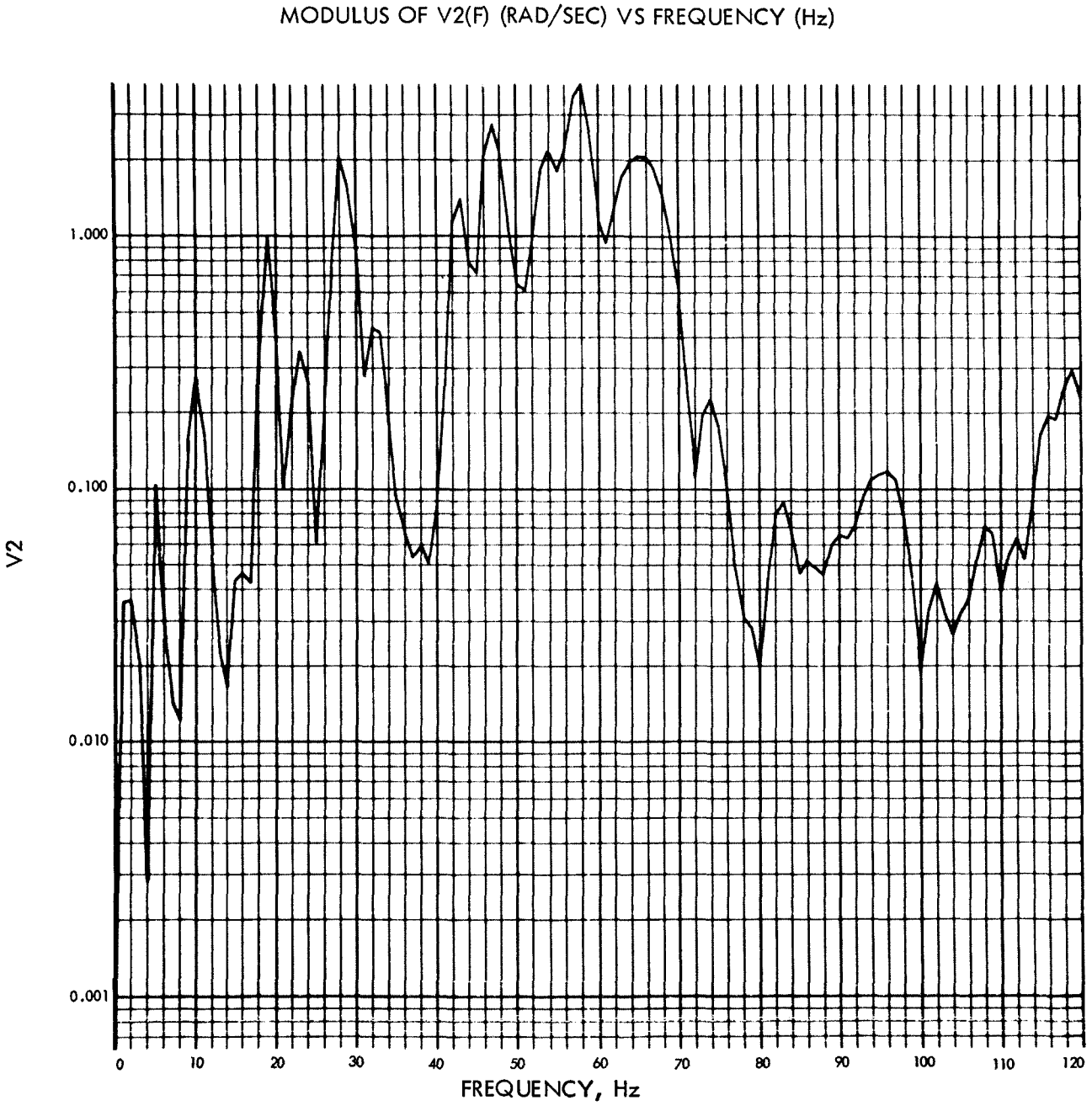

Fig. E-38. Joint 1, x_5 Fourier transform, modulus (pulse 1)

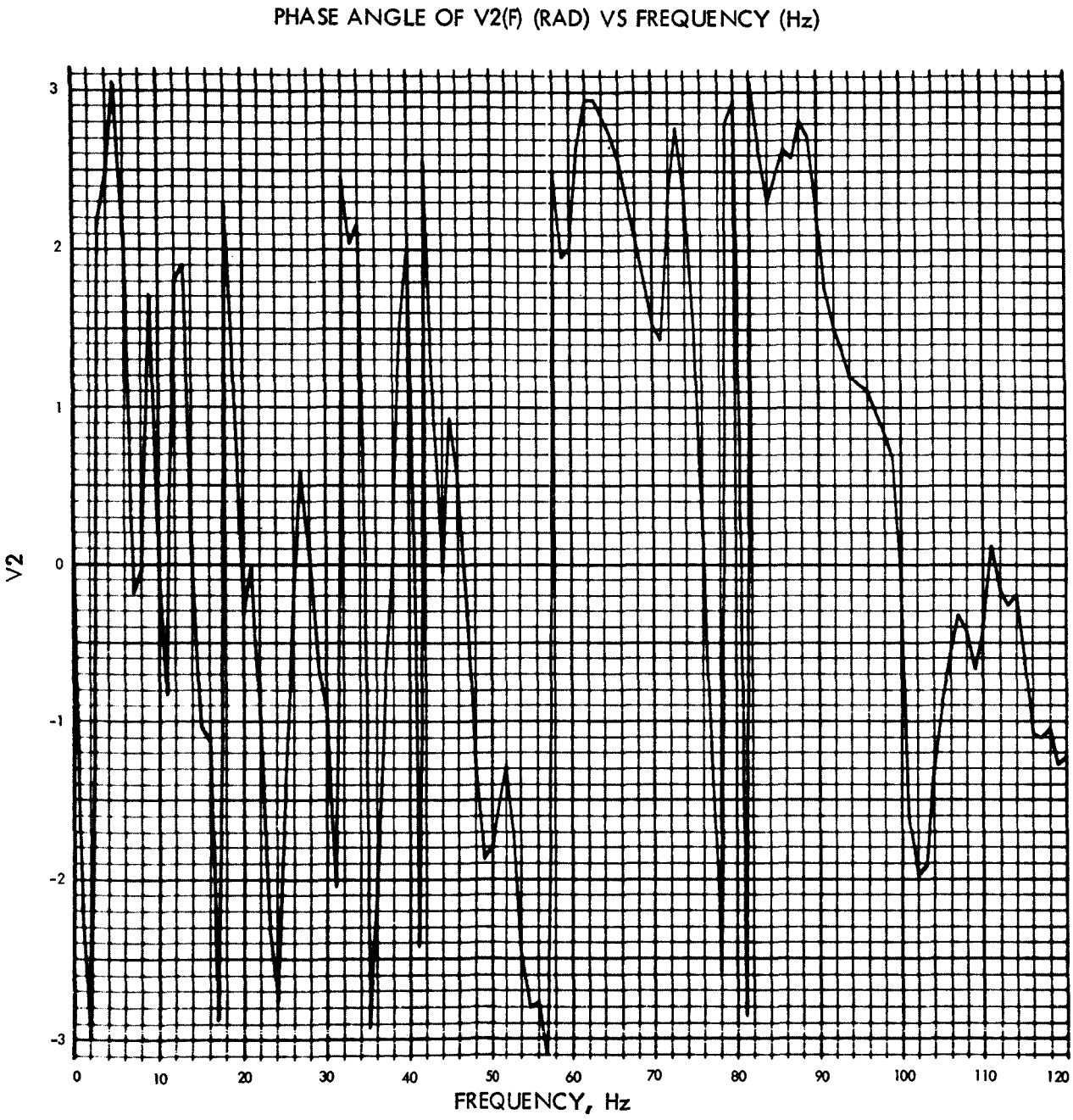

Fig. E-39. Joint 1, x_5 Fourier transform, phase angle (pulse 1)

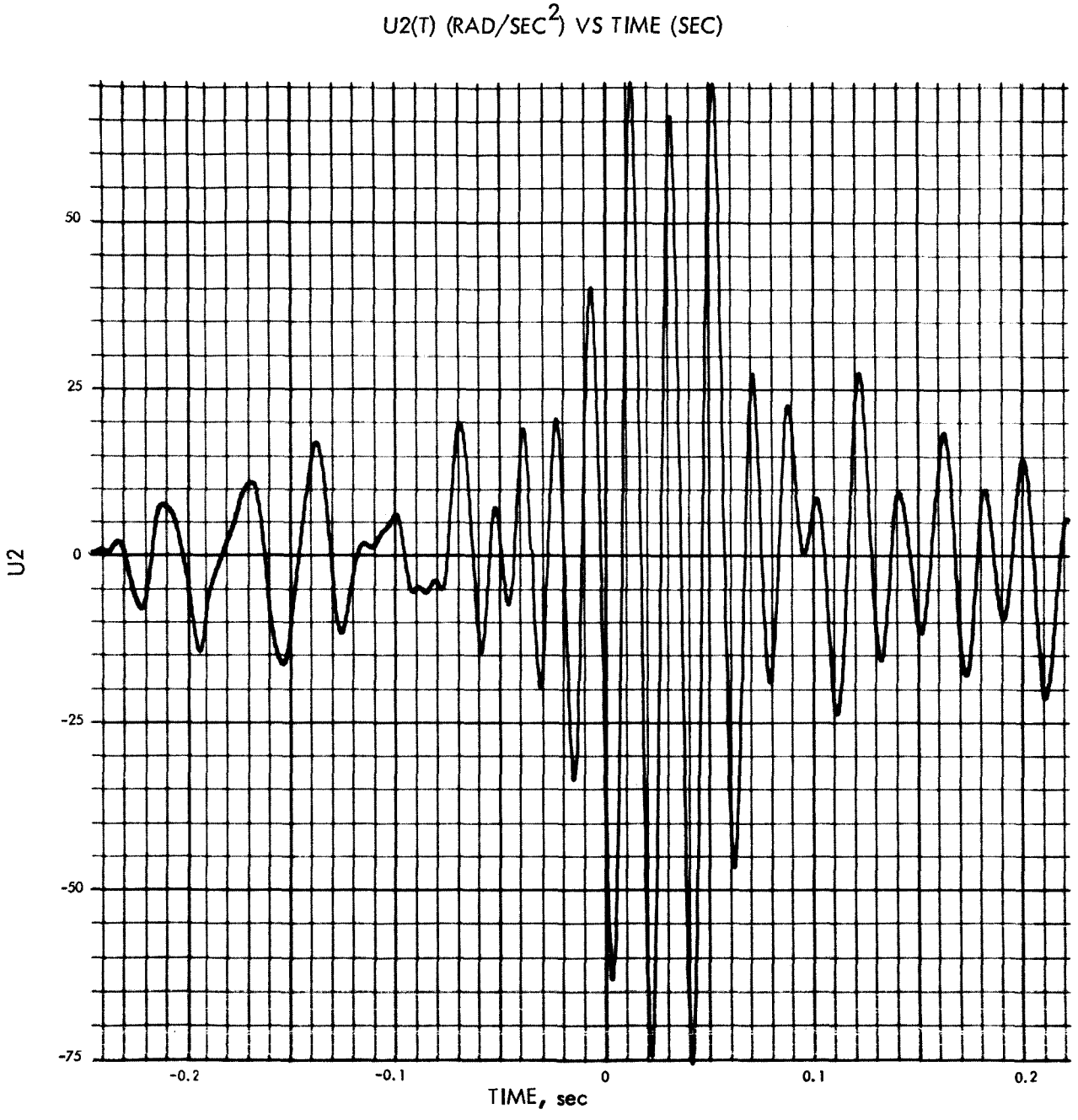

Fig. E-40. Joint 1, x_5 time history (pulse 2)

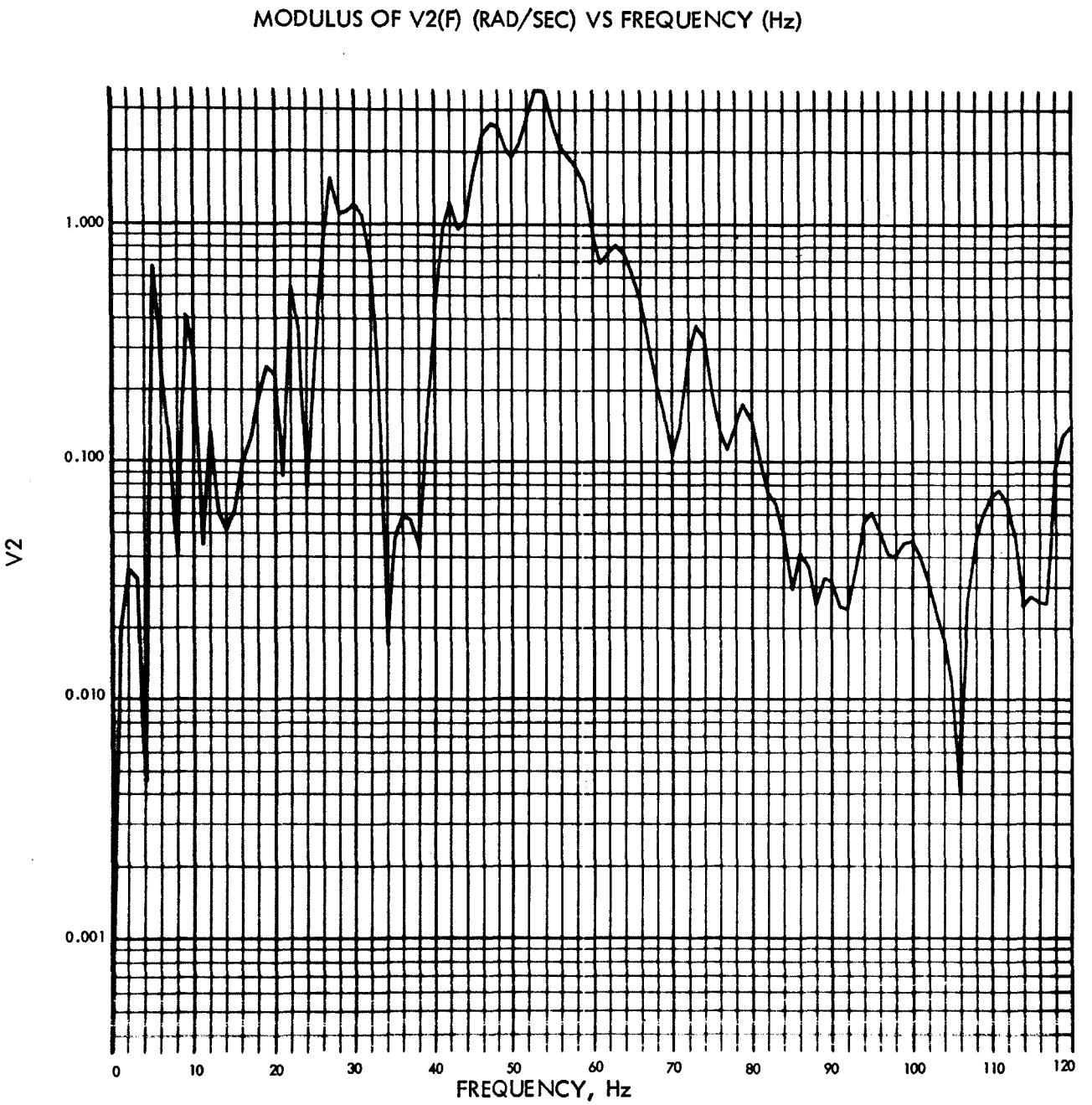

Fig. E-41. Joint 1, x_5 Fourier transform, modulus (pulse 2)

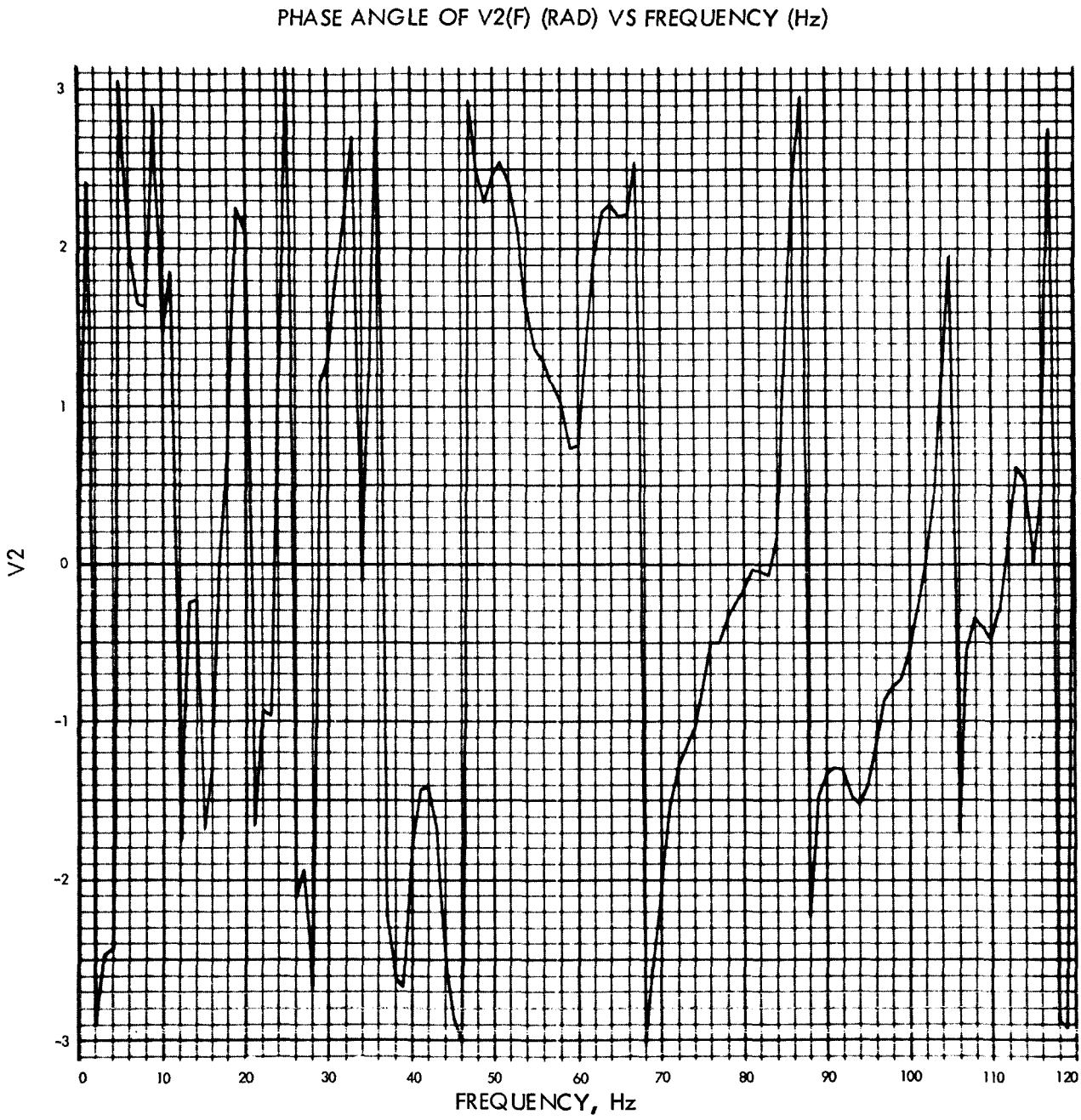

Fig. E-42. Joint 1, x_5 Fourier transform, phase angle (pulse 2)

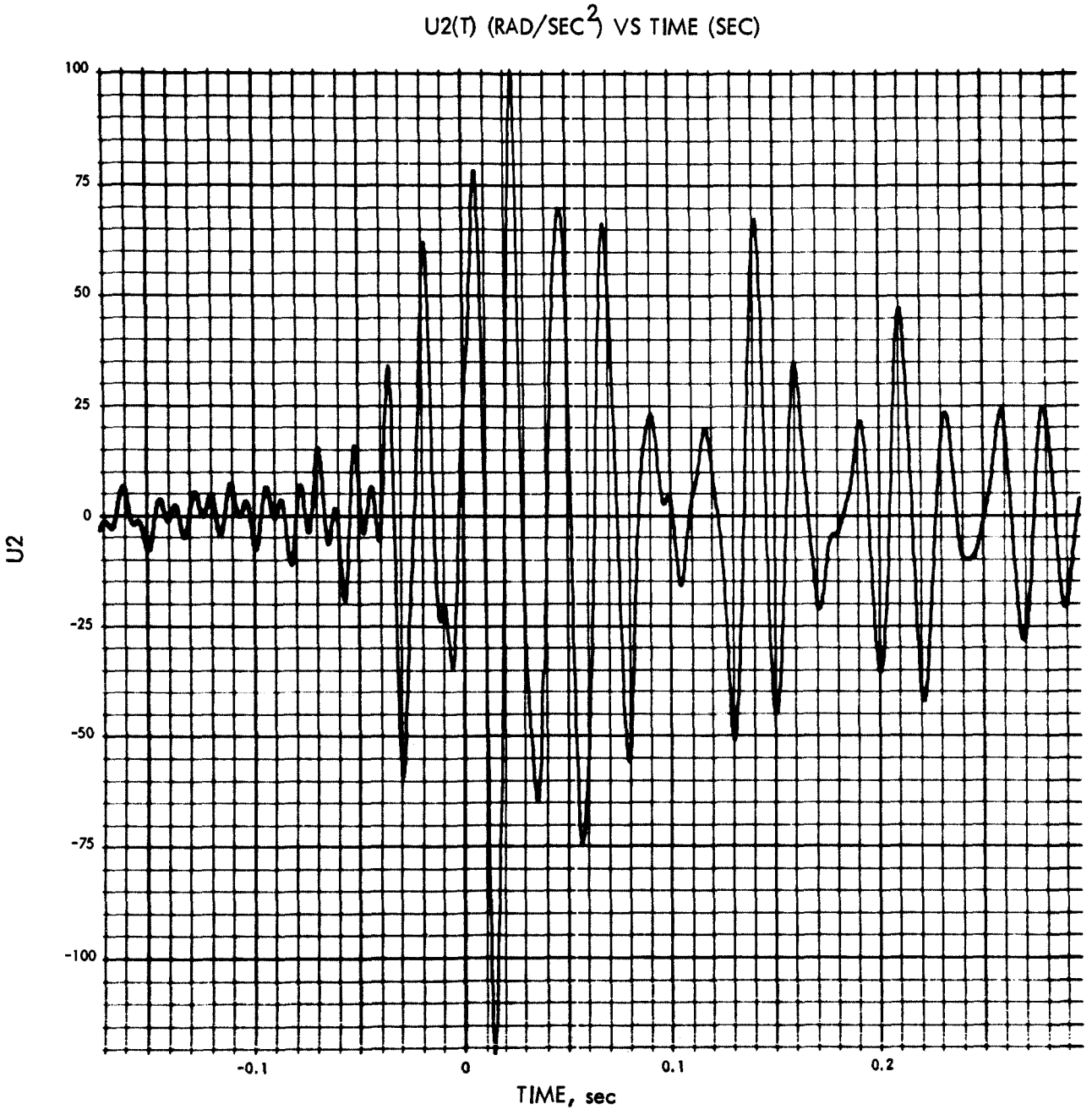

Fig. E-43. Joint 1, x_5 time history (pulse 3)

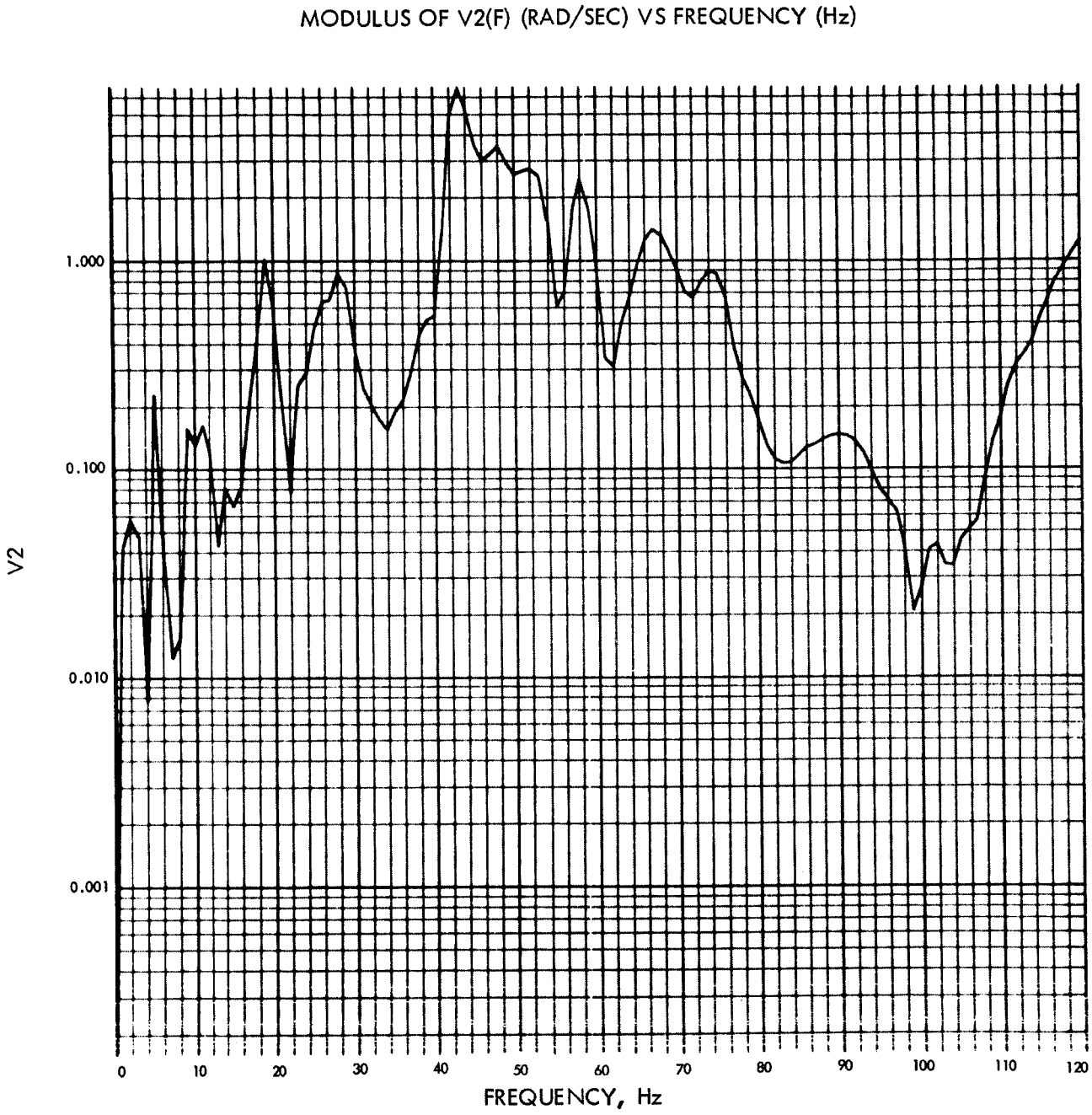

Fig. E-44. Joint 1, x_5 Fourier transform, modulus (pulse 3)

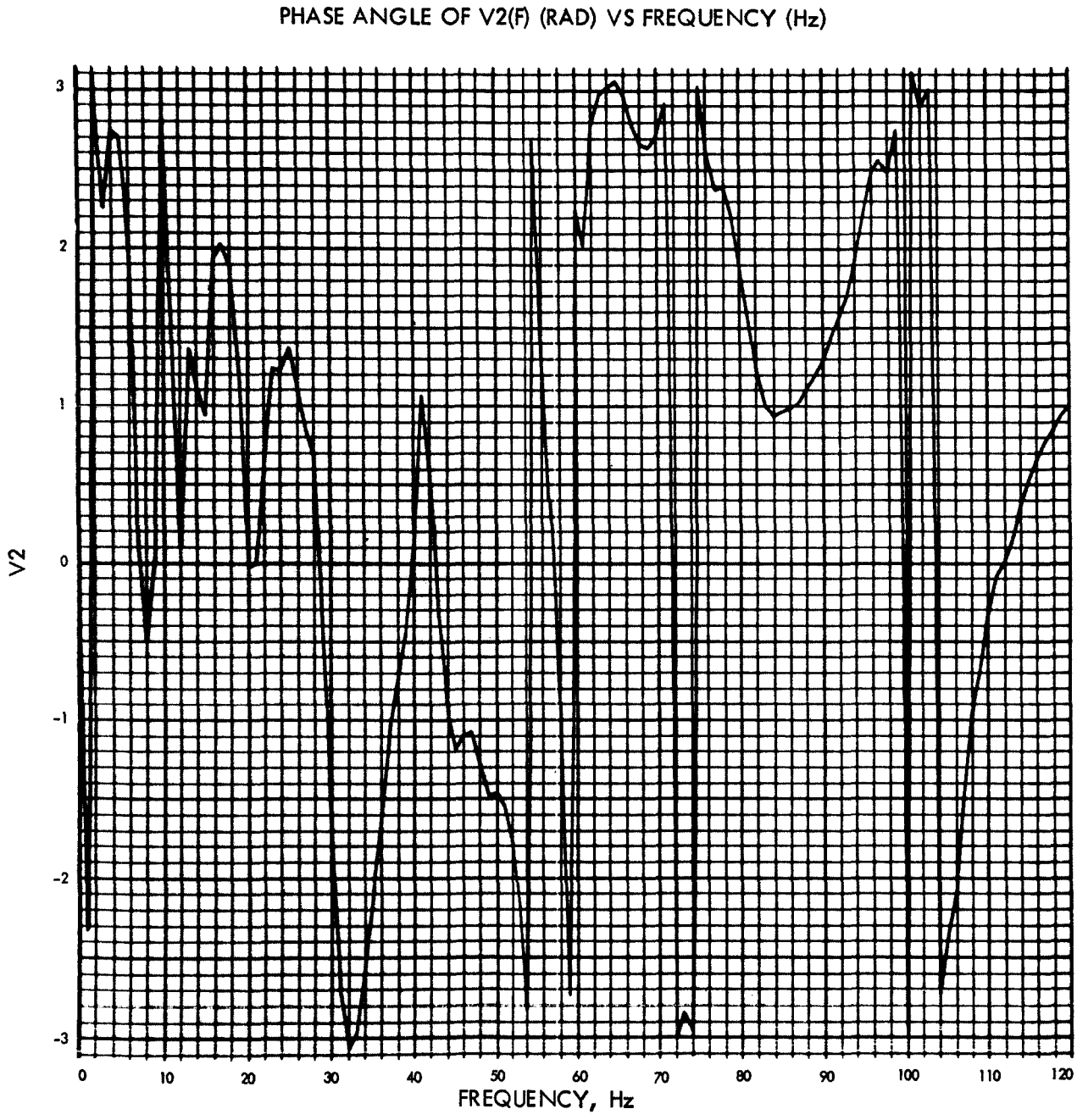

Fig. E-45. Joint 1, x_5 Fourier transform, phase angle (pulse 3)

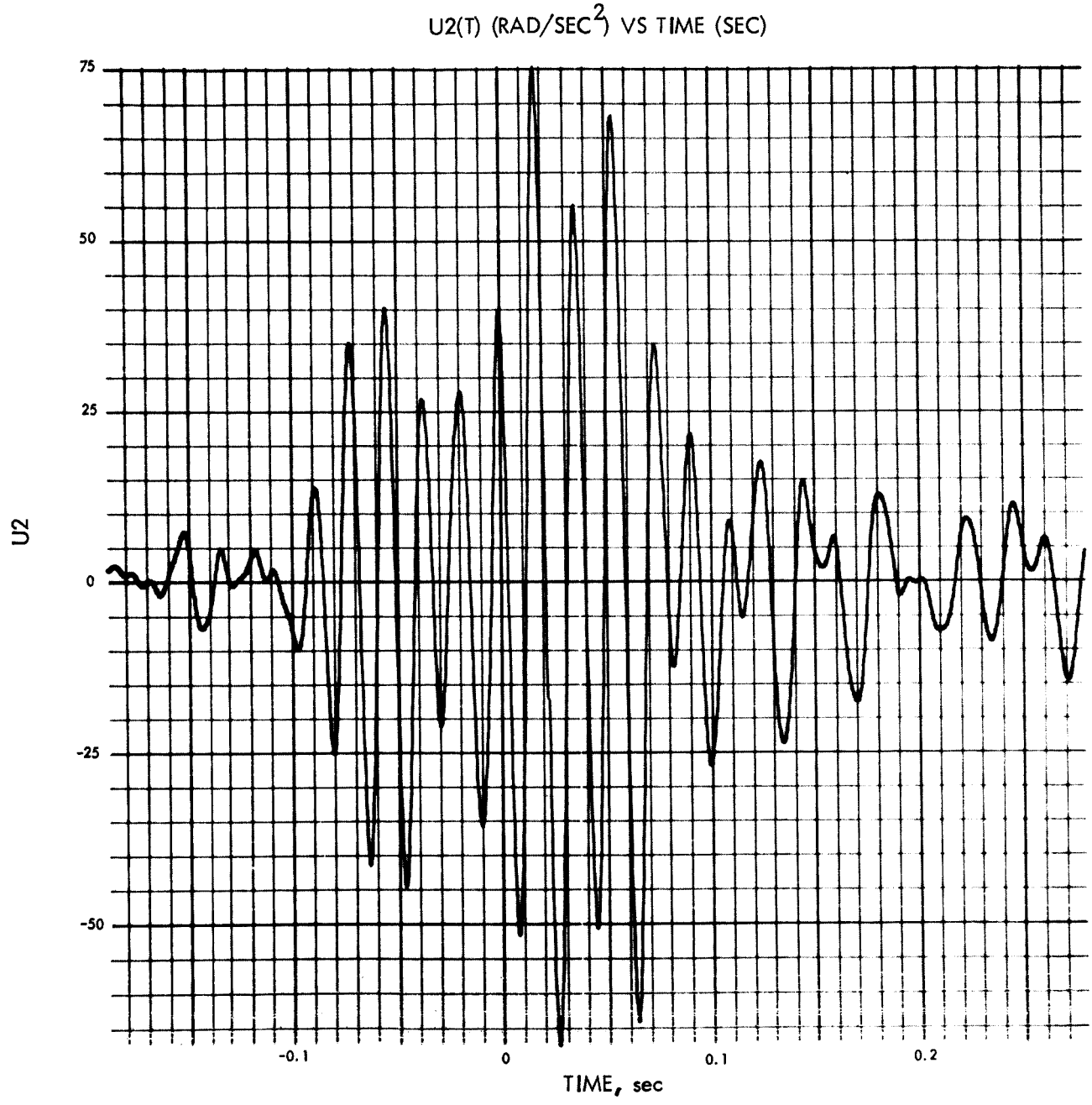

Fig. E-46. Joint 1, x_5 time history (pulse 4)

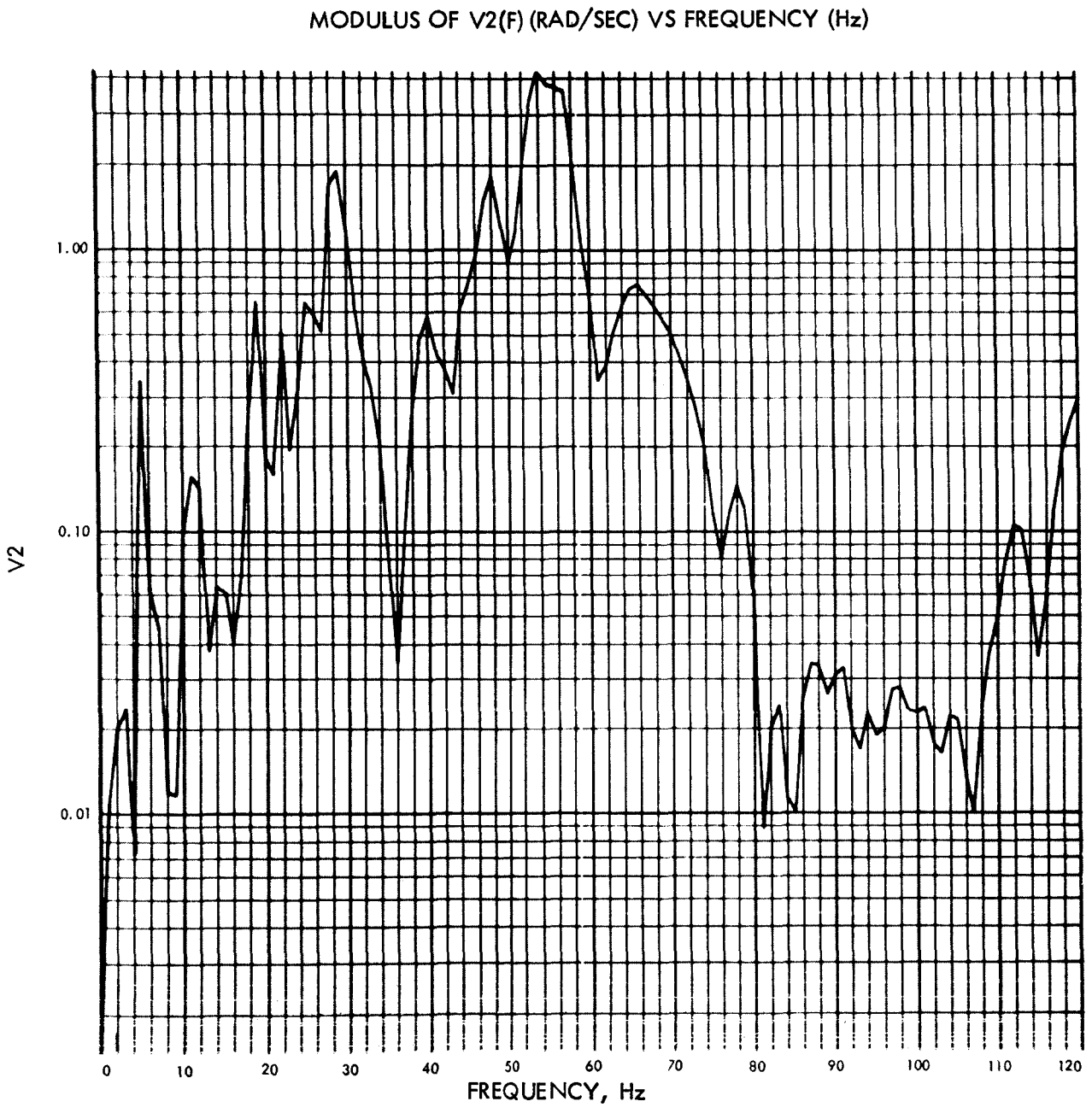

Fig. E-47. Joint 1, x_5 Fourier transform, modulus (pulse 4)

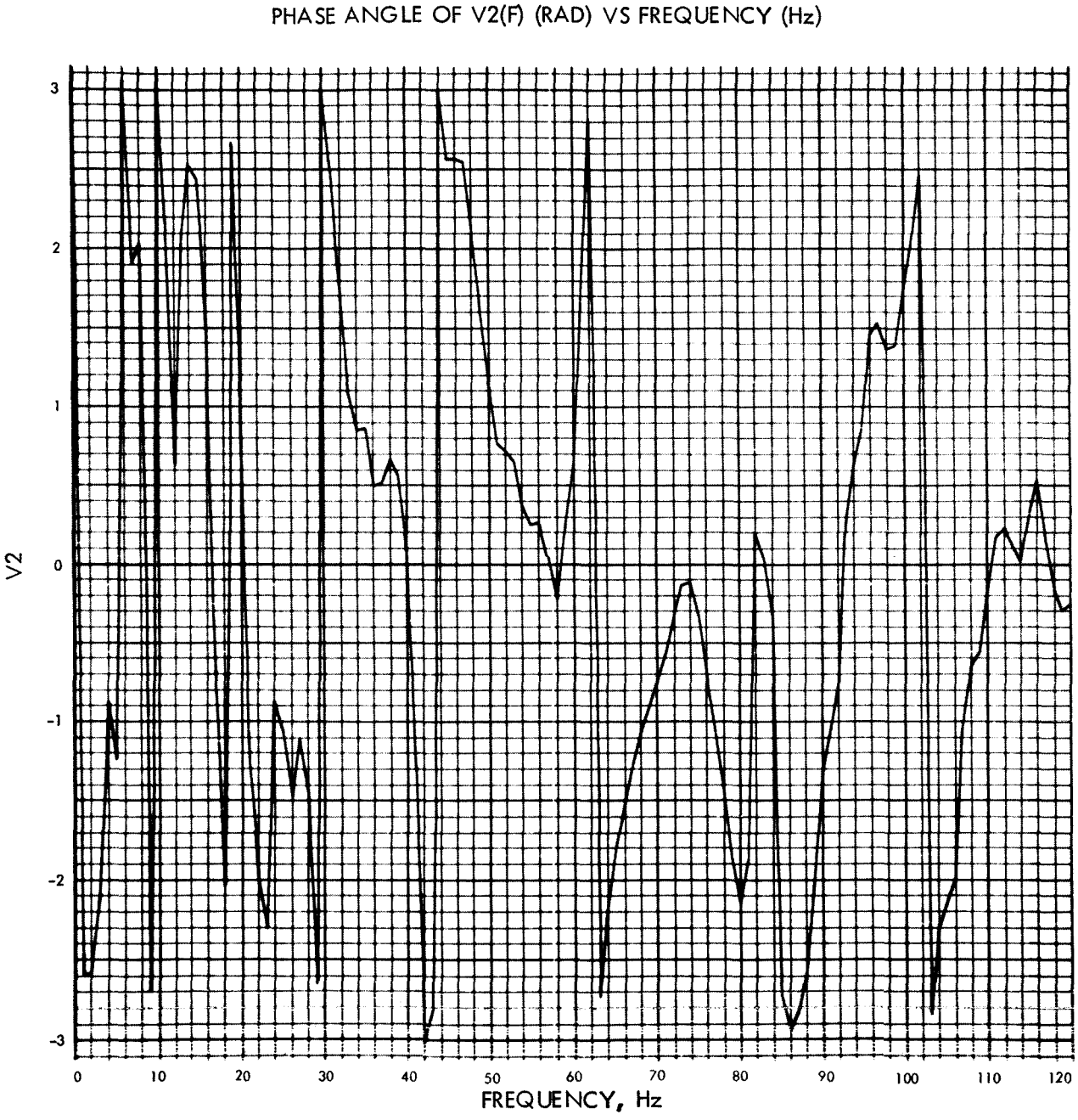

Fig. E-48. Joint 1, x_5 Fourier transform, phase angle (pulse 4)

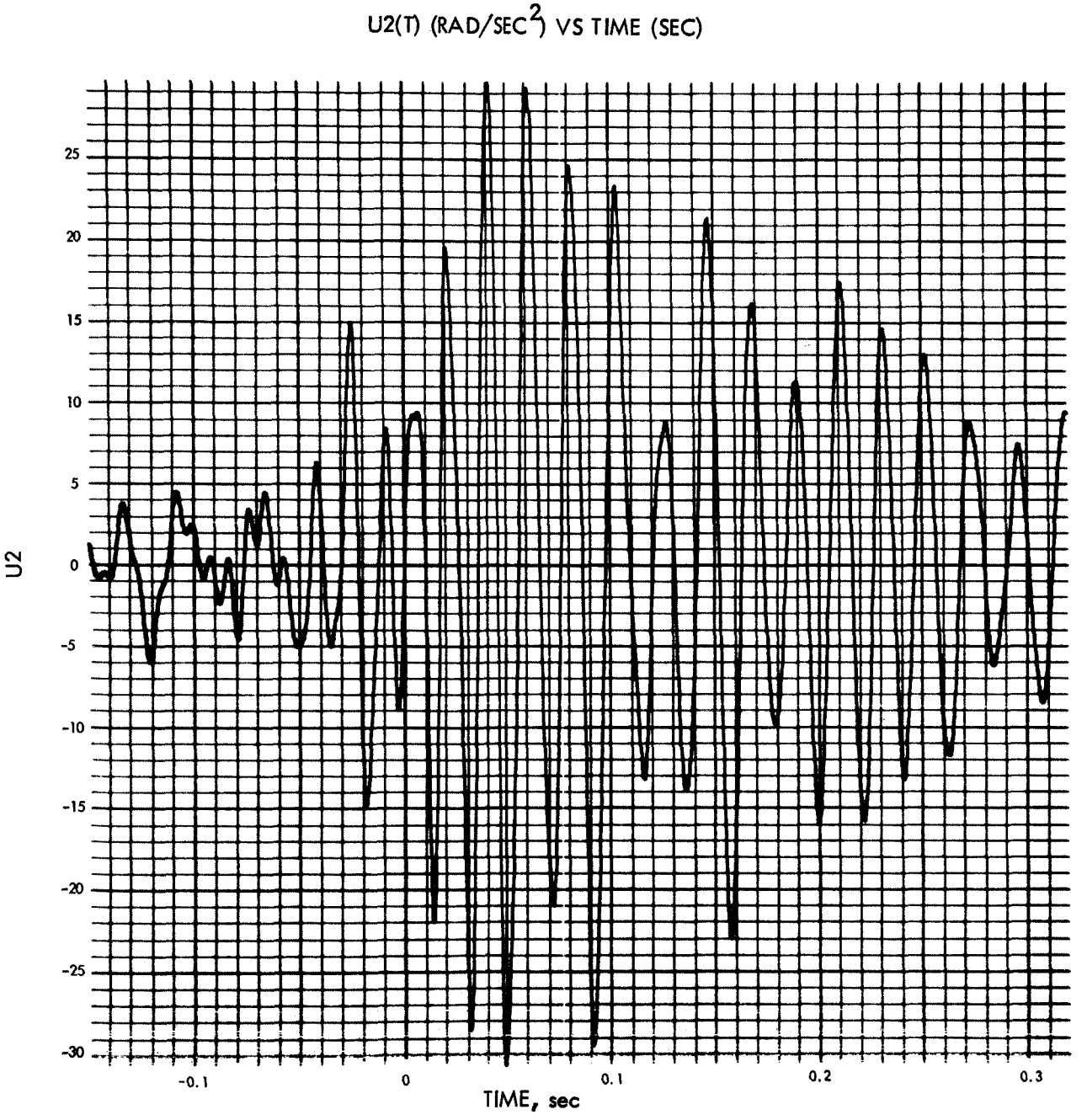

Fig. E-49. Joint 5, x_5 time history (pulse 1)

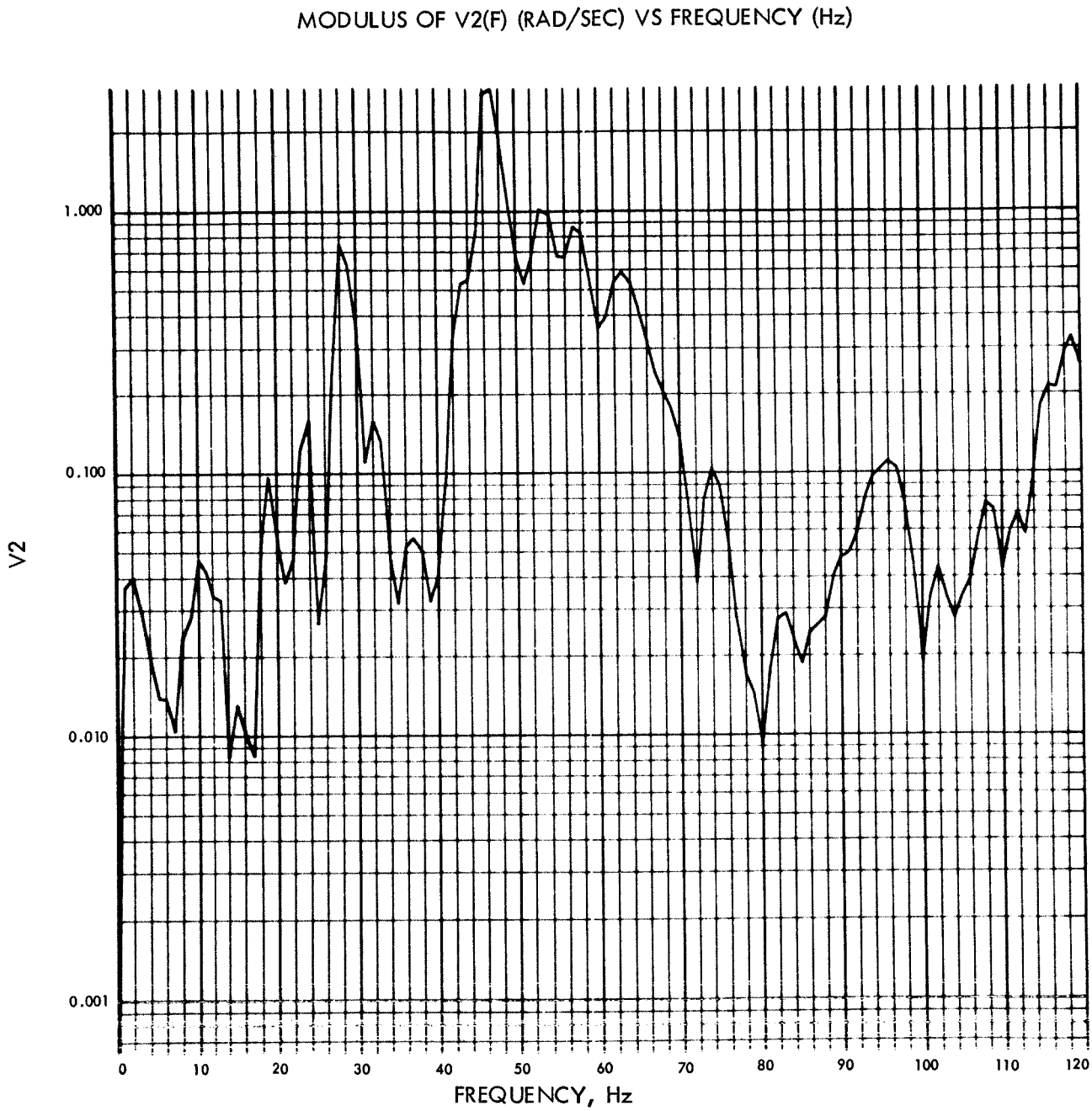

Fig. E-50. Joint 5, x_5 Fourier transform, modulus (pulse 1)

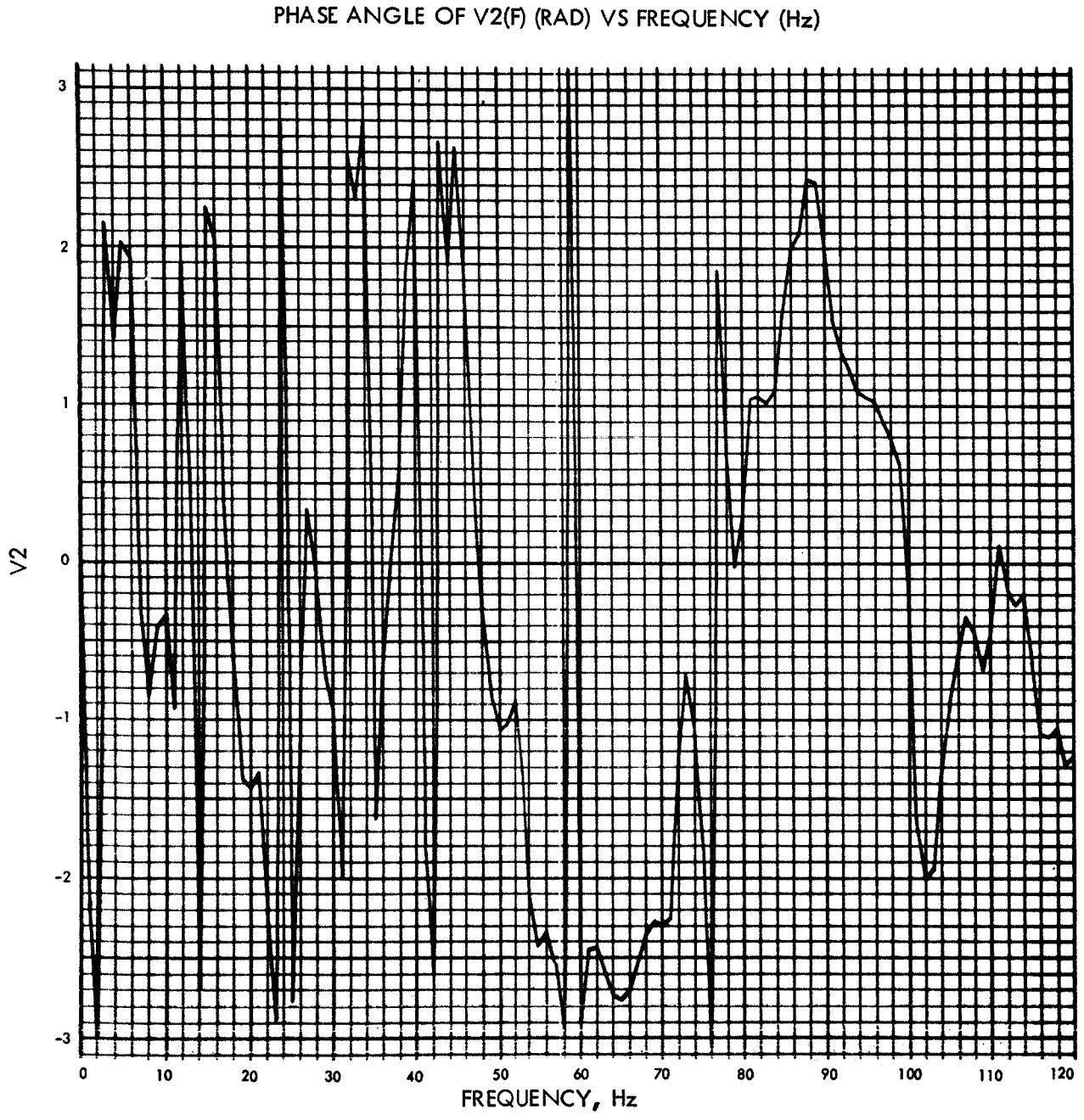

Fig. E-51. Joint 5, x_5 Fourier transform, phase angle (phase 1)

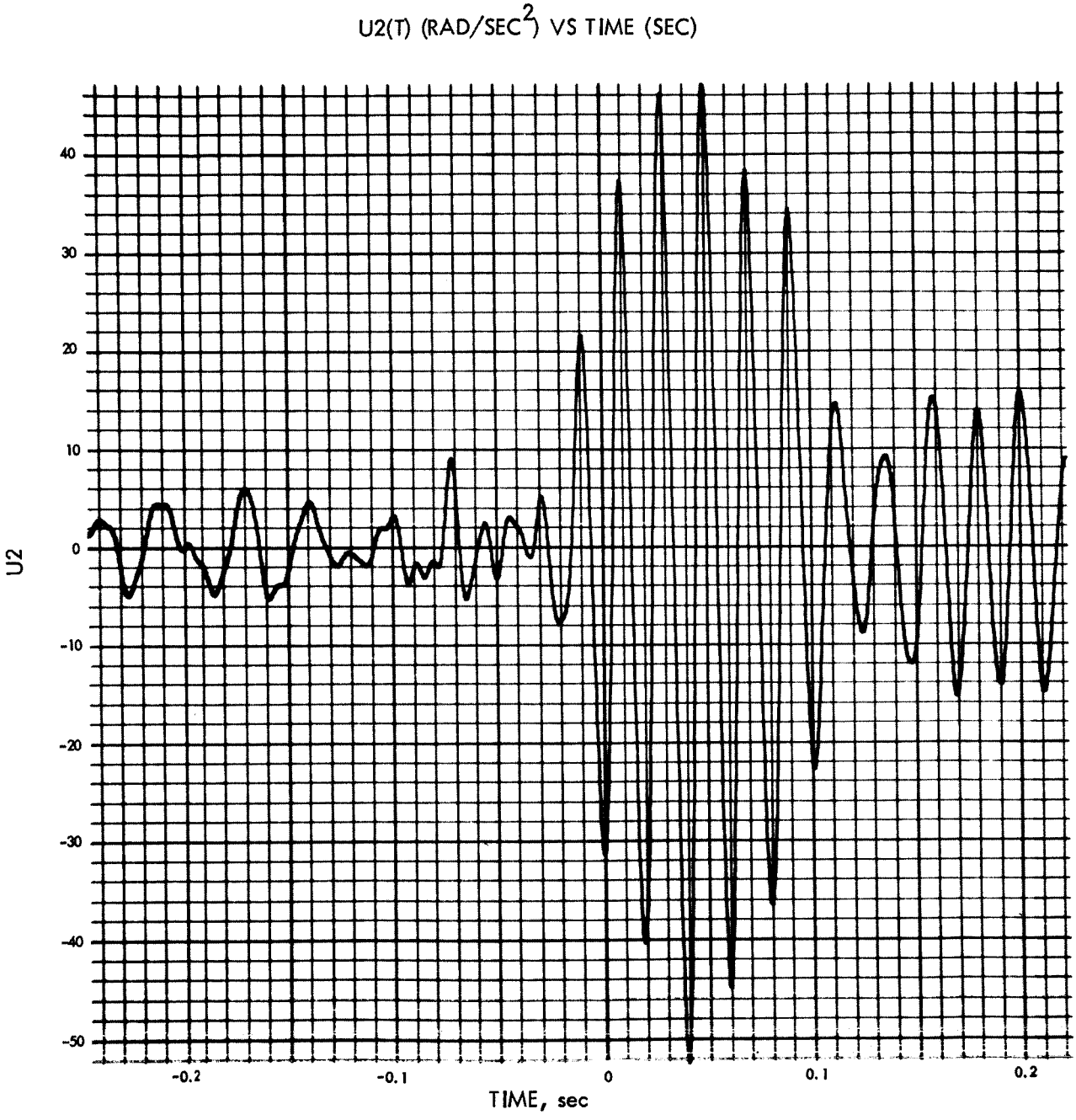

Fig. E-52. Joint 5, x_5 time history (pulse 2)

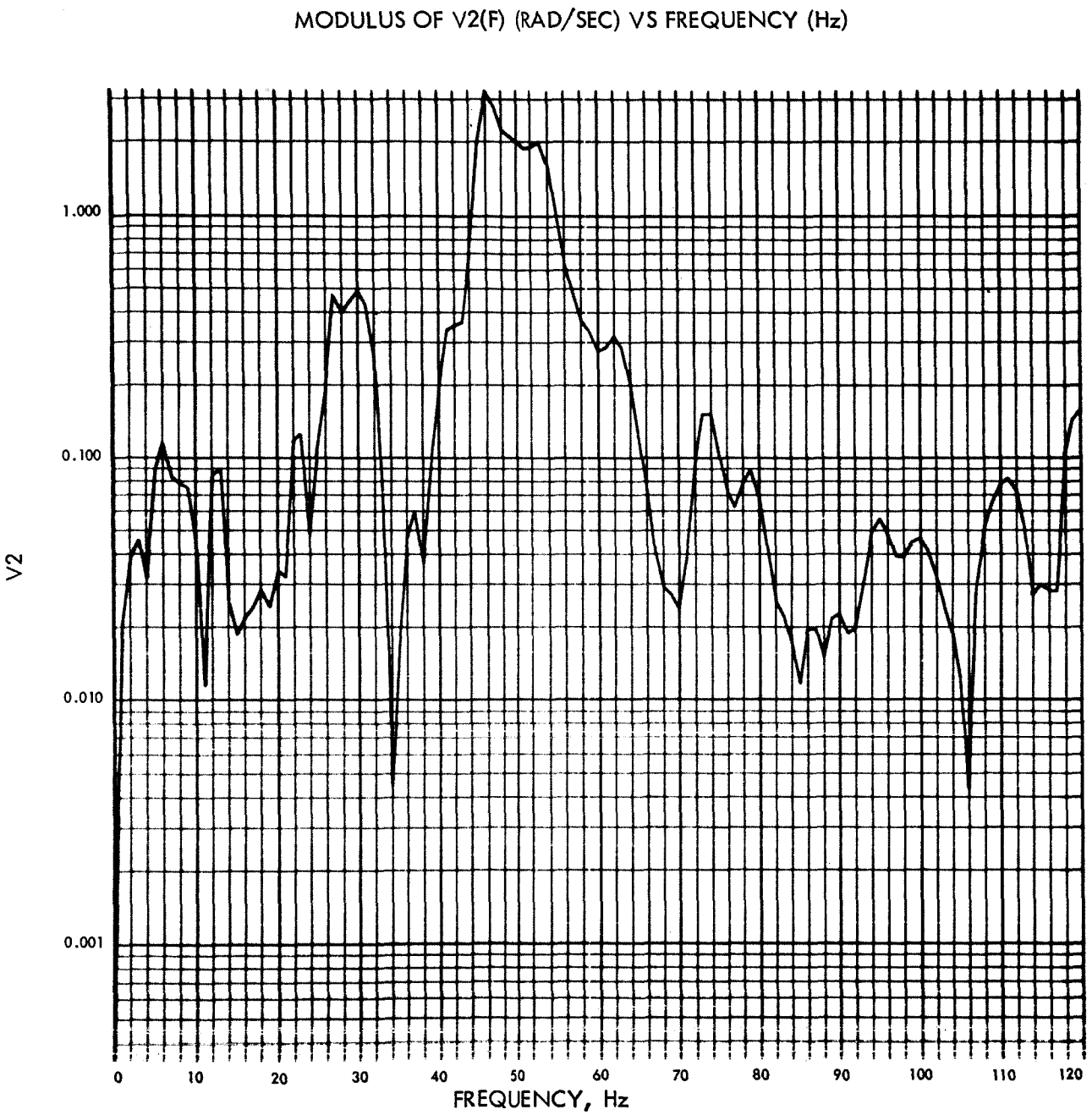

Fig. E-53. Joint 5, x_5 Fourier transform, modulus (pulse 2)

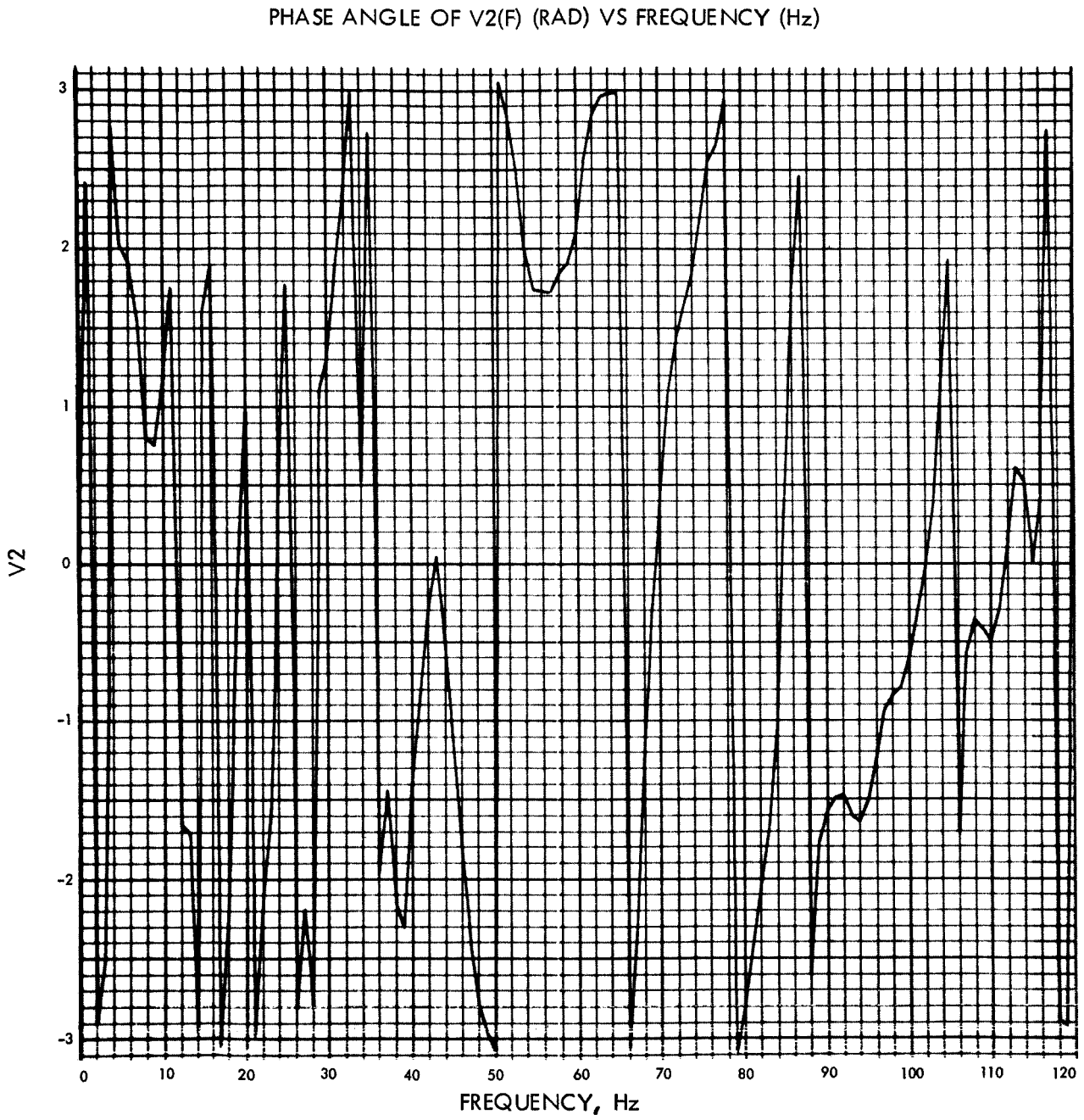

Fig. E-54. Joint 5, x_5 Fourier transform, phase angle (pulse 2)

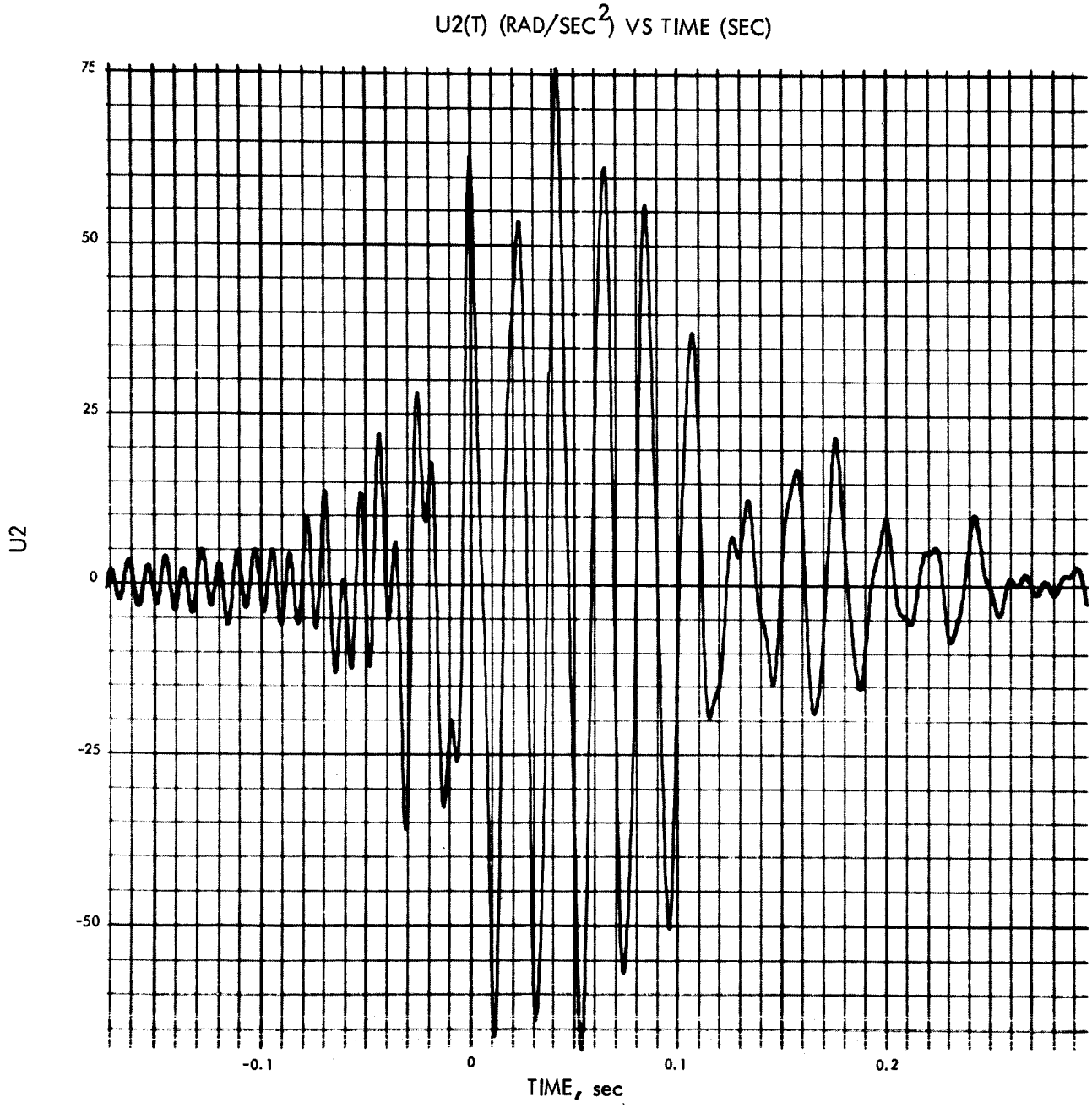

Fig. E-55. Joint 5, x_5 time history (pulse 3)

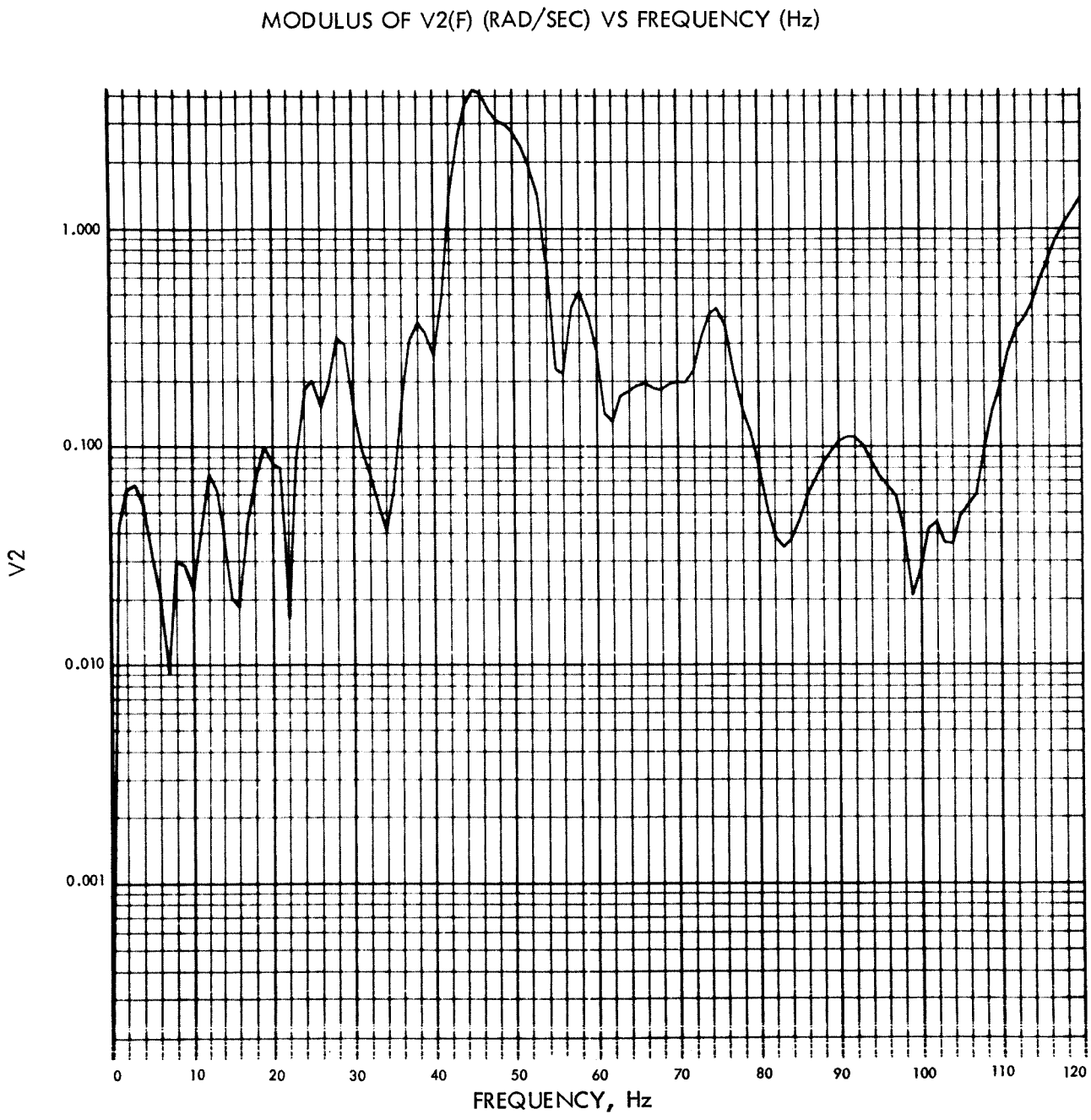

Fig. E-56. Joint 5, x_5 Fourier transform, modulus (pulse 3)

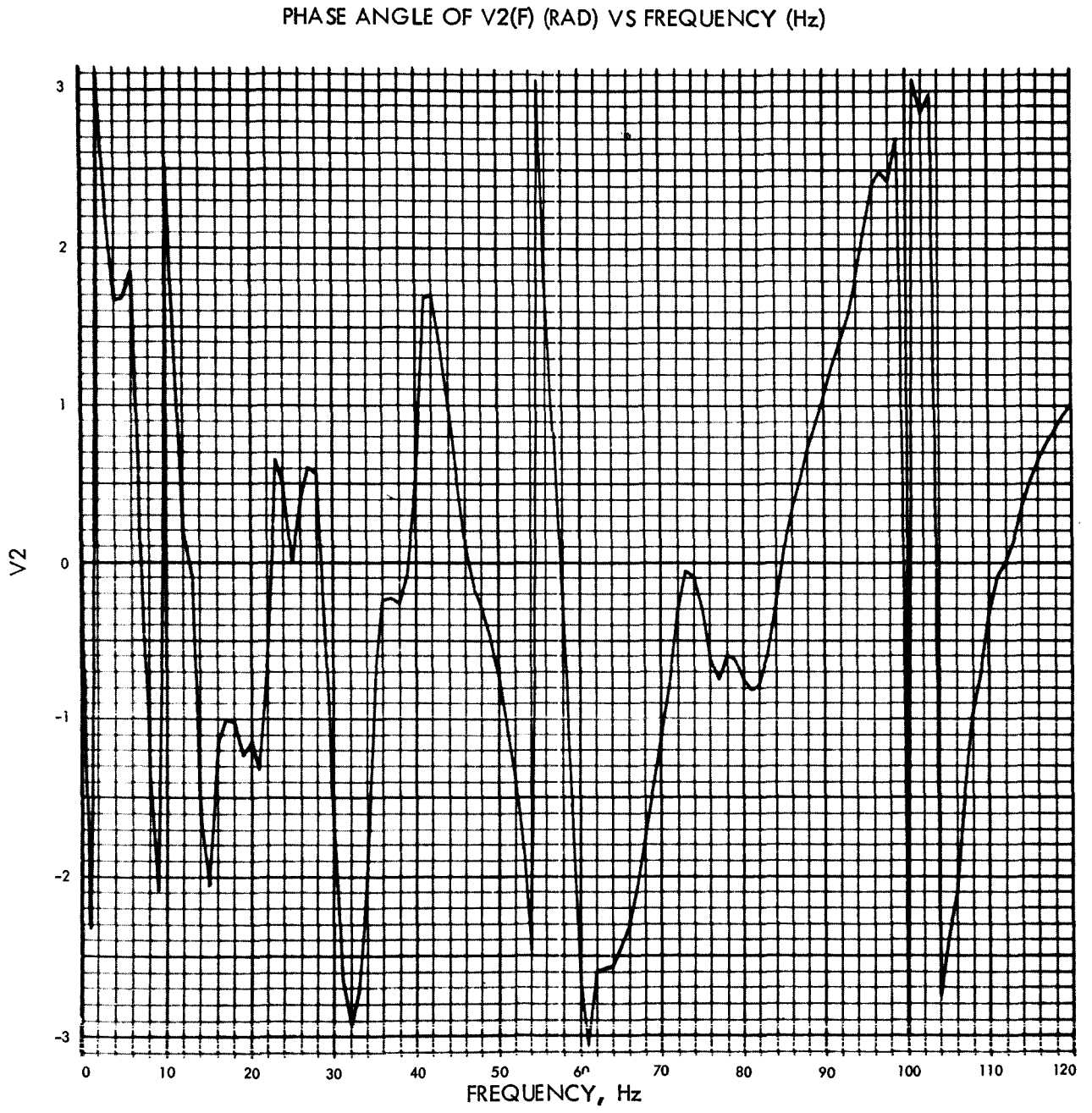

Fig. E-57. Joint 5, x_5 Fourier transform, phase angle (pulse 3)

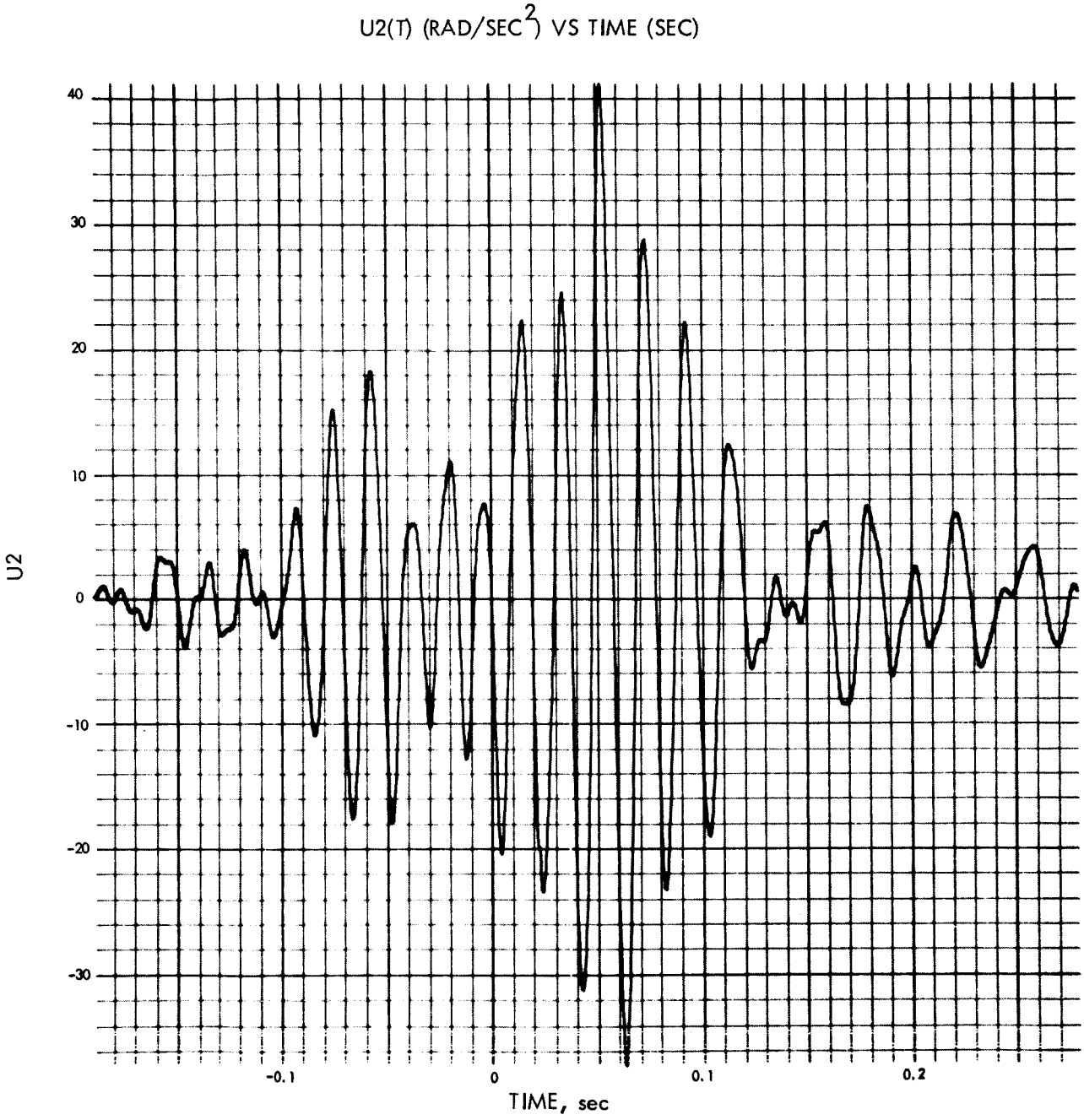

Fig. E-58. Joint 5, x_5 time history (pulse 4)

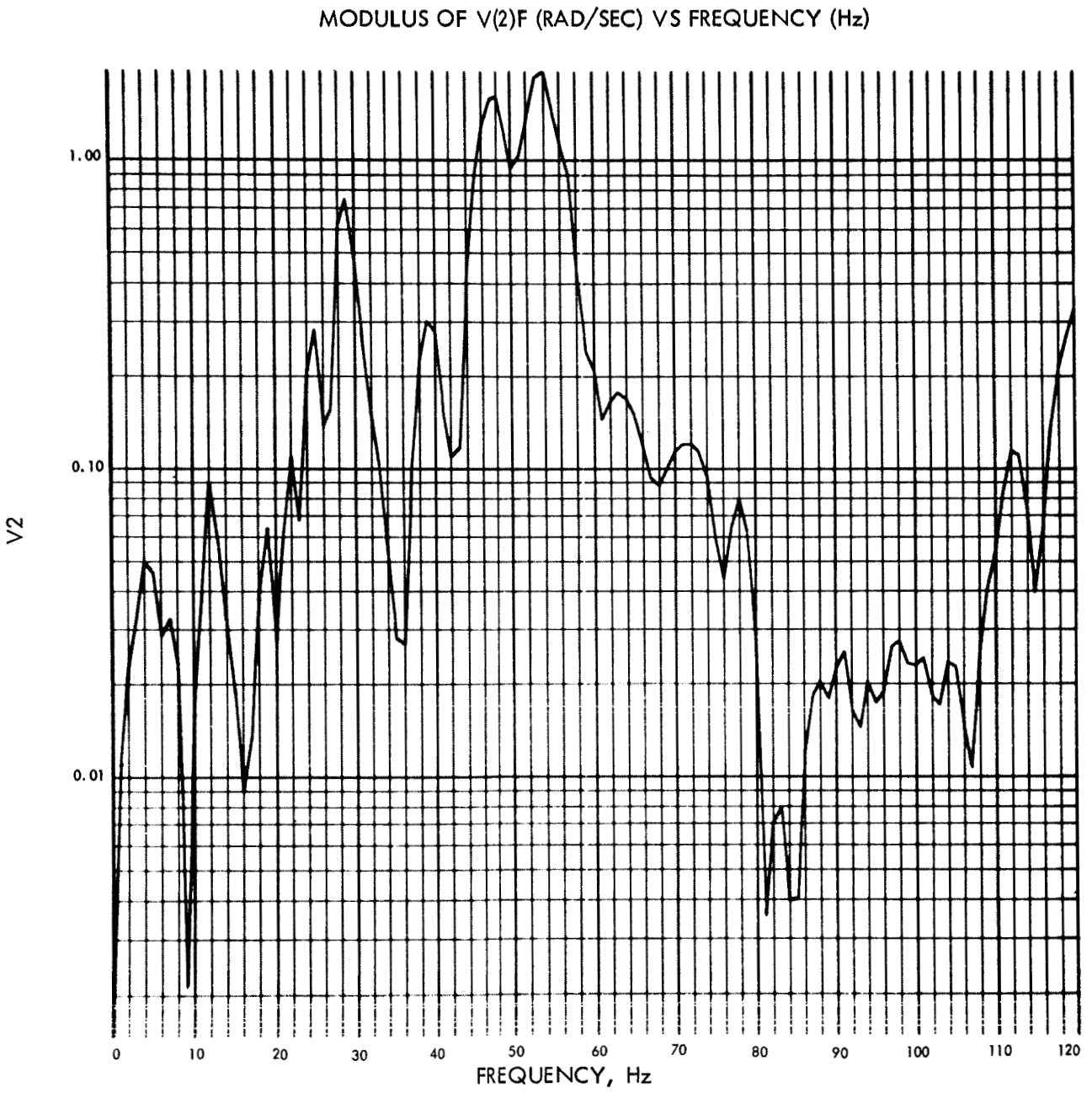

Fig. E-59. Joint 5, x_5 Fourier transform, modulus (pulse 4)

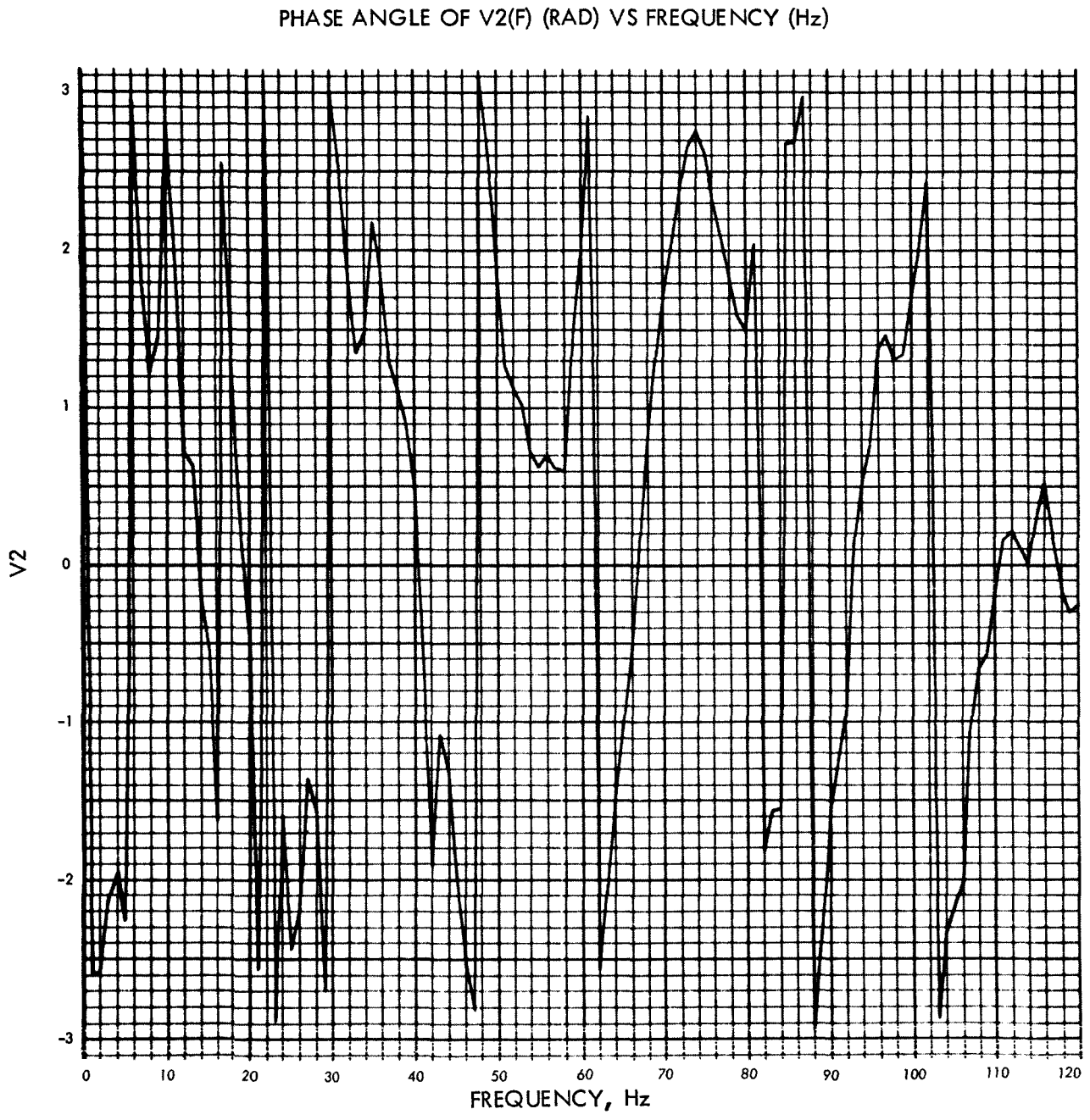

Fig. E-60. Joint 5, x_5 Fourier transform, phase angle (pulse 4)

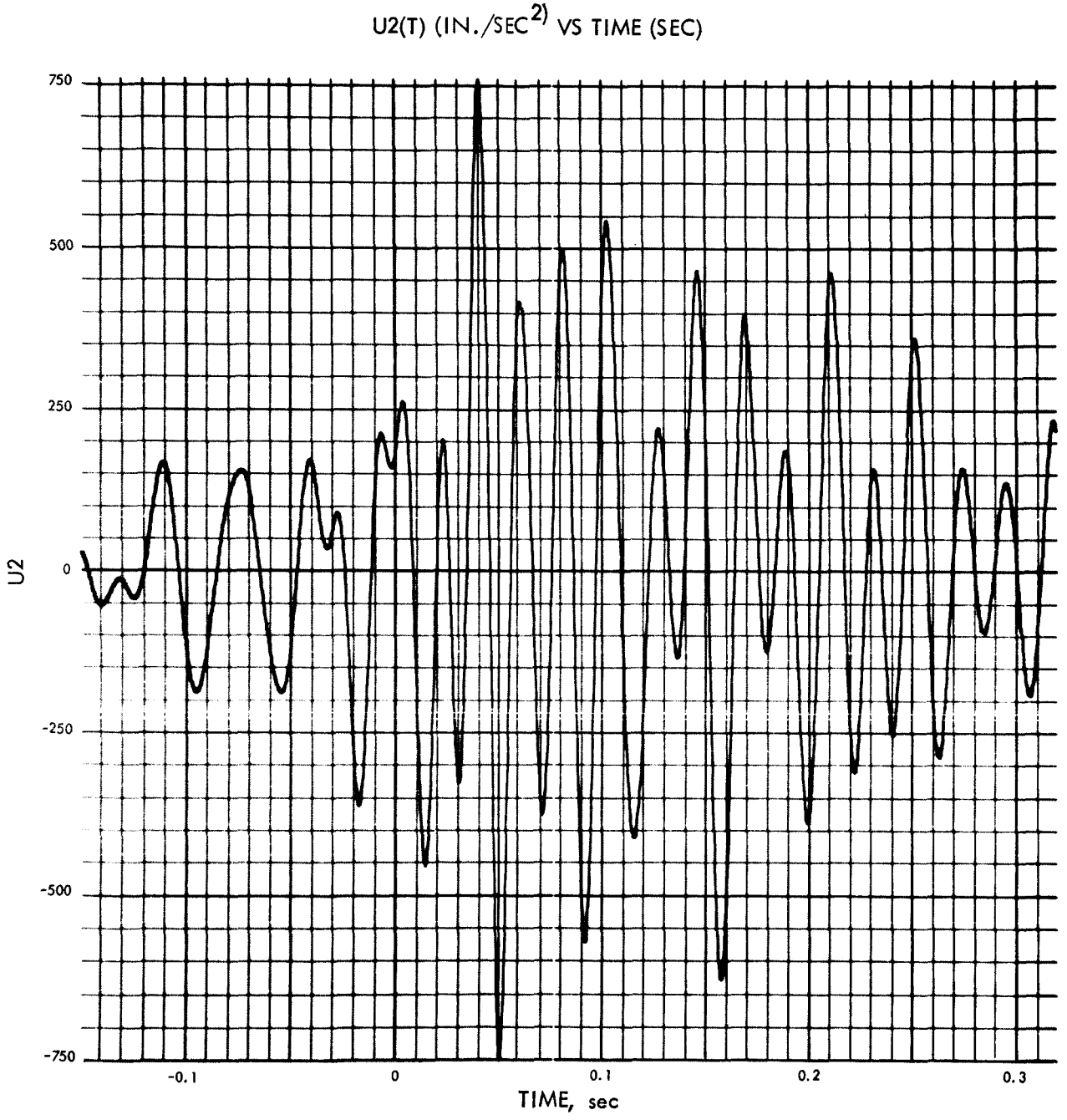

Fig. E-61. Joint 23, x_1 time history (pulse 1)

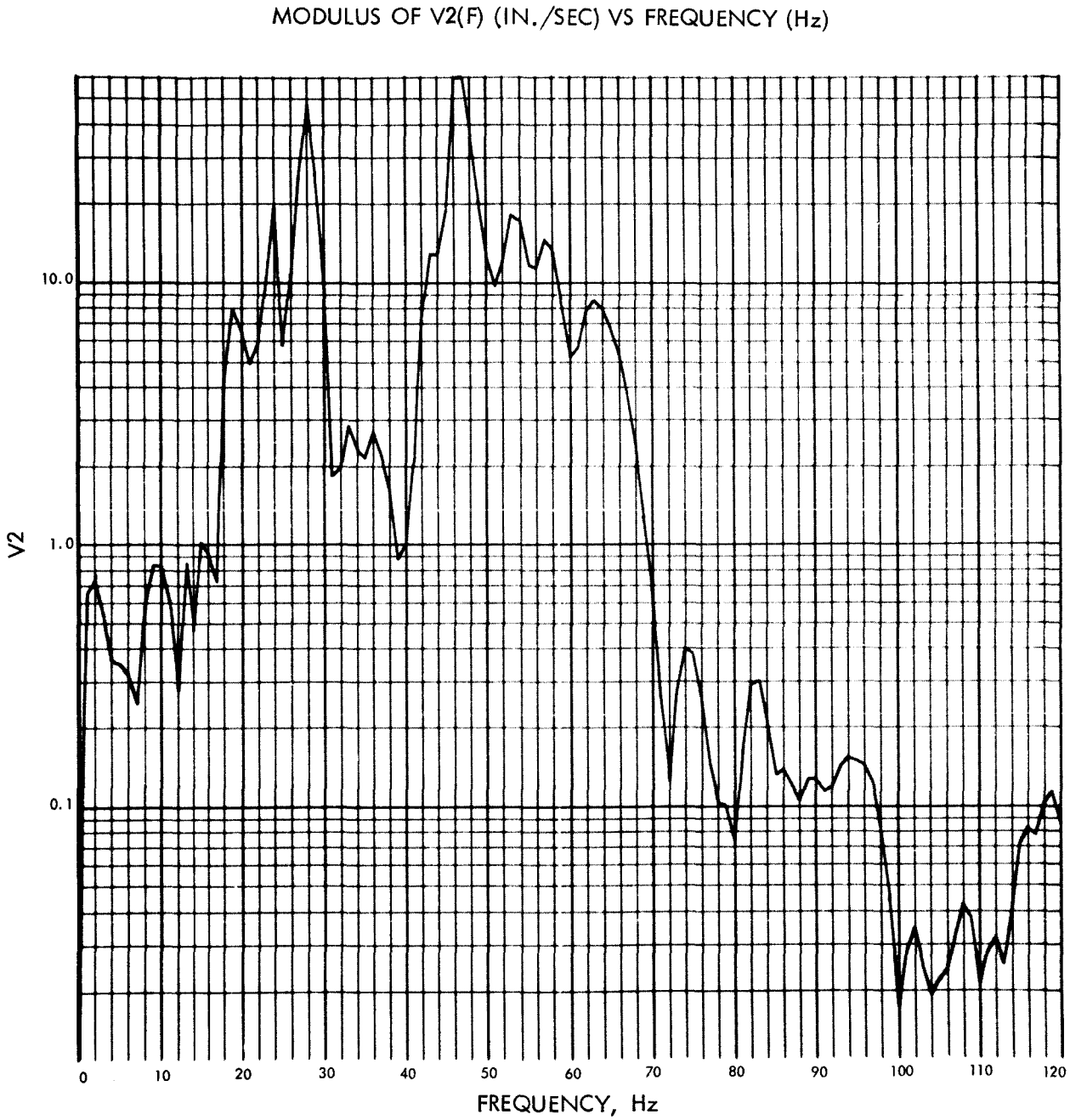

Fig. E-62. Joint 23, x_1 Fourier transform, modulus (pulse 1)

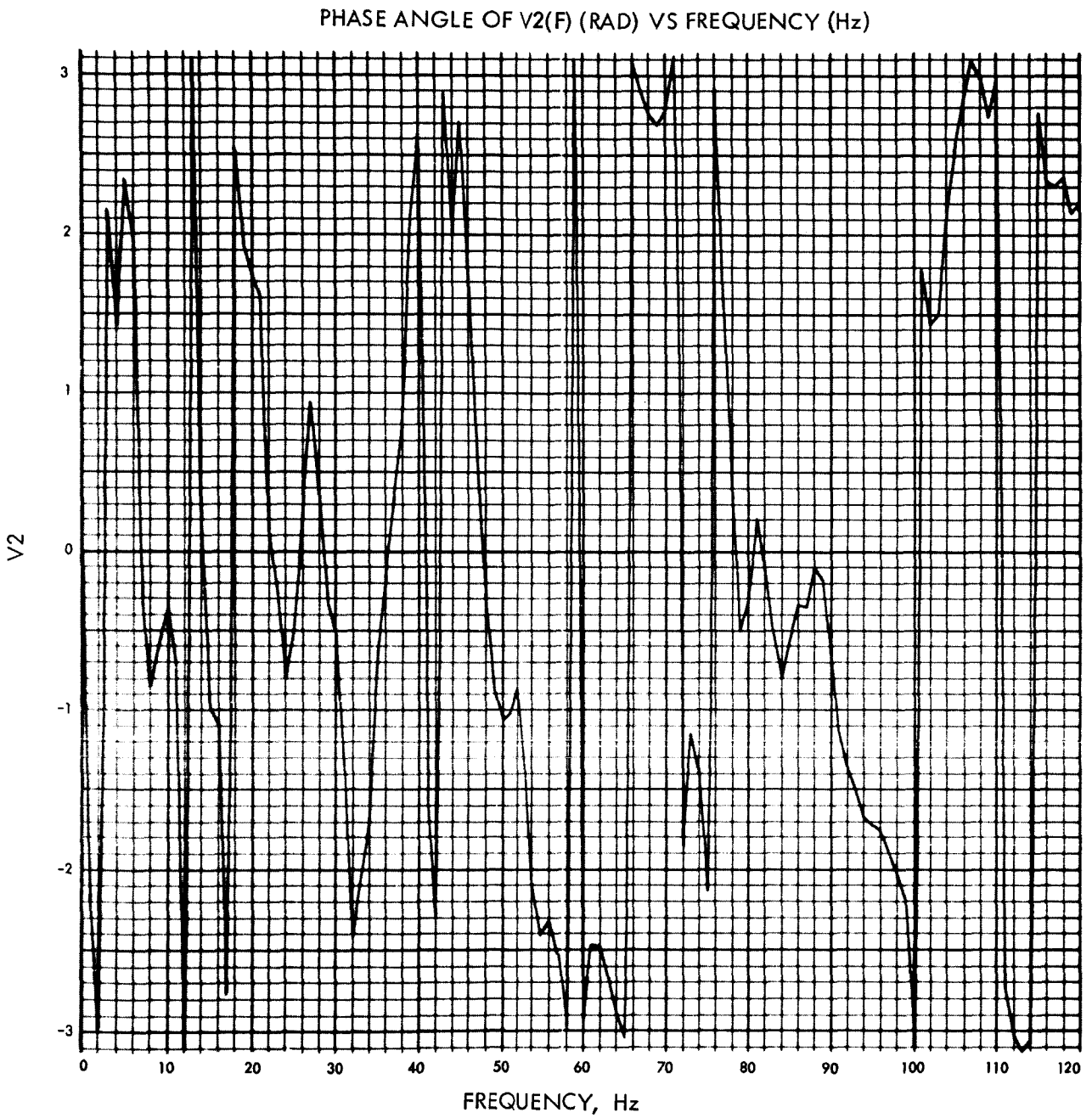

Fig. E-63. Joint 23, x_1 Fourier transform, phase angle (pulse 1)

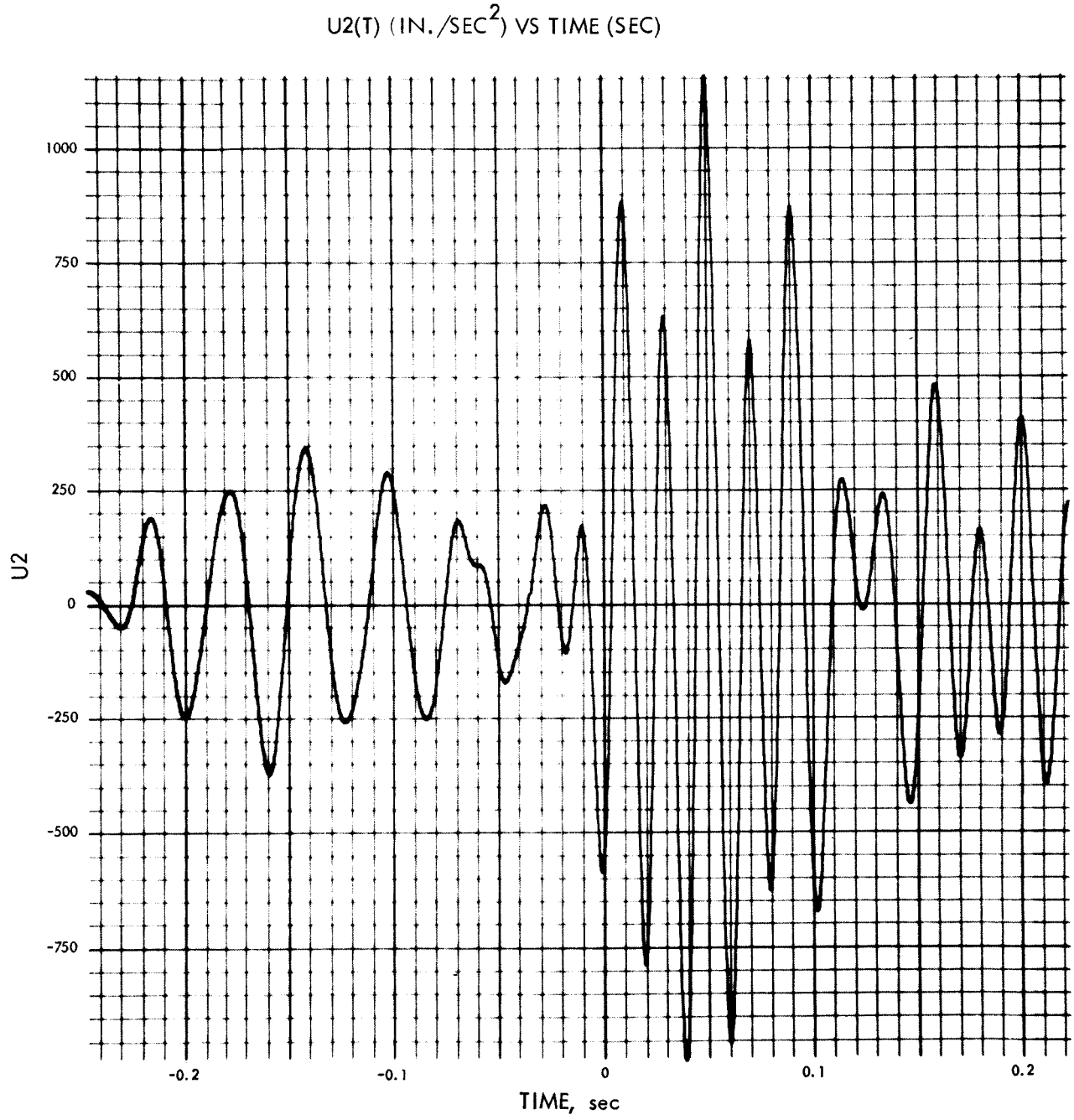

Fig. E-64. Joint 23, x_1 time history (pulse 2)

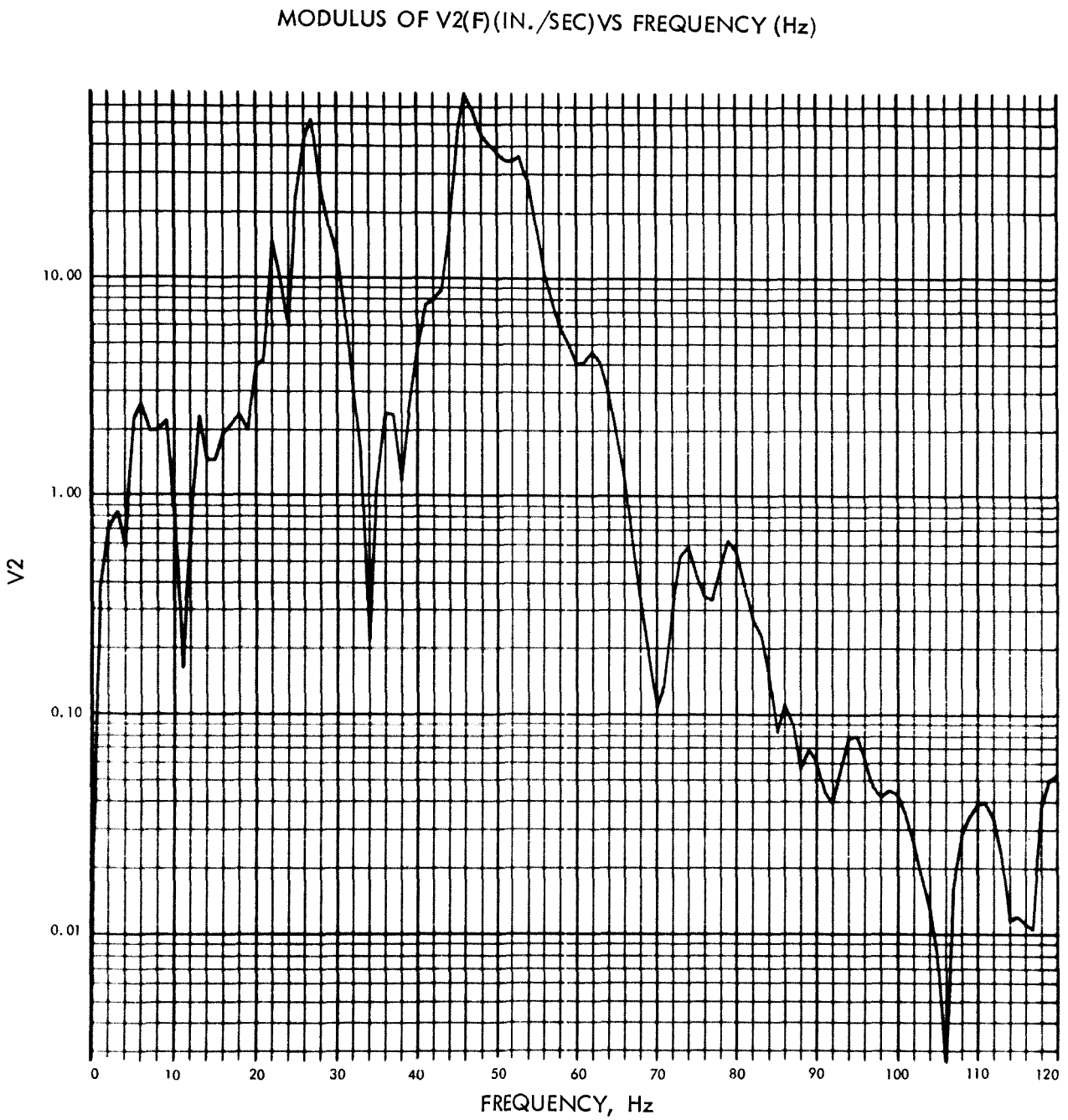

Fig. E-65. Joint 23, x_1 Fourier transform, modulus (pulse 2)

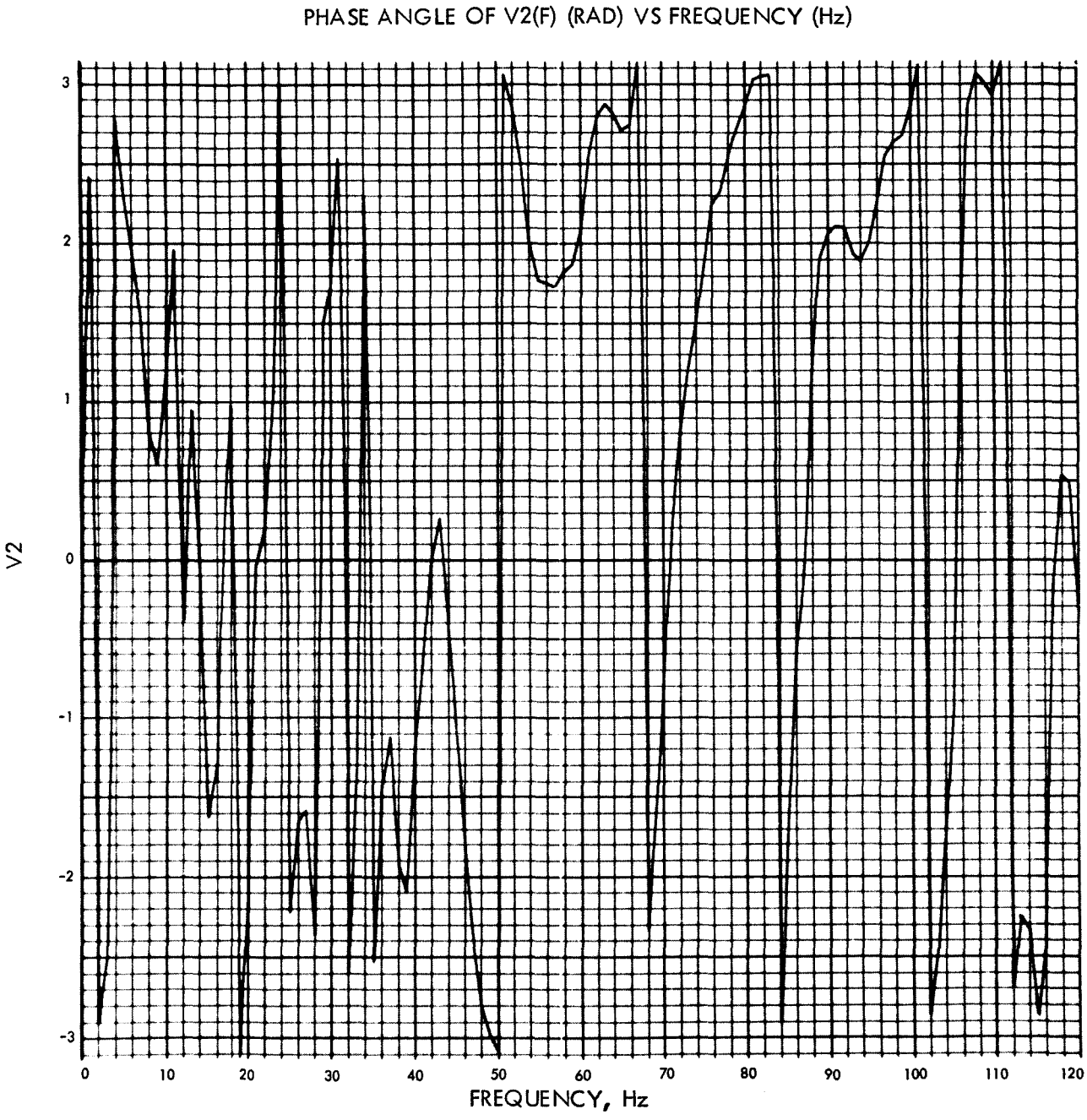

Fig. E-66. Joint 23, x_1 Fourier transform, phase angle (pulse 2)

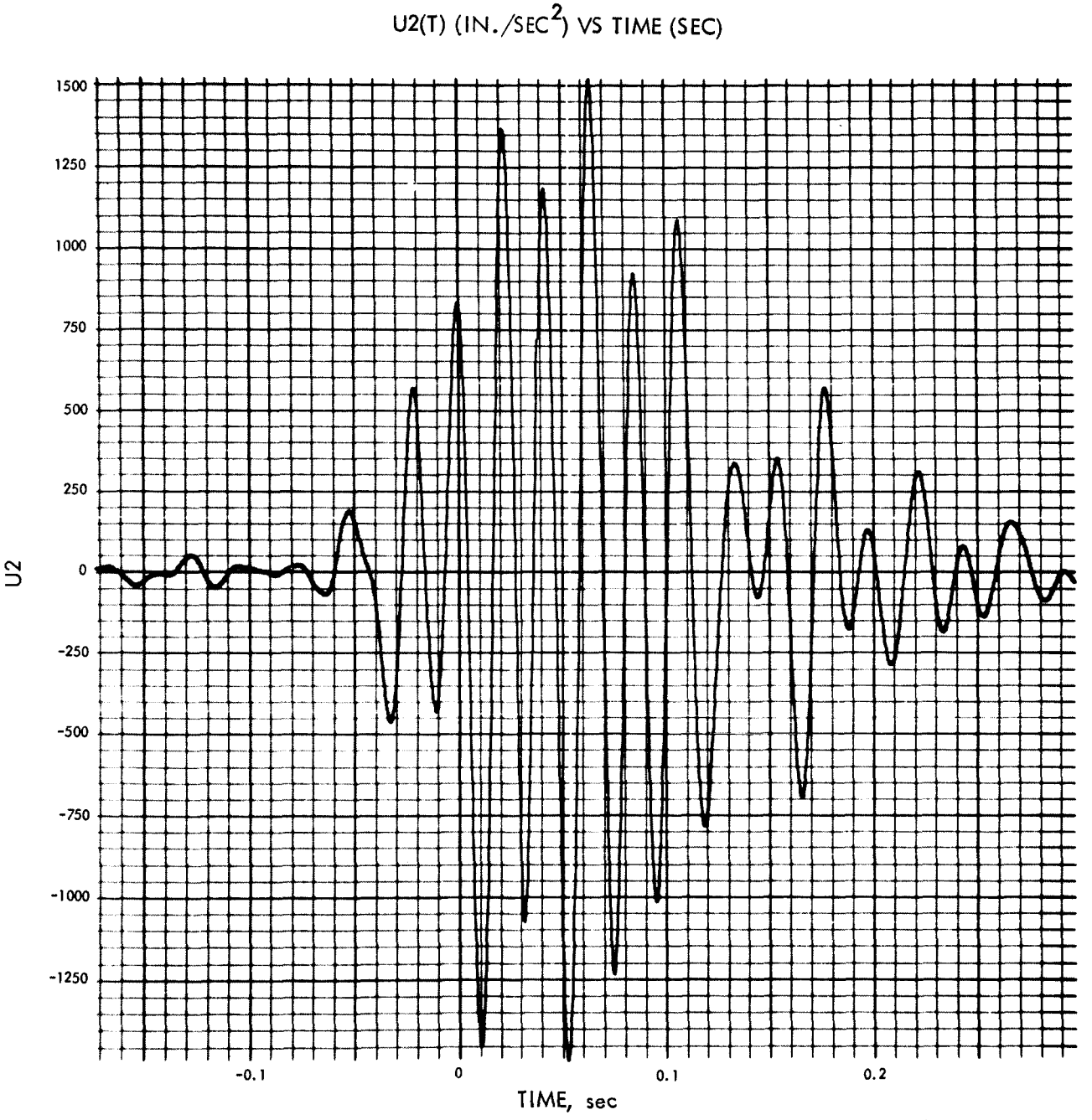

Fig. E-67. Joint 23, x_1 time history (pulse 3)

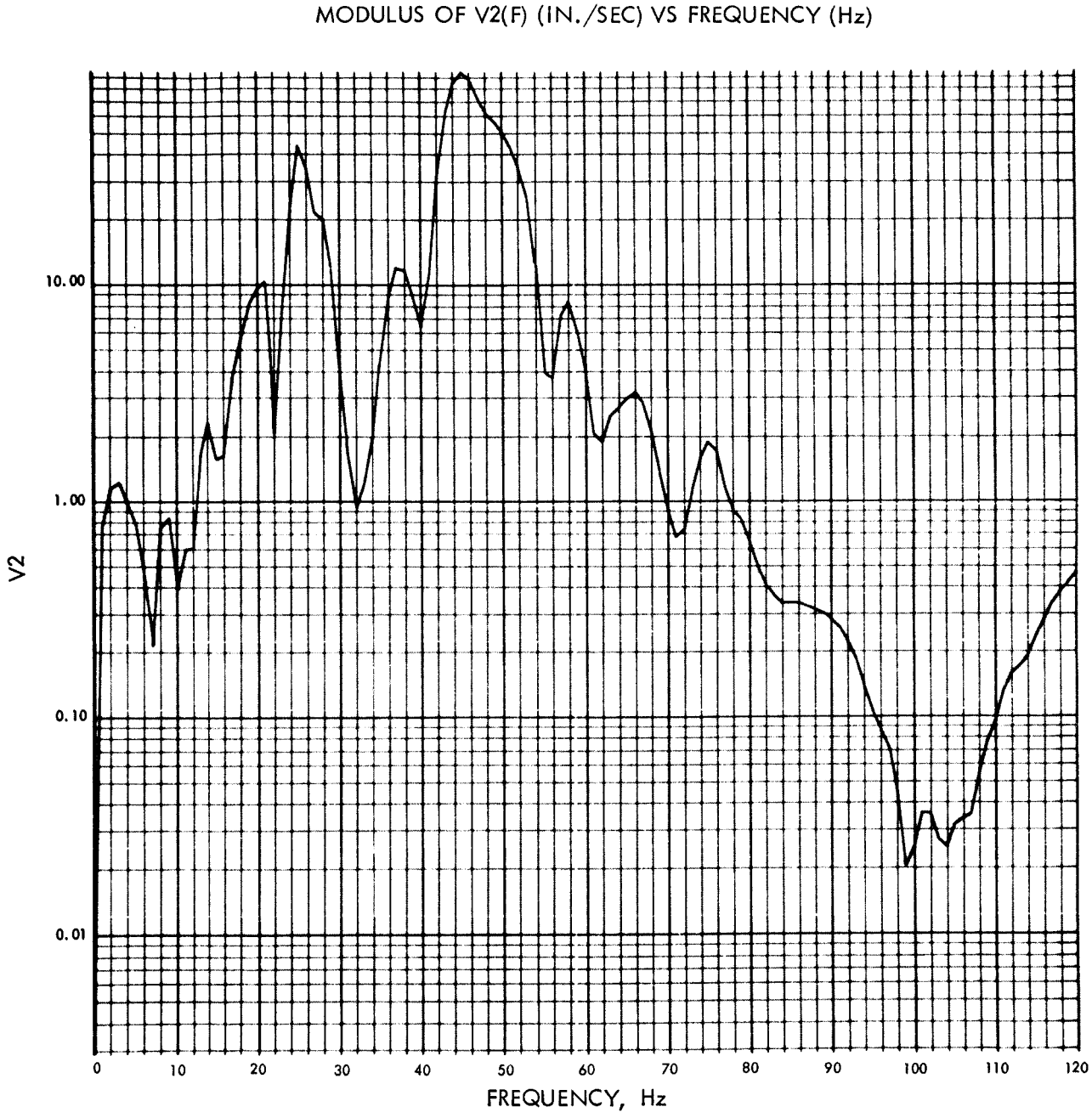

Fig. E-68. Joint 23, x_1 Fourier transform, modulus (pulse 3)

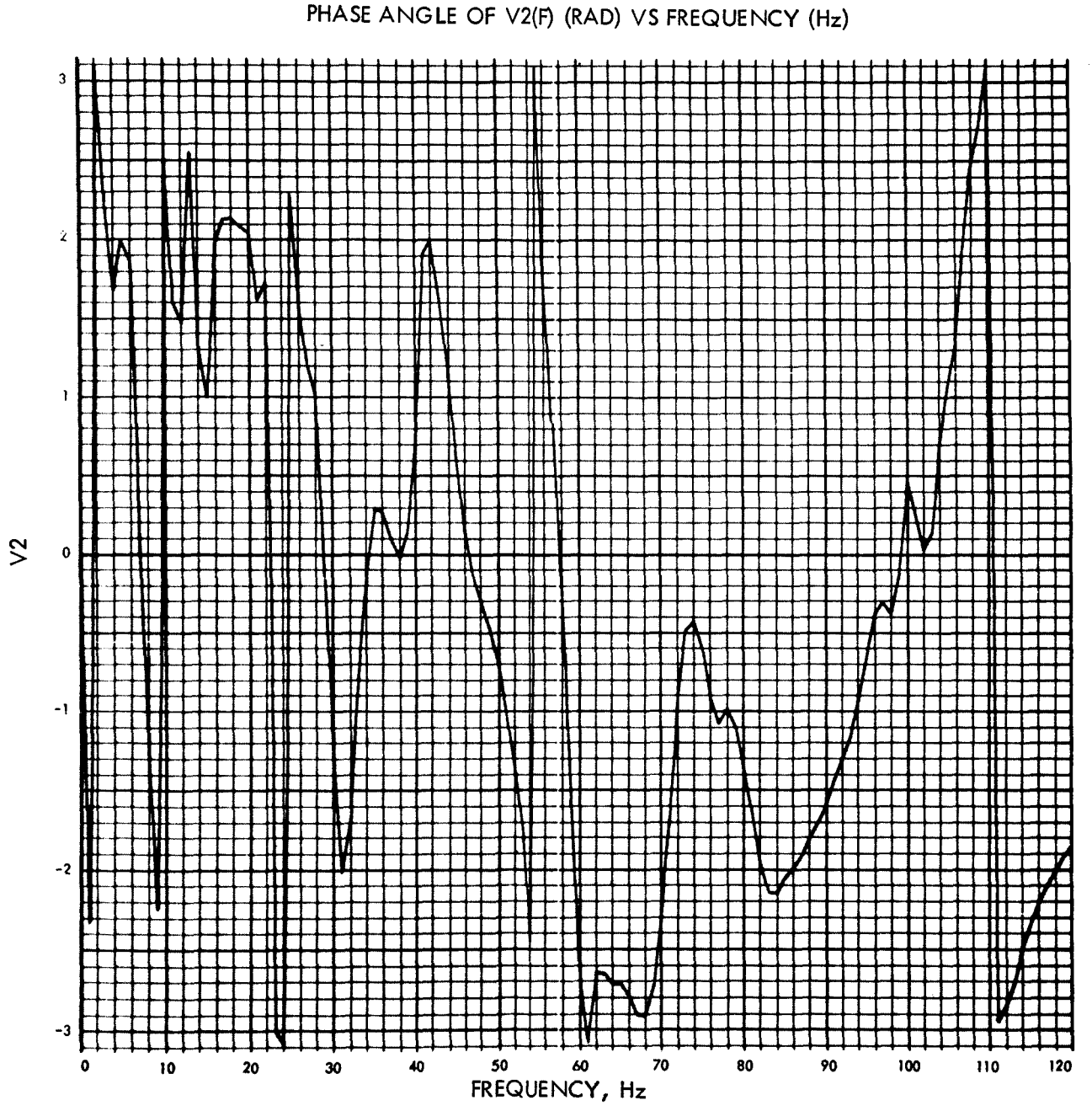

Fig. E-69. Joint 23, x_1 Fourier transform, phase angle (pulse 3)

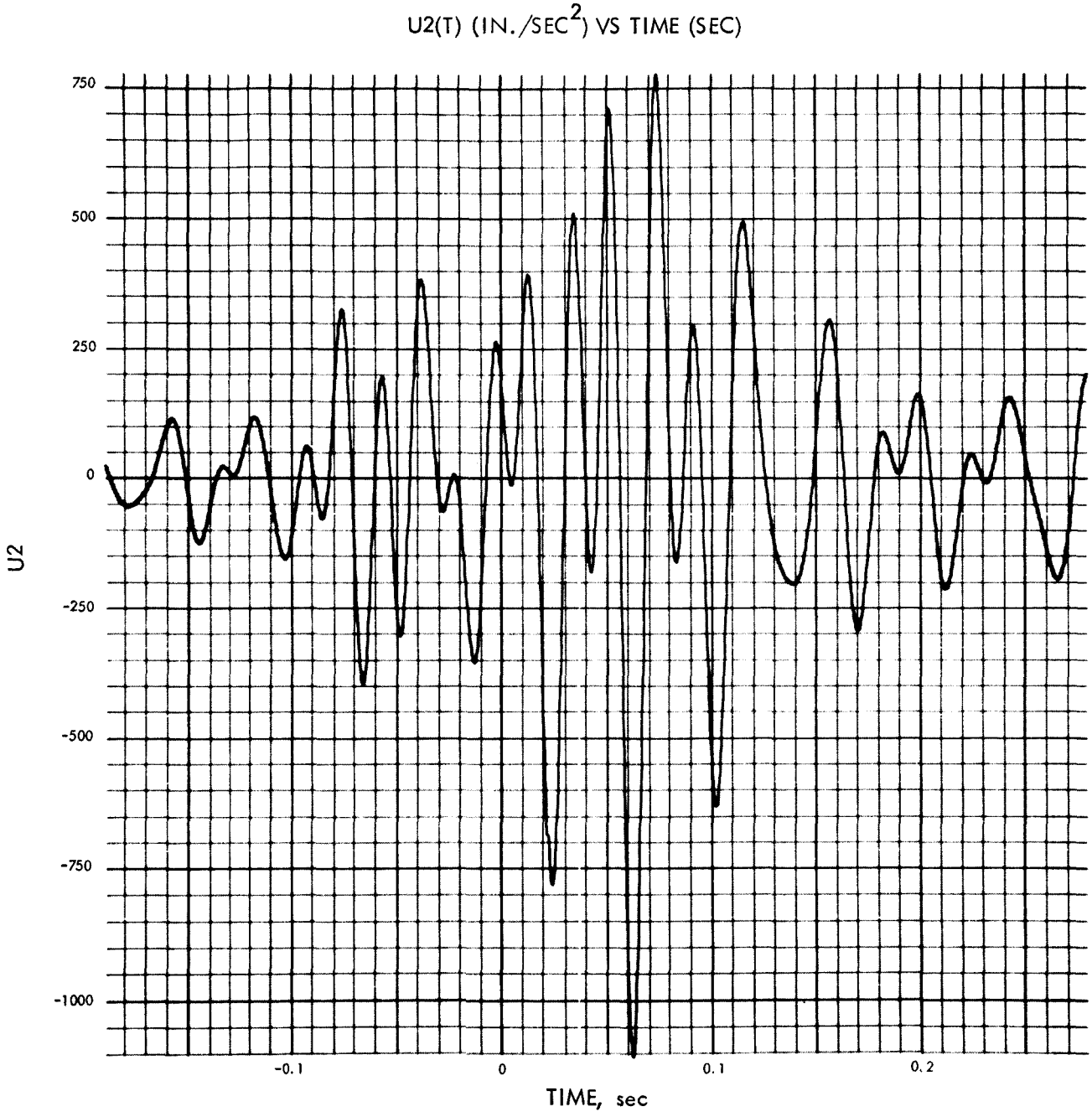

Fig. E-70. Joint 23, x_1 time history (pulse 4)

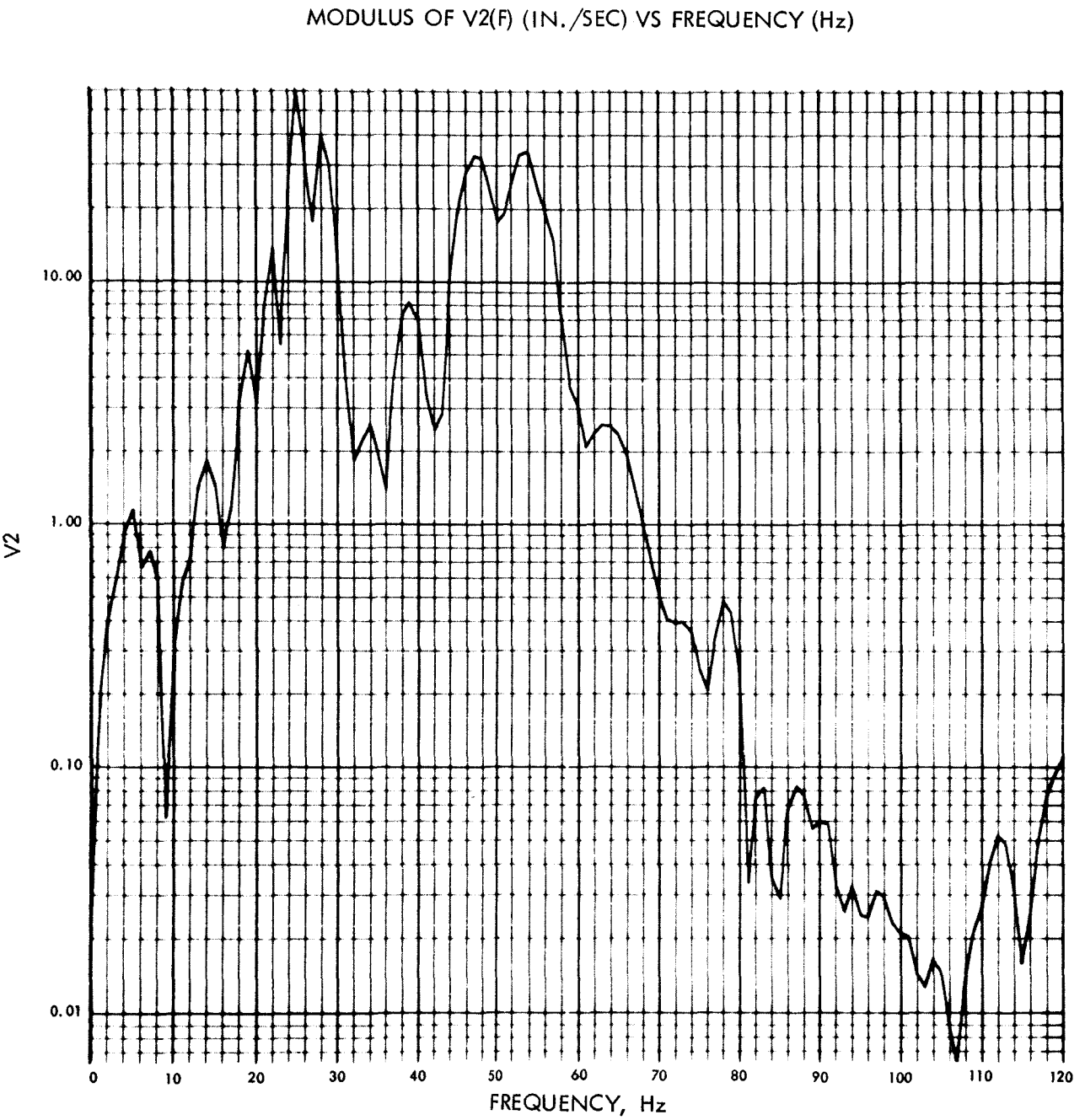

Fig. E-71. Joint 23, x_1 Fourier transform, modulus (pulse 4)

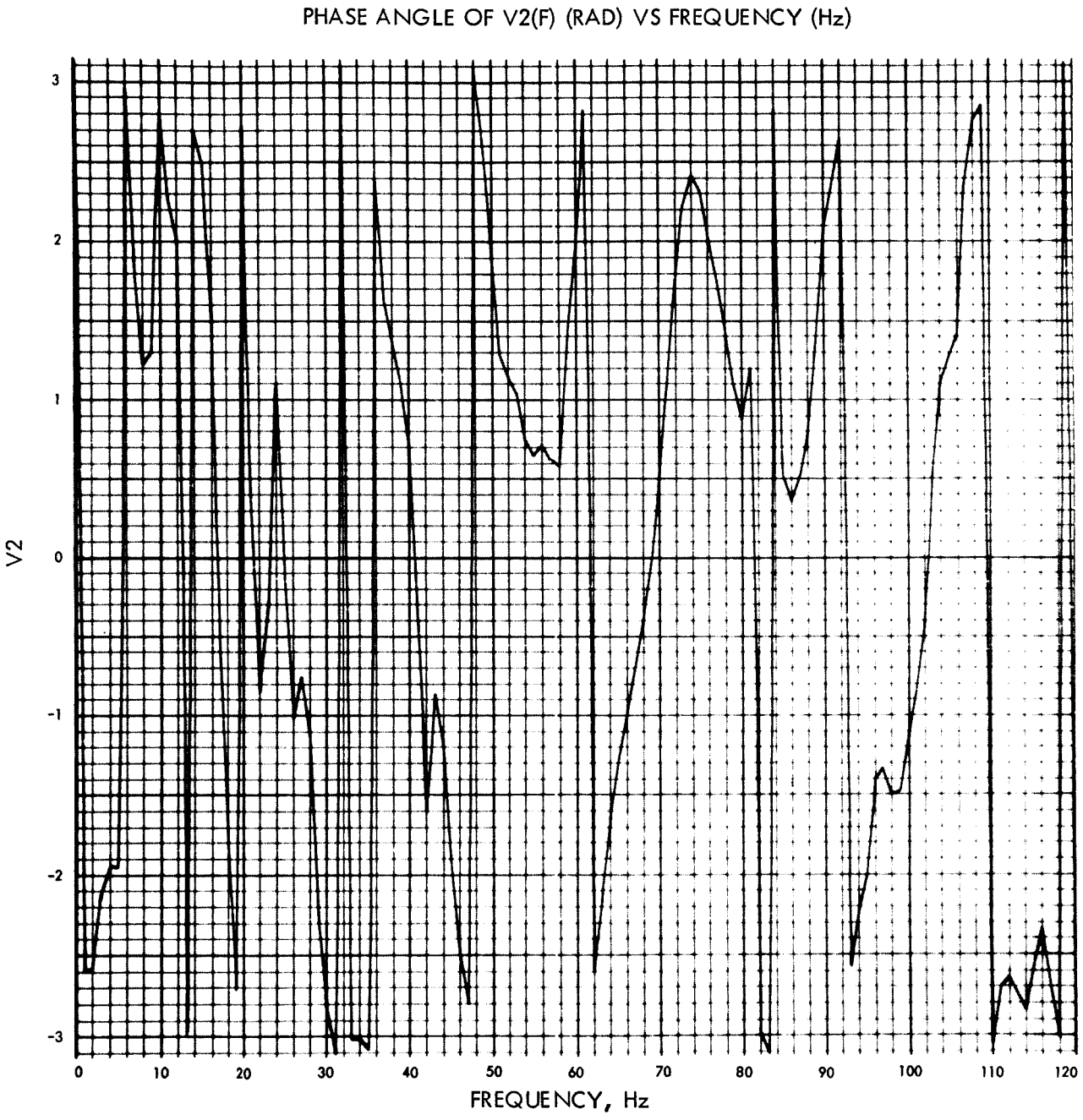

Fig. E-72. Joint 23, x_1 Fourier transform, phase angle (pulse 4)

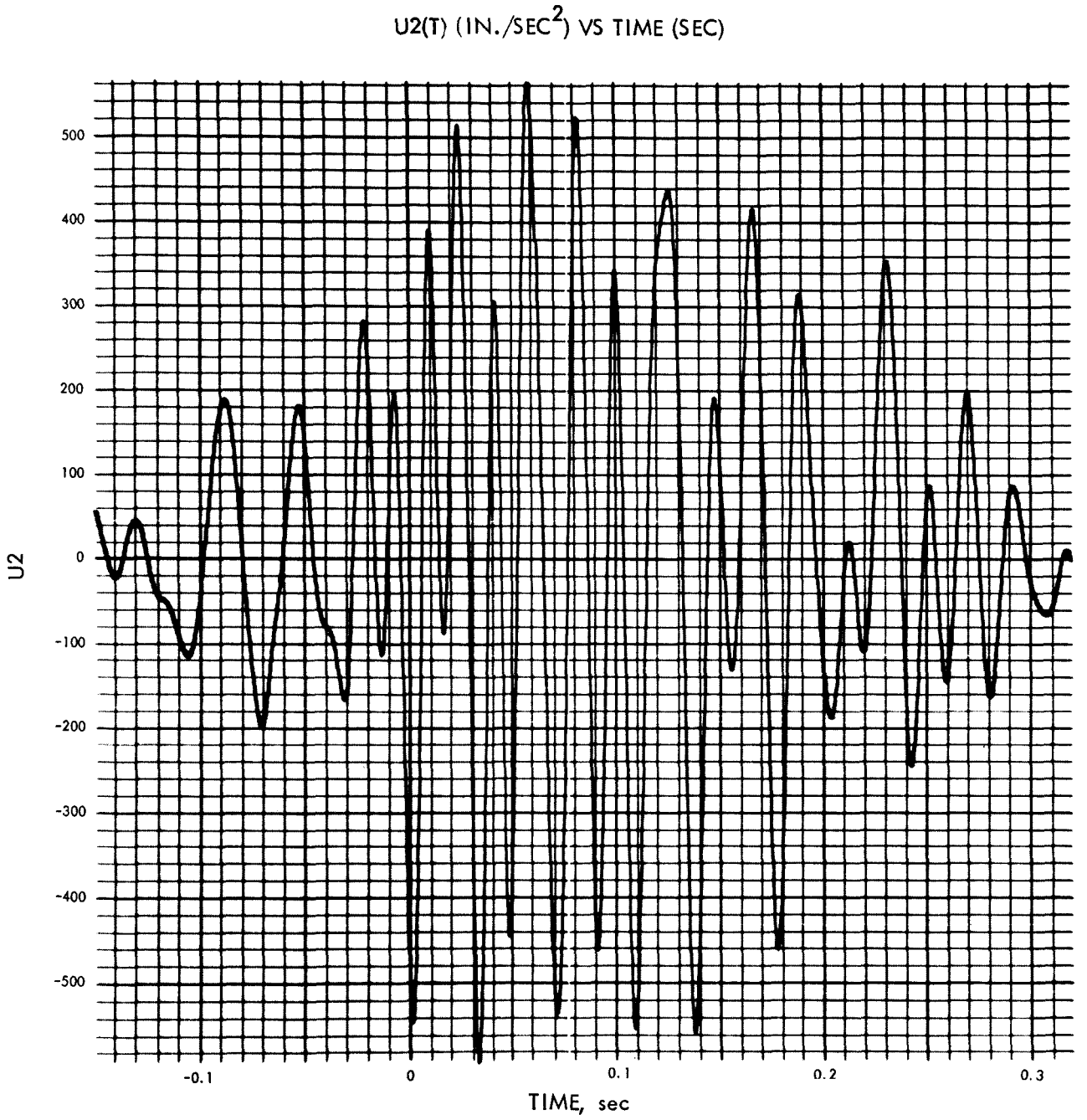

Fig. E-73. Joint 23, x_3 time history (pulse 1)

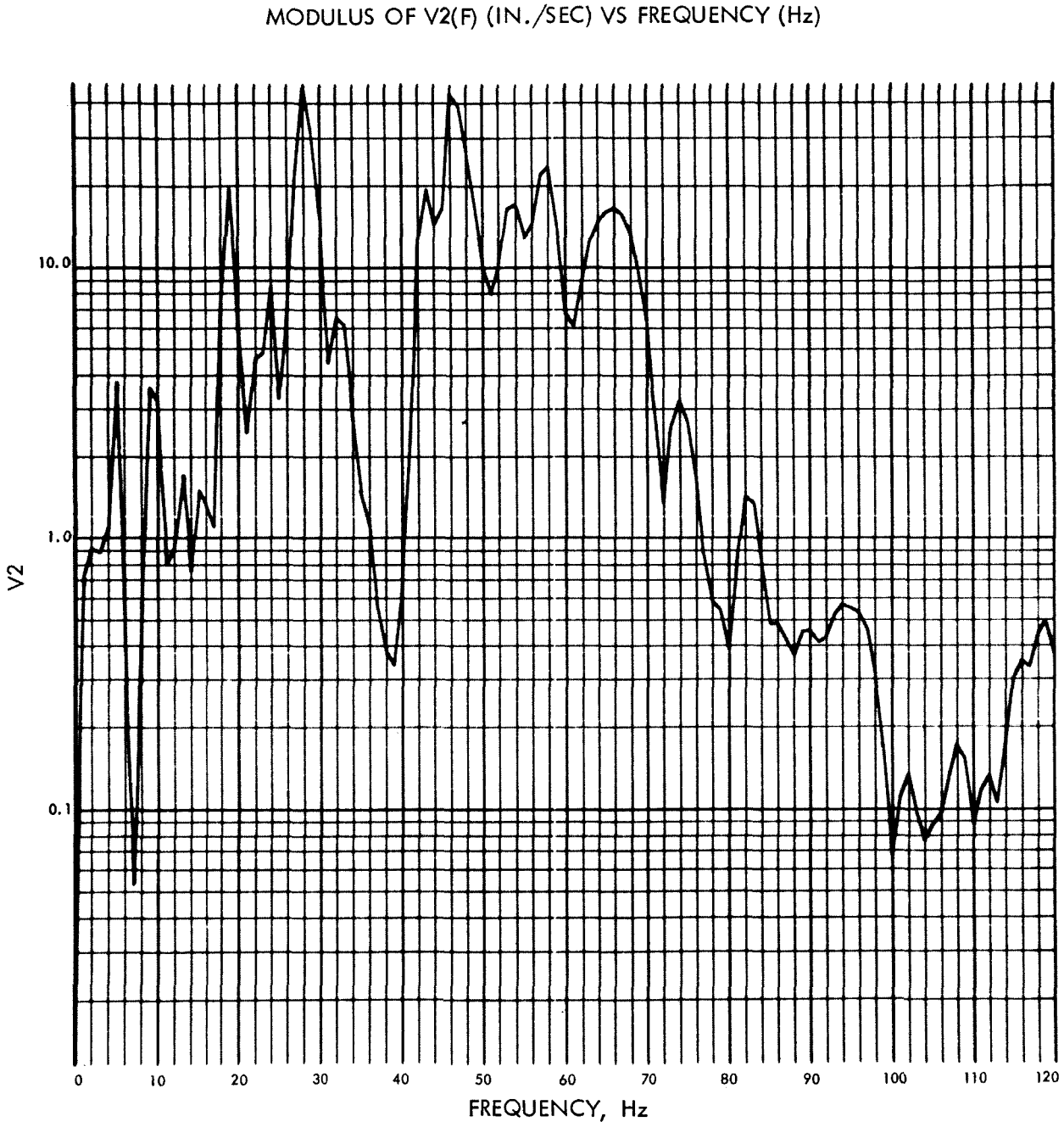

Fig. E-74. Joint 23, x_3 Fourier transform, modulus (pulse 1)

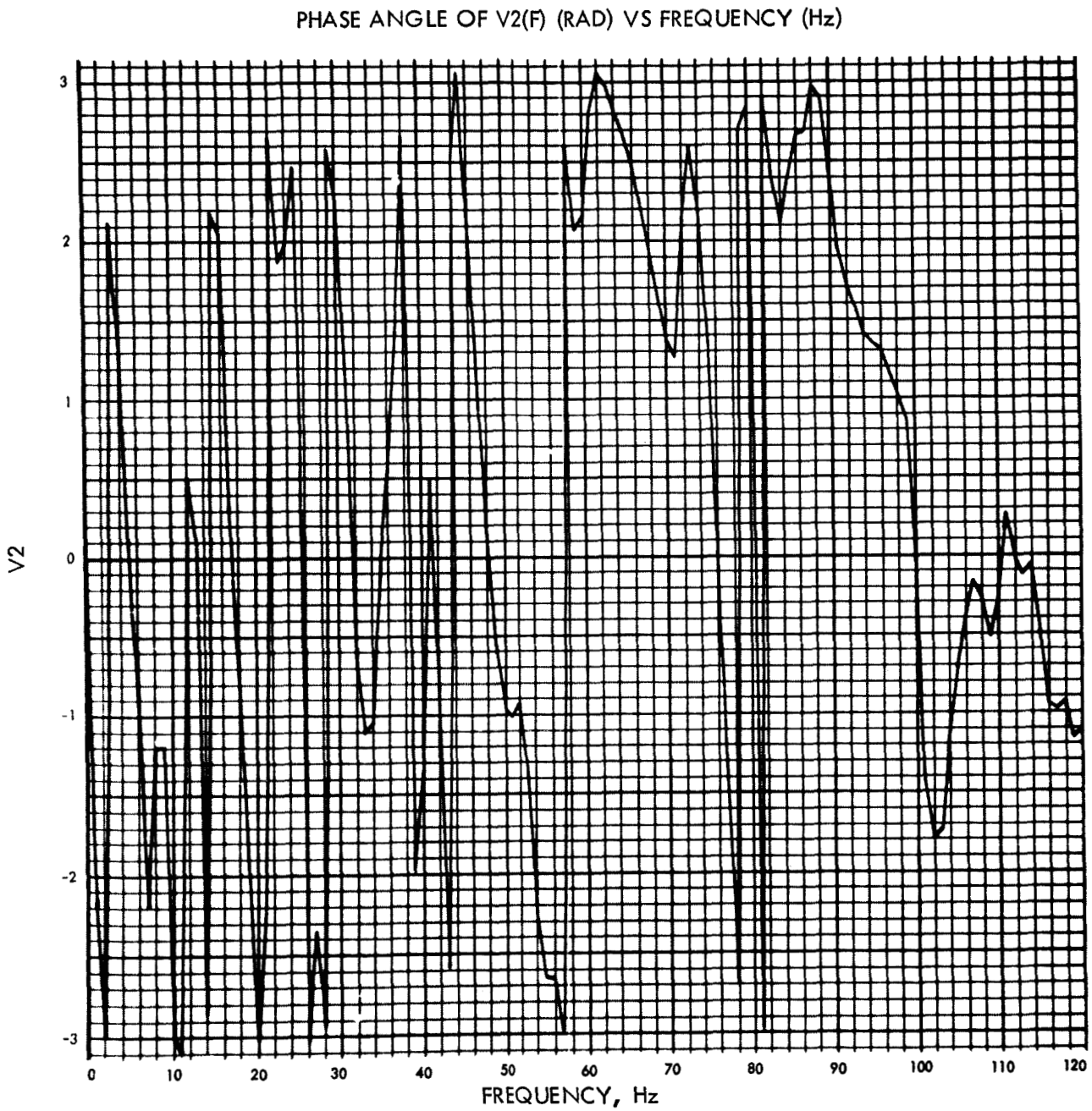

Fig. E-75. Joint 23, x_3 Fourier transform, phase angle (pulse 1)

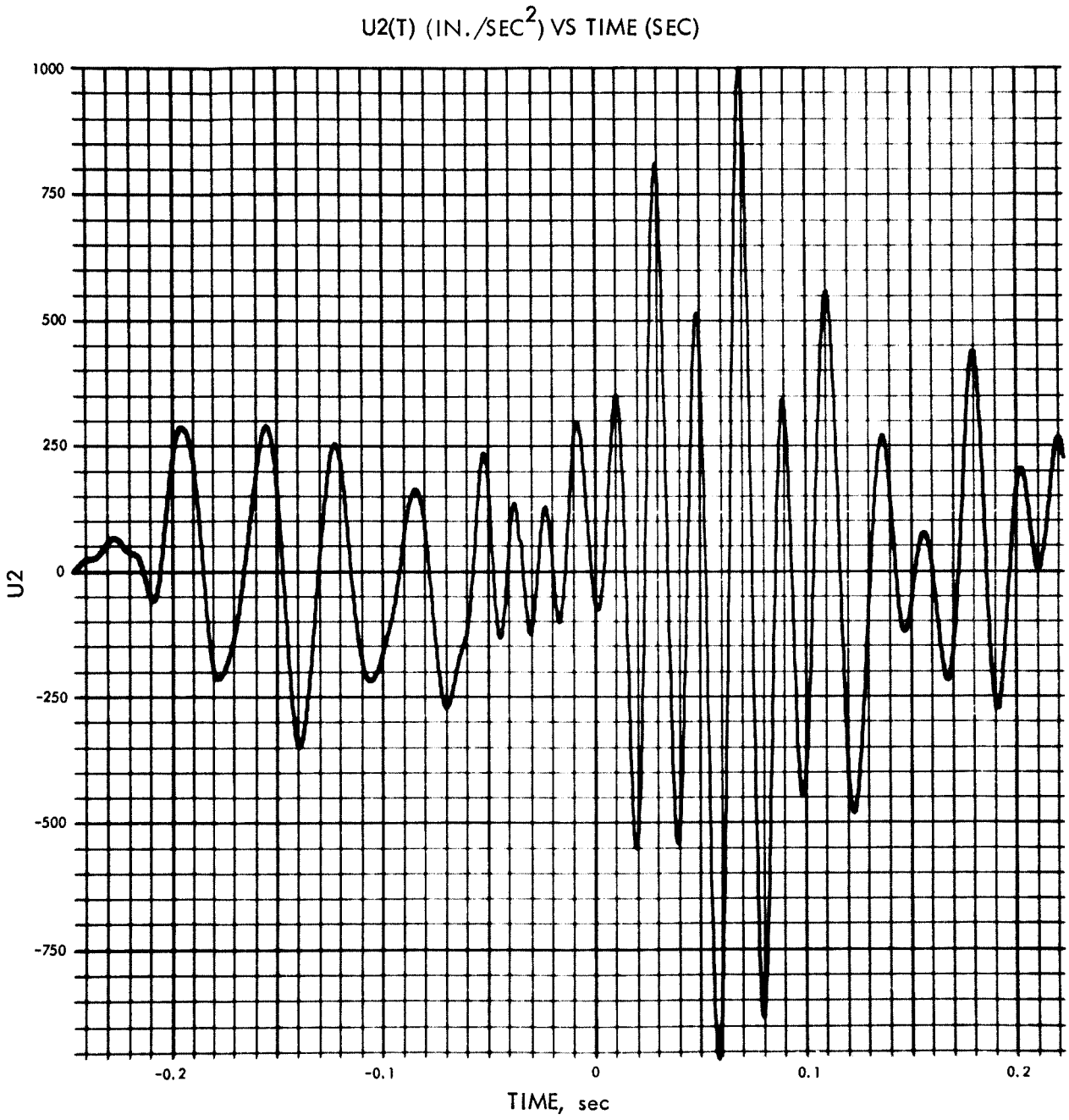

Fig. E-76. Joint 23, x_3 time history (pulse 2)

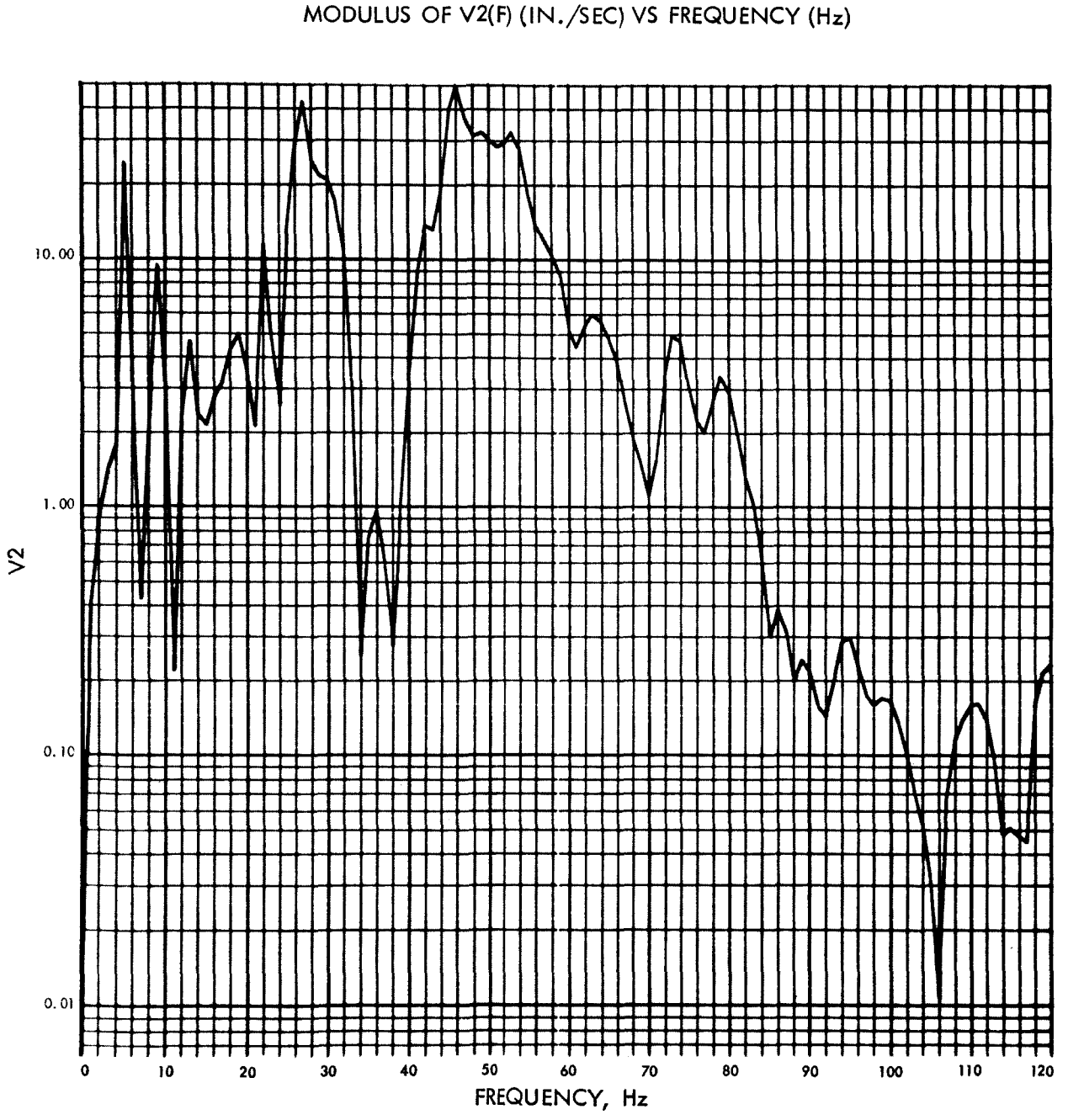

Fig. E-77. Joint 23, x_3 Fourier transform, modulus (pulse 2)

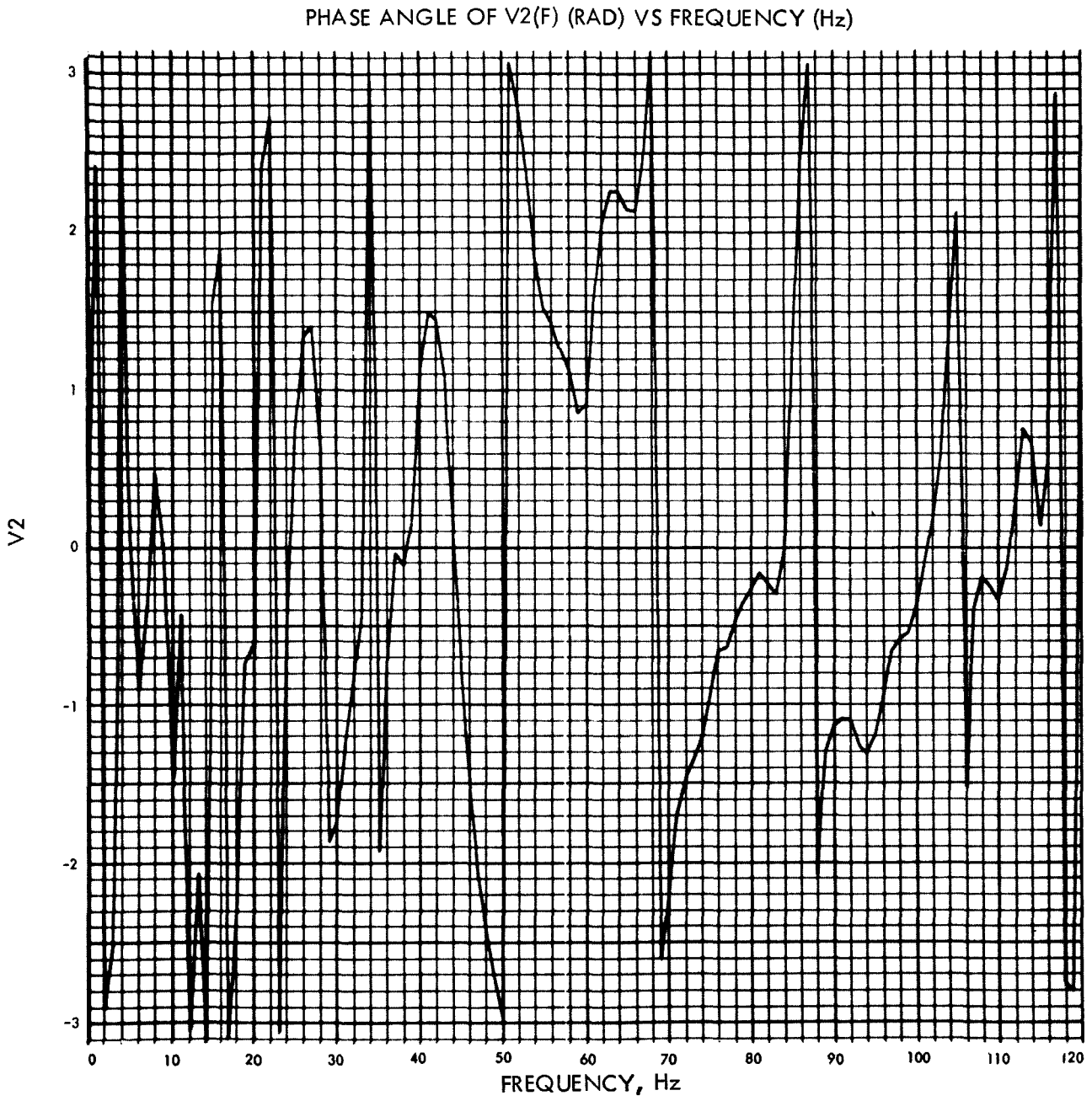

Fig. E-78. Joint 23, x_3 Fourier transform, phase angle (pulse 2)

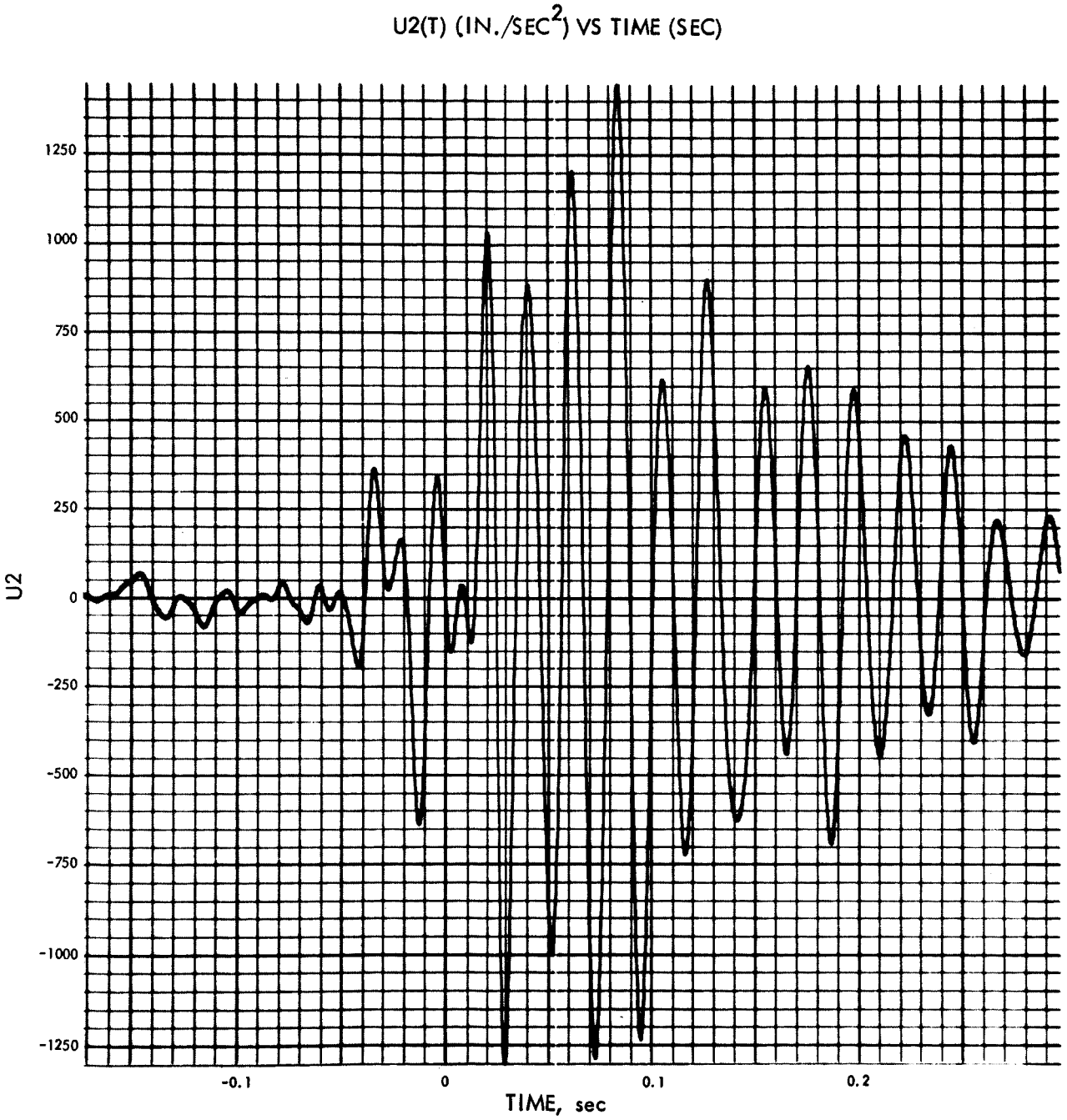

Fig. E-79. Joint 23, x_3 time history (pulse 3)

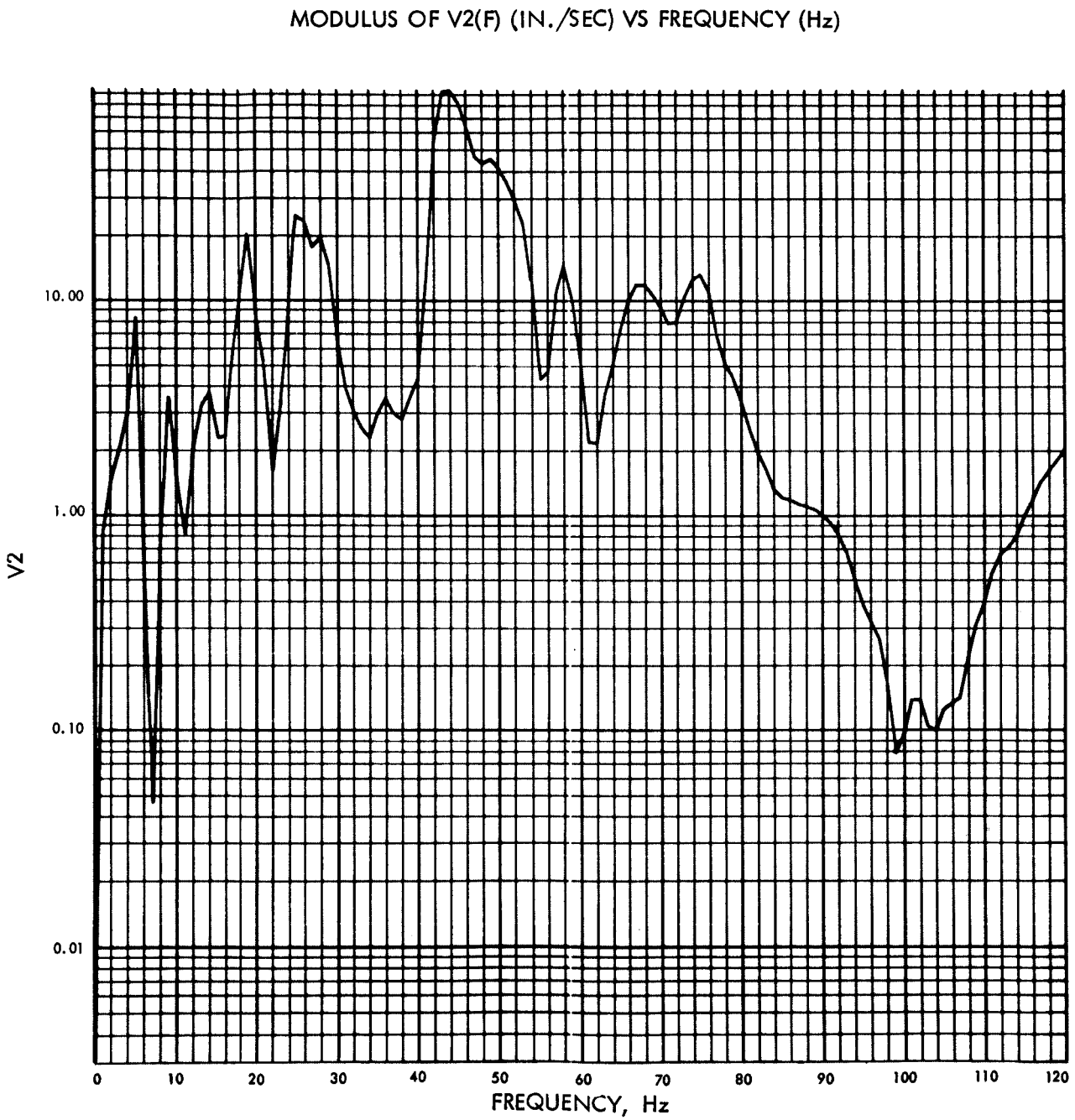

Fig. E-80. Joint 23, x_3 Fourier transform, modulus (pulse 3)

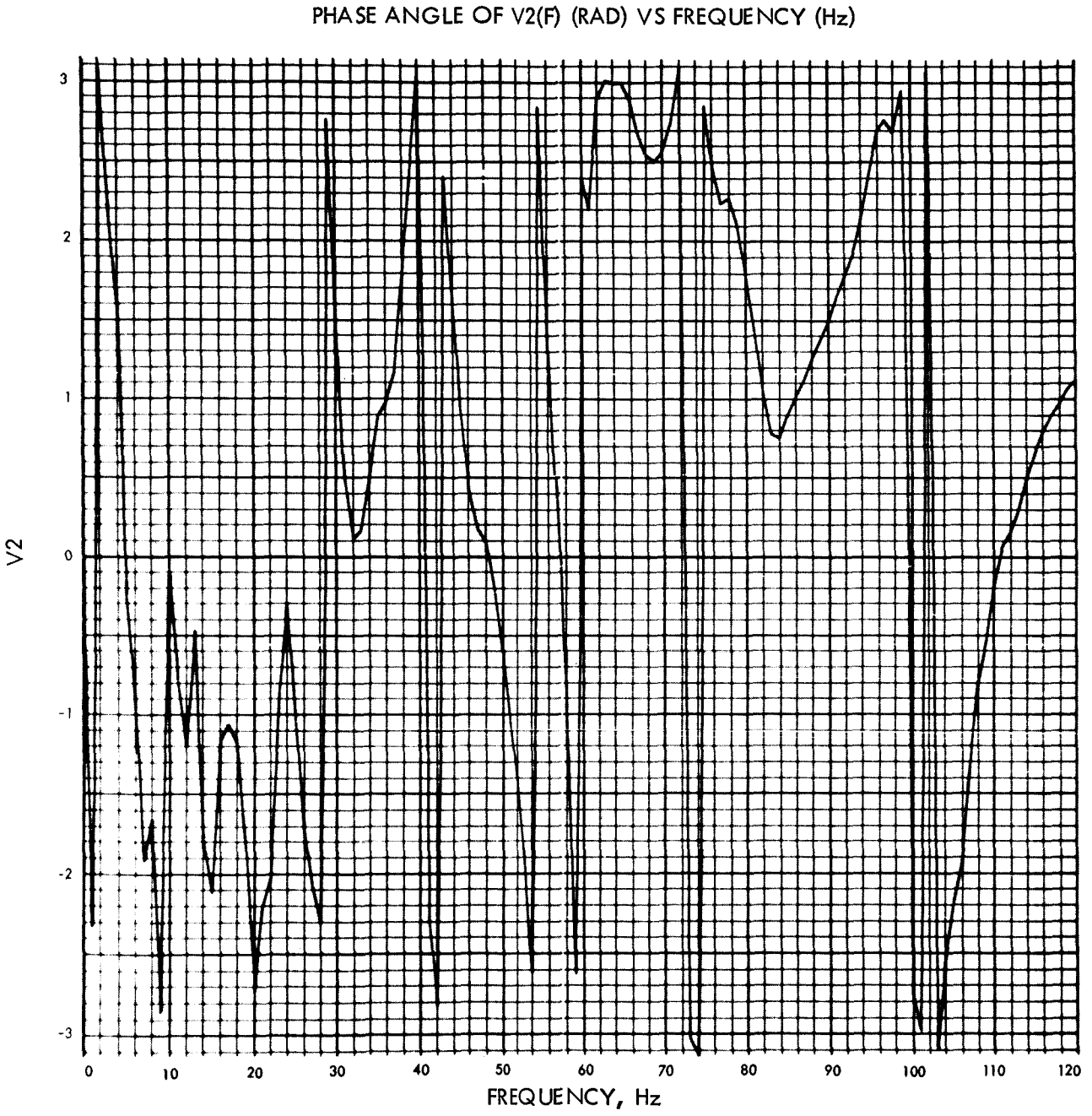

Fig. E-81. Joint 23, x_3 Fourier transform, phase angle (pulse 3)

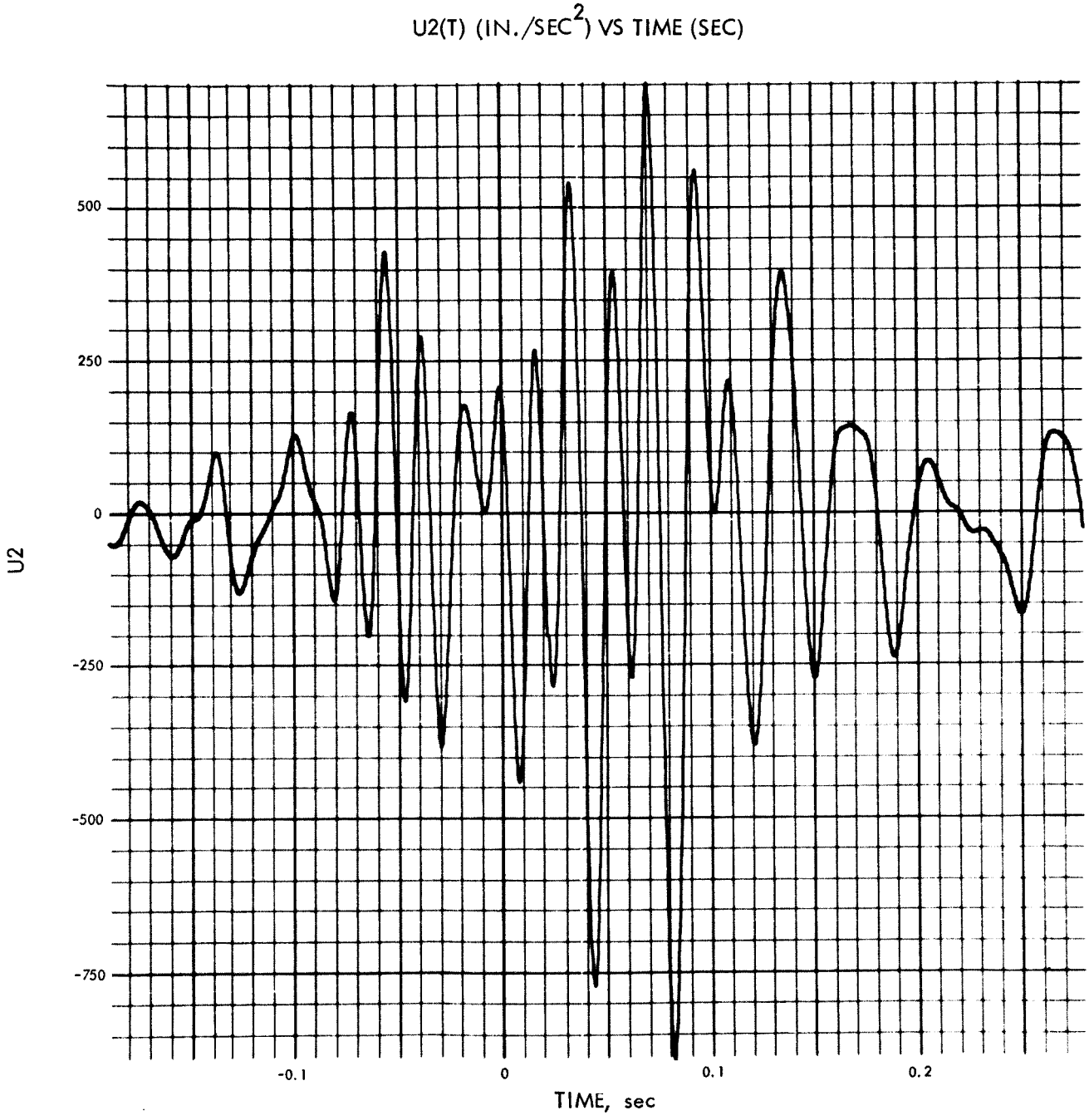

Fig. E-82. Joint 23, x_3 time history (pulse 4)

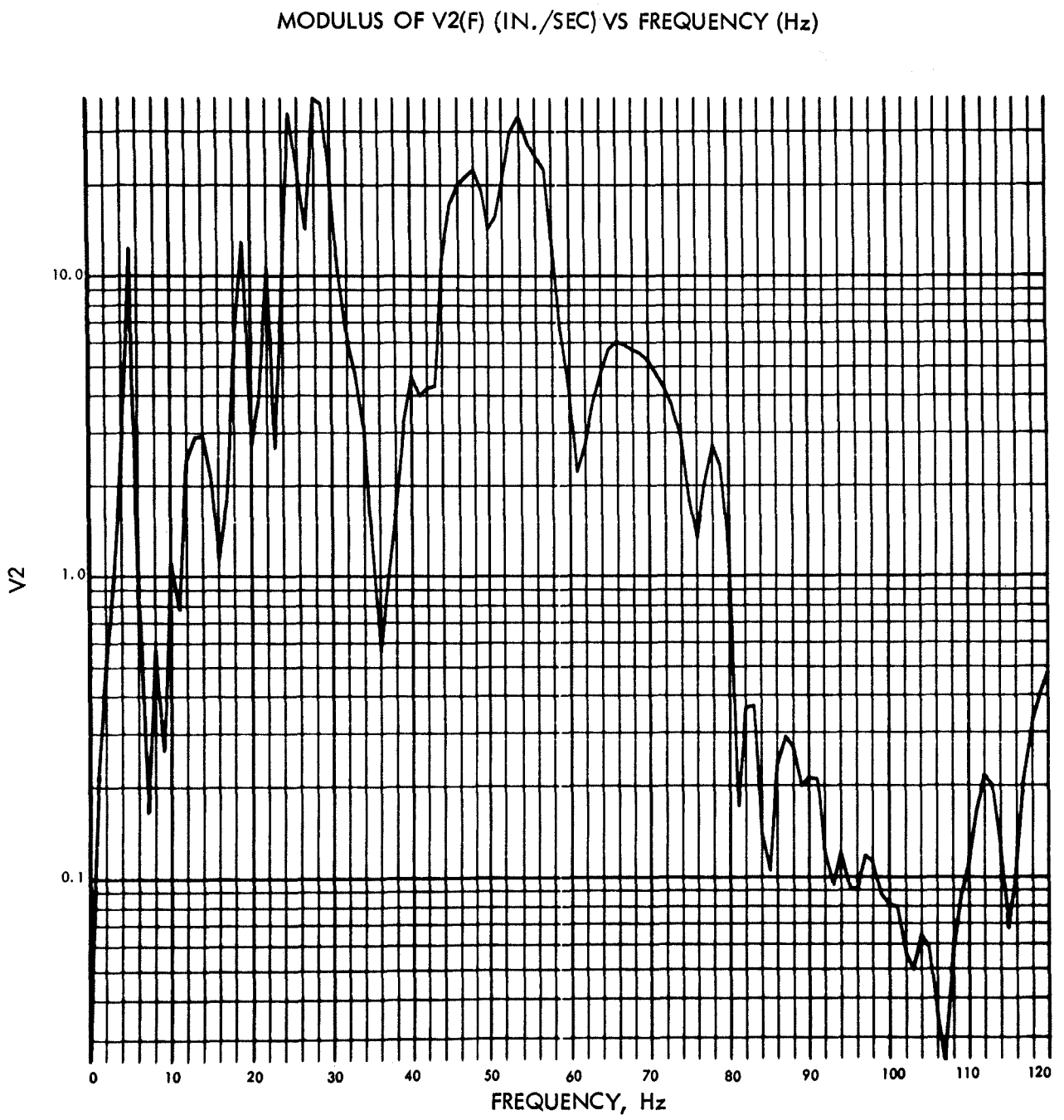

Fig. E-83. Joint 23, x_3 Fourier transform, modulus (pulse 4)

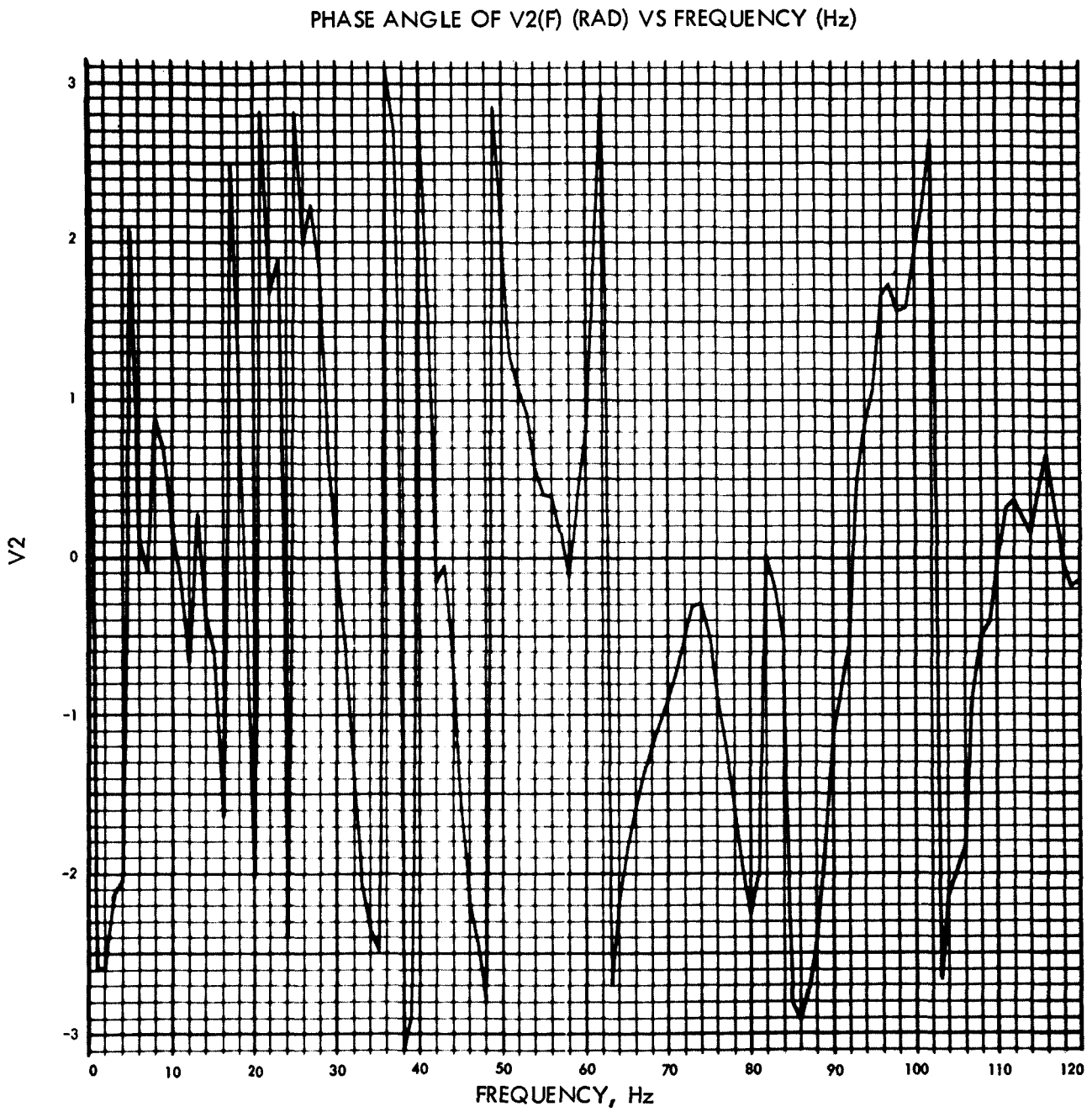

Fig. E-84. Joint 23, x_3 Fourier transform, phase angle (pulse 4)

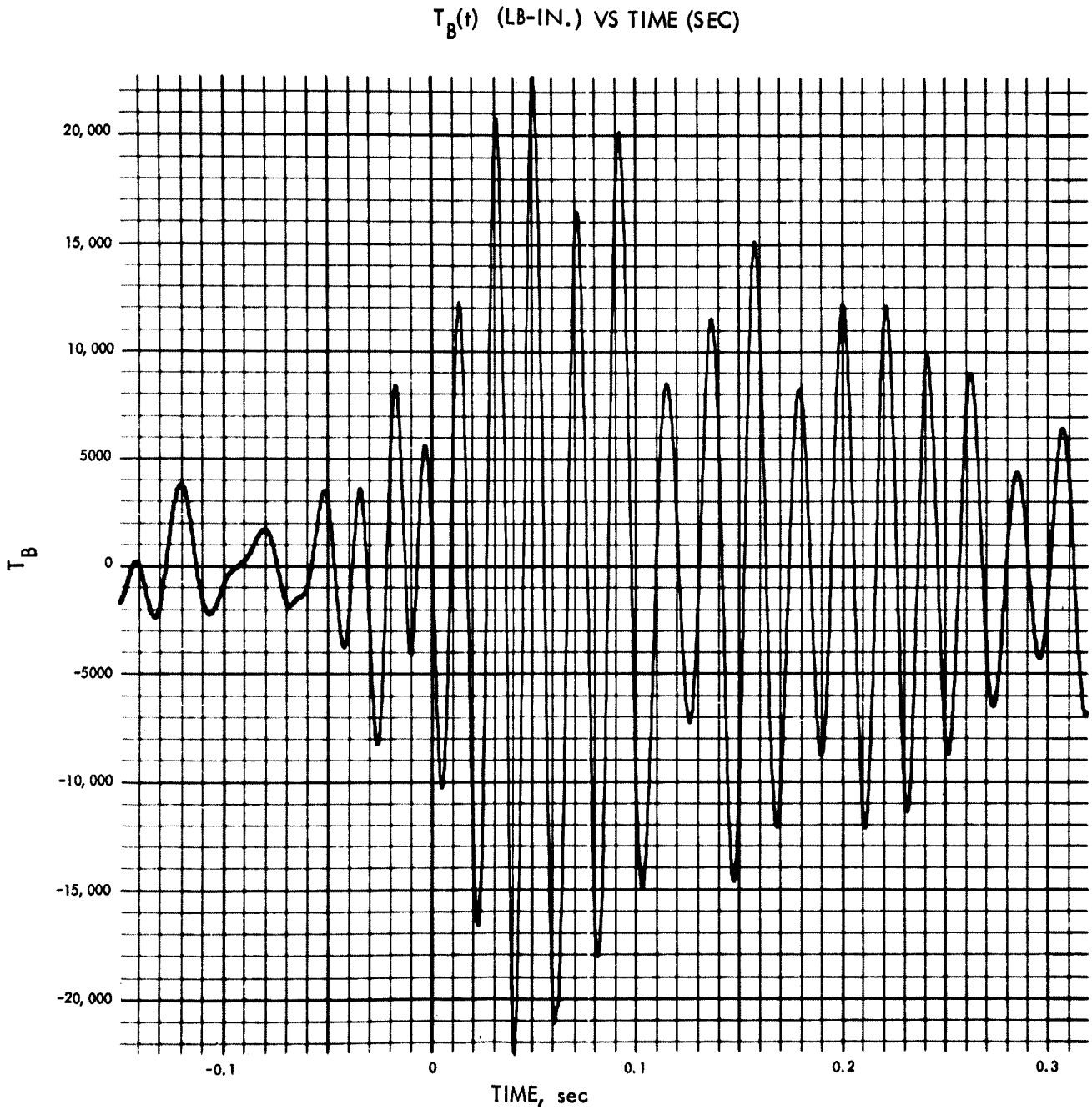

Fig. E-85. Base of spacecraft torque, Joint 7, time history (pulse 1)

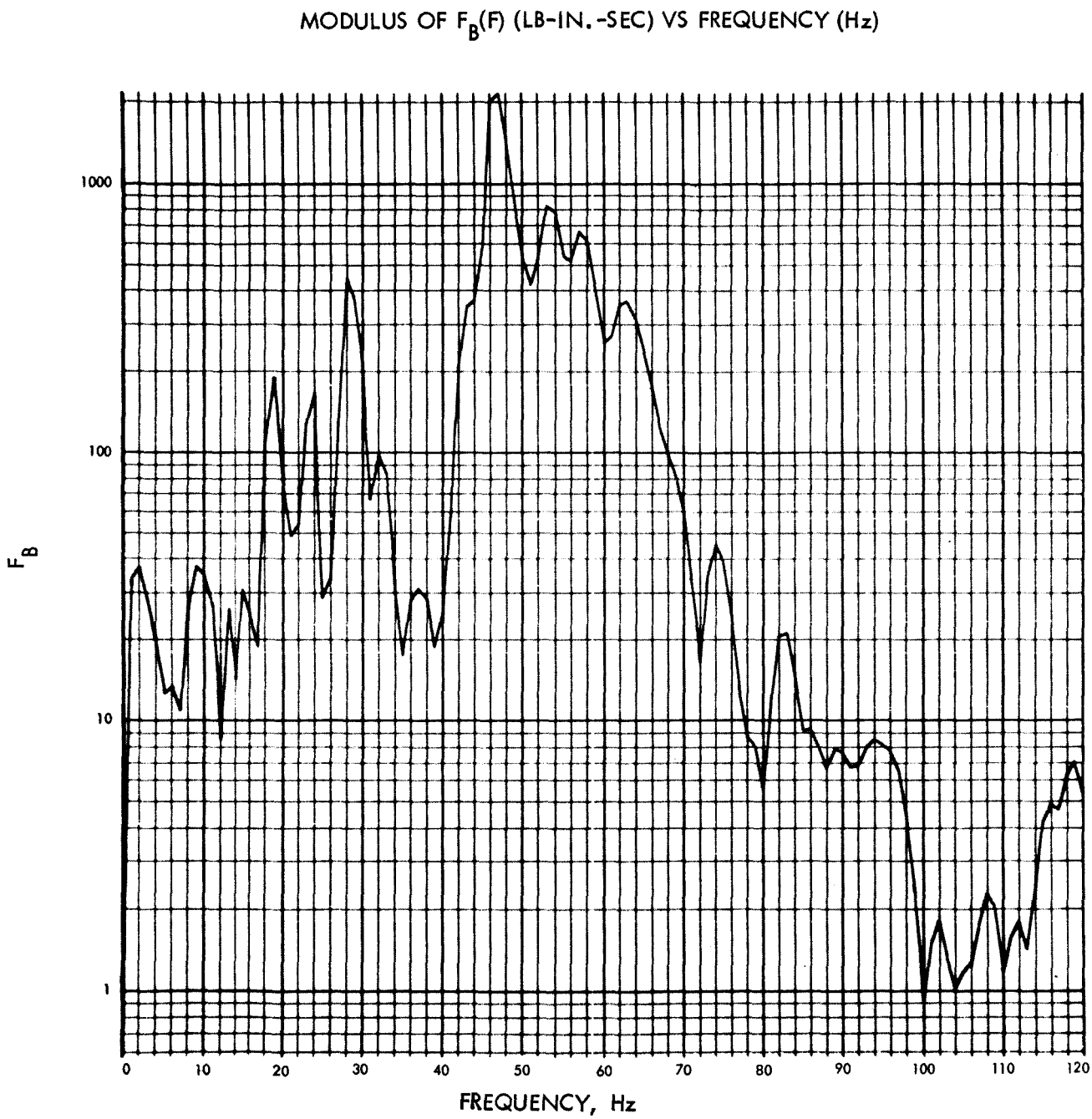

Fig. E-86. Base of spacecraft torque, Fourier transform, modulus (pulse 1)

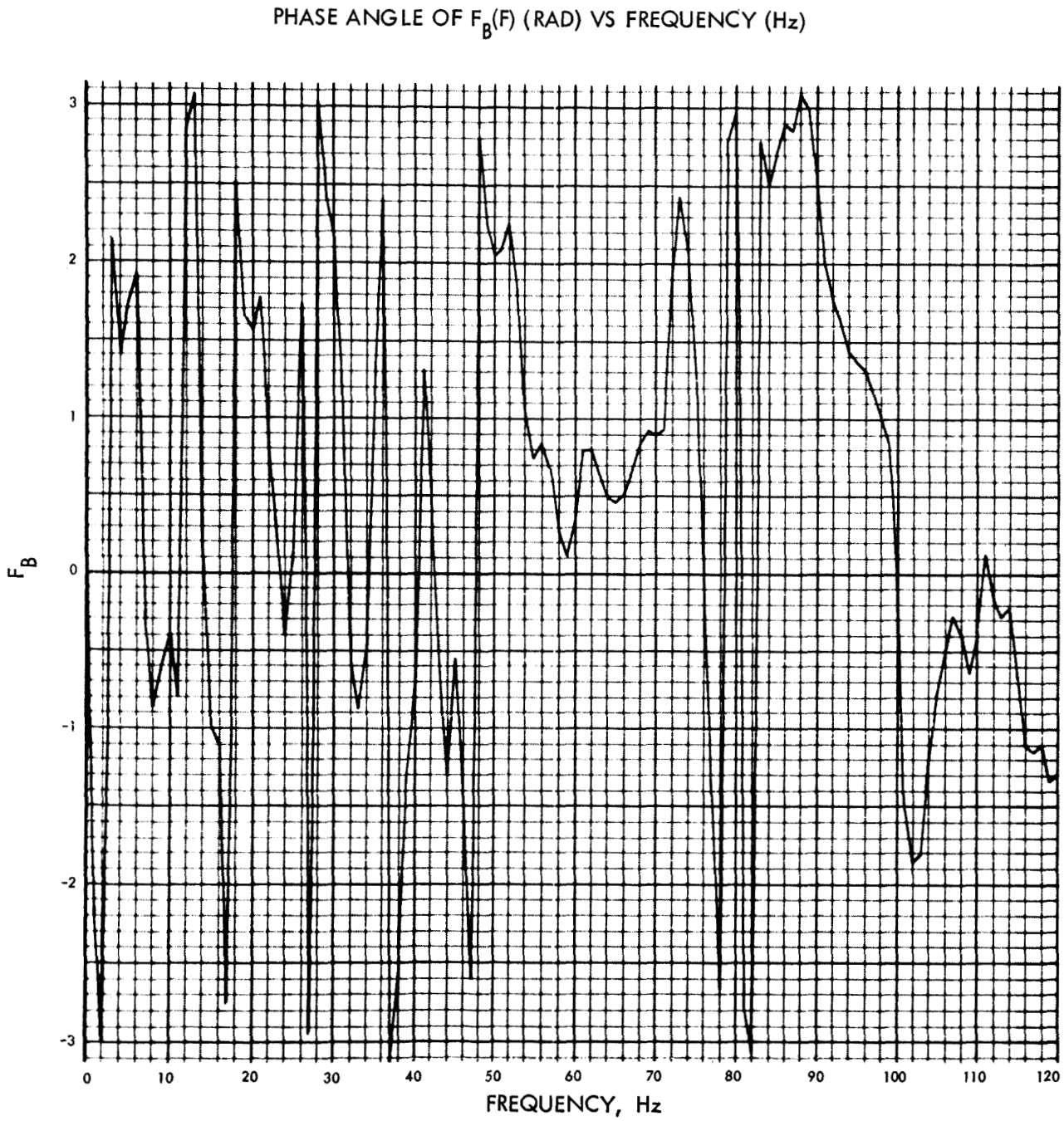

Fig. E-87. Base of spacecraft torque, Joint 7, Fourier transform, phase angle (pulse 1)

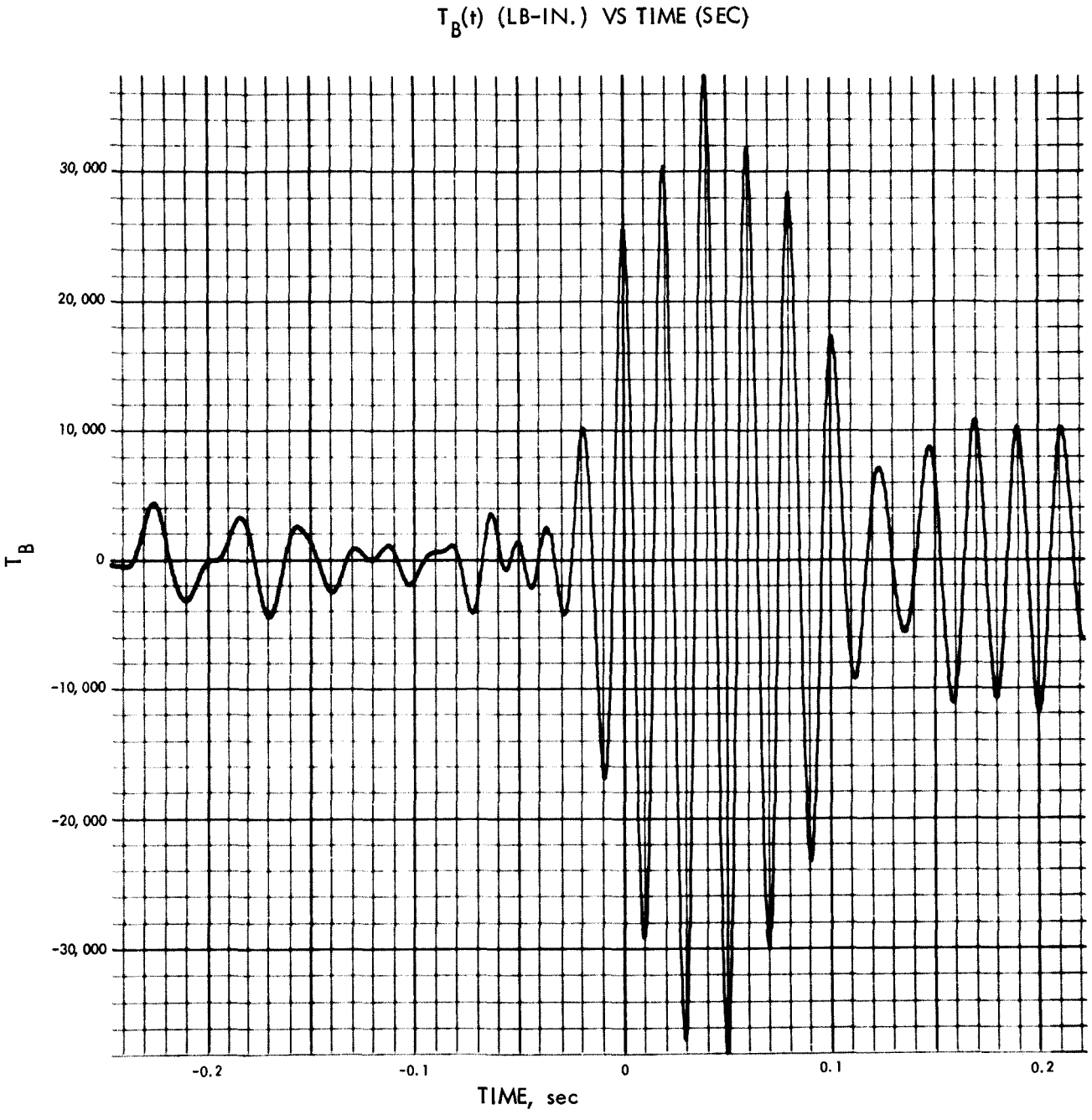

Fig. E-88. Base of spacecraft torque, Joint 7, time history (pulse 2)

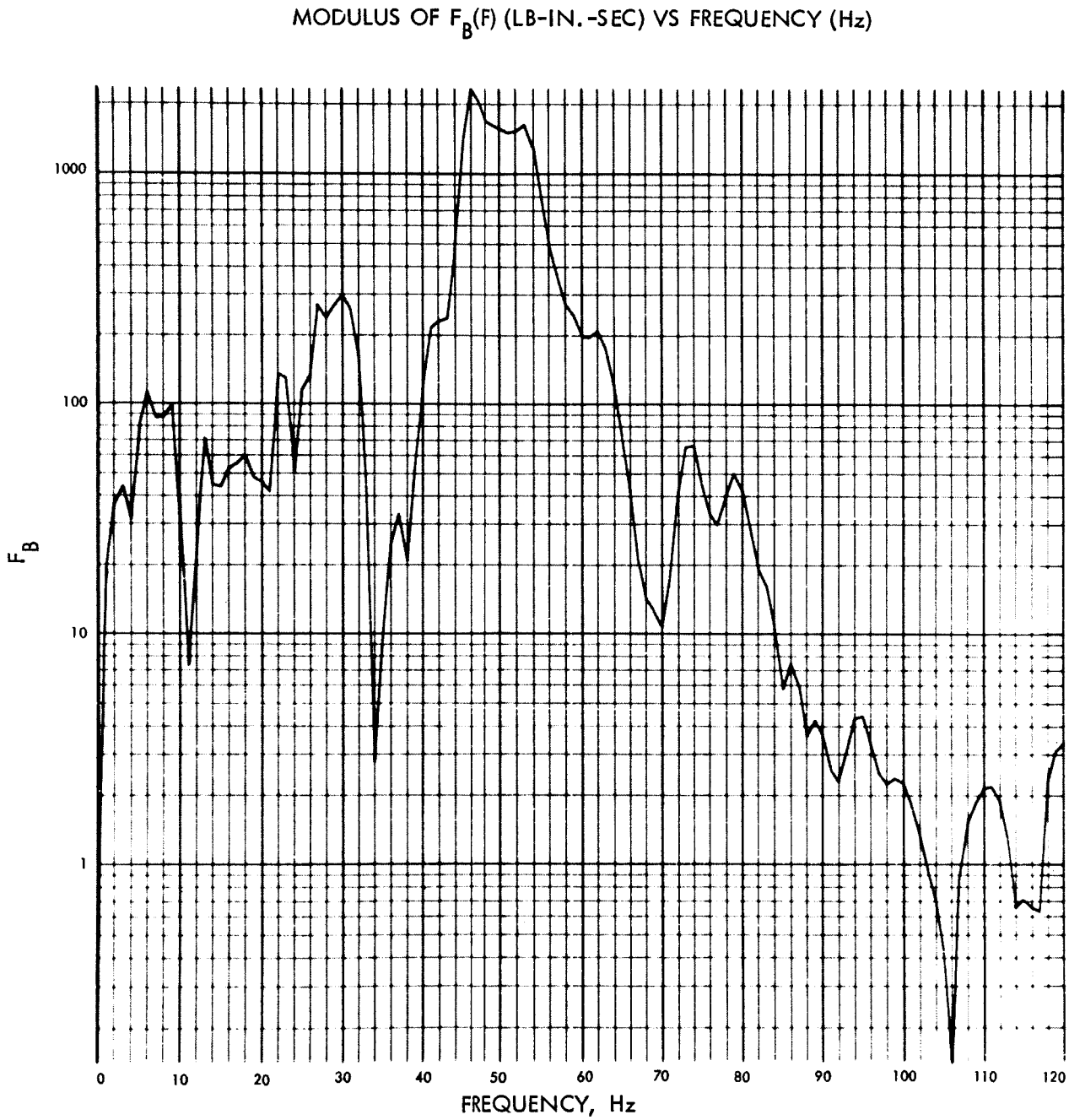

Fig. E-89. Base of spacecraft torque, Fourier transform, modulus (pulse 2)

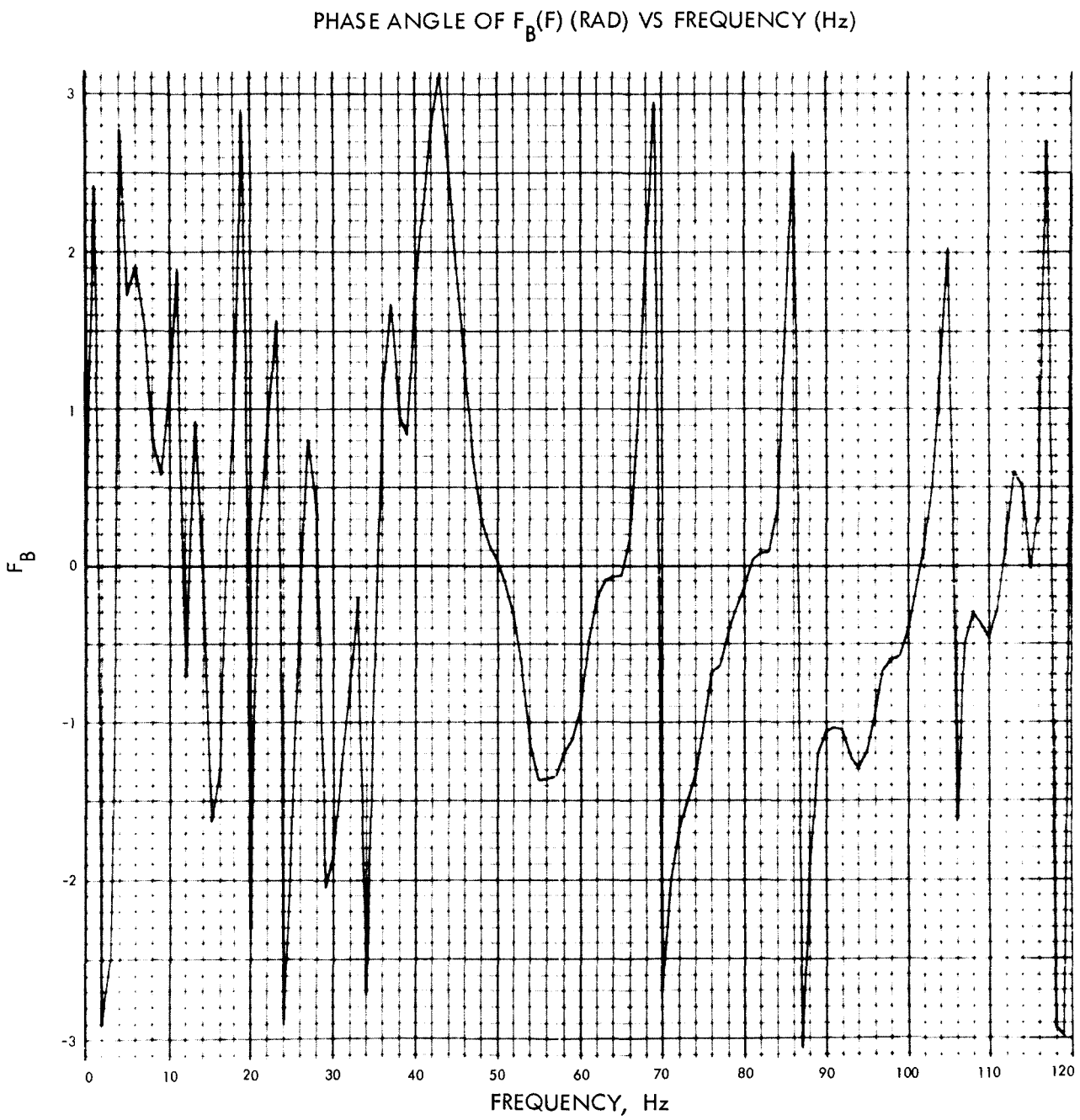

Fig. E-90. Base of spacecraft torque, Joint 7, Fourier transform, phase angle (pulse 2)

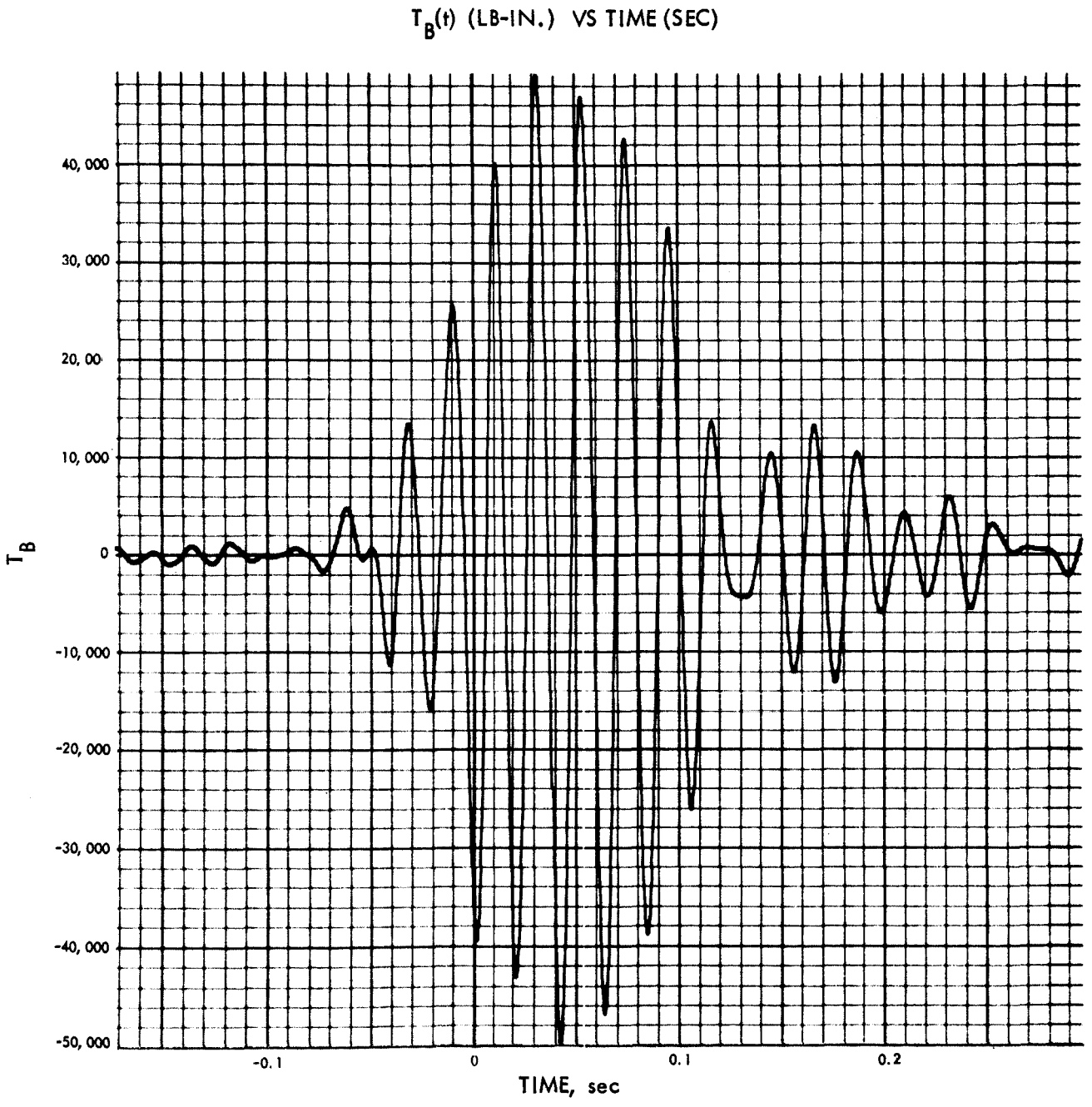

Fig. E-91. Base of spacecraft torque, Joint 7, time history (pulse 3)

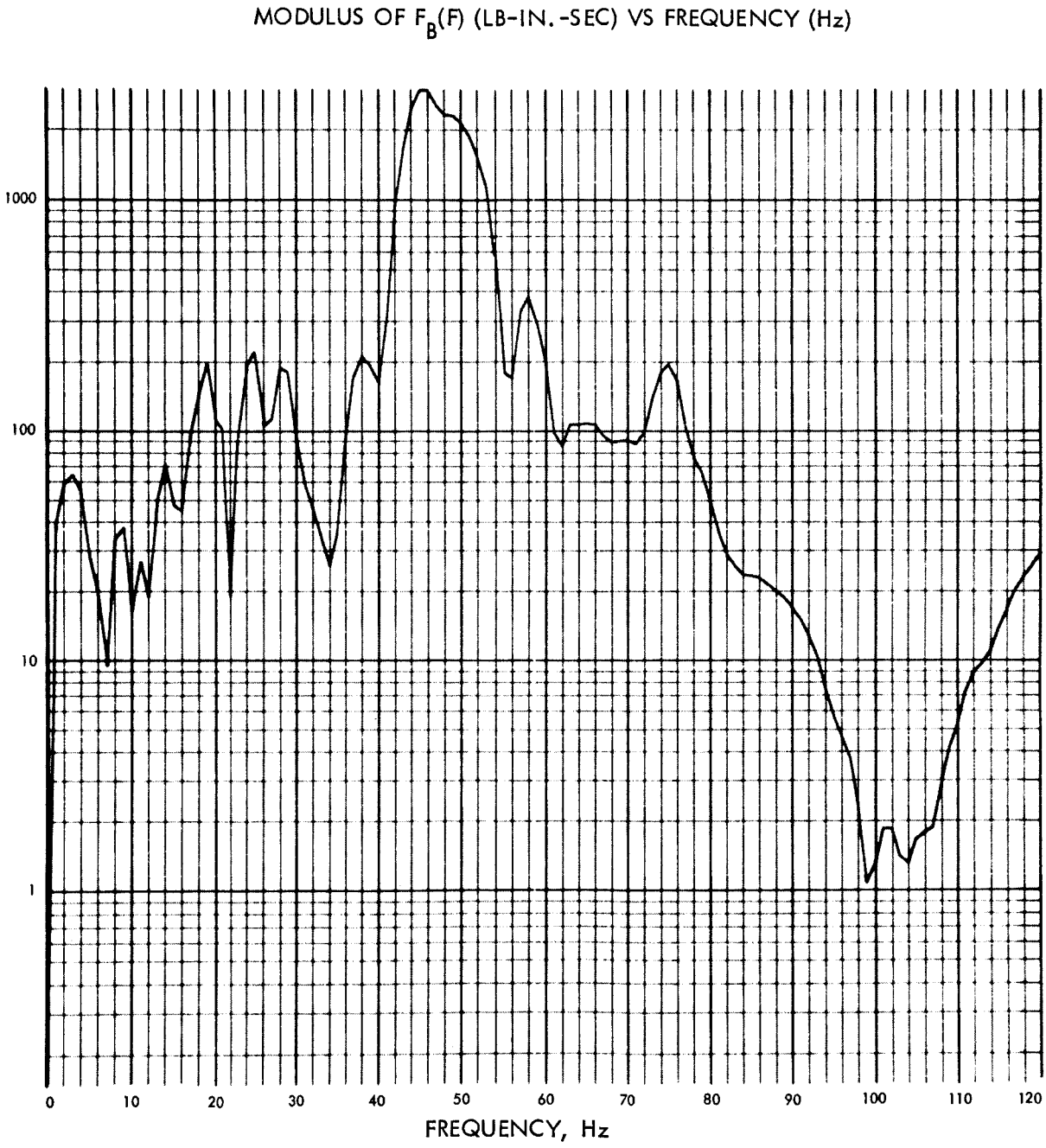

Fig. E-92. Base of spacecraft torque, Fourier transform, modulus (pulse 3)

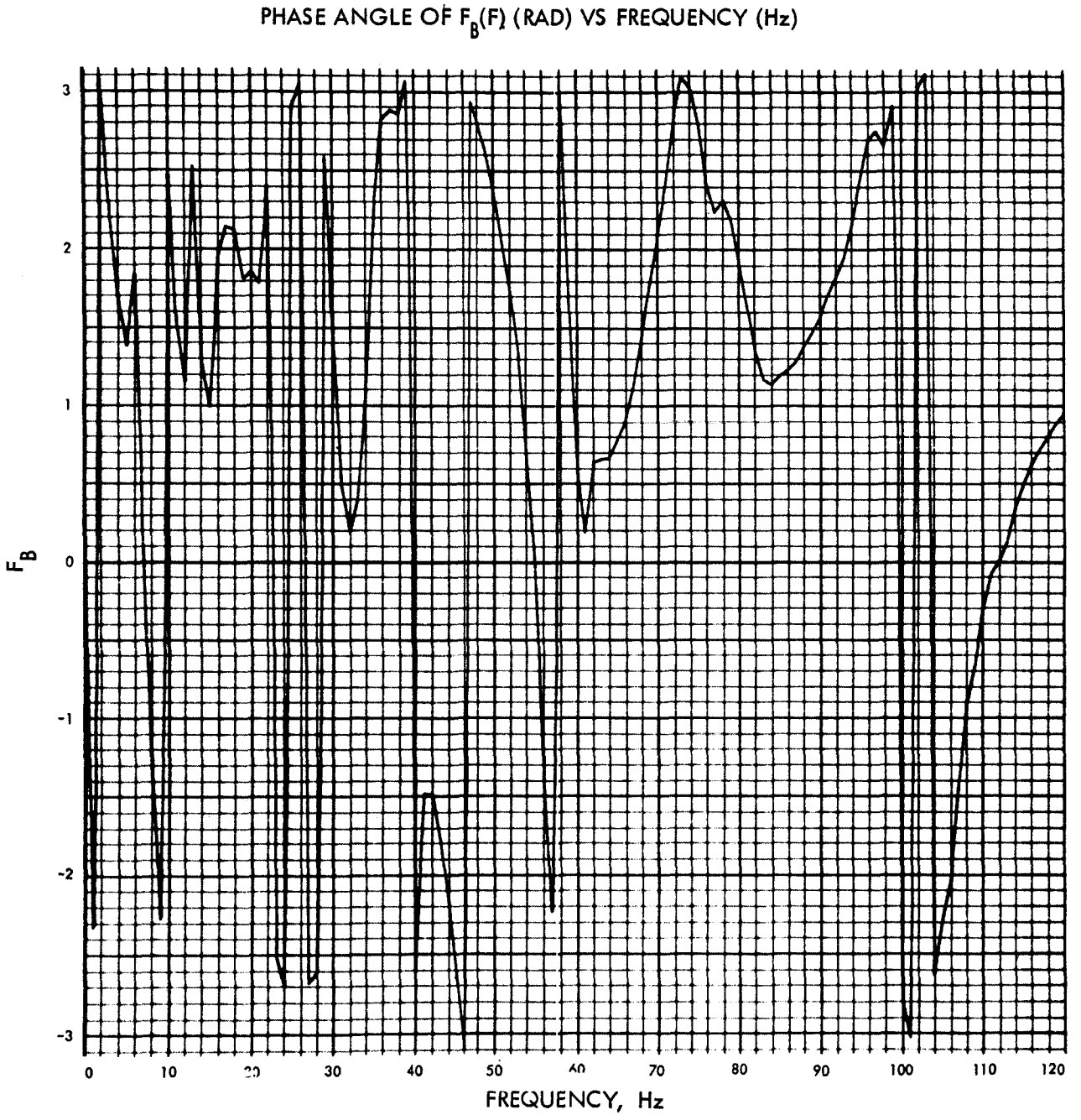

Fig. E-93. Base of spacecraft torque, Joint 7, Fourier transform, phase angle (pulse 3)

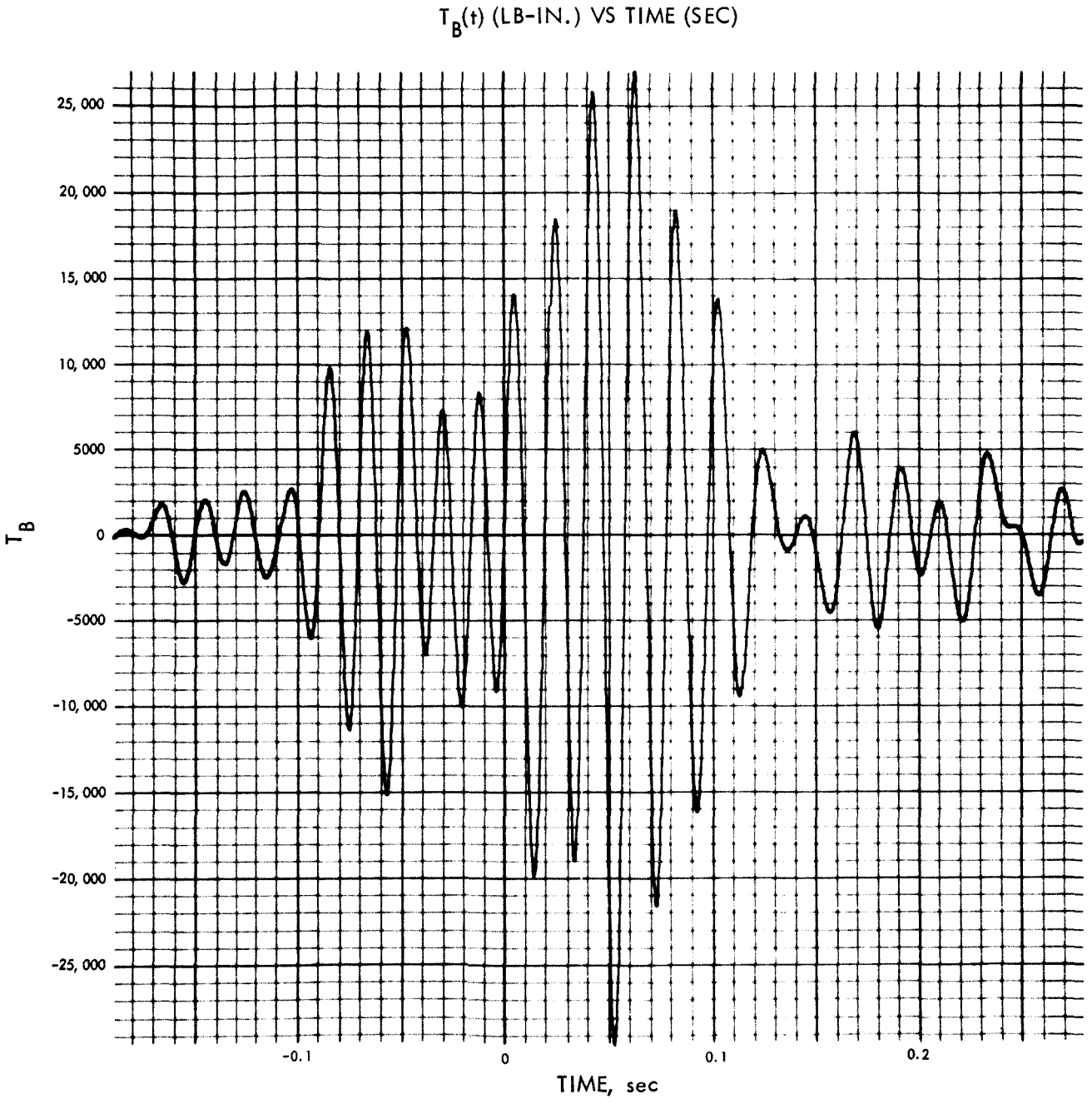

Fig. E-94. Base of spacecraft torque, Joint 7, time history (pulse 4)

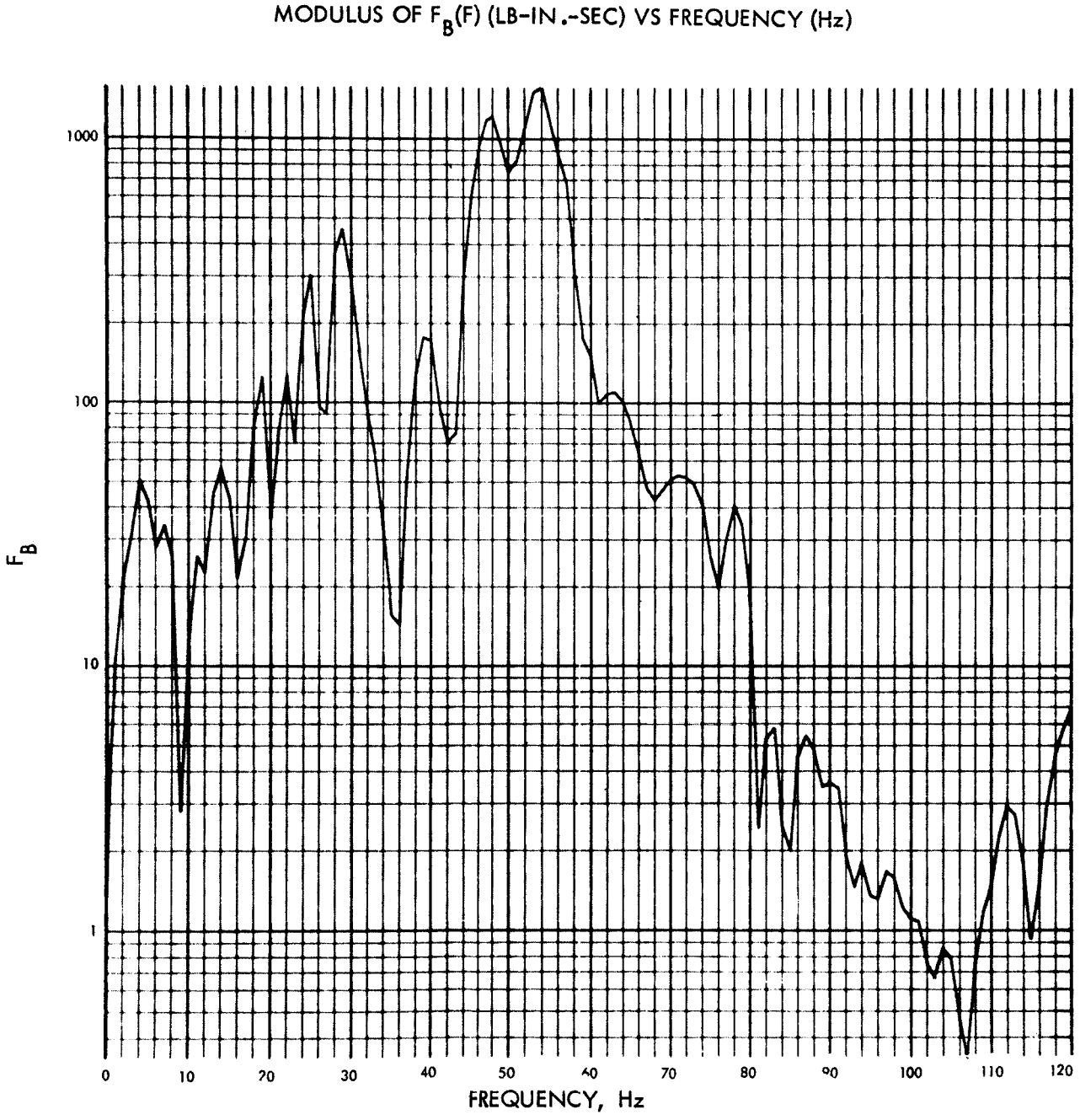

Fig. E-95. Base of spacecraft torque, Joint 7, Fourier transform, modulus (pulse 4)

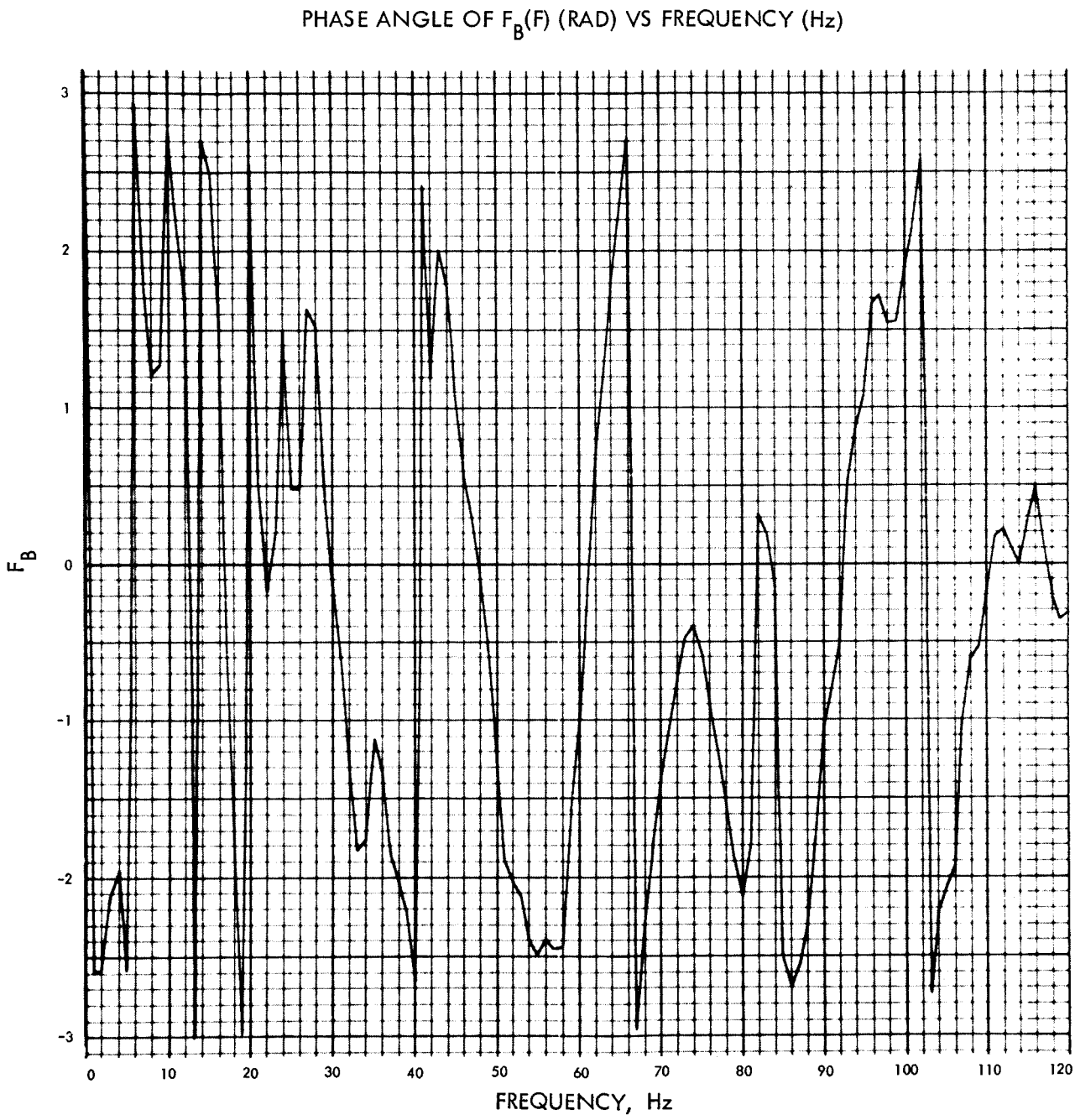

Fig. E-96. Base of spacecraft torque, Joint 7, Fourier transform, phase angle (pulse 4)

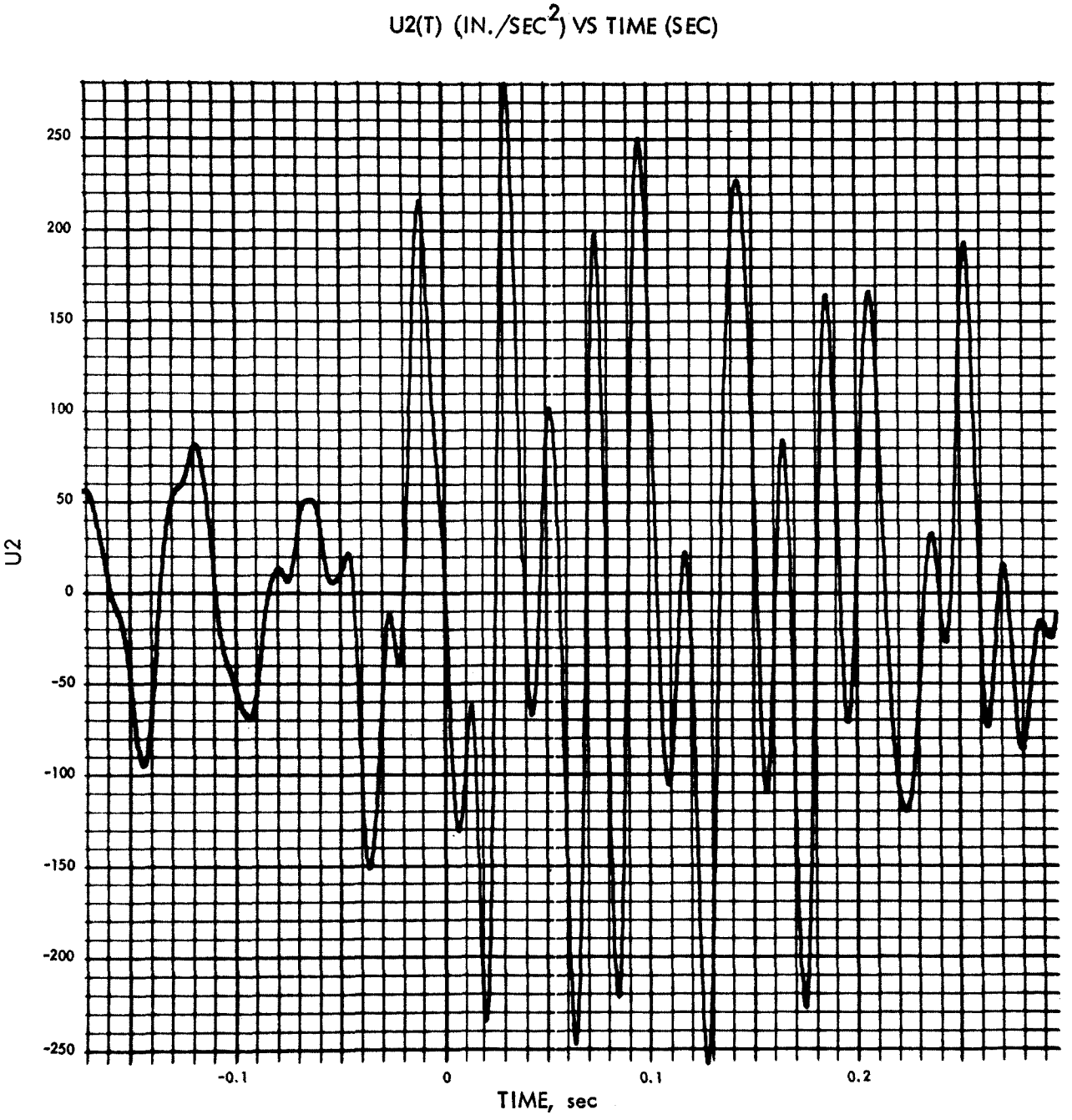

Fig. E-97. Joint 1, x_1 time history (pulse 3) 1% damping

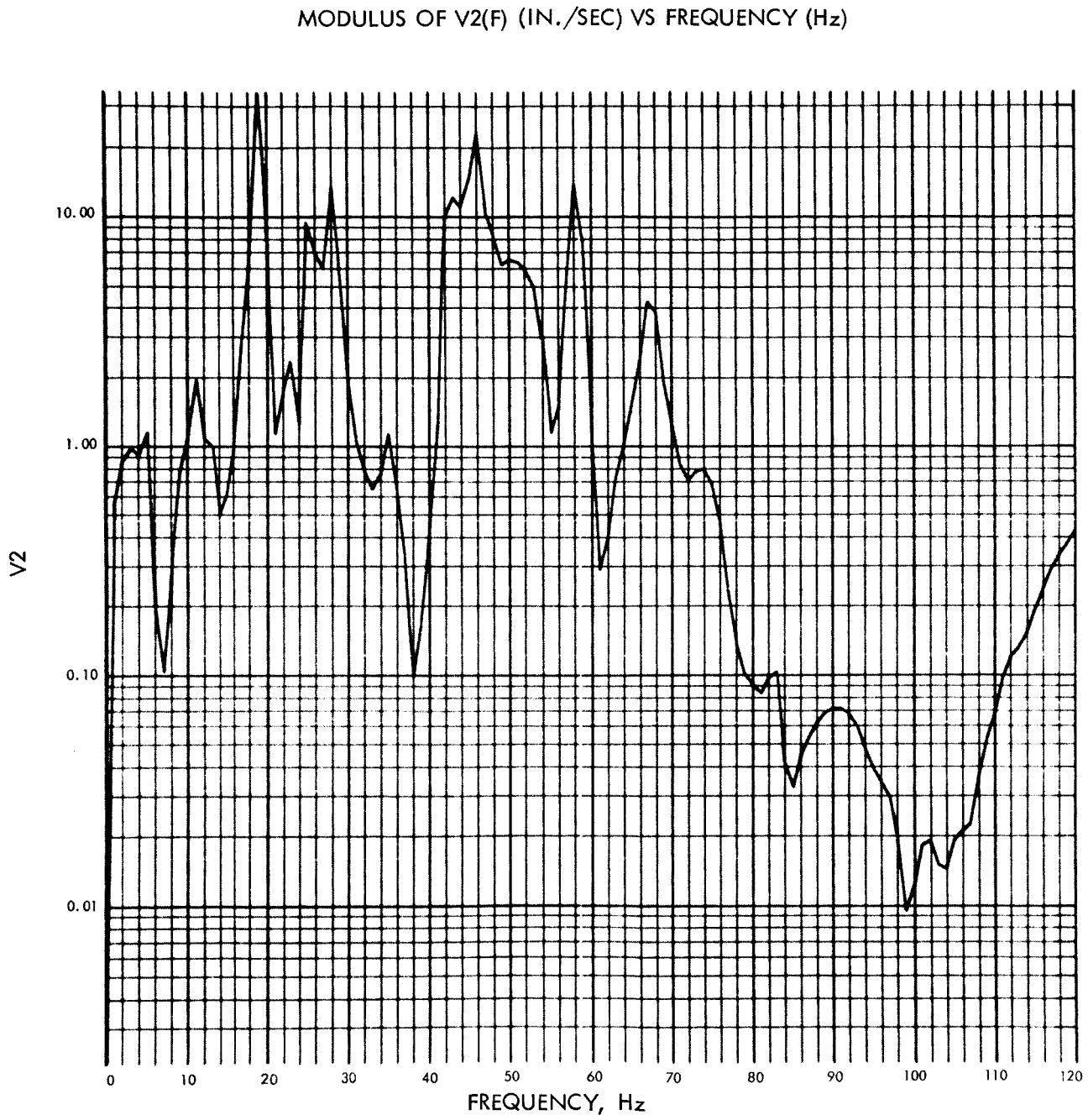

Fig. E-98. Joint 1, x_1 Fourier transform, modulus (pulse 3)
1% damping

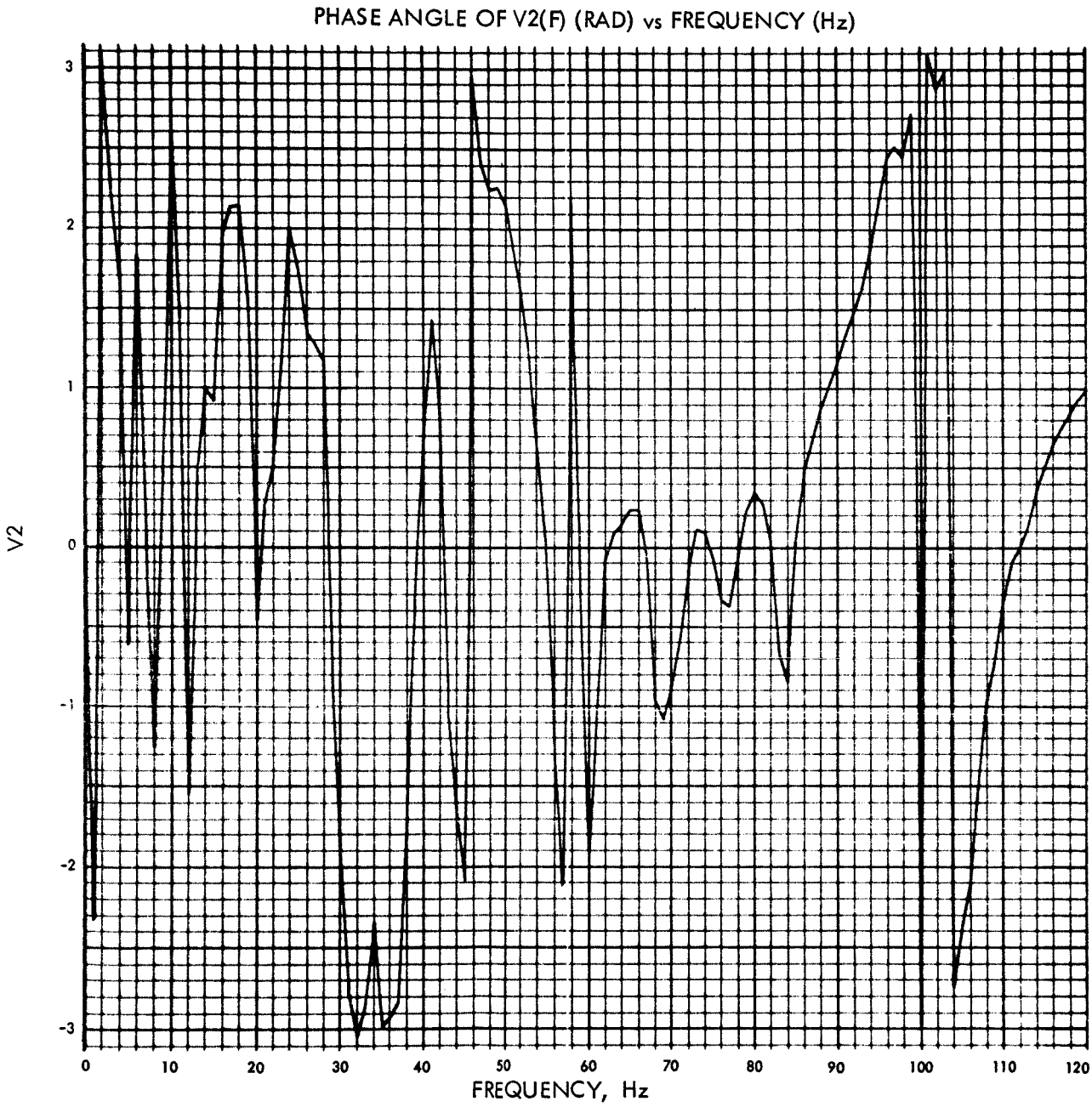

Fig. E-99. Joint 1, x_1 Fourier transform, phase angle (pulse 3) 1% damping

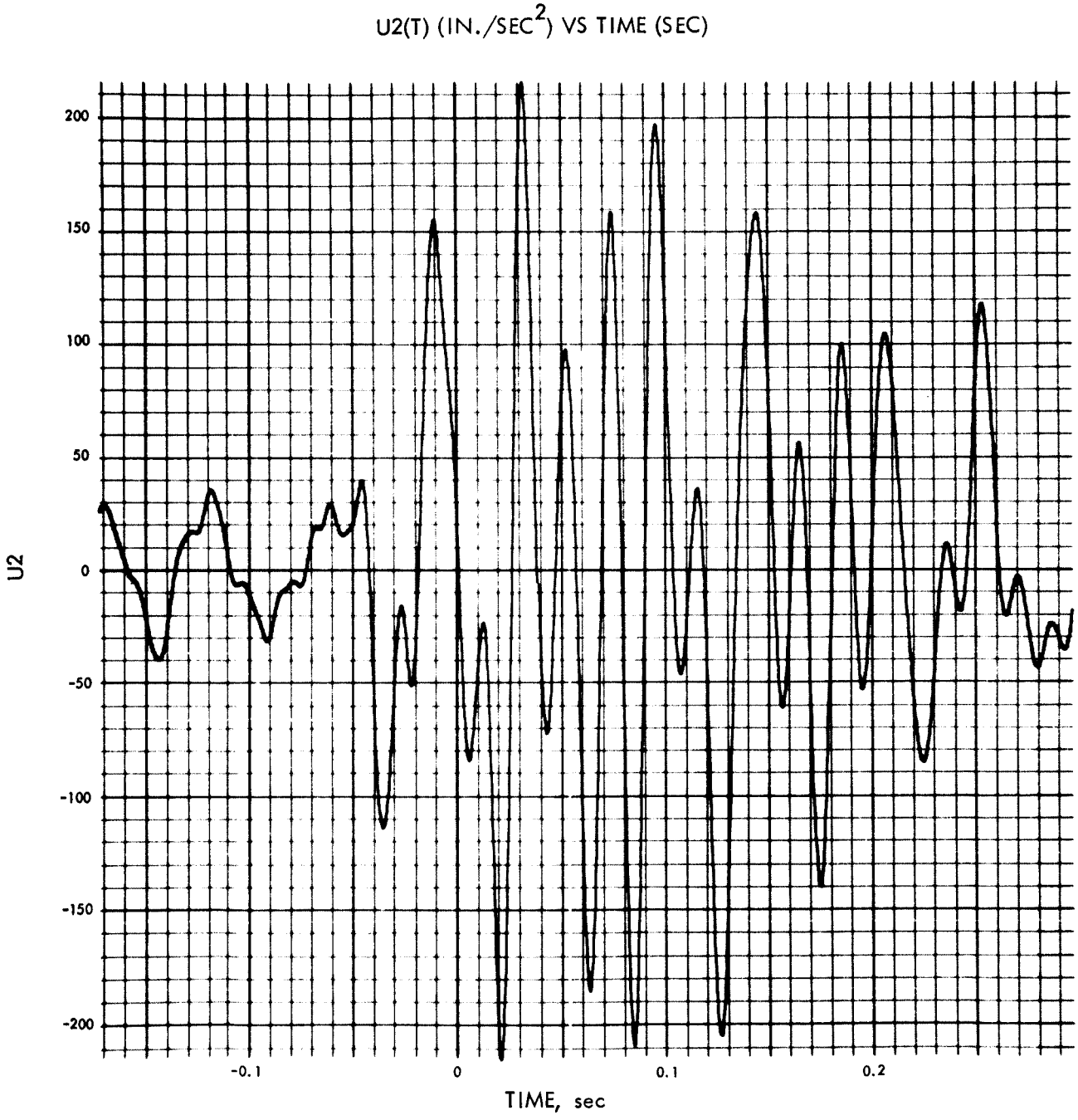

Fig. E-100. Joint 1, x_1 time history (pulse 3) 2% damping

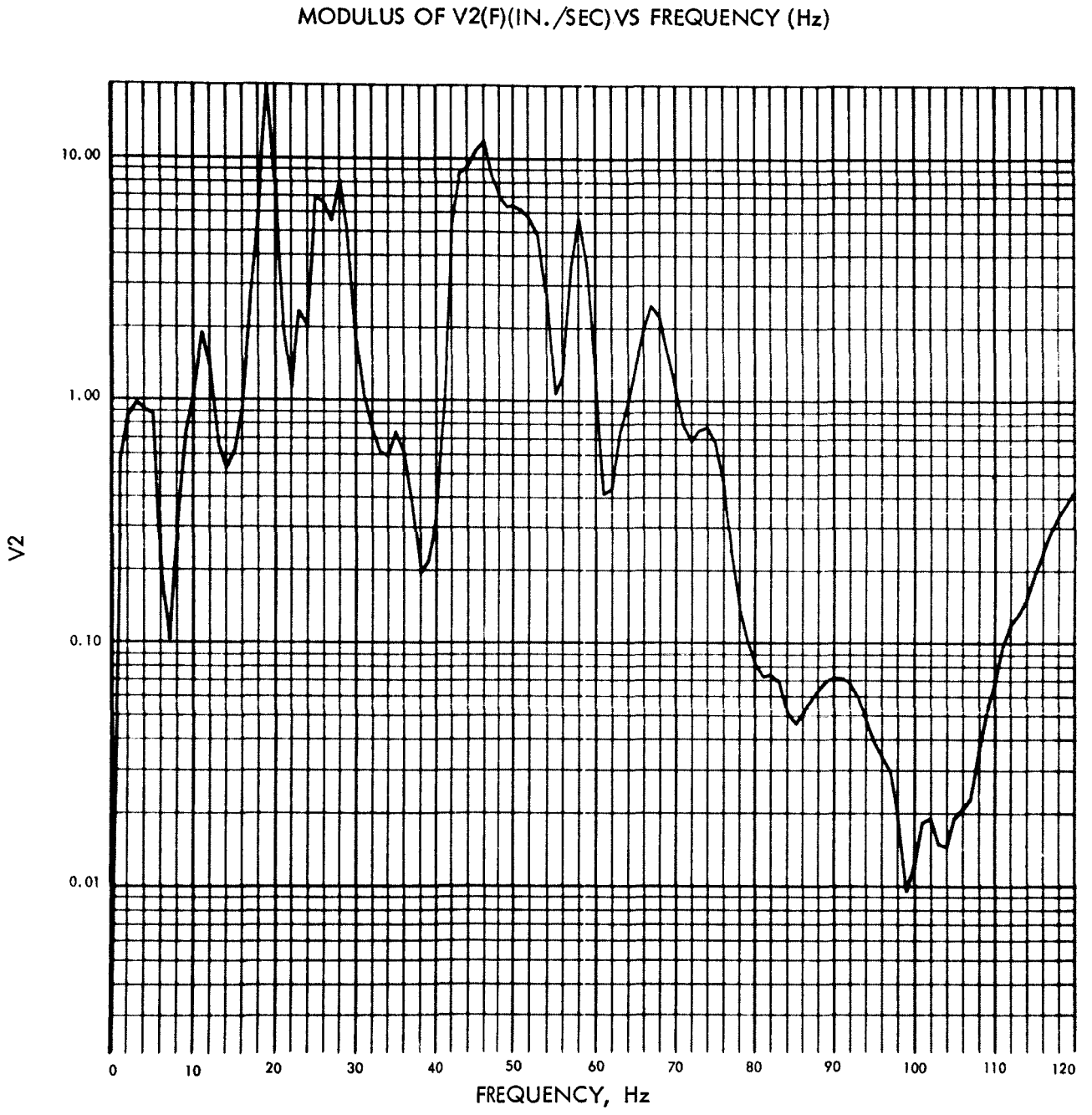

Fig. E-101. Joint 1, x_1 Fourier transform, modulus (pulse 3) 2% damping

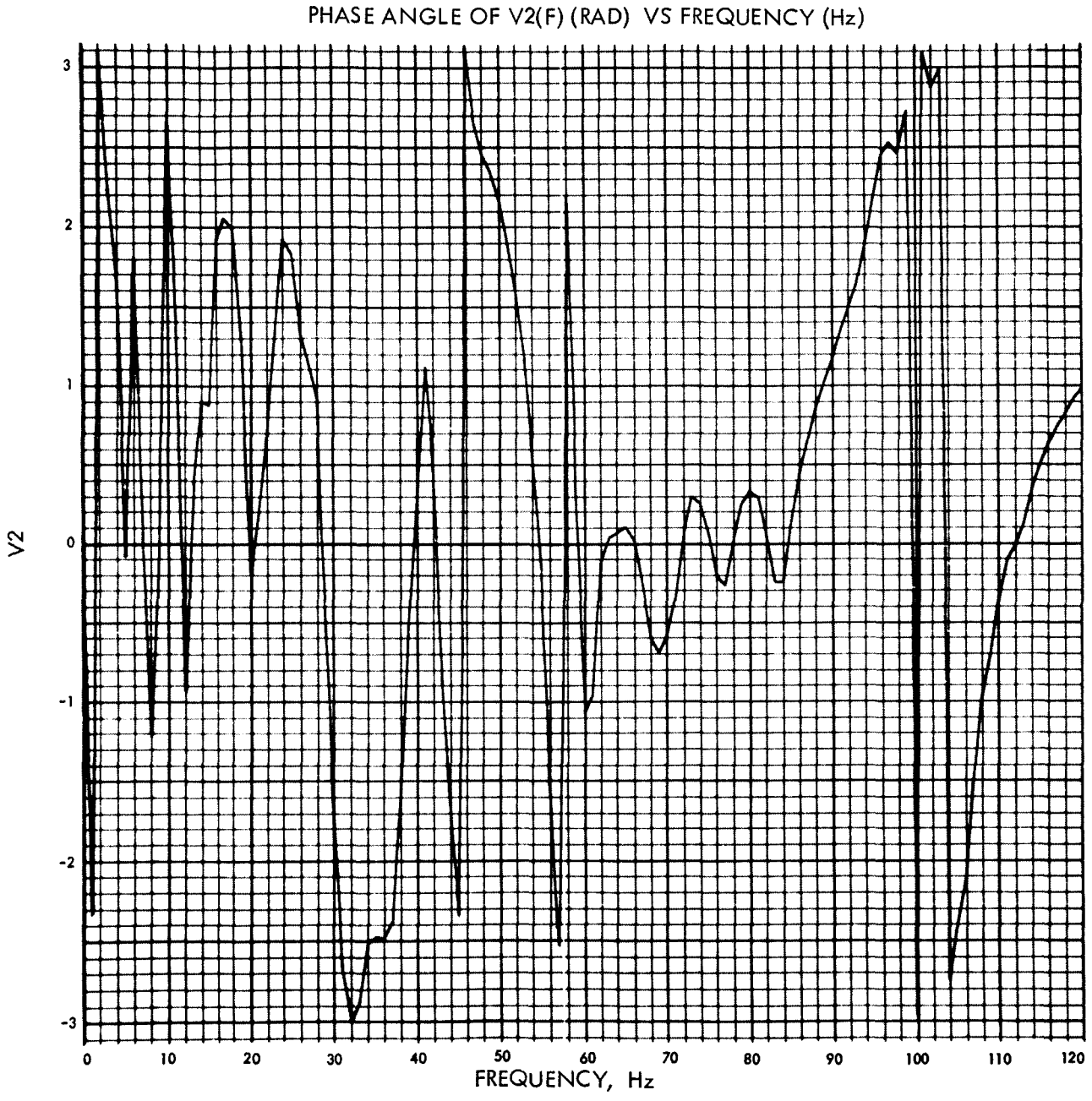

Fig. E-102. Joint 1, x_1 Fourier transform, phase angle (pulse 3) 2% damping

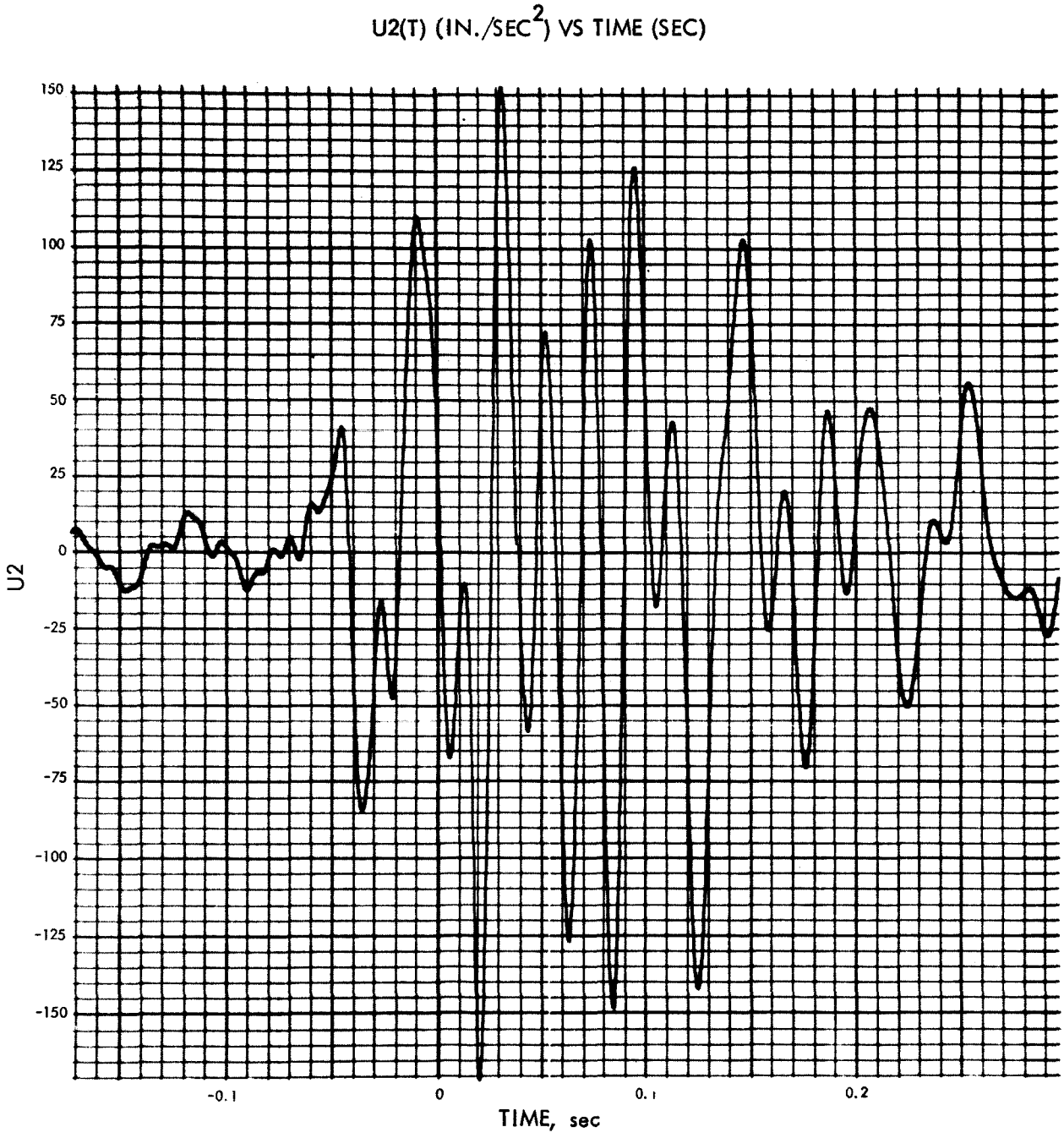

Fig. E-103. Joint 1, x_1 time history (pulse 3) 4% damping

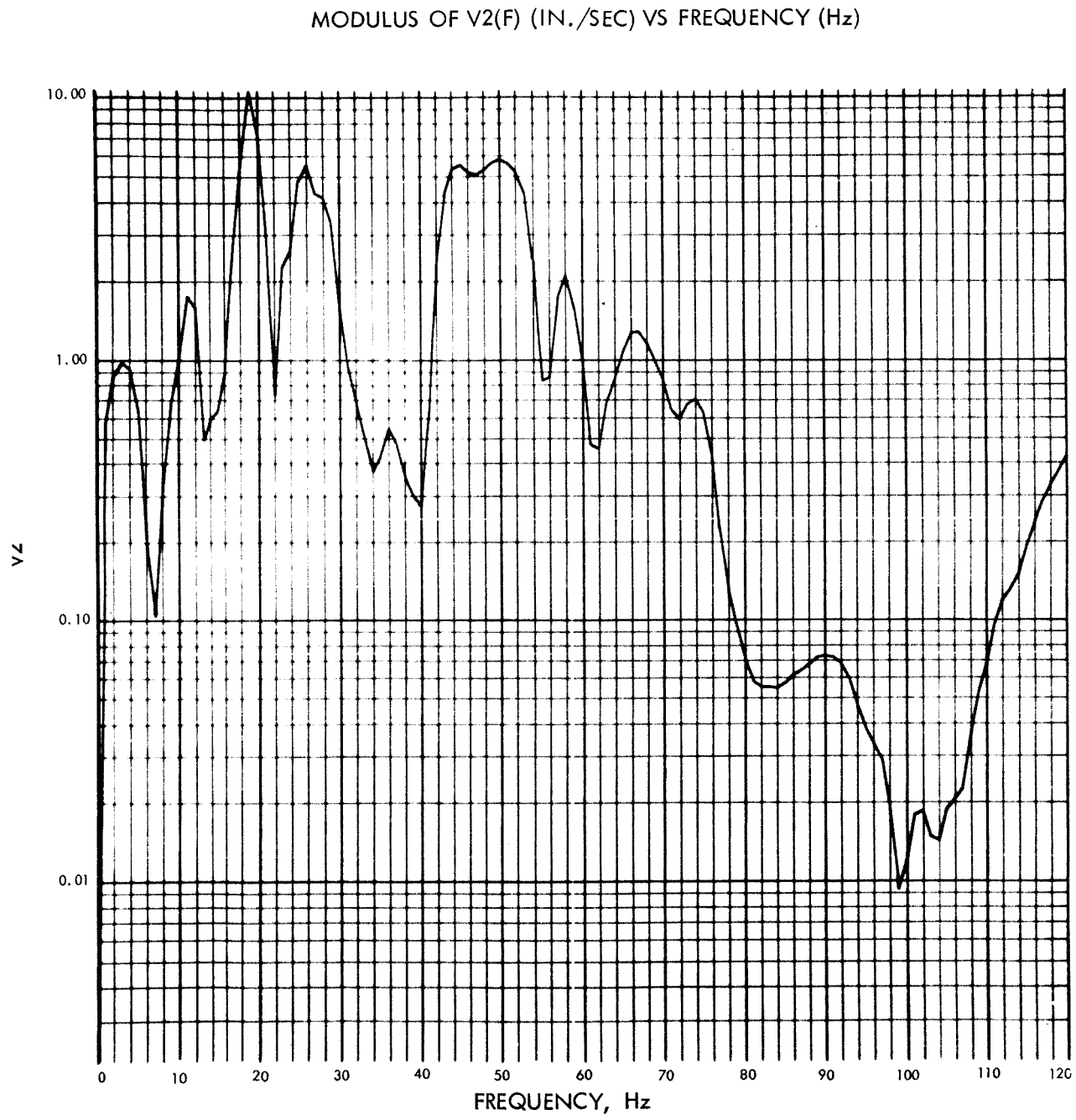

Fig. E-104. Joint 1, x_1 Fourier transform, modulus (pulse 3) 4% damping

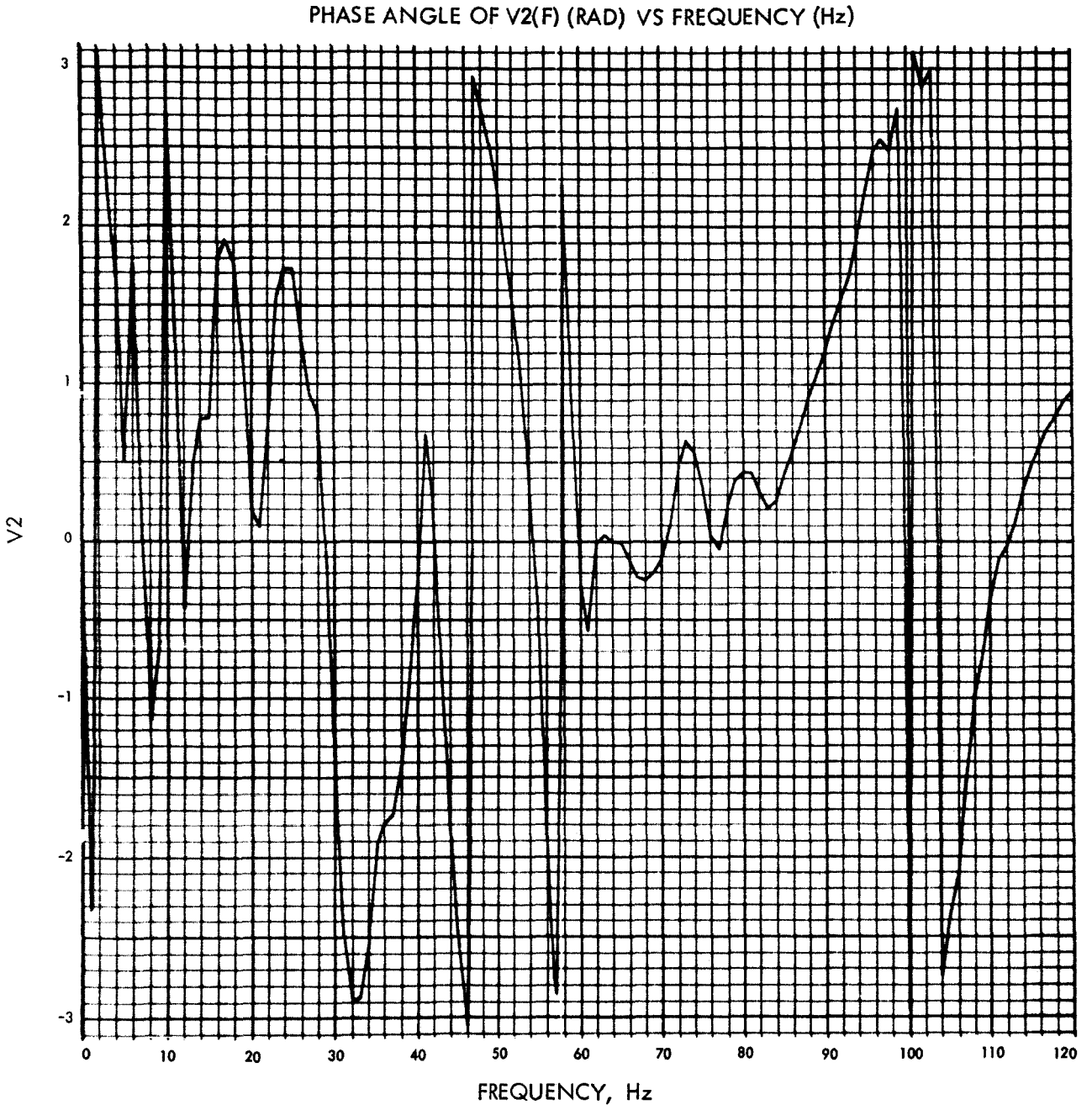

Fig. E-105. Joint 1, x_1 Fourier transform, phase angle (pulse 3) 4% damping

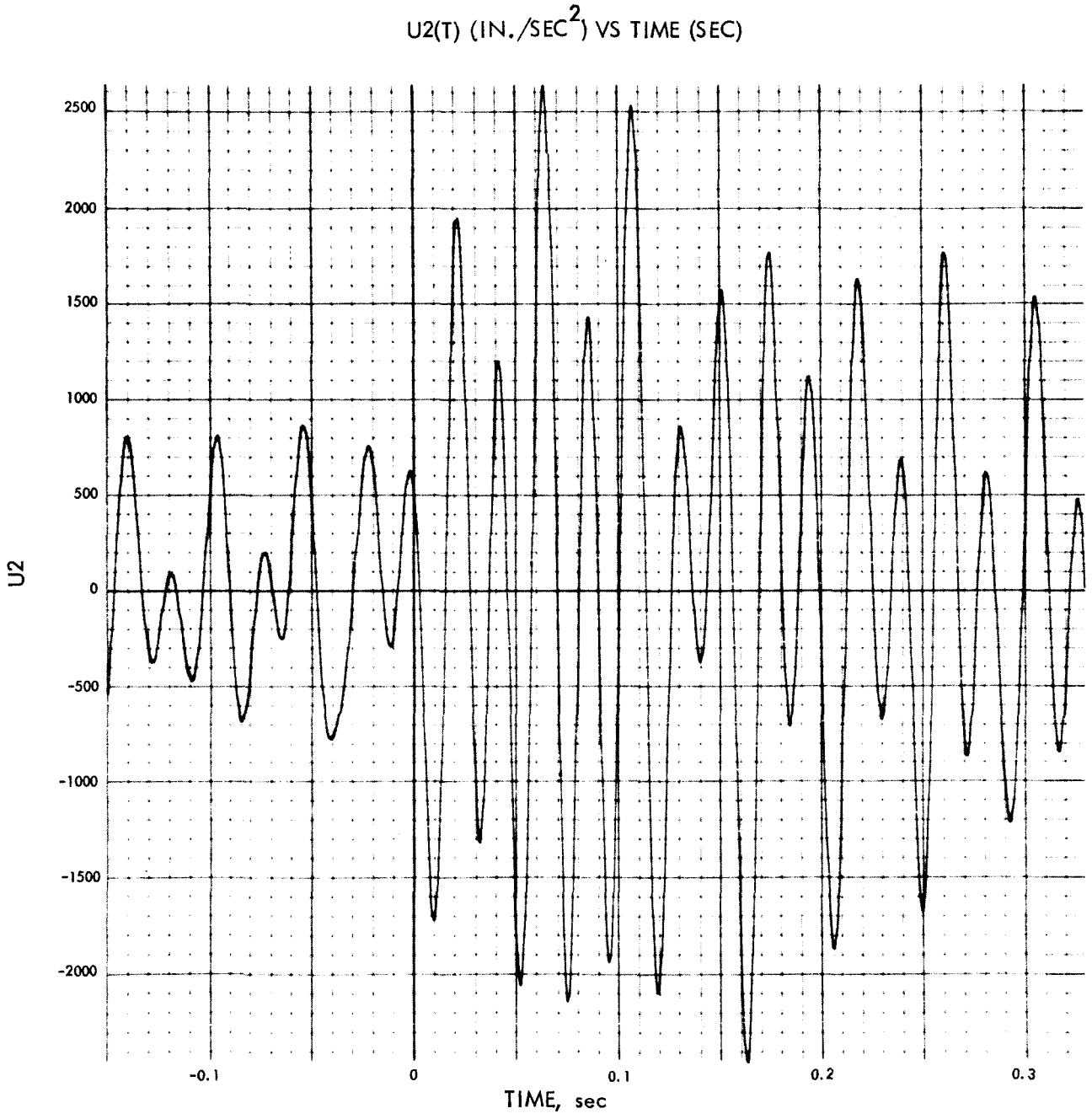

Fig. E-106. Joint 23, x_1 time history (pulse 3) 0.1% damping

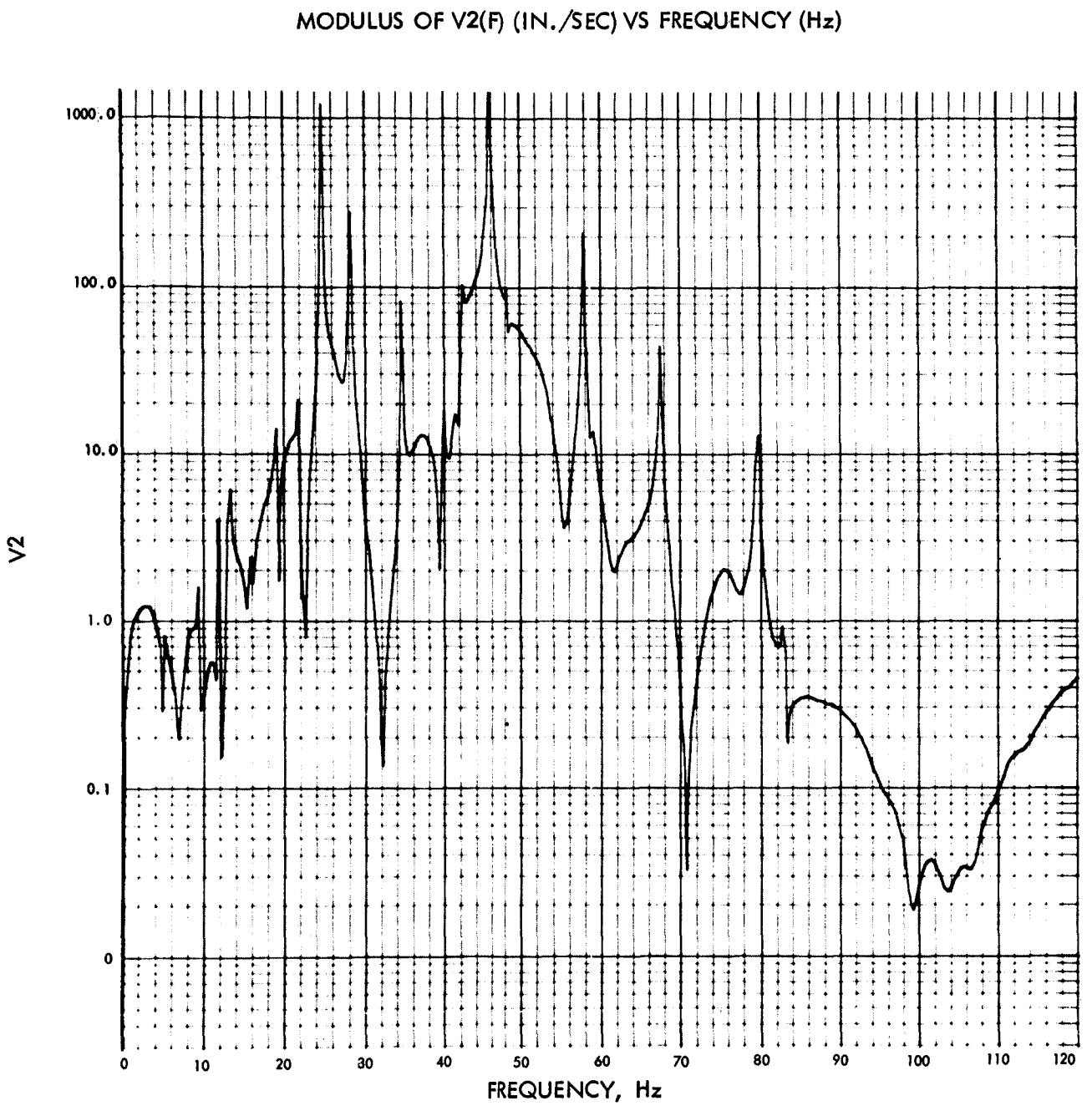

Fig. E-107. Joint 23, x_1 Fourier transform, modulus, (pulse 3) 0.1% damping

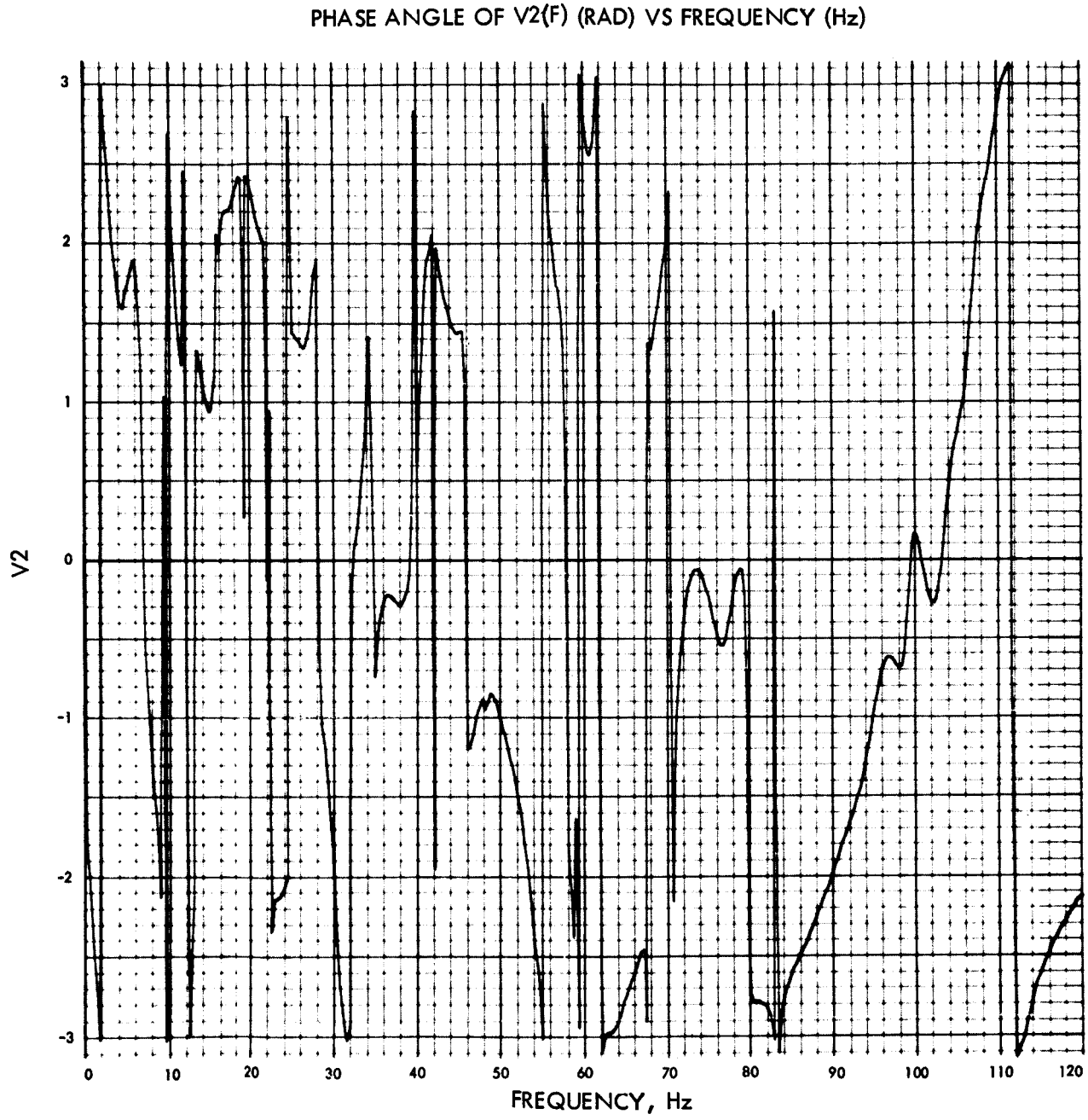

Fig. E-108. Joint 23, x_1 Fourier transform, phase angle, (pulse 3) 0.1% damping

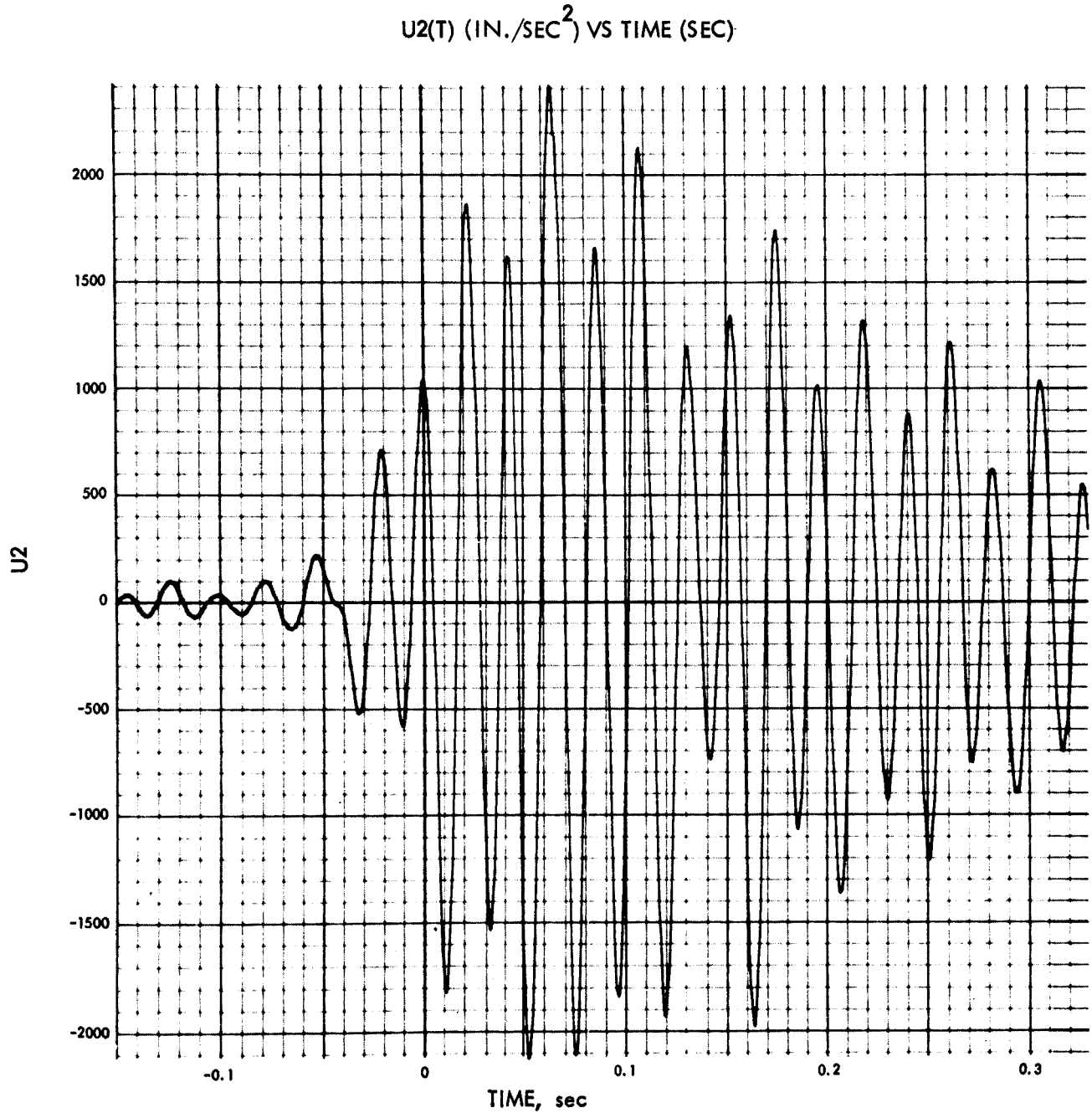

Fig. E-109. Joint 23, x_1 time history (pulse 3) 0.5% damping

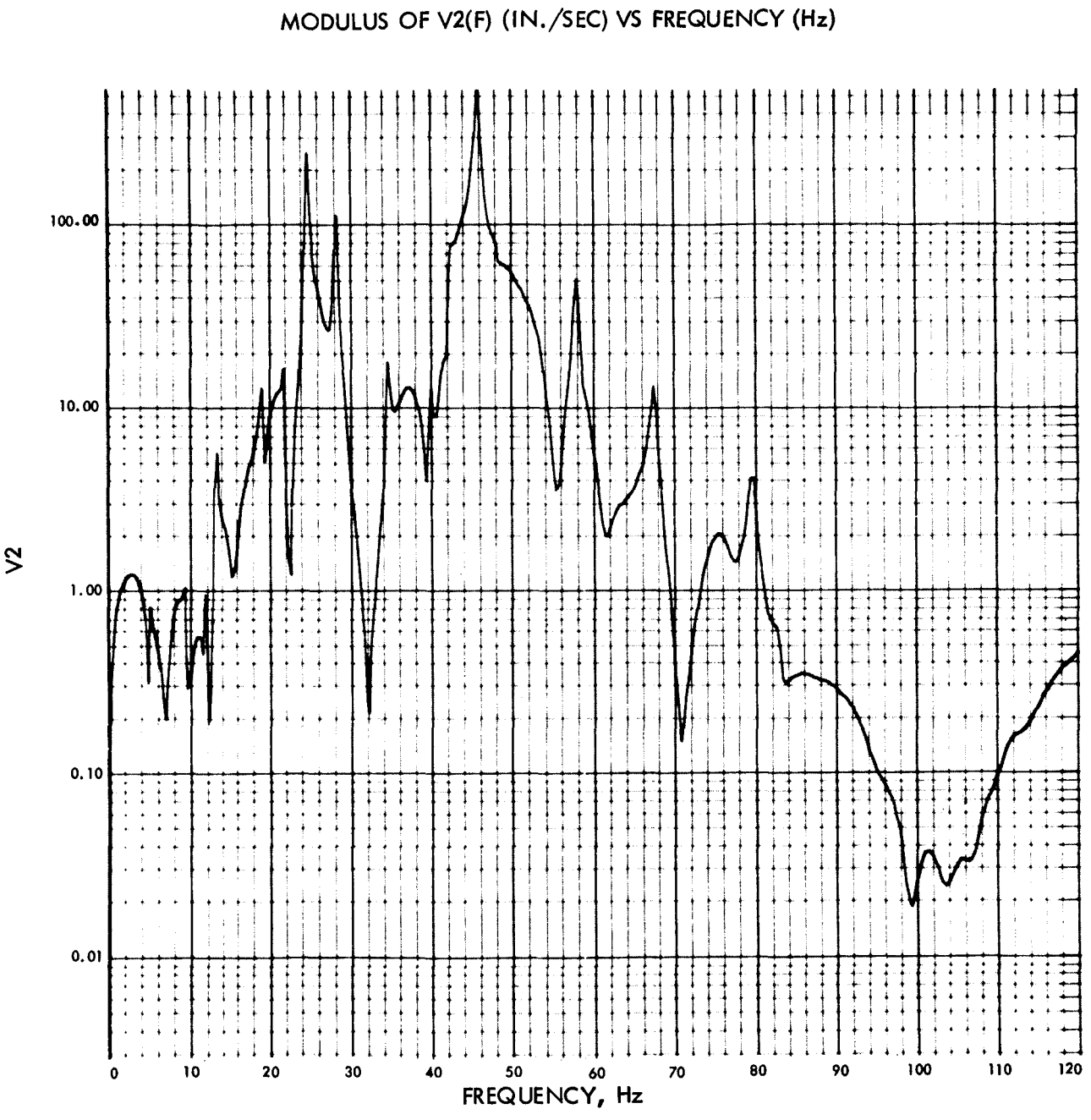

Fig. E-110. Joint 23, x_1 Fourier transform, modulus, (pulse 3) 0.5% damping

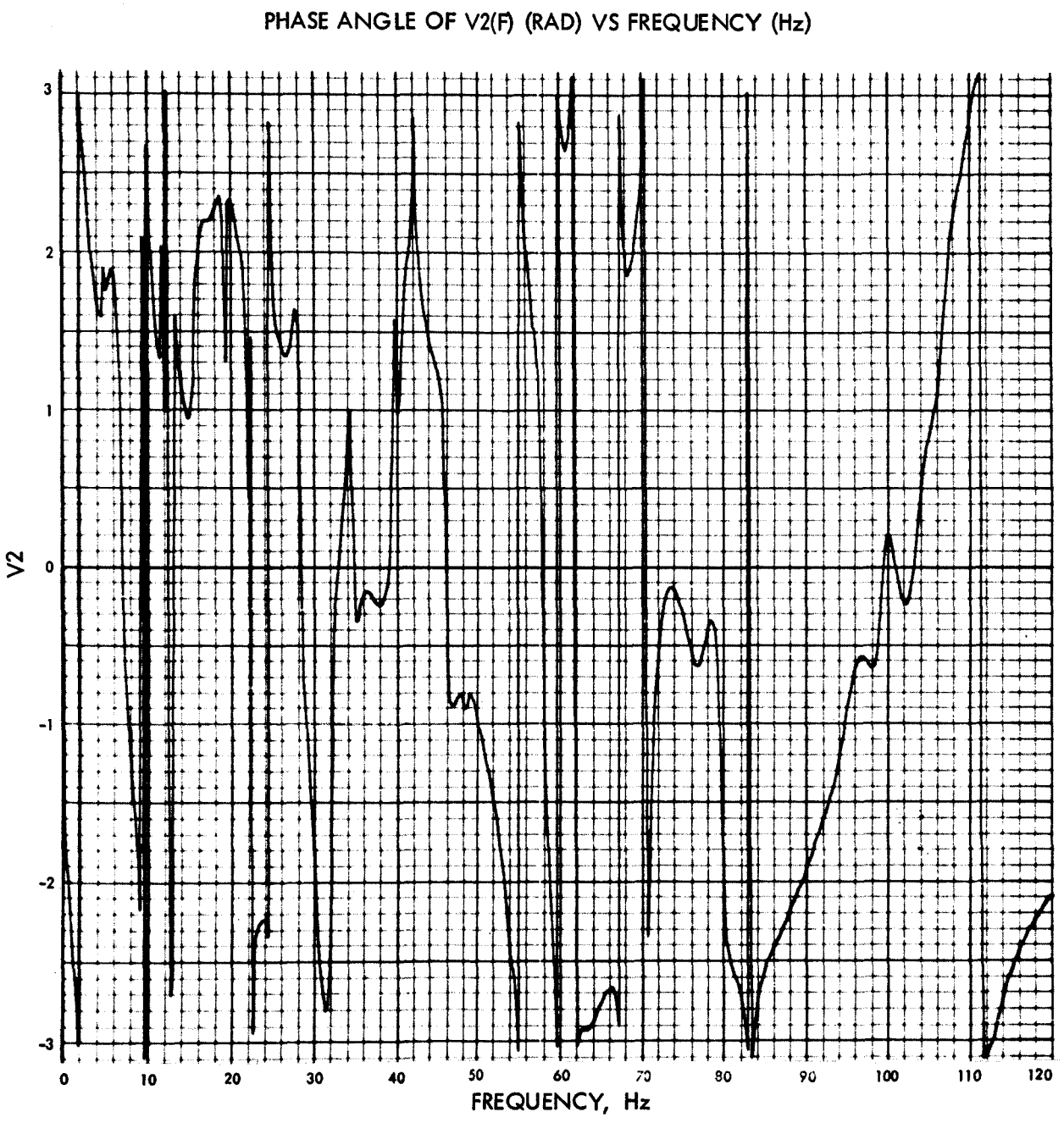

Fig. E-111. Joint 23, x_1 Fourier transform, phase angle (pulse 3) 0.5% damping

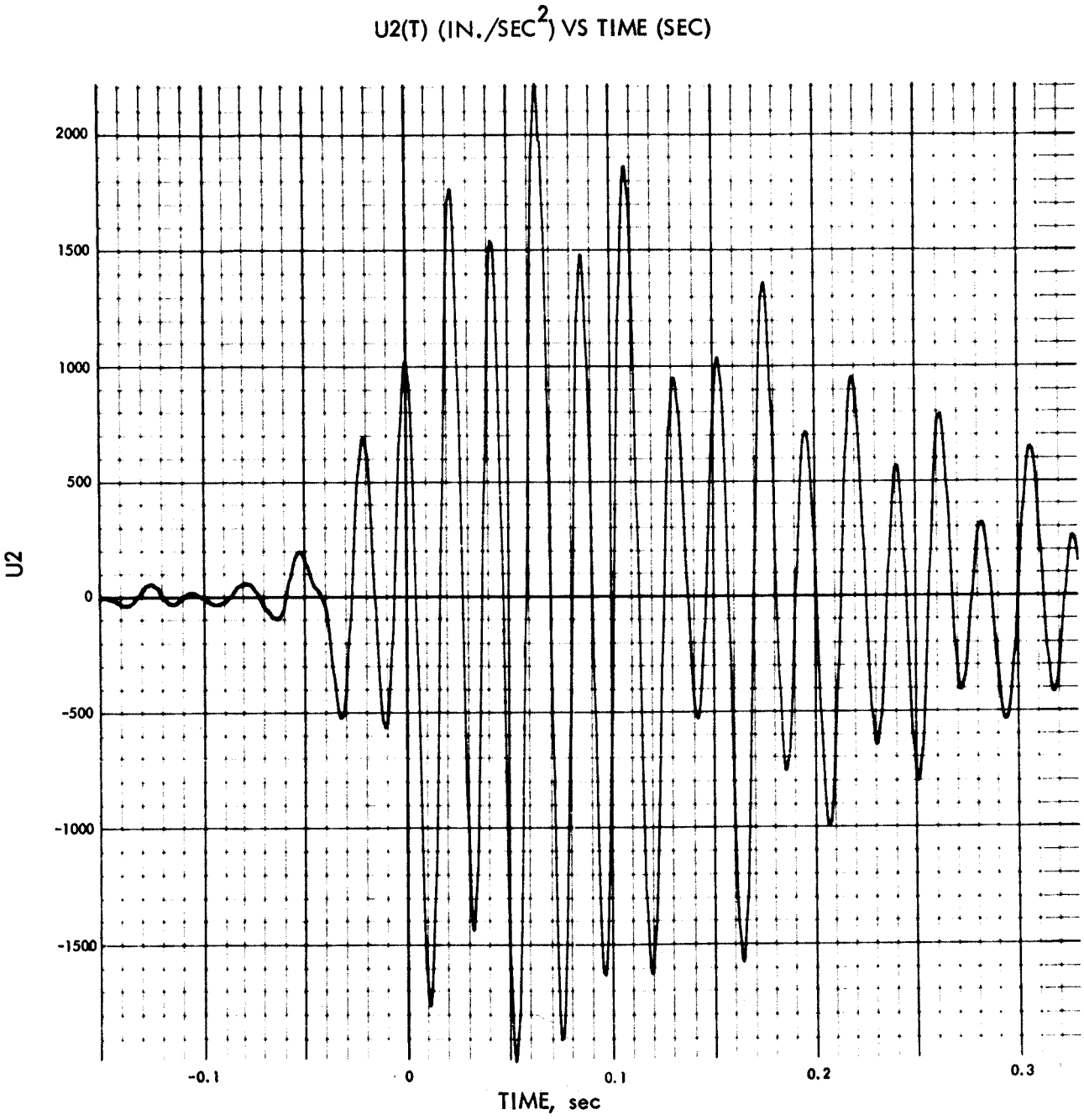

Fig. E-112. Joint 23, x_1 time history (pulse 3) 1% damping

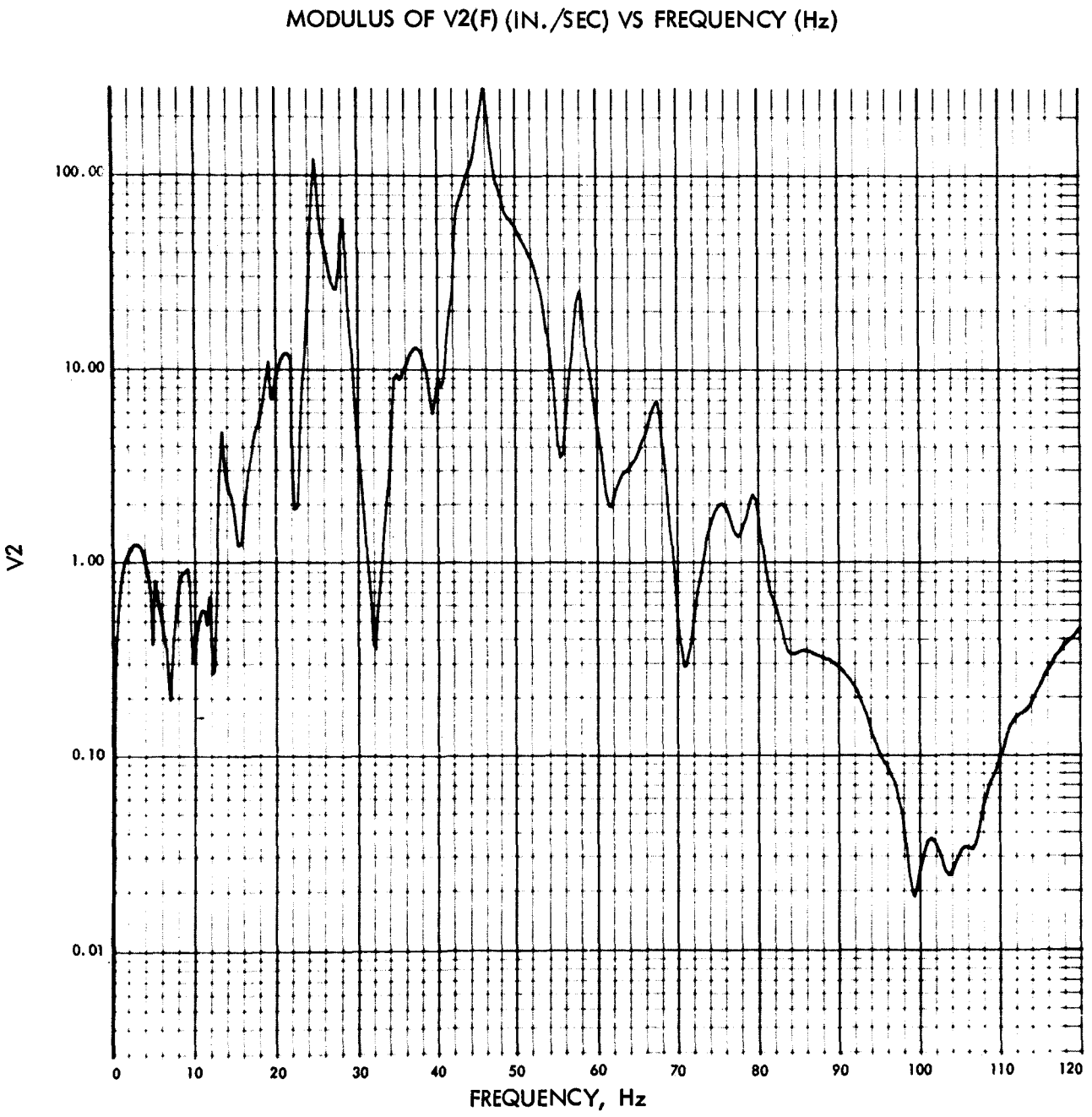

Fig. E-113. Joint 23, x_1 Fourier transform, modulus (pulse 3) 1% damping

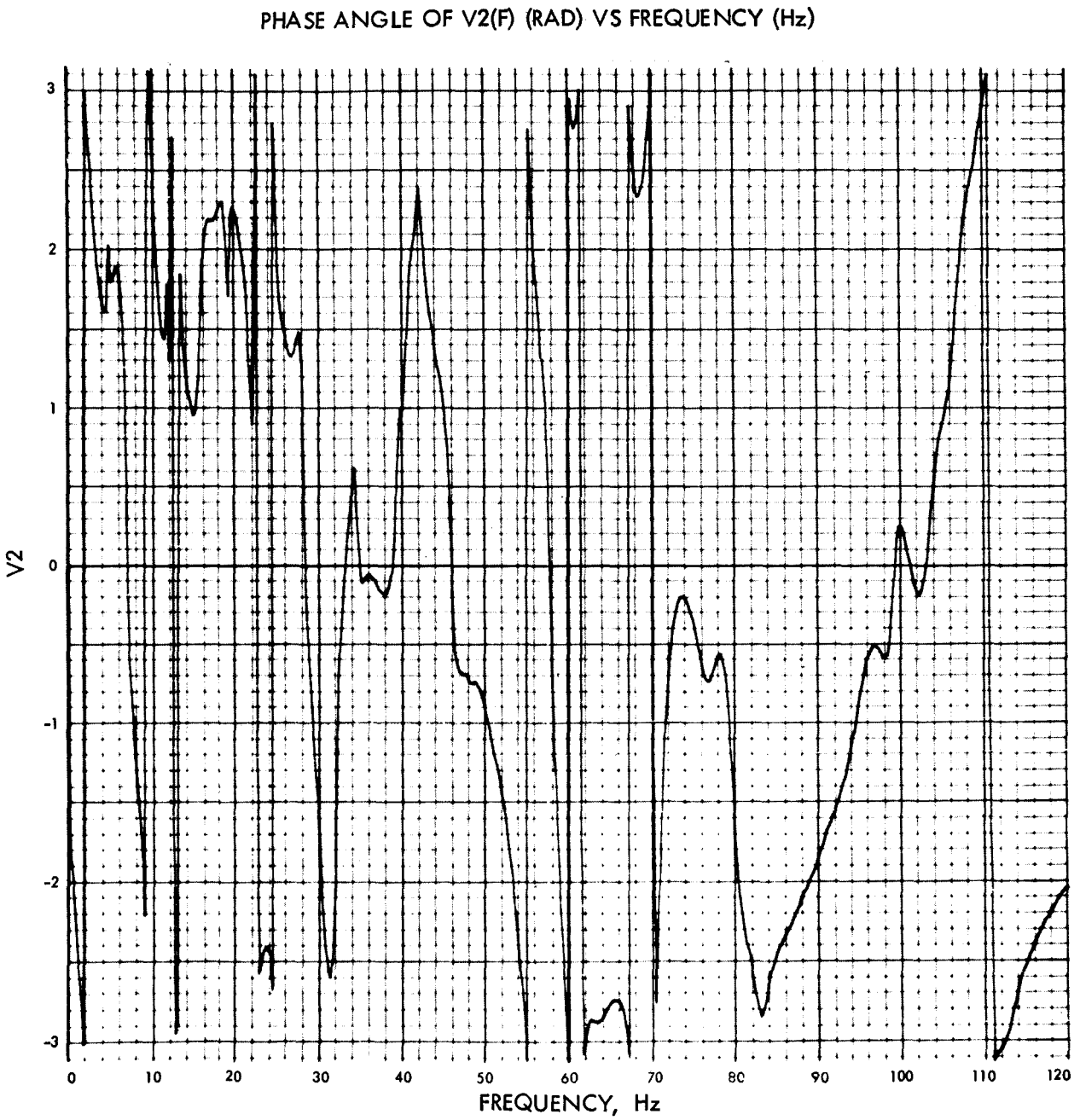

Fig. E-114. Joint 23, x_1 Fourier transform, phase angle (pulse 3) 1% damping

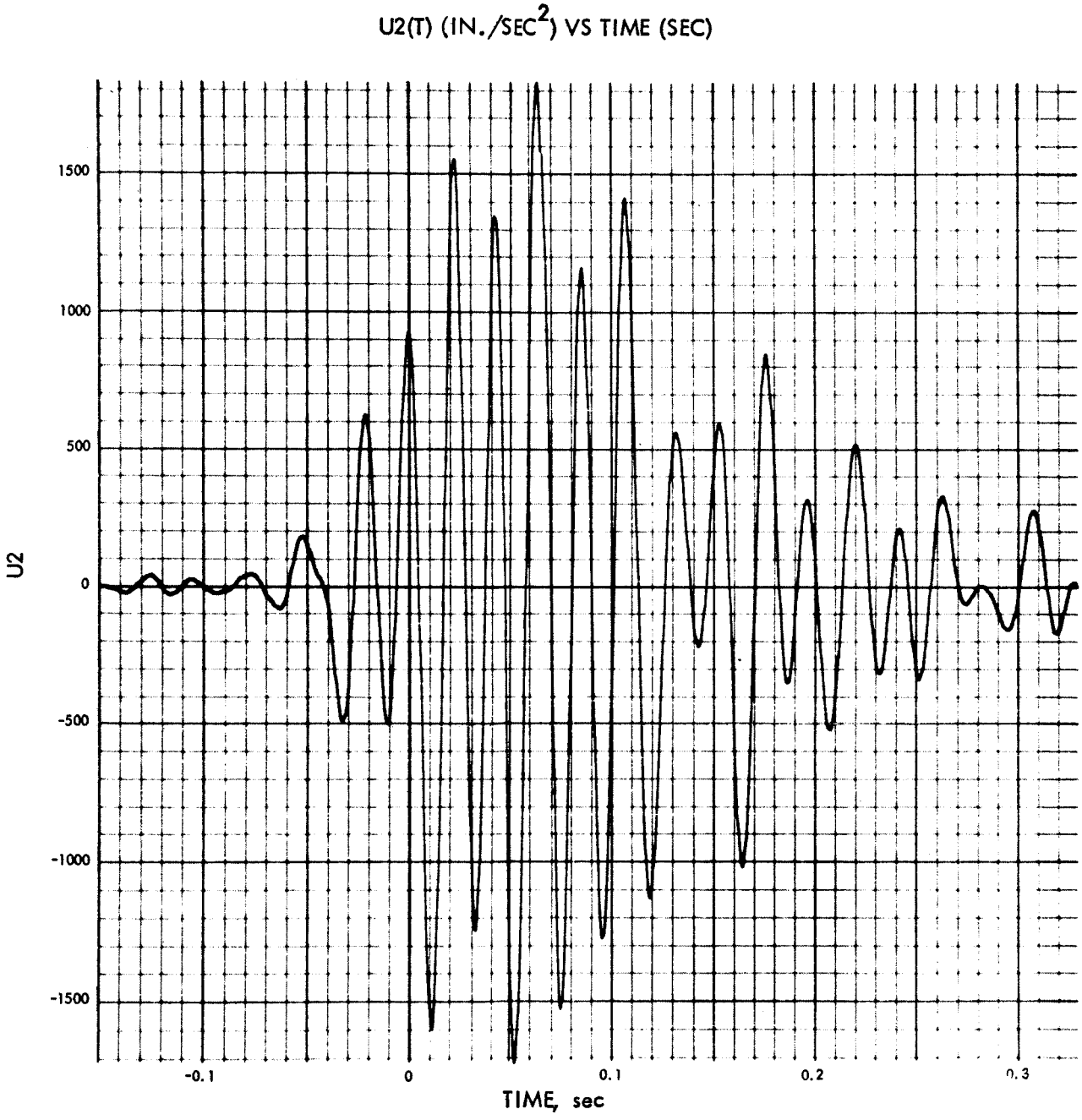

Fig. E-115. Joint 23, x_1 time history (pulse 3) 2% damping

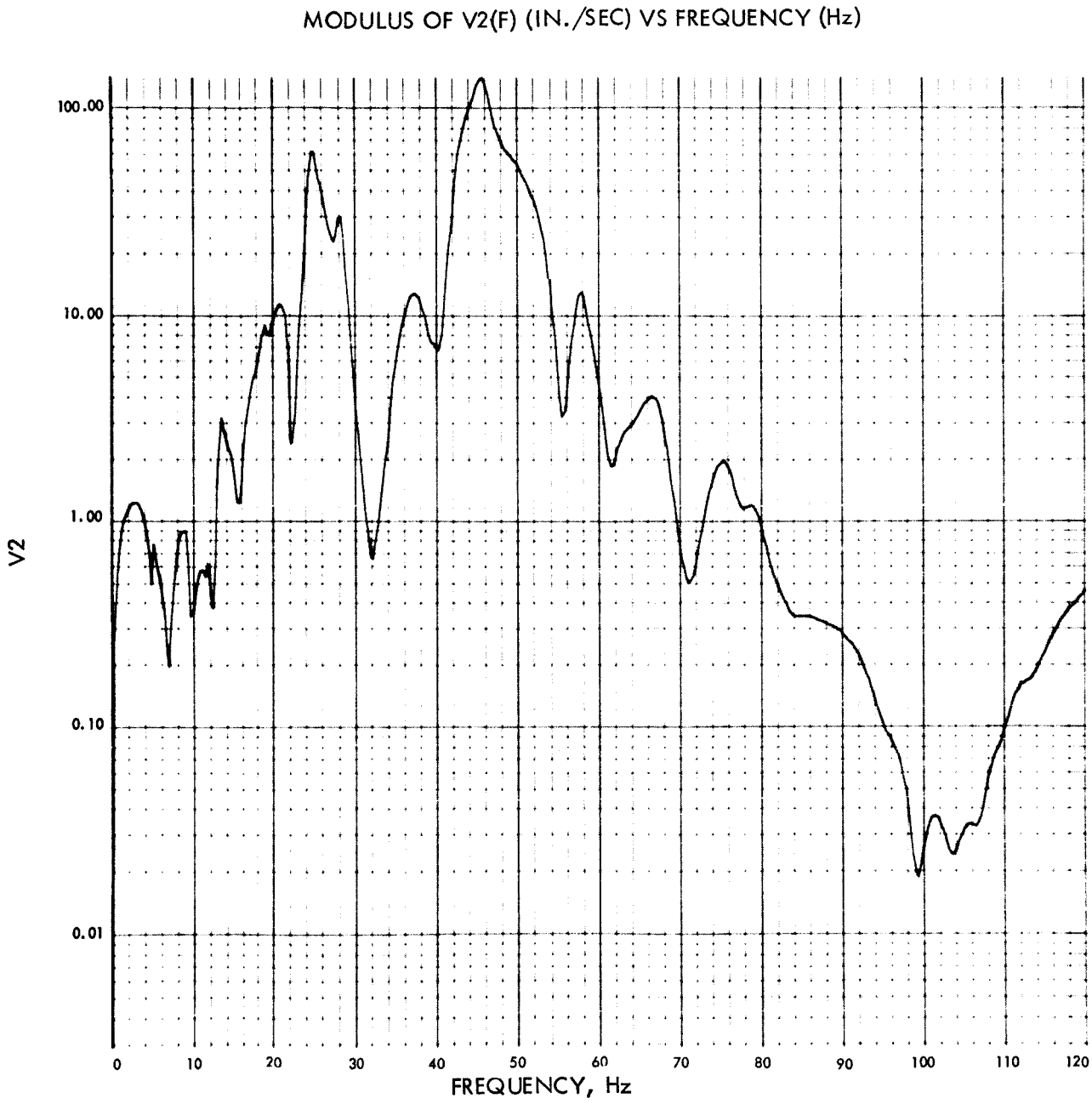

Fig. E-116. Joint 23, x_1 Fourier transform, modulus (pulse 3) 2% damping

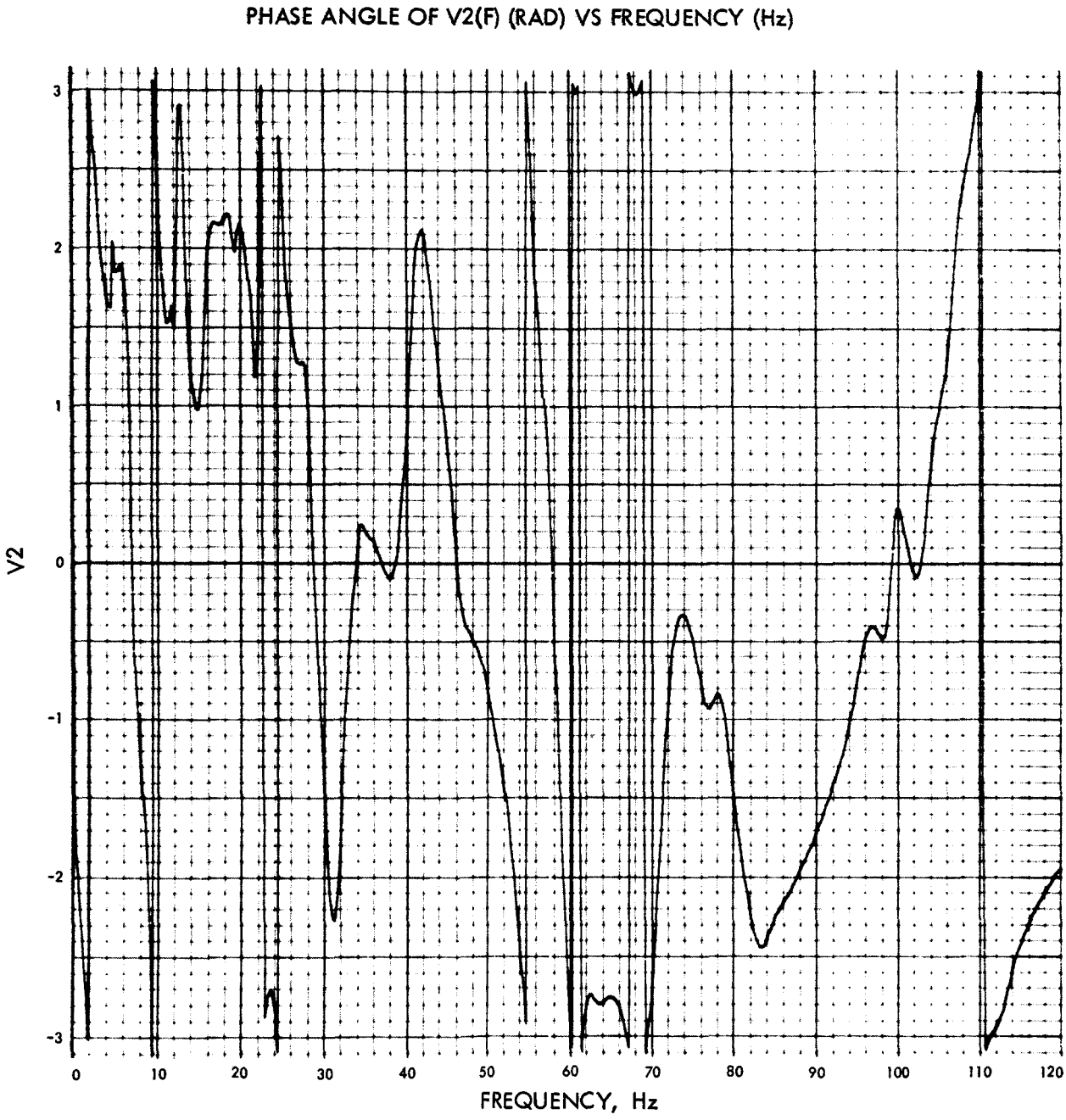

Fig. E-117. Joint 23, x_1 Fourier transform, phase angle (pulse 3) 2% damping

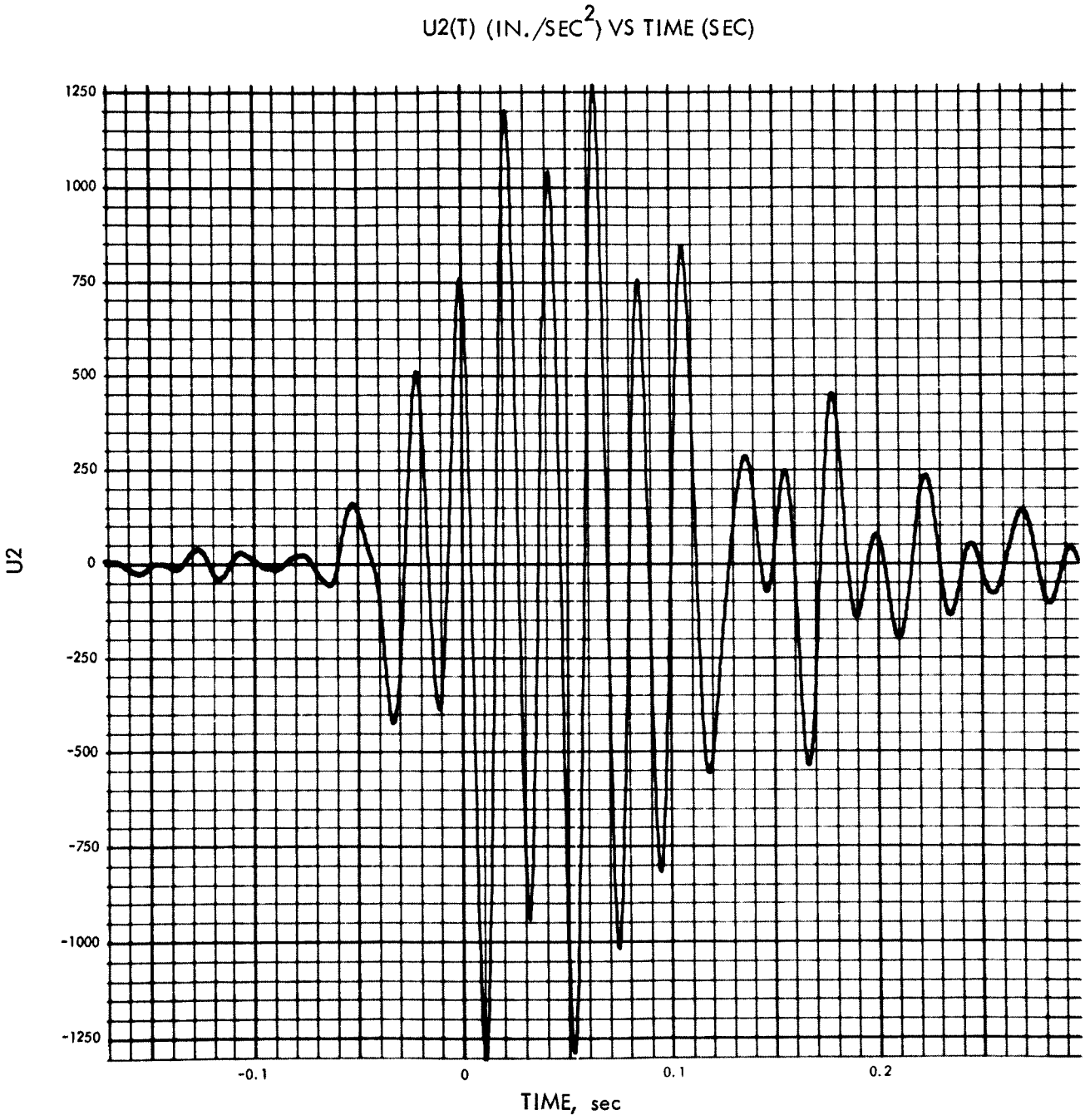

Fig. E-118. Joint 23, x_1 time history (pulse 3) 4% damping

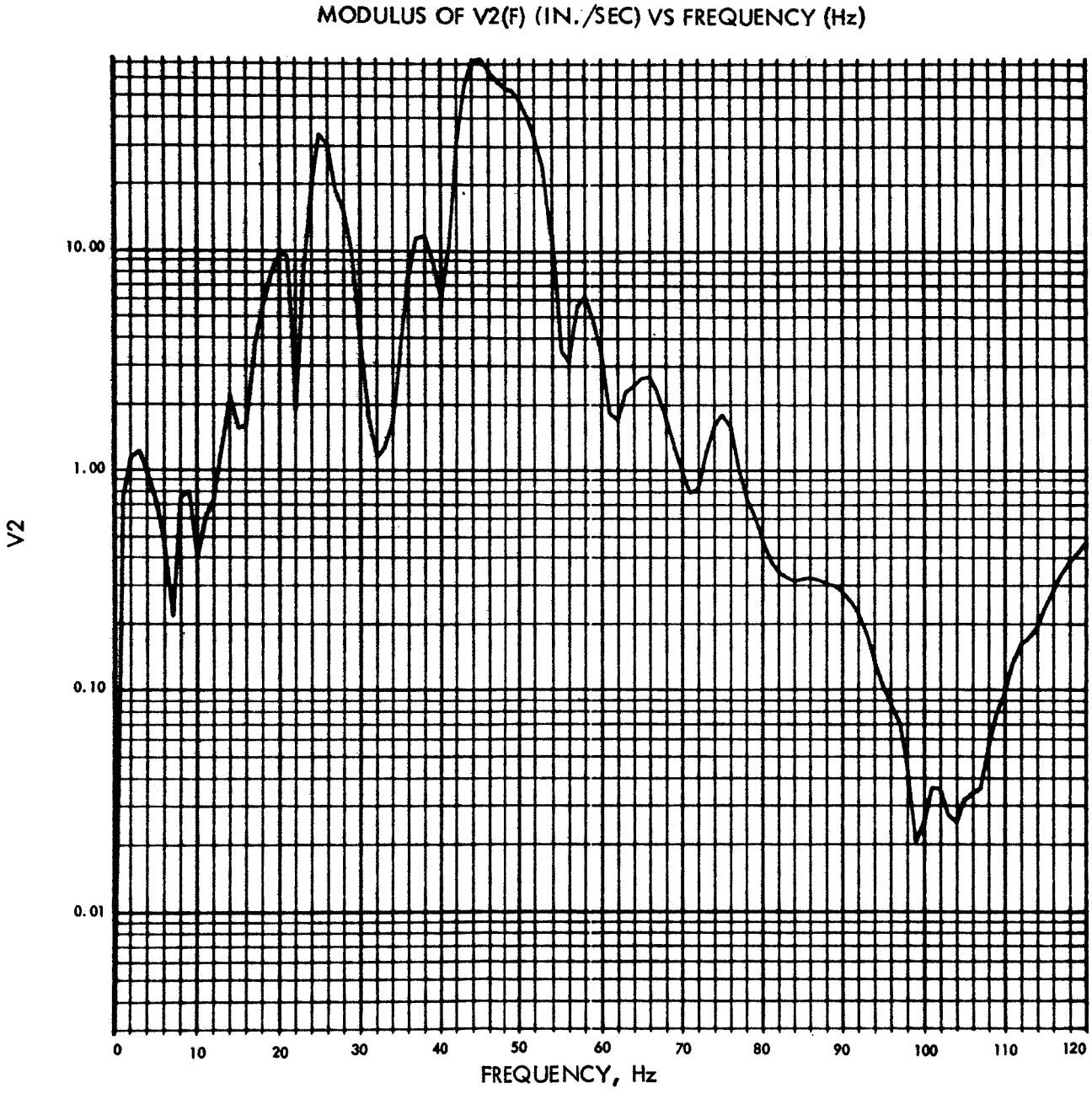

Fig. E-119. Joint 23, x_1 Fourier transform, modulus (pulse 3) 4% damping

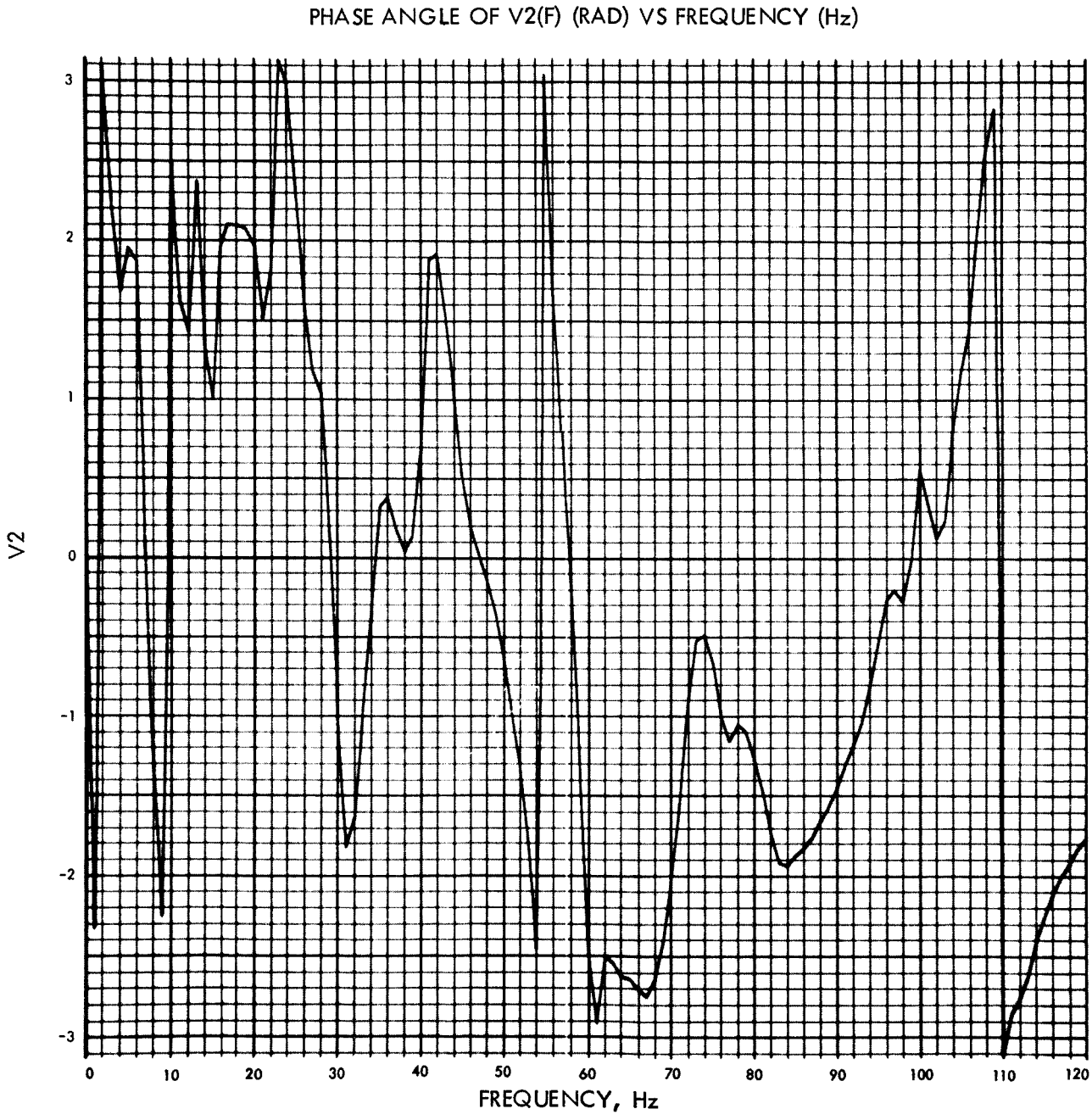

Fig. E-120. Joint 23, x_1 Fourier transform, phase angle (pulse 3) 4% damping

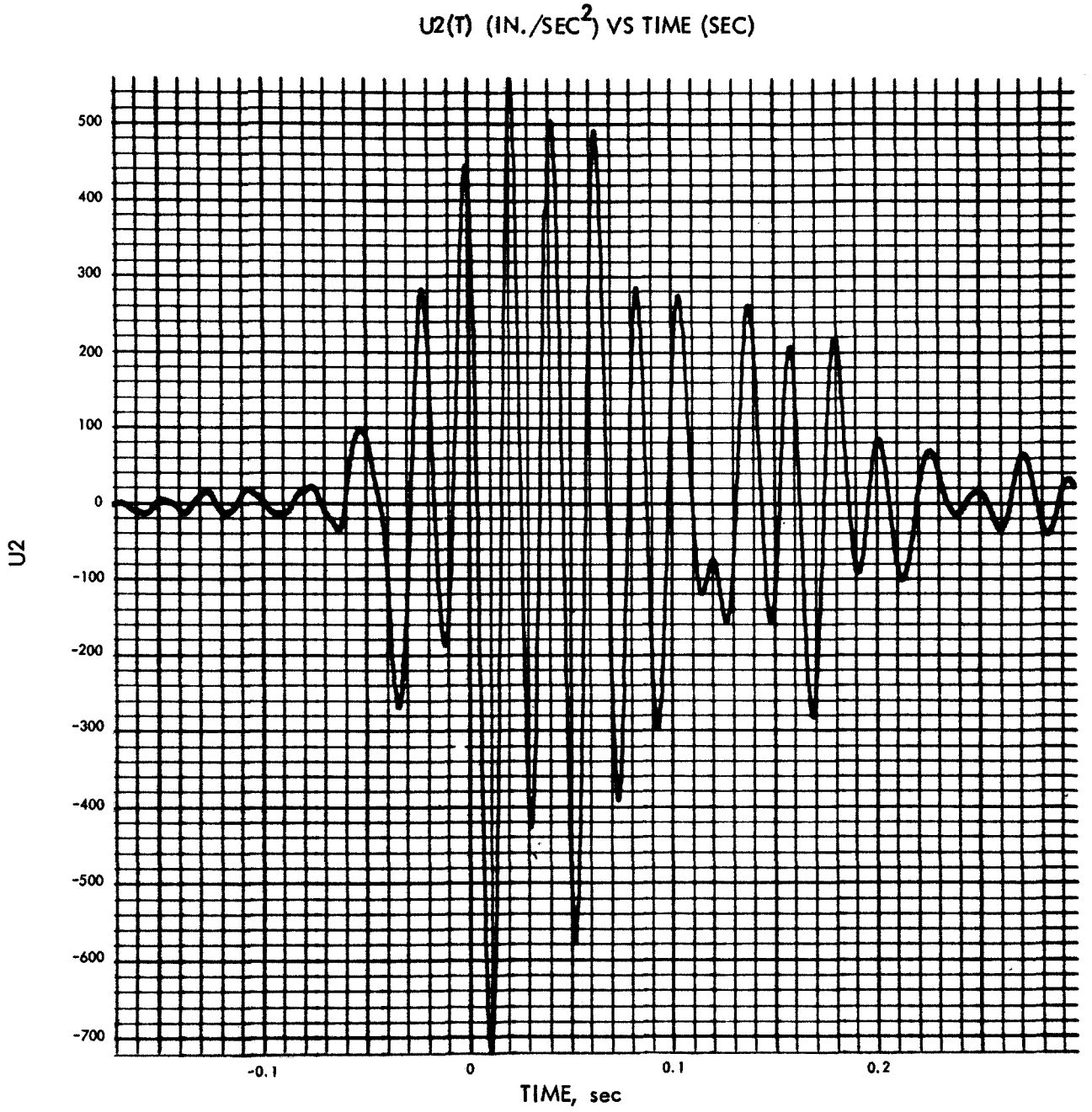

Fig. E-121. Joint 23, x_1 time history (pulse 3) 10% damping

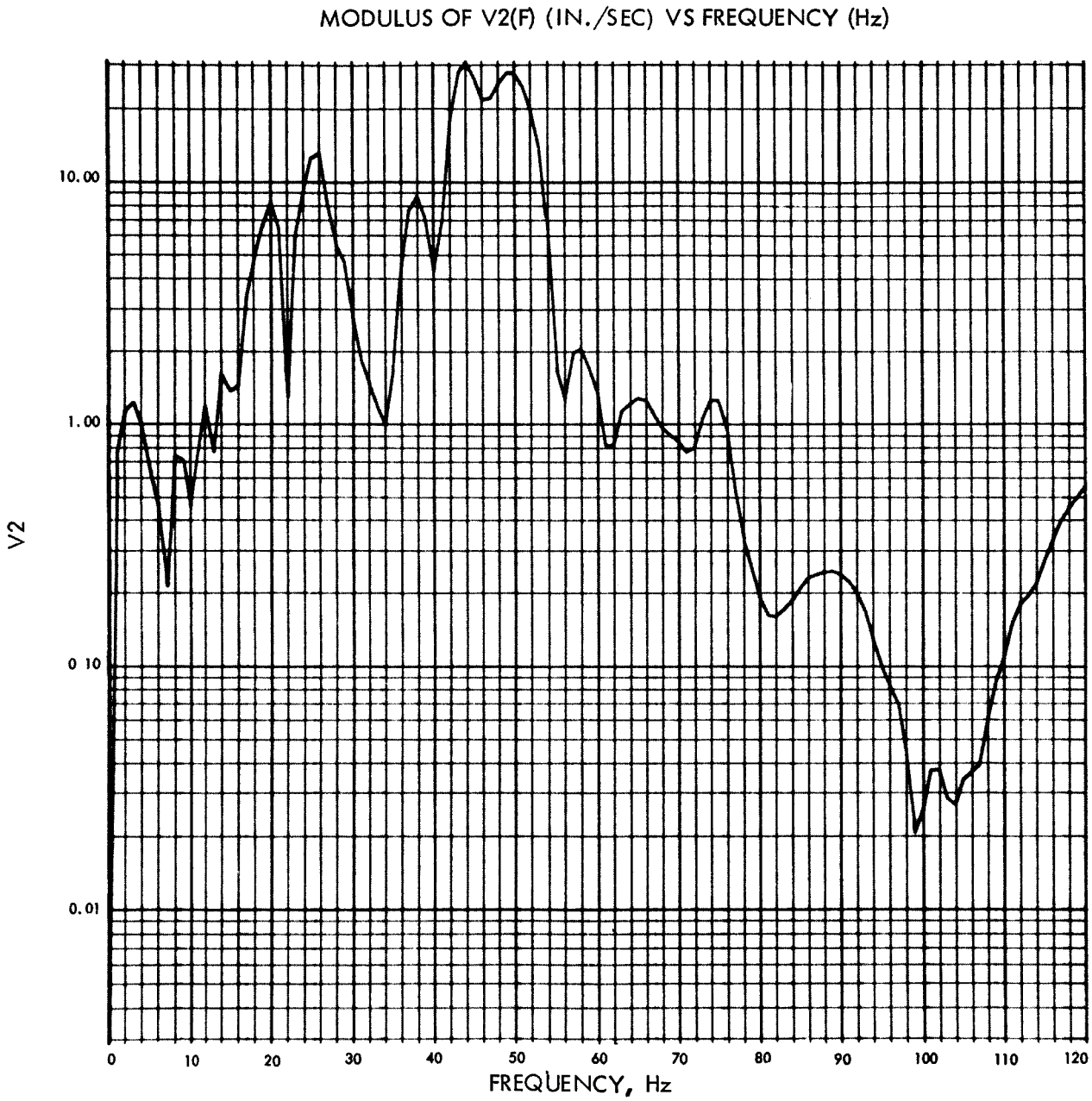

Fig. E-122. Joint 23, x_1 Fourier transform, modulus (pulse 3) 10% damping

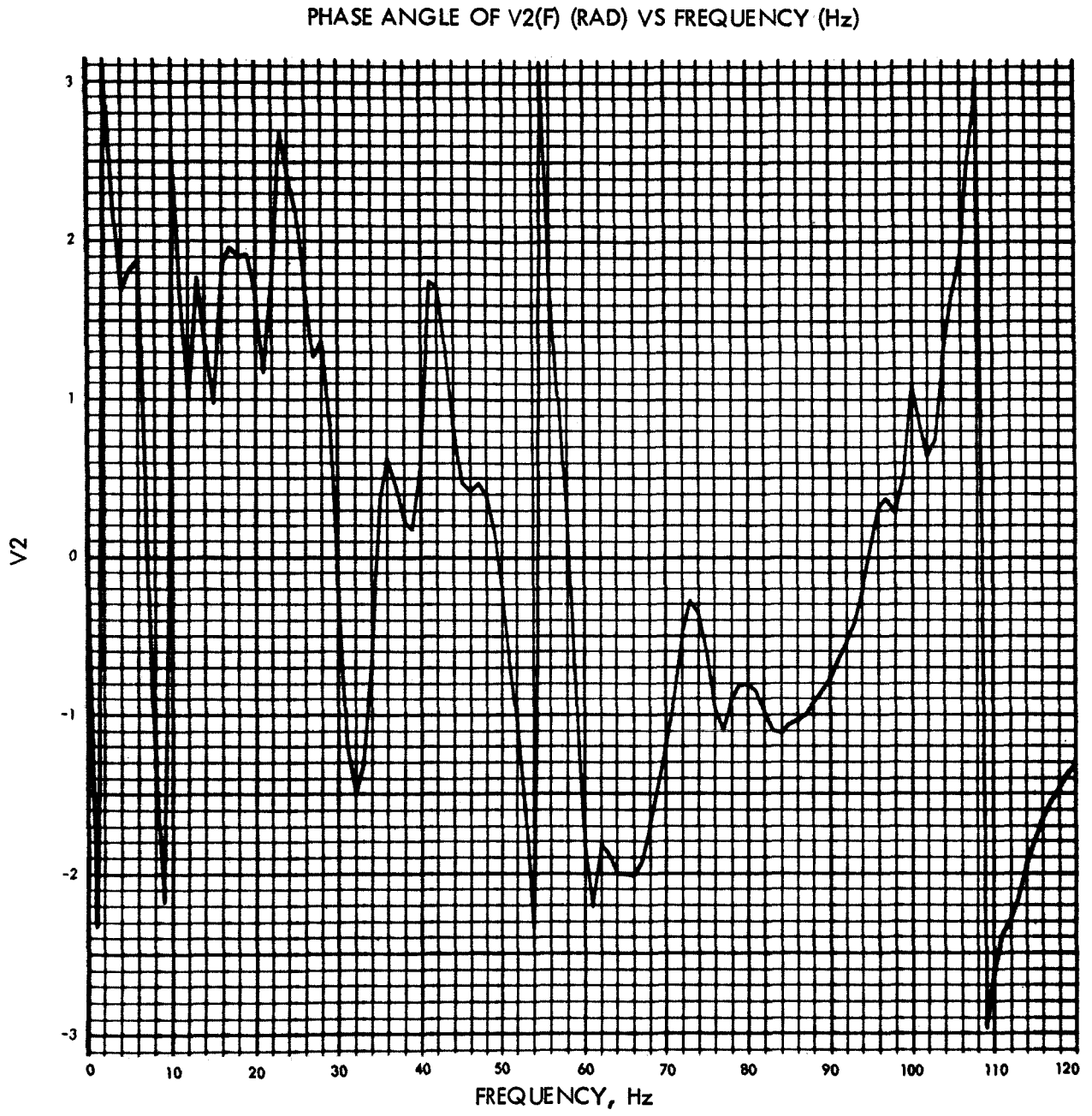

Fig. E-123. Joint 23, x_1 Fourier transform, phase angle (pulse 3) 10% damping

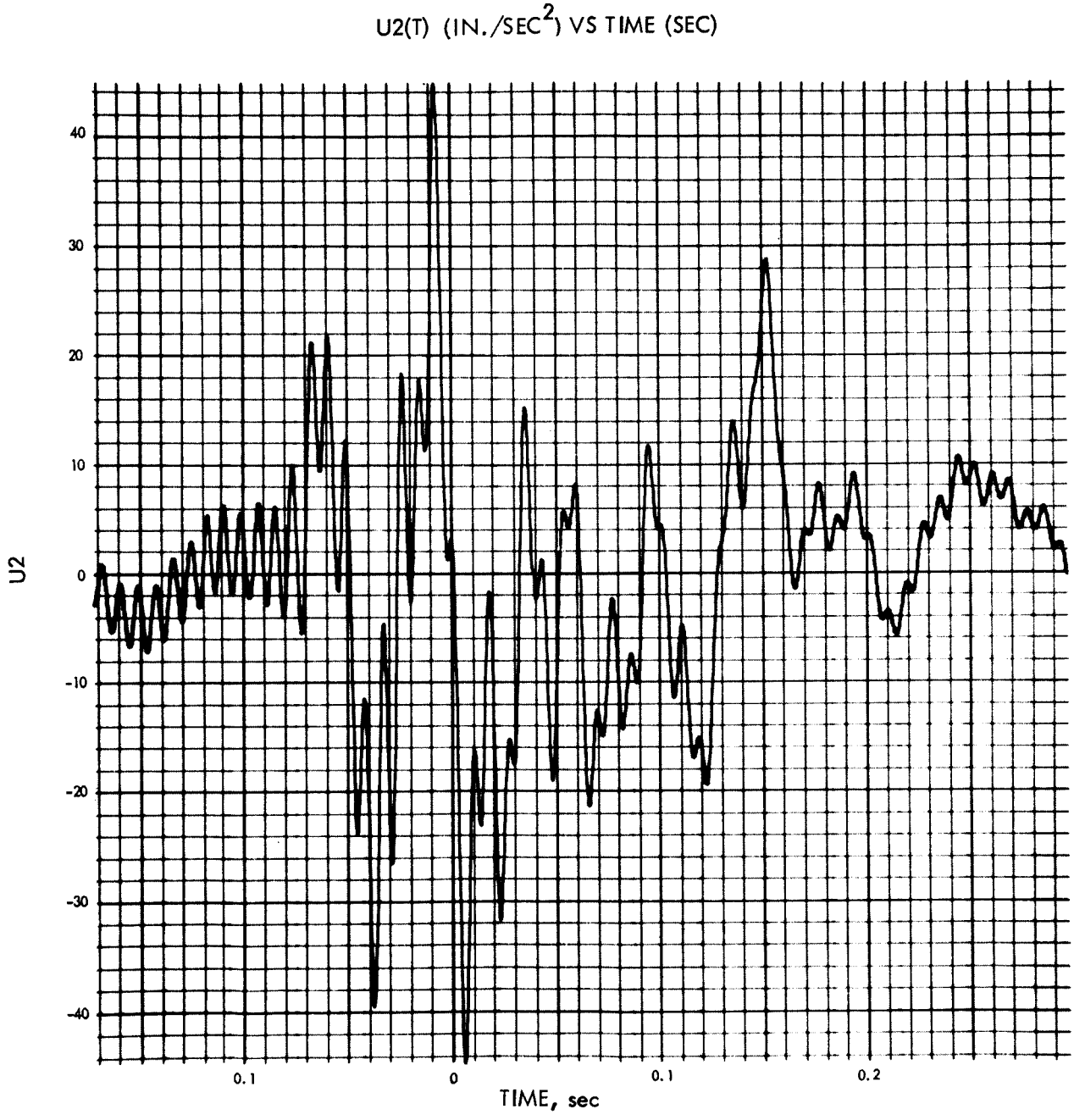

Fig. E-124. Joint 23, x_1 time history (pulse 3) 50% damping

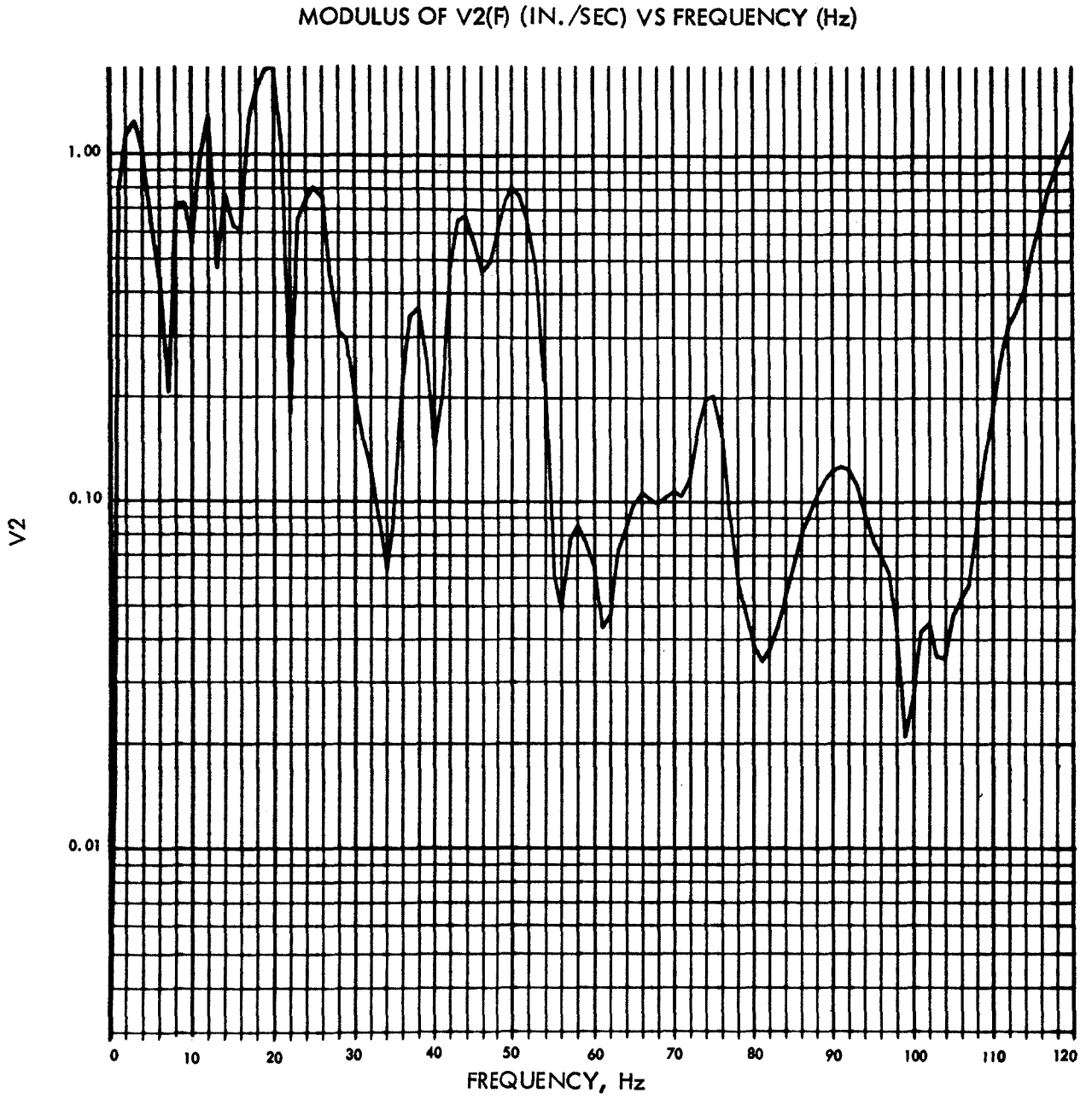

Fig. E-125. Joint 23, x_1 Fourier transform, modulus (pulse 3) 50% damping

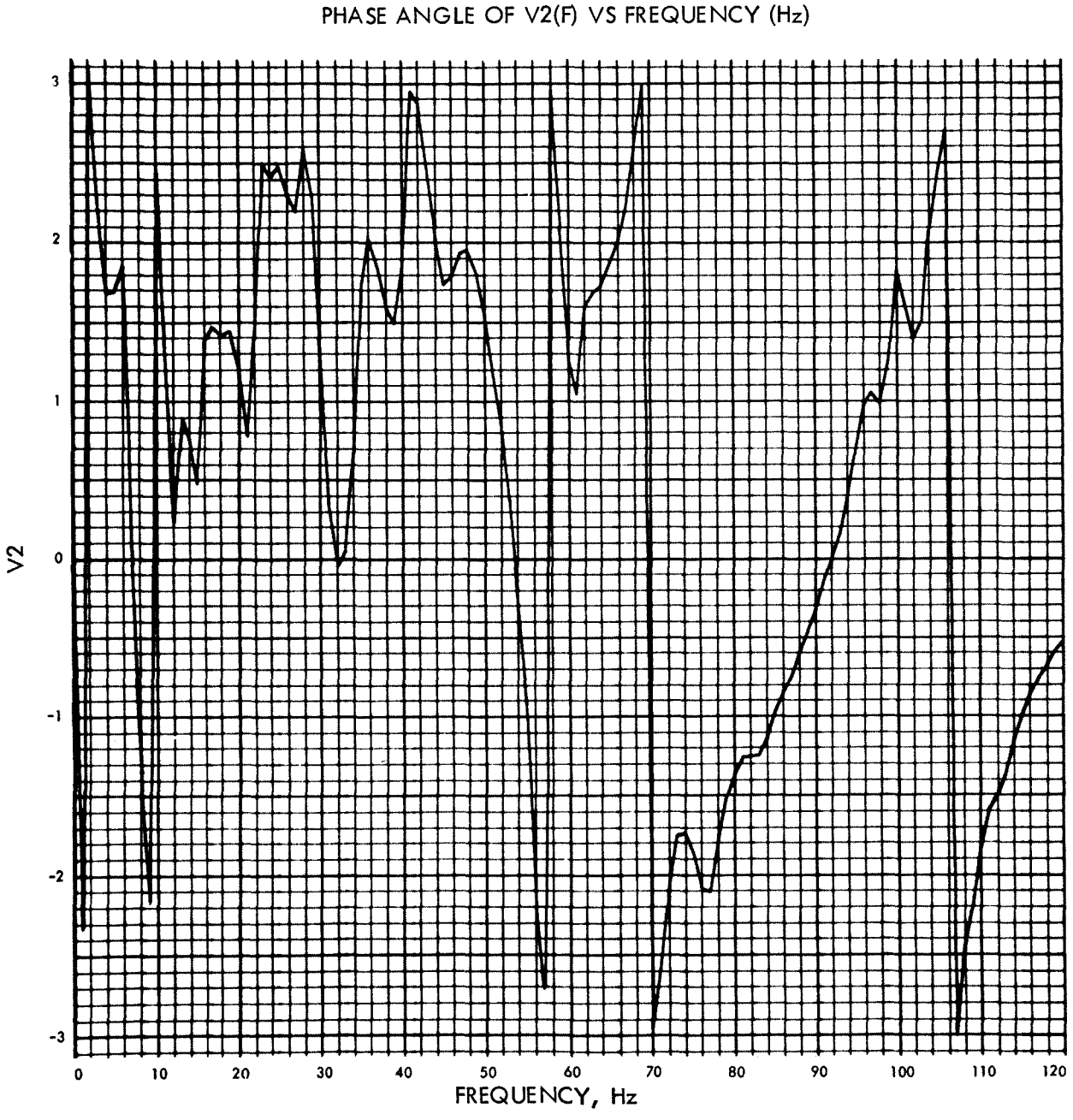

Fig. E-126. Joint 23, x_1 Fourier transform, phase angle (pulse 3) 50% damping

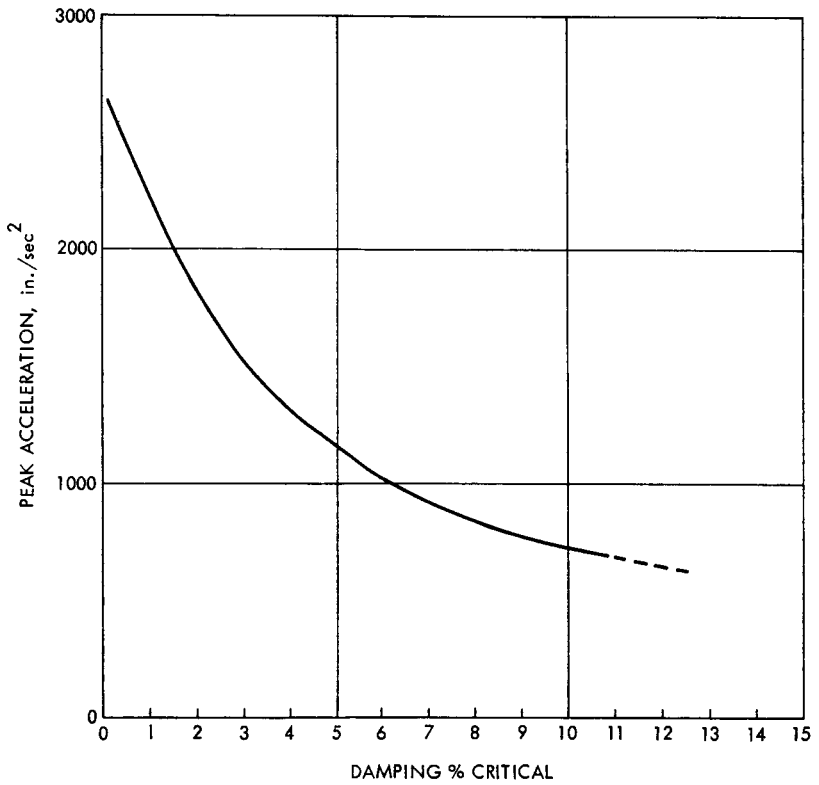

Fig. E-127. Variations of peak acceleration with Atlas/Agena/OGO modal damping